



HAL
open science

Modeling of Pickering Emulsion Polymerization

Barthélémy Brunier

► **To cite this version:**

Barthélémy Brunier. Modeling of Pickering Emulsion Polymerization. Chemical and Process Engineering. Université Claude Bernard - Lyon I, 2015. English. NNT : 2015LYO10320 . tel-01523793

HAL Id: tel-01523793

<https://theses.hal.science/tel-01523793>

Submitted on 17 May 2017

HAL is a multi-disciplinary open access archive for the deposit and dissemination of scientific research documents, whether they are published or not. The documents may come from teaching and research institutions in France or abroad, or from public or private research centers.

L'archive ouverte pluridisciplinaire **HAL**, est destinée au dépôt et à la diffusion de documents scientifiques de niveau recherche, publiés ou non, émanant des établissements d'enseignement et de recherche français ou étrangers, des laboratoires publics ou privés.

UNIVERSITÉ CLAUDE BERNARD - LYON 1
ÉCOLE DOCTORALE DE CHIMIE

THÈSE

pour l'obtention du

DIPLOME DE DOCTORAT

Spécialité : GÉNIE DES PROCÉDÉS

Présentée et soutenue par

Barthélémy BRUNIER

Modeling of Pickering Emulsion Polymerization

Thèse dirigée par Nida SHEIBAT-OTHMAN

préparée au LAGEP/ESCPE-lyon, Projet ANR PICKEP

soutenue le 4 décembre 2015

Jury :

<i>Rapporteurs :</i>	Christophe SERRA	-	Université de Strasbourg (ICPEES)
	Nathalie LE SAUZE	-	Université Paul Sabatier (LGC)
<i>Directeur :</i>	Nida SHEIBAT-OTHMAN	-	CNRS (LAGEP)
<i>Co-encadrant :</i>	Elodie BOURGEAT-LAMI	-	CNRS (LCP-CP2)
	Yves CHEVALIER	-	CNRS (LAGEP)
<i>Examineurs :</i>	Laurent FALK	-	CNRS (LRGP)
	Salima BOUTTI	-	Arkema (Lyon)
	Koffi FIATY	-	Université Lyon1 (LAGEP)

Remerciements

Ces travaux étaient réalisés au sein du Laboratoire d'Automatique et de Génie des Procédés (LAGEP). Je remercie le Professeur Hatem Fessi, directeur du LAGEP, de m'avoir permis d'effectuer ces travaux dans les meilleures conditions.

J'adresse mes remerciements à tous les membres du jury. Je remercie Madame Nathalie Le Sauze et Monsieur Christophe Serra de m'avoir fait l'honneur d'être rapporteurs de cette thèse, pour leur réactivité, leur honnêteté et pour leur relecture attentive malgré de courts délais. Je remercie fortement Monsieur Laurent Falk pour avoir présidé mon jury de thèse, son attention, ses remarques et ses commentaires m'ont vraiment touché. Je tiens à exprimer toute ma reconnaissance à Madame Salima Boutti et Monsieur Koffi Fiatty d'avoir accepté d'évaluer ces travaux. J'ai eu grand plaisir à avoir dans mon jury toutes ces personnes qui font référence dans le domaine du Génie des Procédés en France.

Mes remerciements maintenant se tournent tout naturellement vers ceux sans qui ce travail n'aurait pu aboutir. Ces trois années ont été très enrichissantes, j'ai beaucoup appris autant du point de vue professionnel que personnel. Ceci n'a été possible que grâce à toi Nida Sheibat-Othman. Merci pour ton aide, tes conseils et la grande confiance que tu m'as témoignée. Je suis ravi d'avoir travaillé en ta compagnie et ces moments partagés resteront gravés dans ma mémoire. Merci aussi à Yves Chevalier pour son soutien, sa disponibilité et son honnêteté parfois crue mais qui permet d'avancer. Sa faculté à tout remettre en question m'a beaucoup appris. Et merci à Elodie Bourgeat-Lami, d'avoir été toujours disponible et à l'écoute. Ses compétences, sa rigueur scientifique et sa clairvoyance ont été essentielles pour ce travail. Vous avez été disponibles jusqu'au bout sans faille, jusqu'aux derniers

détails, malgré les délais de relectures contraignants. Je suis fier d'avoir présenté cette thèse avec et grâce à vous trois.

Il me sera très difficile de remercier tout le monde car c'est grâce à l'aide de nombreuses personnes que j'ai pu mener cette thèse à son terme.

J'exprime toute ma reconnaissance à, Madame Nicole Gilon-Delepine de m'avoir permis de passer de nombreuses heures à écouter cette belle machine qu'est l'ICP-OES et surtout pour la disponibilité et la gentillesse dont elle a fait preuve. Je remercie également Géraldine Agusti pour toutes ces séances de microscope et pour tous ses conseils au Laboratoire ainsi que Monsieur Pierre-Yves Dugas de m'avoir accordé son temps et sa patience durant les séances de Cryo-MEB et HR-TEM. Egalement merci à Xavier Jaurand pour son expertise et son coup d'œil afin d'obtenir les plus belles photos de microscope. Un grand merci aussi à Alexandre Monnier qui a fait des mesures de balance à quartz sans contrepartie.

Un merci particulier pour Jean-Pierre et Sébastien pour leurs conseils techniques, leur gentillesse et toutes les petites réparations.

Un grand merci à tous ces jeunes qui ont aussi traversé cette aventure. J'ai beaucoup appris à leur côté, merci à Julien, Nadjat, Boutaina, Mathilde et Mehdi.

Je tiens à remercier les membres du LAGEP, vous m'avez aussi beaucoup appris humainement. Merci à Laure, Jess et Fabrice pour m'avoir accueilli les bras ouverts même si je n'ai toujours pas compris la technique de la biscotte. Un grand merci à tous ceux avec qui j'ai partagé de bons moments au Laboratoire et ainsi que devant une bonne bière, je coinche cette thèse pour vous. Merci à tous les collègues de la salle café du LAGEP qui par quelques mots, une raclette et un croissant partagés, ont rendu ces trois années conviviales.

Je n'oublie pas ma famille, mes parents, ma sœur et mes grands-parents. Merci pour vos encouragements et pour cette confiance inébranlable que vous m'avez accordée tout au long de mes études.

Merci aussi à vous, les gars, ma deuxième famille. Grandir à vos côtés fut une sacré belle aventure, merci à vous pour ces moments et pour ceux à venir.

Et enfin, mon papillon, merci d'être tout simplement là. Ces trois années n'ont pas toujours été faciles et j'espère du fond du cœur que le plus beau reste à vivre.

Résumé

Modélisation de la polymérisation en émulsion stabilisée par des particules inorganiques

L'objectif du présent travail est de développer une méthodologie pour la modélisation fondamentale du procédé de polymérisation en émulsion sans tensioactif stabilisée par des particules inorganiques, appelée "polymérisation en émulsion Pickering (Pickering emulsion polymerization)". Le modèle doit être en mesure de décrire la cinétique de réaction dans les différentes phases, le transfert de masse entre les phases (ex radicaux.) et l'évolution de la distribution de taille des particules (PSD), qui est une propriété importante du latex final. Le modèle recherché sera basé sur des sous-modèles fondamentaux représentant la nucléation des particules, la croissance, la coagulation, le partage de particules inorganiques et la cinétique de la réaction. Ces sous-modèles sont des pièces autonomes qui sont identifiées individuellement et validées expérimentalement représentant un mécanisme élémentaire. La méthodologie développée devrait être applicable à différents systèmes de polymérisation en émulsion stabilisée par des particules inorganiques.

Le modèle permet d'améliorer la compréhension du procédé et pourra être utilisé dans les stratégies de contrôle afin d'améliorer la qualité du produit, principalement pour augmenter la teneur en solide du latex pour l'intérêt industriel.

La stabilisation « Pickering » a récemment émergé comme une nouvelle méthode pour créer des colloïdes nanocomposites par adsorption de particules solides aux interfaces solide-liquide. L'élaboration de latex composites permet d'allier les propriétés des solides inorganiques avec les avantages des polymères organiques, par exemple, ceci permet d'améliorer les propriétés mécaniques et la résistance à l'eau

des films produits avec ces matériaux nanocomposites.

Jusqu'à présent, il n'y a pas eu d'études de modélisations consacrées aux systèmes de polymérisation en émulsion Pickering. Cependant, il y a des différences fondamentales entre la polymérisation en émulsion dite « classique » (avec tensioactif) et Pickering :

- Tout d'abord, la présence de particules inorganiques chargées à la surface des particules de polymères, apporte une stabilité électrostatique et forme une barrière mécanique pouvant influencer l'entrée et la sortie des radicaux, ce qui a une forte influence sur la croissance des particules.
- Dans un second temps, le mécanisme de formation des particules de polymère est différent puisqu'il n'y a plus la présence de micelles de tensioactifs, donc le processus de nucléation ne peut pas être décrit par des modèles de nucléation micellaire habituels.
- Aussi, le mécanisme de partage (ainsi que la dynamique de partage) de particules inorganiques entre les différentes phases (eau, surface des particules polymériques ou gouttelettes de monomère), leur arrangement à la surface des particules polymériques et leur interaction entre eux ou avec cette surface ne sont pas connus.
- 4. Enfin, l'effet stabilisant des particules inorganiques n'est pas défini.

C'est pourquoi, le procédé de polymérisation en émulsion Pickering mérite une modélisation spécifique.

Dans un premier temps (chapitre 2), il a été nécessaire de comprendre le partage de l'argile, qui est la Laponite[®] dans cette thèse, lors du procédé de polymérisation. Il n'était pas possible de déterminer la répartition des particules inorganiques directement lors de la polymérisation, c'est pourquoi nous avons réalisé cette étude sur un latex de polystyrène, avec différentes forces ioniques, produit dans les mêmes conditions. Une adsorption en multicouche a été observée et modélisée par un isotherme d'adsorption suivant la loi B.E.T.. Plusieurs méthodes d'analyse ont

été utilisées : Quartz Crystal Microbalance (QCM-D), la conductimétrie et Inductively Coupled Plasma-Atomic Emission Spectroscopy (ICP-AES). L'étude sur polystyrène pur (non chargé) par ces trois méthodes a permis de démontrer que les interactions non électrostatiques entre l'argile et le polystyrène peuvent surmonter les répulsions électrostatiques nécessaires à l'adsorption. La présence d'un électrolyte améliore cette adsorption car il permet de cranter les charges des plaquettes de l'argile et donc son empilement à la surface des particules polymériques. La présence de multicouche a été vérifiée par microscopie électronique à transmission (TEM) couplée à une méthode de spectroscopie dispersive en énergie (EDS). Le modèle d'adsorption développé, résumé ci-dessous, sera utile pour la modélisation et la compréhension de l'ensemble du processus de polymérisation.

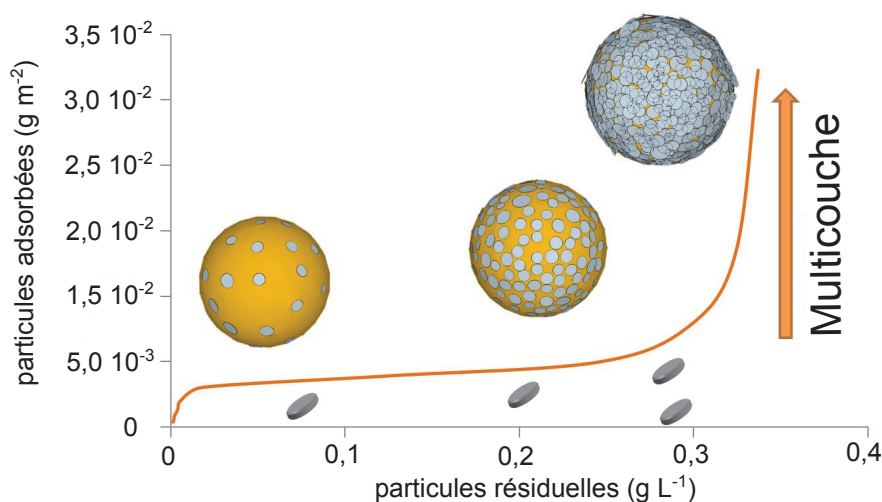


Figure 1: Adsorption isotherm

Dans un second temps (chapitre 3), un grand nombre de réactions de polymérisation ont été réalisées afin de comprendre les différents facteurs expérimentaux entrant en jeu dans le procédé de polymérisation du styrène stabilisés par des particules inorganiques de Laponite[®]. La polymérisation du styrène initiée par un amorceur soluble dans l'eau (le persulfate de potassium) a été choisie car c'est une réaction référence dans la littérature et très bien décrite en terme de cinétique. Nous avons pu démontrer que la vitesse d'agitation et la concentration

initiale du monomère n'ont aucun effet sur la distribution de taille de particules de polymère obtenues. Ceci valide le processus de polymérisation en émulsion et écarte la possibilité de nucléation de gouttelettes (comme dans la polymérisation en mini-émulsion). Aussi, on déduit que le partage de monomère entre les différentes phases est instantané et similaire à la polymérisation en émulsion classique. Donc, la présence d'argile à la surface des particules polymériques n'a pas d'effet sur la solubilité de monomère dans les particules. Des polymérisations semi-continues ont permis de mieux comprendre comment contrôler la vitesse de polymérisation. Une première partie batch permet la formation des particules de polymère. Ce nombre reste ensuite constant lors de la partie semi-continue. De plus en jouant sur le débit et le temps de début d'injection, il est possible de maintenir la réaction en régime saturé (intervalle II) ou en régime affamé (intervalle III). Ces résultats seront très utiles pour la modélisation afin de sélectionner des plages de réaction où certains paramètres restent constants. Notamment, la modélisation des intervalles I, où la nucléation des particules a lieu, ainsi que l'intervalle II (sous saturation) seront considérées dans un premier temps. Dans ces intervalles, la diffusion de radicaux dans les particules et dans l'eau reste constante, car la concentration de monomères dans les différentes phases est constante. Donc, les différents paramètres de réactions peuvent être considérés constants.

Plusieurs types de Laponite[®] ont été ensuite testés (chapitre 4) : la Laponite[®] RDS, la Laponite[®] XLS, la Laponite[®] S482 et la Laponite[®] JS lors de polymérisation en émulsion semi continue. Les différences de stabilisation de chacune ont pu être décrites de manière expérimentale.

L'ensemble de ces études a permis de mieux décomposer les étapes de la polymérisation, ce qui a permis de travailler sur les différents sous modèles de manières indépendantes. En effet, le chapitre 5 traite l'étude des paramètres de capture et de désorption de radicaux pour un nombre de particules stables (sans nucléation ni coagulation). Pour cela, une série d'expériences dans laquelle la nucléation et la coagulation étaient évitées, nous a permis de travailler uniquement sur le modèle de croissance. La croissance est régie par la capture et la désorption des radicaux. Plusieurs modèles de la littérature du coefficient d'absorption et du coef-

ficient de désorption de radicaux ont été comparés. La confrontation de ces modèles avec les résultats expérimentaux nous a permis de choisir le meilleur couple modèle d'absorption/modèle de désorption. La présence de particules inorganiques n'entre pas en compte dans les modèles choisis. Donc, il n'y aurait pas d'influence de la Laponite[®] sur l'entrée et la sortie des radicaux dans les particules de polystyrène. Ce modèle est valable sous saturation en monomère (en intervalle II).

Le chapitre 6 ensuite, traite l'étude de la nucléation et la coagulation des particules en utilisant le modèle d'échange de radicaux développé dans le chapitre 5. Les deux modèles sont valables sous saturation en monomère. Un modèle de nucléation coagulative a permis de comprendre les mécanismes mis en jeu lors de la formation de particules de polymères. Une nucléation homogène permet de générer un grand nombre de particules primaires. Les particules inorganiques viennent stabiliser ces particules primaires. En grossissant, les particules polymériques deviennent instables et coagulent entre elles pour réduire leur tension de surface et améliorer leur stabilité. Ainsi une plus grande quantité de particules inorganiques permet une meilleure stabilisation et donc la nucléation d'un plus grand nombre de particules polymériques. Le nombre effectif de plaquettes participant à cette stabilisation a été déterminé en utilisant le bilan de population et le modèle DLVO pour la détermination du coefficient de coagulation. Il en ressort que le nombre effectif de plaquettes participant la stabilisation des particules polymériques est supérieur au nombre permettant la saturation de la surface des particules polymériques au moment de la fin de la nucléation, mais inférieur à cette surface vers la fin de la polymérisation. Le mécanisme multicouche contribue donc à une stabilisation différente de la polymérisation en émulsion classique.

Abstract

Modeling of Pickering Emulsion Polymerization

The aim of the present project is to develop a methodology for fundamental modeling of surfactant-free emulsion polymerization processes stabilized by inorganic particles, referred to as “Pickering emulsion polymerization”. Modeling emulsion polymerization systems requires modeling the particle size distribution (PSD), which is an important end-use property of the latex. This PSD includes sub-models dedicated to particle nucleation, mass transfer between the different phases (monomer, radicals, stabilizer), and particle coagulation. These models should preferably be individually identified and validated experimentally. The first main part of the work is dedicated to the experimental study. This part can be divided in three parts. The first part describes the adsorption of inorganic particles on polymer without reaction. Multilayer adsorption was observed and B.E.T. isotherm was able to describe this adsorption. The adsorption was found to be enhanced at higher ionic strength. The adsorption dynamics were found fast and therefore clay partitioning can be considered at equilibrium during polymerization. The second part concerned the investigation of different reaction parameters on the particles number and reaction rate in *ab initio* polymerizations. The effect of mixing, initial monomer concentration and initiator concentration were considered. Optimization of these conditions was useful for the modeling part. The last part described the differences between several Laponite[®] grades through the *ab initio* emulsion polymerization of styrene. The second main part of the manuscript focused on the modeling of the Pickering emulsion polymerization. The population balance model and average number of radicals balance were adapted regarding the effect of in-

organic particles. The growth of the polymer particles was optimized by fitting the models of radicals' entry and desorption described available in literature to the experimental data. No modification was needed, which allowed us to conclude that the clay had no influence on radical exchange. However, Laponite[®] stabilization played an important role in polymer particles production. Coagulative nucleation model was able to describe the nucleation rate and predict the total number of particles.

Introduction

Pickering stabilization has recently emerged as a new method to create colloidal nanocomposite particles by adsorption of solid particles at solid-liquid interfaces. The elaboration of composite latexes allows combining attributes of inorganic solids with the processing and handling advantages of organic polymers which allows for instance to improve mechanical and water-resistance properties of films.

So far, there is no modeling studies devoted to Pickering emulsion polymerization systems, including particles sizes distribution (PSD) (while well established for conventional emulsifier-based emulsion polymerization, comprising PSD and molecular weight distribution). Though, there are fundamental differences between conventional and Pickering emulsion polymerization. First of all, the stabilization of Pickering polymerizations takes place mainly by steric repulsions between adsorbed solid particles besides probable electrostatic repulsions. The later form a rigid mechanical barrier that prevents the polymer latexes from coalescing. Second, the nucleation mechanism is different since there are no micelles and it cannot be described by homogeneous nucleation models. Finally, the presence of inorganic particles on the surface of latex particles affects radical absorption and desorption which affects particle growth. Therefore, Pickering emulsion polymerization process deserves specific modeling.

The developed methodology should be applicable to different inorganic systems. The obtained model will improve process understanding and used in control strategies in order to improve the product quality, mainly to increase the solid contents of the latex for industrial interest.

This work was funded by Agence Nationale de la Recherche grant n° ANR-12-JS09-0007-01.

Outline of the manuscript

The manuscript comprises six chapters, organized as follow:

Chapter 1 offers a short literature review of the aspect of emulsion polymerization used in this work.

Chapter 2 describes the experimental investigation of the partitioning of clay platelets in emulsion polymerization of styrene. Different analysis techniques are used: QCM-D, conductimetry and ICP-AES to obtain the adsorption isotherm of Laponite® on polystyrene

Chapter 3 deals with the experimental comparison of several Laponite® grades in the *ab initio* emulsion polymerization of styrene. The effect of Laponite® composition on the polymer stabilization is discussed.

Chapter 4 concerns the influence of process parameters on emulsion polymerization. This part is useful to validate some assumptions made in modeling.

Chapter 5 reports the influence of clay platelets on the modeling of the radical exchange during emulsion polymerization. Several entry and desorption models are discussed and use to determine the best couple to fit to the experimental data.

Chapter 6 focuses on the nucleation mechanism during emulsion polymerization. Coagulative nucleation model is adapted to experimental particle formation.

The following publications resulted from this project : **Journal publication:**

- Barthélémy Brunier, Nida Sheibat-Othman, Yves Chevalier, Elodie Bourgeat-Lami, “Partitioning of clay platelets in Pickering emulsion polymerization” is submitted to Langmuir (DOI: 10.1021/acs.langmuir.5b03576)(chapitre 2)
- Results of chapter 3, 4, 5 and 6 will be submitted soon.

Conferences and Workshops

Oral communications

- **10th European Congress of Chemical Engineering (ECCE 15)**, Nice; Barthélémy Brunier, Nida Sheibat-Othman, Yves Chevalier, Elodie Bourgeat-Lami; “Modelling of Pickering surfactant-free Emulsion Polymerization”
- **Working Party on Polymer Reaction Engineering 2013 (WPPRE 13)**, Hamburg; Barthélémy Brunier, Nida Sheibat-Othman, Yves Chevalier, Elodie Bourgeat-Lami; “Investigation of Pickering emulsion polymerization processes”
- **Working Party on Polymer Reaction Engineering 2015 (WPPRE 15)**, Munich; Barthélémy Brunier, Nida Sheibat-Othman, Yves Chevalier, Elodie Bourgeat-Lami; “Analysis of the effect of Laponite® on Radical exchange in seeded semibatch Pickering Emulsion Polymerization”
- **Journée du CODEGEPRA 2014**, Lyon; Barthélémy Brunier, Nida Sheibat-Othman, Yves Chevalier, Elodie Bourgeat-Lami; “Modélisation des procédés de polymérisation en émulsion stabilisés par des particules inorganiques (stabilisation Pickering)”

Poster communications

- **Working Party on Polymer Reaction Engineering 2013 (WPPRE 13)**, Hamburg, Barthélémy Brunier, Nida Sheibat-Othman, Yves Chevalier, Elodie Bourgeat-Lami; “Investigation of Pickering emulsion polymerization processes”
- **Journée de l’institut de chimie de Lyon 2013 (ICL)**, Lyon; Barthélémy Brunier, Nida Sheibat-Othman, Yves Chevalier, Elodie Bourgeat-Lami; “Modélisation des procédés de polymérisation en émulsion stabilisés par des particules inorganiques”
- **Frontier of Polymer Colloids (FPCOL 2014)**, Prague, Barthélémy

Brunier, Nida Sheibat-Othman, Yves Chevalier, Elodie Bourgeat-Lami; “Evaluation of Laponite[®] partitioning in Pickering emulsion polymerization”

- **Les Rencontres Scientifiques d’IFP Energies nouvelles** (NextLab 2014), IFPEN/Rueil-Malmaison; Barthélémy Brunier, Nida Sheibat-Othman, Yves Chevalier, Elodie Bourgeat-Lami; “Evaluation of Laponite[®] partitioning in Pickering emulsion polymerization”
- **Working Party on Polymer Reaction Engineering 2015** (WPPRE 15), Munich, Barthélémy Brunier, Nida Sheibat-Othman, Yves Chevalier, Elodie Bourgeat-Lami; “Evaluation of Laponite[®] partitioning in Pickering emulsion polymerization”
- **Polymer Reaction Engineering 2016** (PRE 16), Hambourg, Barthélémy Brunier, Nida Sheibat-Othman, Yves Chevalier, Elodie Bourgeat-Lami; “Modelling Pickering Emulsion Polymerization”
- **11th Workshop on Polymer Reaction Engineering** (PRE 16), Hambourg, Barthélémy Brunier, Nida Sheibat-Othman, Yves Chevalier, Elodie Bourgeat-Lami; “Modelling Pickering Emulsion Polymerization”

Contents

Remerciements	iii
Résumé	v
Abstract	xi
Introduction	xiii
Nomenclature	xxiii
I Literature review	1
1 Fundamentals of Emulsion Polymerization	3
1.1 Introduction	3
1.2 Fundamentals of Polymerization	3
1.2.1 Polymerization reaction	4
1.2.2 Process description	6
1.3 Fundamentals of Emulsion Polymerization	7
1.3.1 Description	7
1.3.2 Nucleation mechanism	9
1.4 Pickering Emulsion polymerization	11
1.4.1 State of art	11
1.4.2 Laponite [®]	14
1.5 Difference with classical emulsion polymerization	17
1.5.1 Pickering Emulsion Polymerization with Laponite [®]	17

II	Experimental study of Pickering emulsion polymerization of styrene	23
2	Partitioning of clays platelets in Pickering emulsion polymerization	25
2.1	Introduction	28
2.2	Materials and Methods	29
2.2.1	Materials	29
2.2.2	Laponite RDS	29
2.2.3	Laponite dispersion in water	29
2.2.4	Reactor set-up and operation	30
2.2.5	Preparation of clay-armored polystyrene seed particles at 20 wt% solids content	31
2.2.6	Seeded Polymerizations	31
2.2.7	<i>Ab initio</i> experiments	32
2.2.8	Characterization of the particle size	32
2.2.9	Transmission Electron Microscopy (TEM)	33
2.2.10	Surfactant-free polystyrene seed particles	33
2.2.11	Conductivity measurements	33
2.2.12	Inductively Coupled Plasma - Atomic Emission Spectroscopy (ICP-AES)	34
2.2.13	Quartz Crystal Microbalance (QCM-D)	34
2.3	Results and Discussion	35
2.3.1	Investigation of the role of clay in emulsion polymerization	35
2.3.2	Adsorption of Laponite on surfactant-free polystyrene latex particles	40
2.4	Conclusions	54
2.5	Supporting Information	56
3	Laponite comparison in Pickering emulsion polymerization of styrene	61
3.1	Introduction	62

3.2	Materials and Methods	63
3.2.1	Materials	63
3.2.2	Laponite [®] dispersion in water	64
3.2.3	<i>Ab initio</i> Polymerizations	64
3.2.4	Surfactant-free polystyrene seed latex	64
3.3	Results and discussion	65
3.3.1	Investigation of clay adsorption on polystyrene	65
3.3.2	Investigation of the role of clay in <i>ab initio</i> emulsion polymerization	66
3.4	Conclusion	74
4	Preliminary experimental observations	77
4.1	Introduction	78
4.2	Materials and Methods	78
4.3	Results and discussion	79
4.3.1	Effect of mixing	79
4.3.2	Effect of initial concentration of monomer in the bulk medium	81
4.3.3	Effect of initial concentration of initiator	83
4.3.4	Effect of monomer flowrate	85
4.3.5	Investigation of radical diffusion limitations	88
4.4	Conclusion	90
III	Modeling of Pickering Emulsion Polymerization	91
5	Effect of Pickering stabilization on radical exchange in emulsion polymerization	93
5.1	Introduction	95
5.2	Materials and Methods	98
5.3	Modelling	98
5.3.1	Polymer particles population balance	98
5.3.2	Average number of radicals in the particles	99

5.3.3	Aqueous phase reactions	102
5.3.4	Monomeric radicals	105
5.3.5	Monomer balance	106
5.3.6	Clay partitioning	106
5.4	Investigation of radical entry and desorption models	107
5.4.1	Radical entry	107
5.4.2	Radical desorption models	114
5.5	Pickering emulsion polymerization (interval II)	125
5.5.1	Experimental observations	125
5.5.2	Capture/desorption models for Pickering emulsion polymer- ization	128
5.5.3	Effect of clay concentration	130
5.5.4	Comparison to conventional SDS stabilization	132
5.6	Conclusions	132
6	Modeling of nucleation and coagulation in Pickering emulsion poly- merization	133
6.1	Introduction	135
6.2	Materials and Methods	136
6.2.1	Hamaker constant measurement	137
6.3	Modeling	137
6.3.1	Polymer particles population balances	137
6.3.2	Homogeneous nucleation mechanism	139
6.3.3	Particle coagulation	139
6.3.4	Radical, monomer and surfactant balances in the different phases	144
6.4	Results and discussion	146
6.4.1	Experimental observations	146
6.4.2	Modeling	152
6.4.3	Effective number of platelets contributing to surface charge	156
6.5	Conclusion	157

IV	Conclusion	161
A	Transition from interval II to interval III in emulsion polymerization	165
A.1	Introduction	167
A.2	Materials and methods	168
A.2.1	Materials	168
A.2.2	Ab initio semi-continuous polymerization experiments	168
A.3	Modeling	169
A.3.1	Polymer particles population balances	169
A.3.2	Radical exchange	169
A.3.3	Diffusion limitation	170
A.4	Results and discussion	171
A.4.1	Experimental observations	171
A.4.2	Modelling intervals II and III	175
A.5	Conclusion	181
B	Modelling of Emulsion Polymerization	185
B.1	Initiator balance	185
B.2	Monomer balance	185
B.2.1	Total monomer balance	185
B.2.2	Monomer partitioning	186
	Bibliography	191

Nomenclature

Greek letters

α	the parameter used in the diffusion controlled desorption mechanism	-
β	the parameter used in the diffusion controlled desorption mechanism	-
Δm	the mass of adsorbed material in QCM-D	$ng\ cm^{-2}$
δ_h	the thickness of the hairy layer	dm
δ_p	the thickness of the diffusion layer in the polymer phase	dm
δ_s	the Stern layer	dm
δ_w	the thickness of the stagnant layer in the aqueous phase	dm
ϵ_0	the vacuum permittivity	$F\ dm^{-1}$
ϵ_r	the water relative permittivity	-
η	the viscosity of the medium	$Pa\ s$
η_{exp}	the experimental viscosity	$mPa\ s$
η_{ref}	the viscosity of a reference	$mPa\ s$
κ	the Debye length	dm
μ	the shear modulus	$N\ m^{-2}$
Φ_A	the attractive potential	J

Φ_R	the repulsive potential	J
Φ_T	the total potential between two particles	J
Ψ	the surface potential	V
ψ	the zeta potential	V
ρ_c	the density of clay platelet	$g \text{ dm}^{-3}$
ρ_q	the quartz density	$g \text{ cm}^{-3}$
σ_0	the surface charge of one clay platelet	$C \text{ dm}^{-2}$
σ_T	the total surface charge	$C \text{ dm}^{-2}$
σ_{corr}	the rescaled conductivity	$mS \text{ cm}^{-1}$
σ_{exp}	the experimental conductivity	$mS \text{ cm}^{-1}$
σ_I	the initiator surface charge	$C \text{ dm}^{-2}$
σ_{stab}	the inorganic particles surface charge	$C \text{ dm}^{-2}$
ζ	the zeta potential of the polymer particle	V

Roman letters

$[\dot{T}]_w$	the total concentration of radicals in the aqueous phase	$mol \text{ dm}^{-3}$
$[E_i^\bullet]_w$	the concentration of desorbed radicals of size i in the aqueous phase	$mol \text{ dm}^{-3}$
$[IM_i^\bullet]_w$	the concentration of radicals of size i in the aqueous phase	$mol \text{ dm}^{-3}$
$[M_i^\bullet]_w$	the concentration of radicals of size i in the polymer particles	$mol \text{ dm}^{-3}$
\mathcal{G}	the growth rate of particle	$dm \text{ s}^{-1}$
\bar{n}	the average number of radicals per particle	-
\mathfrak{R}^+	the formation rate of particles by coagulation	$part \text{ s}^{-1} \text{ dm}^{-3}$

\mathfrak{R}^-	the depletion rate of particles by coagulation	$part\ s^{-1}\ dm^{-3}$
\mathfrak{R}_n	the nucleation rate	$part\ s^{-1}\ dm^{-3}$
\mathfrak{R}_{coag}	the coagulation rate	$part\ s^{-1}\ dm^{-3}$
\mathfrak{R}_{hom}	the homogeneous nucleation rate	$part\ s^{-1}\ dm^{-3}$
A	the Hamaker constant	J
A_{tot}	the total surface of polymer particles	dm^2
B	the coagulation rate coefficient	$dm^{-1}\ s^{-1}$
C	the mass sensitivity constant	$ng\ cm^{-2}\ Hz^{-1}$
c	the BET constant	-
C_s	the concentration at saturation of the solute in B.E.T. adsorption model	$mg\ L^{-1}$
$C_{e,i}$	the electrolyte concentration of ionic species i	$mol\ dm^{-3}$
C_{eq}	the equilibrium solution concentration	$g\ L^{-1}$
CCC	the critical coagulation concentration	$mol\ dm^{-3}$
CMC	the critical micellar concentration	$mol\ dm^{-3}$
D_h	the radical diffusion coefficient in the hairy layer	$dm^2\ s^{-1}$
D_p	the radical diffusion coefficient in the particle	$dm^2\ s^{-1}$
d_p	the diameter of a polymer particle	dm
D_w	the radical diffusion coefficient of in water	$dm^2\ s^{-1}$
E_1	the heat of adsorption for the first clay layer	$J\ mol^{-1}$
E_N	the heat of adsorption for the second and higher clay layers	$J\ mol^{-1}$
E_{des}	the activation energy of desorption	J

$f(v, t)$	the volume distribution of particle size	$part\ dm^{-3}\ dm^{-3}$
f_0	the intrinsic crystal frequency	Hz
f_c	the resonance frequency	Hz
f_e	the frequency at which monomeric radicals may exit	s^{-1}
F_i	the ionic force	$mol\ dm^{-3}$
f_I	the efficiency factor of initiator decomposition	—
F_m	the monomer flowrate	$mol\ s^{-1}$
f_p	the efficiency factor of radical capture	-
h_c	the thickness of one clay platelet	dm
I	the number of mole of initiator at any time	mol
I_0	the initial number of mole of initiator	mol
j_{crit}	the critical size	-
k_0	equilibrium radical desorption parameter	s^{-1}
k_b	the Boltzman constant	$J\ K^{-1}$
k_e	the radical entry coefficient	$dm^3\ mol^{-1}\ s^{-1}$
k_I	the decomposition coefficient of initiator	s^{-1}
K_L	the adsorption equilibrium constant of upper clay layers	$L\ g^{-1}$
k_p	the propagation rate constant	$dm^3\ mol^{-1}\ s^{-1}$
K_S	the adsorption equilibrium constant of the 1st clay layer	$L\ g^{-1}$
k_{des}	the coefficient of radical desorption	s^{-1}
k_{fm}	the radical transfert to monomer rate coefficient	$dm^3\ mol^{-1}\ s^{-1}$
k_{p1}	the propagation rate coefficient of the oligoradical of size 1	$dm^3\ mol^{-1}\ s^{-1}$

k_{p2}	the propagation rate coefficient of the oligoradical of size 2	$dm^3 mol^{-1} s^{-1}$
k_{tp}	the radical termination rate coefficient in the particle	$dm^3 mol^{-1} s^{-1}$
k_{tw}	the radical termination rate coefficient in water	$dm^3 mol^{-1} s^{-1}$
L	the edge to edge distance between particles	dm
m	the partition coefficient of the radicals between the polymer particles and the aqueous phase	—
m_c	the mass of clay introduced	g
$n(r, t)$	the number of particles of diameter between r and Δr	$part dm^{-1}$
N	the number of monomer-swollen polymer particles per unit volume of water	$part dm^{-3}$
$n(r, t)$	the radius distribution of particle size	$part dm^{-1} dm^{-3}$
N_A	the Avogadro's number	mol^{-1}
N_c	the number of clay platelets introduced	$part$
N_c^{eff}	the effective number of platelets contributing to the charge	$part$
N_m	the number of moles of free monomer in the reactor	mol
n_o	the overtone number in Sauerbrey equation	—
P	the probability of the radical to escape the particle before undergoing other reaction	—
q	the surface density of adsorbed species	$mg m^{-2}$
q_m	the surface density of adsorbed species for a hypothetical monolayer	$mg m^{-2}$
q_c	the clay platelets charge	C
R	the center to center interparticle distance	dm
r	the radius of a polymer particle	dm

r_c	the radius of one clay platelet	dm
r_{nuc}	the nucleation radius	dm
R_{pp}	the reaction rate in the polymer particles	$mol\ s^{-1}\ dm^{-3}$
R_{pw}	the reaction rate in the aqueous phase	$mol\ s^{-1}\ dm^{-3}$
S_c	the surface of the face of a clay platelet	dm^2
S_{Lap}	the surfac of one face of clay platelet	dm^2
SC	the solid content	%
T	the temperature	K
v	the volume of a polymer particle	dm^3
V_p	the total volume of polymer	dm^3
V_w	the total volume of the aqueous phase	dm^3
W	the stability ratio	dm^{-1}
x	the ratio of the partial pressure of the adsorbate to its saturation partial pressure at the system temperature	-
z_+	the valence of a cation	-
z_i	the valence of ionic species i	-
$[I]$	the initiator concentration in water	$mol\ dm^{-3}$
$[I_0]$	the initial concentration of initiator in water	$mol\ dm^{-3}$
$[IM]_{j_{crit}}$	the concentration of radical with the critical size	$mol\ dm^{-3}$
$[M]_p$	the monomer concentration in the monomer-swollen polymer particles	$mol\ dm^{-3}$

Part I

Literature review

Chapter 1

Fundamentals of Emulsion Polymerization

*“ Real knowledge is to know the
extent of one’s ignorance. ”*

Confucius - Chinese Philosopher

1.1 Introduction

In this chapter, we briefly describe polymerization processes, as well as the various mechanisms in the emulsion polymerization.

1.2 Fundamentals of Polymerization

A polymer is a set of the same chemical nature macromolecules formed by the covalent bond by association of many smaller molecules, called monomers. A polymer may be of natural origin, obtained by modifying a natural polymer or entirely chemically synthesized by polymerization reaction. The molecular structure of a polymer is homopolymer when it results from the polymerization of a single monomer, and copolymer when the reaction involves more than one type of monomer [Kiparissides, 1996].

1.2.1 Polymerization reaction

The kinetic mechanisms used in the polymerization can be divided into two categories depending on the growth process of the polymer:

- The step-growth and polycondensation are based on successive reactions in which bi-functional or multifunctional monomers react to form first dimers, then trimers, longer oligomers and eventually long chain polymers. Polyamides, polyesters, silicones, and polyurethanes are the polymers obtained by polycondensation.
- The chain-growth polymerization and polyaddition correspond to a reaction resulting in the sequential addition of monomer molecules in an active center. In the case of radical polymerization, free radicals are responsible of the formation of active centers. Chain reactions have three major stages: initiation leading to the formation of active centers, the propagation where the polymer grow by monomer radicals addition and termination when the free radicals combine and it is the end of the polymerization of the chain.

The polymerization processes are not only dependent on the reaction kinetics mechanisms but also the reaction process must be considered. Polymerization processes can be at first divided in two category, homogeneous polymerization and the heterogeneous polymerization. In homogeneous polymerization, as the name suggests, all the reactants are soluble in the solvent and compatible with the resulting polymer. In the heterogeneous polymerization systems, the monomer and the polymer are insoluble in the solvent. Homogeneous polymerization comprises bulk (or mass) polymerization or solution systems while heterogeneous reactions may be categorized as bulk, solution suspension precipitation, emulsion, gas phase and interfacial polymerization.

1.2.1.1 Emulsion polymerization

The emulsion polymerization is a quite important process used in the industrie of polymer. The annual production of polymer by emulsion polymerization is around

twenty thousand tons which represents around 10% of the total polymer production. Polymers produced by emulsion polymerization can be divided into three rough categories : the synthetic rubber, the plastics and the dispersion. Many of these polymers were used in every day life like polybutadiene (synthetic rubber) in tires, polystyrene (plastic) in plastic cups or polyacrylic (dispersion) in the acrylic paints. The process of emulsion polymerization is described below.

The term emulsion polymerization and mini-emulsion polymerization can lead to confusion in the literature. An emulsion is defined as a dispersion of droplets of a liquid phase (for example oil) into a continuous liquid phase (for example water). When the oil droplets is a monomer it can be polymerized, but it's not an emulsion polymerization. This heterogeneous polymerization process whereby droplets containing monomer are converted into polymer particles is referred to as a suspension or miniemulsion polymerization. In contrast, the nucleation locus in an emulsion polymerization process is the water phase. New particles are newly formed in the reaction mixture upon initiation in the water phase. Particle formation is generally confined to the initial stages of the emulsion polymerization process, and occurs through either micellar or homogeneous nucleation. The monomer droplets can be seen as temporary storage containers for excess amount of monomer and serve to compensate monomer consumption in the growing particles. The main reaction locus is therefore the polymer particles. The final dispersion of polymer particles in the continuous phase (water) is also known as polymer latex.

One may ask oneself why the monomer droplets do not polymerize into polymer beads in an emulsion polymerization. The answer lies in the probability of a growing radicals oligomer in the water phase entering in a monomer droplet. Indeed the total surface area of the monomer droplet is low in comparison to the combined surface area of micelles or the polymer latex particles. One could increase the probability of entry of radicals into the monomer droplets by decreasing the size of the droplets (to sub-micron diameter), thereby shifting the locus of polymerization into the monomer droplets. Therefore reaction mechanism moved to a miniemulsion process.

The “conventional” polymerization mechanism can be resumed as follow. A

colloidal dispersion of monomer is converted by free-radical chain polymerization in a stable dispersion of polymer particles. At first, an emulsion comprising the dispersing medium, monomer, and a surfactant is mixed in the reactor. Excess of surfactants forms micelles in aqueous phase. A small portion of the monomer is dissolved in the aqueous phase, but the monomer remains mostly in the droplets. A water soluble initiator is added and the reaction starts. Monomers are transformed in polymer by propagation reaction in the water phase. The oligoradicals formed can enter in a micelle or continue to react in water. After a certain size (critical size), oligoradicals precipitate in water. These precipitated radicals are stabilized by surfactant, this lead to the formation of a primary waterborne particle. Therefore the polymerization does not take place in the monomer droplets, but in micelles or in the aqueous phase. These new formed particles are saturated in monomer which is converted with the presence of radicals. The particles growth and reaction ends when no more monomer is present in the medium. The low viscosity of the reaction medium helps controlling the reactor temperature. The high polymerization rate and conversion rate of nearly 100% are part of the advantageous characteristics of the emulsion polymerization in view of other methods, and are due to the radical compartmentalisation.

1.2.2 Process description

In our study, it is question of two types of synthetisize methods: batch and semi-continuous processes. Note that most emulsion polymerization industrial processes are done by these methods.

1.2.2.1 Batch process

A typical batch reactor consists of a tank with an agitator and integral heating/cooling system. These vessels may vary in size from less than 1 liter to more than 15 000 liters. All reagents are charged into the reactor at the outset. In industry, the advantages of the batch reactor lie with its versatility. A single vessel can carry out a sequence of different operations without the need to change the setup.

This is particularly useful when processing toxic or highly potent compounds. But many difficulties are associated to this process; the mixture homogenization and heat transfer are only provided by the agitation and the heat transfer at the interface with jacket. This leads to a non-homogeneous mixture. Baffles can be added to enhance the mixing. But mixing in large batch reactors is constrained by the amount of energy that can be applied. Fast temperature control response and uniform jacket heating is often required in some reaction process but it has to be recognized that large batch reactors with external cooling jackets have severe heat transfer constraints by virtue of design. It is necessary to well control the cooling of the reaction to avoid the uncontrolled heat runaway.

1.2.2.2 Semi-continuous process

Semi-continuous process is similar to the batch process, the main difference lies in the fact that reagents are introduced continuously in the reactor. Semi-continuous operations are those that can be characterized by batch process that run continuously with periodic start-ups and shutdowns. An addition over time allows better control of the reaction in term of final properties of the product or heat transfer control. Moreover, in case of thermic runaway, addition of reagents can be stopped, reaction will end rapidly. In emulsion polymerization, addition of monomer or sometimes surfactant, water and initiator can be done by semi-continuous process.

1.3 Fundamentals of Emulsion Polymerization

1.3.1 Description

The emulsion polymerization mechanism is based on the representation of Harkins [Harkins, 1947]. According to this theory, three intervals can be distinguished [Fortuny Heredia, 2002]:

1.3.1.1 Interval I

The system is composed of monomer droplets which are stabilized by the surfactant, an aqueous phase in which are found the surfactant, monomer, free surfactants

and surfactant micelles. The initiator also present in the aqueous phase allows the initiation and formation of new particles. The nucleation occurs according to different mechanisms described below, and the number of particles increases with a substantial rate of reaction. The free surfactant in aqueous phase and the micelles are consumed to stabilize the particles. Interval I ends when the number of particle remains constant and often coincides with the disappearance of the micelles in the aqueous phase in the conventional emulsion polymerization.

1.3.1.2 Interval II

The surfactant is primarily adsorbed to the particles' surface, but is solubilized in the aqueous phase and adsorbed on the monomer droplets. The particles are swollen with monomer, the monomer is continuously transferred from droplets to polymer particles by diffusion through the aqueous phase. Monomer concentrations in the aqueous phase and the particles are in saturation. Interval II is complete when the monomer droplets have disappeared and monomer concentration in the particle is not at the saturation.

1.3.1.3 Interval III

The medium contains no more droplet, only polymer particles are in the reactor. The monomer concentration in the particles decreases until total conversion. The decrease of monomer concentration in the polymer particles leads to a decrease in the mobility of radicals in the polymer particles which may affect radical termination capture and desorption. At high viscosities, this may cause an auto-acceleration of the reaction. This auto-acceleration (Gel Effect or Trommsdorff-Norrish Effect) is a dangerous reaction behavior. It is due to the localized increase in viscosity of the polymerizing system that slow termination reactions between huge oligomer. The small monomer molecules present in the particle are less affected by the increase of viscosity so the propagation rate coefficient stays constant. This causes an increase in the the overall reaction rate, leading to a high increase in temperature and a possible reaction runaway.

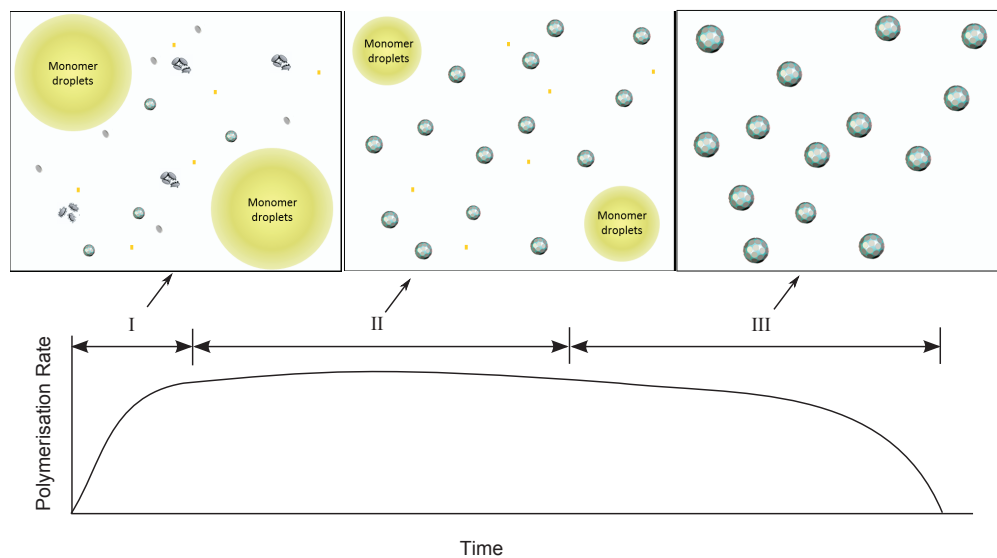


Figure 1.1: Three intervals with the dependence of polymerization rate in emulsion polymerization

Figure 1.1 illustrates the evolution of emulsion polymerization rate during these three intervals. The kinetic curve contains three stage relating to the three intervals: a relatively short stage I, characterized by the growing polymerization rate, stage II of a constant rate of the process, and stage III, where the polymerization rate decreases.

1.3.2 Nucleation mechanism

Nucleation is one of the most important phenomena in emulsion polymerization. The formation of the first particles is fast and takes place according to different mechanisms presented below. The experimental study of nucleation is difficult because there are technical limitations, such as the measurement of particle size.

1.3.2.1 Micellar nucleation

The basics of micellar nucleation mechanism were given by Harkins [Harkins, 1945]. It applies to cases where the free surfactant concentration in the aqueous phase is greater than the critical micelle concentration (CMC). The critical micellar concen-

tration (CMC) is defined as the concentration of surfactants above which micelles form and all additional surfactants added to the system go to micelles.

Upon introduction of surfactants into the system, they will initially partition into the interface, reducing the system free energy by lowering the energy of the interface and removing the hydrophobic parts of the surfactant from contact with water. Subsequently, when the surface coverage by the surfactants increases, the surface free energy decreases and the surfactants start aggregating into micelles, thus again decreasing the system's free energy by decreasing the contact area of hydrophobic parts of the surfactant with water. Upon reaching CMC, any further addition of surfactants will just increase the number of micelles. In emulsion polymerization, surfactant molecules stabilize the droplets reservoir or are free in the aqueous phase. Upon the CMC free surfactants form micelles; these micelles are swollen by monomer.

On the other hand, radicals from the initiator decomposition react with the monomer and form oligoradicals. Growing oligomers migrate into the swollen micelles. Capturing oligoradicals by reservoir droplets is negligible due to their low surface area compared to that of micelles. Each entry of a radical to a monomer swollen micelles leads to a nucleation event. Micelles become particles and these particles continue to grow. Micelles which did not capture radicals of the period during nucleation are emptied of their monomer and surfactant to feed their growing particles. The micellar nucleation is completed when the free surfactant concentration in the aqueous phase is less than the CMC

This mechanism applies to the polymerization of hydrophobic monomers such as chloroprene, 1,3-butadiene or certain acrylates, whose solubility in water varies from 0.34 to 15 $mmol L^{-1}$ at 25°C [Vanderhoff, 1993]. The solubility of the styrene is, for example, of the order of 0.4 $g L^{-1}$ in water at 50°C .

1.3.2.2 Homogeneous nucleation

This mechanism studied by Roe, Fitch and Tsai, Ugelstad and Hansen [Fitch and Tsai, 1971] [Hansen and Ugelstad, 1978a] is admitted in the case of polymerization in the absence of surfactant, or present at a concentration below its

CMC. The radicals resulting from the decomposition of the initiator propagate in the aqueous phase by addition of monomer molecules dissolved in the continuous phase. They grow until they reach limit value constituent unit. This limit depends on the nature of the monomer; it is 5 in the case of styrene. If the oligoradicals may not enter into a micelle or particle until this limit, they are no longer soluble in the aqueous phase and precipitate. Precipitation of oligomers leads to the formation of primary nanoparticles. Their growth is achieved by swelling of the monomer or by coagulation with other nuclei. The stabilization of the latex particles is mainly ensured by the presence of charged oligoradicals and free surfactant or inorganic particles.

1.3.2.3 Coagulative nucleation

The coagulative nucleation drawn from the work of Gilbert et al. [Feeney et al., 1984] based on two steps. First the precursor particles are formed by micellar or homogeneous nucleation mechanism. The growth of these nuclei is carried by a small quantity of monomer swelling due to their low colloidal stability. The surface charge density required to stabilize these small species is very important, the primary particles are therefore unstable. The particles tend towards reducing the surface area to promote their stability by increasing the surface charge density. So in a second step, these primary particles coagulate with each other and / or on the particles already present. This leads to the formation of mature particles, more stable. These can grow by swelling monomer or capture of other nuclei. Unlike the two other mechanisms, the nucleation step is long and is responsible for a large size polydispersity of the latex particles during this step.

1.4 Pickering Emulsion polymerization

1.4.1 State of art

Nanotechnology has grown to become an important area of research with tremendous scientific and economic potential, including microprocessor and biotechnology industries, allowing the synthesis of nanomaterials with great control regarding their

structures, functions and compositions; e.g. organic/inorganic, polymeric, or biological, providing these materials with electro-mechanical and thermo-mechanical properties. Among the various technologies, manufacturing composite polymer materials including inorganic compounds allows improving end-use properties, such as stiffness and toughness, barrier properties, resistance to fire and ignition or optical properties, while reducing their cost. In this perspective, different kinds of inorganic materials have been used with different structures, including silica, iron oxides, titanium dioxide, metals, and clays [Sill et al., 2009] (see table 1.1).

Anisotropic particles such as clay platelets, carbon nanotubes, gold nanorods or semi-conductor nanowires have raised special interest over the last two decades due to their high aspect ratio resulting in enhanced overall performances [Alexandre and Dubois, 2000]. Anisotropic particles such as clay platelets, carbon nanotubes, gold nanorods or semi-conductor nanowires have raised special interest over the last two decades due to their high aspect ratio resulting in enhanced overall performances [Alexandre and Dubois, 2000]. Layered silicates commonly involved in nanocomposite synthesis belong to the structural family of the 2:1 phyllosilicates (usually from the smectite group) and have a sheet-like structure that consists of silica tetrahedral bonded to alumina or magnesia tetrahedral in a number of ways. Among them, Montmorillonite (MMT) and Laponite[®] (synthetic hectorite clay) are by far the most frequently used as inert modifiers and film-forming agents with attractive rheological properties [Bon and Colver, 2007]. Their lamellar structure consists of two dimensional platelets with a central layer made of $M_{2-3}(O)_6$ octahedra (M being either a divalent or a trivalent metal), sandwiched between two external layers of $Si(O, OH)_4$ tetrahedra. Laponite[®] and MMT are similar in structure and thickness (1 nm), but the diameter of Laponite[®] (30 nm) is smaller than that of MMT (0.1 – 1 μ m). Therefore Laponite[®] clay can be easily exfoliated and dispersed in water as a colloidal suspension, making it particularly interesting for the stabilization of emulsions [Bon and Colver, 2007] or latex particles [Sheibat-Othman et al., 2011]. Laponite and MTT also differ in the nature of the interlayer metal which is Mg for Laponite[®] and Al for MMT. Polymer/clay nanocomposites can be manufactured by various processes including

Table 1.1: Chemical composition for the four Laponite[®] grades

Inorganique Particle	Monomer	Reference	
Oxydes	SiO_2	[P(2-VP)]	[Dupin et al., 2007]
		PMMA	[Colver et al., 2008]
		PSTy PBuA	[Schmid et al., 2009]
	TiO_2	PSTy	[Sheibat-Othman and Bourgeat-Lami, 2009]
		PSTy	[Song et al., 2009]
		PSTy	[Zhao et al., 2010]
		PSTy, AA, AAm	[Schrade et al., 2011]
	Al_2O_3	PSTy	[Lu and Larock, 2007]
	Fe_2O_3	PSTy	[Yin et al., 2012]
		PSTy	[Kim et al., 2013]
ZnO	PSTy	[Chen et al., 2008]	
Graphen	GO	PSTy	[Thickett and Zetterlund, 2013]
		PSTy	[Yin et al., 2013]
Metal	Au	PSTy	[Tang et al., 2014]
Aluminosilicates	Montmorillonite	PMMA	[Choi et al., 2001]
		PMMA	[Lin et al., 2006]
		PSTy	[Sheibat-Othman et al., 2011]
	Laponite	Psty-BuA	[Bourgeat-Lami et al., 2010]
		PSTy	[Sheibat-Othman et al., 2011]

heterocoagulation [Xu et al., 2005] of the clay and the polymer particles, melt intercalation [Sherman and Ford, 2005] [Caruso et al., 2001], polymer intercalation from solution, exfoliation / adsorption, and covalent modification followed by in situ polymerization (bulk, solution and dispersion) [Sun et al., 2004]. Quite recently, waterborne polymer / clay nanocomposites elaborated by in situ free radical emulsion [Sheibat-Othman et al., 2011] or miniemulsion [Bon and Colver, 2007] have emerged. These processes are cheap and environmentally attractive because they do not involve organic solvent and the final products are easy to manipulate due to their low viscosity. In such systems, the production of composite materials implies the reaction of organic monomers in the presence of inorganic colloidal particles [Bourgeat-Lami et al., 2010]. Emulsion polymerization has been first carried out by keeping the surfactant and adding chemically-modified Laponite[®] as a supplementary additive [Ruggerone et al., 2009a] [Ruggerone et al., 2009b] [Herrera et al., 2004] [Negrete-Herrera et al., 2006a] [Herrera et al., 2005] [Herrera et al., 2006] [Negrete-Herrera et al., 2007] [Negrete-Herrera et al., 2006b]. Such functionalized Laponite[®] was coated with either cationic initiators or monomers through ion exchange, or by the reaction of the edge-hydroxyls with suitable organosilane molecules. Stable colloidal aqueous suspensions of composite particles with diameters in the range 50-150 nm were obtained consisting of a polymer core surrounded by an outer shell of clay platelets. It has been subsequently shown that bare (non-modified) Laponite[®] particles could be used in emulsion polymerization without addition of surfactant [Bourgeat-Lami et al., 2007] [Aranda and Ruiz-Hitzky, 1994]. The advantage of using Laponite[®] is due to its uniform shape and smaller diameter, which makes it more attractive in stabilizing emulsions than other bigger clays such as Montmorillonite (MMT). In such surfactant-free heterophase polymerizations known as “Pickering emulsion polymerization”, the adsorbed clay platelets stabilize the dispersion of polymer particles. It is therefore worth investigating to evaluate the partitioning of the platelets on the polymer and the effect of the clay on the reaction rate and polymer properties.

1.4.2 Laponite[®]

Laponite[®] is an entirely synthetic layered silicate developed by Laporte industries between 1965 and 1970 with a structure and composition closely resembling the natural clay mineral hectorite. Now it is a registered trademark of BYK additives Ltd. During the synthesis process, salts of sodium magnesium and lithium are combined with sodium silicate at well controlled rates and temperature. This process gives an amorphous precipitate which is submitted to a high temperature treatment for a partial crystallization. The final product is then filtered, washed, dried and milled, having the appearance of a very fine white powder [technical bulletin, 2003]. The crystalline structure of Laponite[®] unit cell is composed by six octahedral magnesium ions sandwiched between two layers of four tetrahedral silicon atoms. These groups are balanced by twenty oxygen atoms and four hydroxyl groups. The idealized structure shown in Fig. 1.2 is composed of six divalent magnesium ions (Mg^{2+}) in the octahedral layer to give a positive charge of +12 e, where e denotes the elementary charge. However, some magnesium ions are substituted by monovalent cations such as lithium (Li^+) and some positions are empty obtaining a negative charge of -0.7 e in the whole unit cell. During manufacturing process this negative charge is neutralized by the addition of sodium ions (Na^+) that adsorb onto the surfaces of the crystals. The sodium ions are shared by adjacent crystals that are consequently held together in form of stacks schematically shown (facing the rims) in figure 1.3 a. The energy compensation originated by sodium ions is done according to the following molecular formula: $Na_{0.7}^+[(Si_8Mg_{5.5}Li_{0.3})O_{20}(OH)_4]^{0.7-}$

When dispersed in aqueous solvent the sodium ions release from the crystal interlayers (see figure 1.3 b), leading to a homogeneous negative charge on the faces, while a protonation process of the hydroxide groups localized where the crystal structure terminates, originates a positive charge on the rim [Tawari et al., 2001].

Laponites[®] used in this work contain the peptizing agent tetrasodium pyrophosphate (around 10 wt%) adsorbed onto the positively charged rims (edges); the tetravalent negatively charged pyrophosphate ions neutralize the rim charge and decrease electrostatic attractions between the positively charged rims and the neg-

atively charged faces, and therefore avoid gelation. Reducing such interactions contributes to a longer stability of the dispersions in water. Note that low molar mass polyethylene oxide (PEO) molecules have also been reported to delay Laponite[®] aggregation by forming a steric barrier preventing contact between platelets [Mongondry et al., 2004].

Therefore Laponite[®] in aqueous solvent forms a colloidal dispersion of charged disc-like particles with a diameter of 25 nm and a thickness of 1 nm with negative and positive charges distributed on the faces and rims respectively [Tawari et al., 2001]. The thickness of each Laponite[®] disc corresponds to the height of the crystal unit cell shown in figure 1.2.

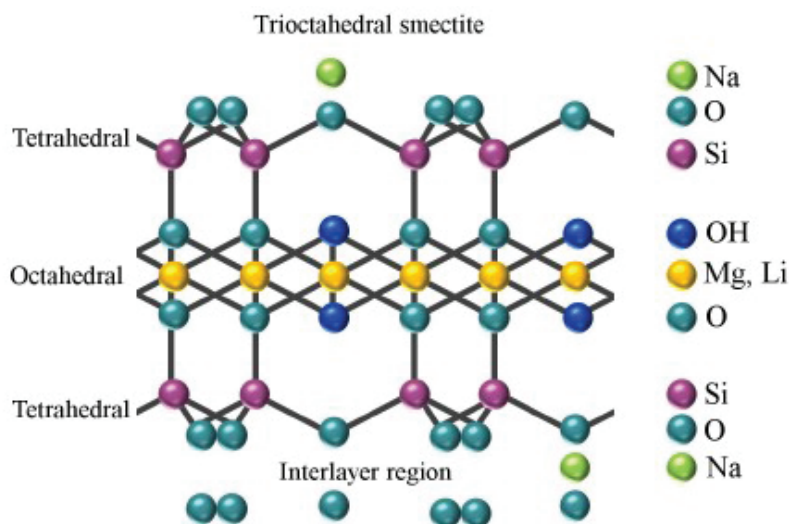
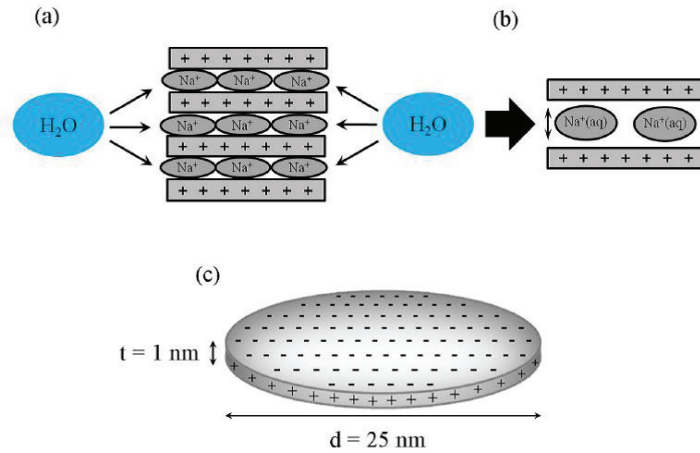


Figure 1.2: Laponite[®] crystal

Laponite[®] dispersions are generally considered as monodisperse suspensions of discs shown in Fig. 1.3. However, Balnois and coauthors by using Atomic Force Microscopy in a very diluted deposition of Laponite[®] (without peptizing agent) solution on mica have found a small polydispersity both in radius and height [Balnois et al., 2003]. Laponite[®] particles appear as ellipses with height of 1 nm and both major and minor radius of 24.0 ± 6.9 nm and 16.8 ± 4.9 nm respectively.

Laponite[®] interaction potential is characterized by an isotropic van der Waals attraction and an anisotropic electrostatic interaction, which can be either repulsive

Figure 1.3: Laponite[®] powder description

(face-face, rim-rim) or attractive (rim-face). Since sodium counter-ions Na^+ are dispersed in the solution, the negative charged faces of the particles are screened by them forming an electrical double layer composed by a Stern and a diffuse layer.

1.5 Difference with classical emulsion polymerization

Using Laponite brings some fundamental changes in reaction mechanisms of emulsion polymerization. It's necessary to identify the difference between conventional and Pickering emulsion polymerization to adjust the "well-known" model of conventional emulsion polymerization to Pickering emulsion polymerization. First of all, the stabilization of Pickering polymerizations takes place mainly by steric repulsions between adsorbed solid particles besides probable electrostatic repulsions. The later form a rigid mechanical barrier that prevents the polymer latexes from coalescing. Second, the nucleation mechanism is different since there are no micelles and it cannot be described by homogeneous nucleation models. Finally, the presence of inorganic particles on the surface of latex particles affects radical absorption and desorption which affects particle growth.

1.5.1 Pickering Emulsion Polymerization with Laponite[®]

The case of a water soluble initiator will be used. The emulsion polymerization mechanism is based on the representation of Harkins [Harkins, 1947] represented in the following diagram.

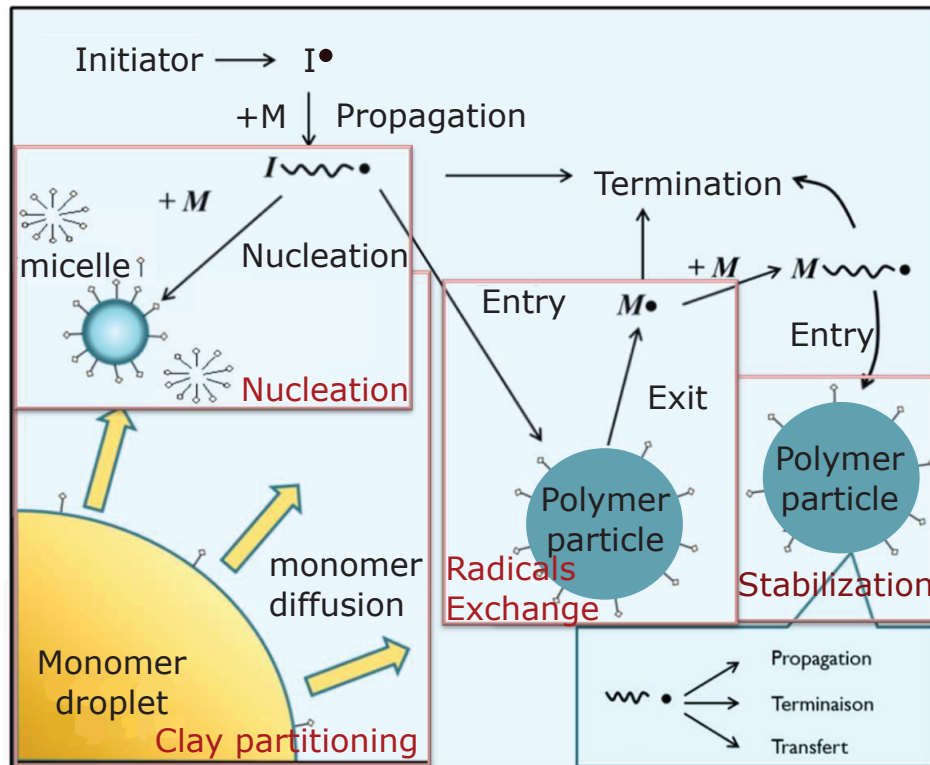


Figure 1.4: Emulsion Polymerization mechanism

First of all, Waterborne free radicals polymerize with monomer molecules dissolved in the continuous aqueous phase. This oligo radical can continue to grow by propagation, hydrophobicity of oligomeric radicals increase. When a critical chain length is achieved, these oligomeric radicals become so hydrophobic that they show a strong tendency to enter the monomer-swollen micelles or precipitate. A new particle is created. This particle is stabilized by surfactants in the case of conventional emulsion polymerization or by inorganic particles in our case. The oligo radicals continue to propagate by reacting with monomer molecules inside the particles. These reactions consume monomer which is supply by the reservoir

monomer droplets in the aqueous phase. The particle is also the loci to other reaction as termination and transfer. The main differences with conventional emulsion polymerization are located in the box area of the figure 1.4 and described below.

1.5.1.1 Nucleation

In conventional system, micellar nucleation predominated in the polymerization kinetic [Chern, 2006]. In Pickering emulsion polymerization, no micelle are formed so the nucleation mechanism model turn towards to the two other model described below namely the homogeneous nucleation and coagulation nucleation.

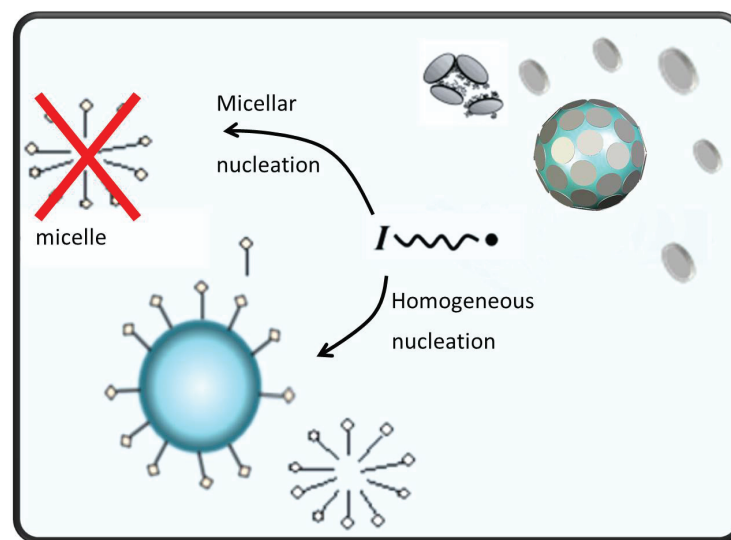


Figure 1.5: Nucleation differences between conventional and Pickering emulsion polymerization

1.5.1.2 Stabilization

Emulsion polymers are colloids, meaning that consist of small discrete particles dispersed in the continuous liquid media. Colloids have many unique and interesting properties as a result of their small size (less than $1\mu\text{m}$) and large interfacial area. Due to this large interfacial area, particles tend to coagulate each other to reduce their instability. Addition of stabilizer is necessary. In general, the anionic surfactants are preferred in many emulsion polymerization systems. Once adsorbed at

the interface, surfactants form a protective layer that imparted the steric and/or electrostatic stabilization effects to the particles and prevented two approaching particles from coagulation during polymerization.

In the electrostatic stabilization mechanism, surfactant molecules dissociate in solution to provide an ionic charge when they adsorb at the particle surface. The surface-charge particles repel one another electrostatically. Anionic surfactant carry a negative ionic charge [Colombié et al., 2000] [Castelvetto et al., 2006], whereas cationic surfactants carry a positive ionic charge [Ramos and Forcada, 2006] [Zaragoza-Contreras et al., 2002]. Changes in the ionic strength of a latex by addition of electrolyte can induce coagulation [Binks and Lumsdon, 1999]. That why sometimes, non-ionic surfactant can be used to improves the stability of latex product against electrolytes, freeze-thaw cycles, water or high shear rates [Yamak, 2013]. In this case, it is the steric stabilization mechanism that protects the interactive particles from coagulation [Ferguson et al., 2005] [Lazaridis et al., 1999]. These stabilizers are believed to cover the system in such a way that long loops and tails extend out into solution. The steric stabilization has been attributed to the thermodynamic penalty when stabilization tries to confine polymeric chains to smaller volumes. Under the circumstances, satisfactory colloidal stability can be achieved via the electrostatic stabilization mechanism [Verwey et al., 1999], the steric stabilization mechanism [Ferguson et al., 2005] [Lazaridis et al., 1999] or both.

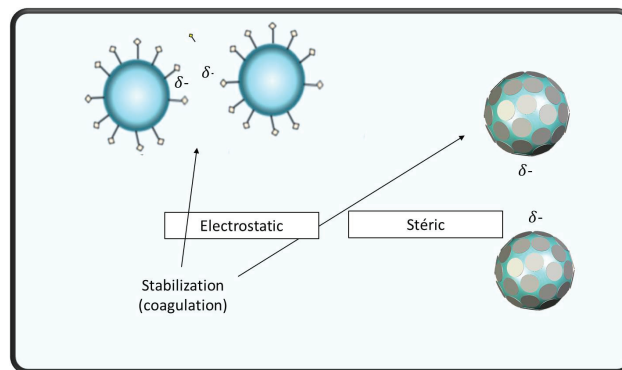


Figure 1.6: Stabilization differences between conventional and Pickering emulsion polymerization

In Pickering emulsion polymerization, the stabilization mechanism remains roughly the same. Adsorption of inorganic particles on the polymer particle forms also a protective layer. This layer is electrostatically charged so the electrostatic repulsion remains to contribute to the stabilization. However, the hairy layers of the surfactants is replaced by a rigid crust around the polymer particles. This mechanical barrier prevents coagulation by steric stabilization [Aveyard et al., 2003] [Chevalier and Bolzinger, 2013]. The inorganic particles have also different effects on stabilization, which was related to slight differences in their compositions and in their adsorption isotherms

1.5.1.3 Radical exchange

The radical exchange is more detail in chapter 5, but in some words, the presence of electrostatically charged layer on the surface of the polymer particles was not found to play a role in radical entry and exit for conventional emulsifiers [Adams et al., 1988]. The case of inorganic particles is not obvious, the mechanical barrier at the surface of the polymer particles may affect the diffusion of the radical to the particle, this was found to play an important role in radical exchange [Smith and Ewart, 1948]. Therefore, it is important to evaluate the impact of the stabilizing layer on radical entry and desorption.

1.5.1.4 Stabilizer partitioning

As described above, inorganic particles seem to have an important role in the emulsion polymerization process, in particular during the nucleation/stabilization stage. Therefore, it is a priority to understand how these particles are distributed between water phase and polymer surface. Quantify the surface coverage of the polymer particles by the inorganic particles will be necessary for the further model.

Part II

Experimental study of Pickering emulsion polymerization of styrene

Chapter 2

Partitioning of clays platelets in Pickering emulsion polymerization

*“ The miracle is this - the more we
share, the more we have ”*

Leonard Nimoy

The research described in this Chapter has been accepted in Langmuir:
Partitioning of Laponite Clay Platelets in Pickering Emulsion Poly-
merization Barthélémy Brunier, Nida Sheibat-Othman, Yves Cheva-
lier, and Elodie Bourgeat-Lami Langmuir 2016 32 (1), 112-124 DOI:
10.1021/acs.langmuir.5b03576

Abstract : Partitioning of Laponite[®] disc-like clay platelets between polymer particles and bulk aqueous phase was investigated in Pickering surfactant-free emulsion polymerization of styrene. Adsorption of clay platelets plays an important role of stabilization in this system, influencing the particles size and number, and hence the reaction rate. Adsorption isotherms show that, while clay platelets are almost fully exfoliated in water, they form multilayers on the surface of polymer particles by the end of polymerization, as confirmed by transmission electron microscopy (TEM). This observation is supported by quartz crystal microbalance, conductivity and TEM measurements which reveal interactions between the clay and polystyrene, as a function of ionic strength. The strong adsorption of clay platelets leaves a low residual concentration in the aqueous phase that cannot cause further nucleation of polymer particles, as demonstrated during seeded emulsion polymerization experiments in the presence of high excess of clay. A BET-type model for Laponite[®] adsorption on polystyrene particles matches the adsorption isotherms.

2.1 Introduction

In surfactant-free heterophase polymerizations known as “Pickering emulsion polymerization”, the adsorbed clay platelets stabilize the dispersion of polymer particles. It is therefore worth investigating the interactions between the clay and the polymer particles and evaluate the partitioning of the platelets between the different phases during the polymerization reaction.

The adsorption of dislike Laponite[®] clay platelets and Ludox[®] silica particles on solid surfaces was firstly studied by Xu et al. [Xu et al., 2010] using a Quartz Crystal Microbalance (QCM). It was concluded that Laponite[®] adsorption depended primarily on the surface charge of the polymer surface rather than the hydrophobic character of its surface. Interestingly, comparison between Ludox[®] silica and Laponite[®] suggested a simple monolayer formation for Ludox[®] silica, but a monolayer-to-multilayer transition for Laponite[®] as the concentration increased. Other adsorption studies of clay (and layered silicates) mainly concerned adsorption on modified surfaces in the objective of optimizing layer-by-layer assembly processes [Podsiadlo et al., 2009]. Clay platelets were reported to undergo fast adsorption; MMT adsorbs as a monolayer together with few overlapping platelets [Ariga et al., 1999] [Lin et al., 2008] and kaolinite clay adsorbs as multilayers [Yan and Masliyah, 1994].

The present study aims at investigating and modeling the partitioning of Laponite[®] clay stabilizing polymer particles during emulsion polymerization. The concentration of clay platelets was below the gelation concentration in order to focus on fluid colloidal suspensions of non-aggregated clay platelets. Assessment of the adsorption of Laponite[®] on polystyrene particles and characterization of Laponite[®] surface-aggregation were done by QCM-D, transmission electron microscopy (TEM), conductivity and elemental analysis (Inductively Coupled Plasma-Atomic Emission Spectroscopy, ICP-AES).

2.2 Materials and Methods

2.2.1 Materials

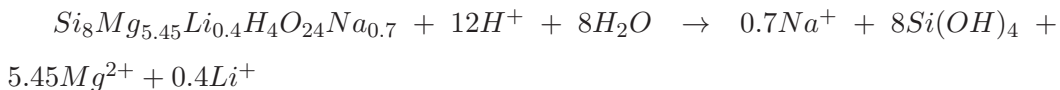
The monomer, styrene (Acros Organics, 99% extra pure, stabilized) was stored in a fridge until used. Potassium persulfate (Sigma-Aldrich, minimum 99%) was used as initiator. The clay Laponite[®] RDS (Rockwood additives) was used as stabilizer. Deionized water of 18 $M\Omega\text{ cm}$ resistivity was used throughout the work.

2.2.2 Laponite RDS

Laponite[®] is a synthetic layered silicate with a structure and composition closely resembling the natural clay hectorite [Coelho et al., 2007]. The used grade Laponite[®] RDS contains the peptizing agent tetrasodium pyrophosphate ($Na_4P_2O_7$) at a concentration of 10 wt% (5.6% Na_2O and 4.4% P_2O_5) based on dry Laponite[®]. Laponite[®] is made of disc-shaped crystals of 25 nm diameter and 0.92 nm thickness. Its density is 2570 kg m^{-3} [Ruzicka et al., 2006] and its melting point is 900°C . The platelet's specific surface area is $358.5\text{ m}^2\text{ g}^{-1}$ [Fripjat et al., 1982]. Each crystal is composed of about 1500 unit cells/sheet, and each cell is composed of six octahedrally coordinated divalent magnesium atoms sandwiched between two layers of four tetrahedral silicon atoms. These groups are balanced by twenty oxygen atoms and four hydroxyl groups. Some magnesium atoms are substituted by monovalent lithium atoms and some positions are empty; such departure from stoichiometry provides a negative surface charge to the platelets that is balanced by sodium cations. The mean chemical composition is 65.82% SiO_2 , 30.15% MgO , 3.20% Na_2O and 0.83% LiO_2 , leading to the following chemical formula: $Na_{0.7}^+[(Si_8Mg_{5.5}Li_{0.3})O_{20}(OH)_4]^{0.7-}$. Besides, Laponite[®] powder contains up to 8 wt% water, which should be either eliminated before weighing (by heating) or taken into consideration in the calculation of concentrations. In the powder form, the crystals share interlayer Na^+ ions forming stacks.

2.2.3 Laponite dispersion in water

Laponite[®] nanoparticles are hydrophilic and the pH of their aqueous dispersions is 8-9. Indeed, a strongly negative charge (700 elementary charges) is present on their basal faces due to the release of the Na^+ ions from the surface and a weakly positive charge appears on the rim of the disks due to protonation of the OH groups with hydrogen atoms of water (for $pH < 11$) [Ruzicka et al., 2006] [Tawari et al., 2001]. This forms a colloidal dispersion of charged disc-like particles with a diameter of 25 nm and a thickness of 1 nm with negative charges on the crystal faces and small pH-dependent positive charges on the edges, typically 10% of the negative charges [Tawari et al., 2001]. The interaction between platelets has been characterized by an isotropic van der Waals attraction and an anisotropic electrostatic interaction, which can be either repulsive (face-face, rim-rim) or attractive (rim-face) [Tawari et al., 2001]. The sodium counterions Na^+ in solution screen the negative charges of the faces forming an electrical double layer. Aqueous Laponite[®] suspensions undergo aging, which is characterized by Mg^{2+} ions leaching taking place according to the following chemical reaction in acidic medium. This reaction that takes place in contact with CO_2 can be avoided by working under inert nitrogen. [Ruzicka et al., 2006]



The Laponite[®] RDS used in this work contains the peptizing agent tetrasodium pyrophosphate (10 wt%) adsorbed onto the positively charged rims (edges); the tetravalent negatively charged pyrophosphate ions neutralize the rim charge and decrease electrostatic attractions between the positively charged rims and the negatively charged faces, and therefore avoid gelation. Reducing such interactions contributes to a longer stability of the dispersions in water. Note that low molar mass polyethylene oxide (PEO) molecules have also been reported to delay Laponite[®] aggregation by forming a steric barrier preventing contact between platelets [Mongondry et al., 2004].

2.2.4 Reactor set-up and operation

A 1 L calorimeter reactor was used with mechanical stirring at 400 rpm using a three blades Bohlender propeller. The reaction was conducted at 70°C, and the reaction temperature was controlled using a thermostat bath. The reactor was equipped with five thermocouples inserted into the reactor, at the jacket inlet and outlet, in the heating bath and in the feed. A balance allowed measuring the flowrate of the introduced monomer in semi-continuous experiments. The reactions were carried out under oxygen free conditions, by degassing the reaction medium using nitrogen stream before the reaction. During the reaction, the stream of nitrogen was moved upwards off the reaction medium to the top of the reactor to maintain saturation of the gaseous atmosphere with nitrogen. These measurements were used to calculate the heat produced by the reaction and the calorimetric conversion [Bourgeat-Lami et al., 2010]. Samples were withdrawn at specific time intervals to measure the solids content (SC) using a thermogravimetric balance and the particle size, which allowed calculating the particle number density (assuming spherical particles). The solids content was used to calculate the amount of polymer and the monomer conversion, after subtraction of the mass of solids of clay and initiator. The ratio of the area of clay platelets' faces to the polymer particles area was calculated in order to get an estimate the surface coverage of the latex particles by the clay and assess any excess of clay [Teixeira et al., 2011].

2.2.5 Preparation of clay-armored polystyrene seed particles at 20 wt% solids content

This latex is to be used for seeded polymerizations. It was prepared batch-wise. 800 g of water containing 1 g L⁻¹ clay was stirred for 30 min at ambient temperature, degassed using nitrogen and heated to 70°C in the reactor. Then, 200 g of styrene was added and the polymerization was initiated by adding 1.6 g of potassium persulfate. The final mean particle size of the seed was 280 nm and the solids content was 20%.

2.2.6 Seeded Polymerizations

200 g of the above-described 20% solids content seed were mixed in the reactor with 640 g of deionized water. 40 g of styrene was added to swell the seed particles for 1 h at ambient temperature under stirring at 200 rpm. Then, different amounts of clay were dispersed in the latex. Two series of experiments were performed: in the first one, the dispersion was allowed to equilibrate for one hour, and in the second one, for 12 h. The dispersion was then heated up to 70°C, degassed, and the initiator was added to start the polymerization. After the depletion of monomer from the droplets (as determined by calorimetric estimation of the conversion), which corresponded to about 50% conversion, 160 g of monomer was added semi-continuously at a flowrate of 0.02 g s^{-1} (therefore under monomer-starved conditions). At the end of monomer addition, a batch polymerization period of 30 min was applied to raise the conversion of the monomer above 90%.

2.2.7 *Ab initio* experiments

A batch period was first considered for particle nucleation followed by a semi-continuous part similar to seeded polymerizations. For the batch part, first 800 g of water containing different concentrations of clay was stirred for 30 min at ambient temperature and degassed using nitrogen and heating to 70°C in the reactor. This was followed by the addition of 40 g of styrene, heating to 70°C and the polymerization was initiated by adding 1.6 g of potassium persulfate.

2.2.8 Characterization of the particle size

Particle mean size and size distribution were measured by dynamic light scattering (Zetasizer, nano ZS, Malvern) at 25°C at a fixed scattering angle of 90°. The z-average hydrodynamic diameter (D , nm) is: $D = \frac{\sum n_i D_i^6}{\sum n_i D_i^5}$, where n_i is the number density of particles of diameter D_i . The measured particle size was corrected for the amount of monomer that diffused from the particles to water due to dilution necessary for the measurement; but the corrected sizes were found close to the measured ones, as the particles were not saturated with monomer during most of

the polymerization time. The particle size was not corrected with regards to the adsorbed platelets thickness. Indeed, it was assumed that the platelets laid flat on the polymer particles (as will be demonstrated later using TEM) and therefore did not significantly contribute to the measured particle size, due to their small thickness (1 nm) compared to the particles diameter (of the order of 200 nm).

2.2.9 Transmission Electron Microscopy (TEM)

A JEOL 2100F microscope, (“Centre Technologique des Microstructures” (CT μ), University of Lyon, Villeurbanne, France), was used to observe the clay-armored latexes at high angle annular dark field mode. A small drop of diluted latex (5 wt%) was deposited on a microscope grid (carbon-coated copper support), slowly dried in open air, and observed under 200 keV acceleration voltage. Image analysis (using Digital Micrograph software) was used to evaluate the platelet and the interstitial water layer thicknesses. Using this TEM and the same procedure, **Energy-Dispersive X-ray Spectroscopy (EDS)** mapping of elements was carried out to determine the spatial distribution of carbon, oxygen, silicon and magnesium elements in the clay-armored particles. Laponite[®] RDS dispersion in water was investigated by image analysis of TEM as well as cryo-TEM (see Supporting Information).

2.2.10 Surfactant-free polystyrene seed particles

This seed was done for conductivity and ICP-AES analyses. It was prepared batch-wise using 4 g potassium persulfate in 800 mL degassed water in a 1 L reactor. In order to produce different particles sizes (200, 400 and 750 nm), the reaction was carried out with different styrene concentrations (2, 4 and 10 wt%). The final latexes were concentrated in a Rotavapor[®] up to 20 wt% solids content. Such high concentration is required since both the conductivity and ICP-AES studies involve diluting the latex with a dispersion of clay. The latex was cleaned several times (about 10 times) with ion exchange resins (*Dowex[®] MarathonTM*) to eliminate free ionic species resulting from initiator decomposition and hydrosoluble species.

Washing steps were repeated until a constant conductivity was obtained.

2.2.11 Conductivity measurements

The cleaned surfactant-free polystyrene latex described above was used (SC = 20%). A dispersion of clay in water was prepared and gently stirred for 24 h, then added to the cleaned latex and allowed to equilibrate for 12 h. Deionized water was added to reach the same solids content (5 wt%) for all samples, with different clay concentrations. The conductivity was corrected for the effect of viscosity (measured with a MCR 302 Rheometer) by assuming a linear relationship between the conductivity and the viscosity. Indeed the mobility of ionic species varies linearly with respect to the viscosity of the medium. Conductivities were rescaled in order to eliminate the effect of viscosity on conductivity as follows: $\sigma_{corr} = \sigma_{exp} \frac{\eta_{ref}}{\eta_{exp}}$, with $\eta_{ref} = 1.003 \text{ mPa s}$ for all samples, and η_{exp} measured with a Anton Paar MCR 302 rheometer.

2.2.12 Inductively Coupled Plasma - Atomic Emission Spectroscopy (ICP-AES)

Adsorption of clay platelets on polystyrene latex was investigated by measuring the residual magnesium (Mg), silicon (Si) and lithium (Li) in water. A titration method was employed using at least two distinct wavelengths for each element: 279.8 nm, 280.3 nm and 285.2 nm for Mg; 252.9 nm, 255.6 nm and 288.2 nm for Si, and finally 610.4 nm and 670.8 nm for Li. The surfactant-free latex described above was used. Three series of experiments were realized: with cleaned, uncleaned latex, and uncleaned latex followed by ionic strength adjustment by addition of KCl. The clay dispersion was prepared as in the conductivity study, and the concentrations of the samples were all adjusted to 5 wt% solids content. Two methods of separation of polystyrene from free clay platelets in water were considered: (1) ultra-centrifugation of the samples at 40 000 rpm for 20 min (after validating that the platelets do not settle during centrifugation under such conditions), and (2) filtration through a syringe filter of 200 nm pore diameter (a test was also done to

validate that particles do not pass through the filter but that the clay does).

2.2.13 Quartz Crystal Microbalance (QCM-D)

A QCM apparatus with dissipation monitoring technology (model D300, Q-Sense) was used to study the kinetics of clay adsorption. The measurements were performed in a cell coated with neutral polystyrene (QSX-305, Lot Oriel). All experiments were performed at $20^{\circ}\text{C} \pm 0.01^{\circ}\text{C}$, after achieving a stable baseline of resonance frequency (f_c) and energy dissipation (D). Four harmonics were detected (1st fundamental harmonic, 3rd, 5th and 7th overtones) for the frequency and dissipation (normalized energy lost per oscillation period which corresponds to the bandwidth divided by the resonance frequency). Two different concentrations of clay platelets were studied (2 g L^{-1} and 10 g L^{-1}). First deionized water was injected into the measurement cell; after 2 min delay for a stable baseline of frequency was achieved, three successive injections of fresh solution of clay platelets in water were made followed by a 2 min equilibration period before each measurement.

2.3 Results and Discussion

2.3.1 Investigation of the role of clay in emulsion polymerization

Surfactant-free emulsion polymerization of styrene was carried out in the presence of clay by semi-continuous monomer addition, either in *ab initio* or in seeded modes, in order to infer the role of clay in particles on the nucleation and stabilization of polymer particles.

2.3.1.1 Effect of clay concentration in *ab initio* semi-continuous polymerization

The objective of these experiments is to investigate the relationships between the clay concentration and the number density of nucleated particles and their stability. figure 2.1 shows the results of a series of *ab initio* semi-continuous experiments with different clay concentrations. At the beginning, the number of particles in-

creased during a first period called nucleation period (figure 2.1a). The end of the nucleation period, where the number of particles stopped increasing, was observed between 45 and 90 min. The number of particles increased as a function of the clay concentration; the dependence on clay concentration was less important for high concentrations, the dependence on clay concentration was less at the high concentrations but no clear levelling off was observed. This led to an increase in the reaction rate and smaller particles at the same solids content (figure 2.1b,c). As a second result, the clay particles were found to be quite efficient in ensuring particles' stability since the particles number remained constant until the end of the reaction, with SC = 20%, revealing neither coagulation nor renucleation.

The clay particles were nicely dispersed in water as non-aggregated elementary particles. Indeed, dispersion of clay in water (without latex) was investigated by different methods (see Supporting Information). In short, conductimetry indicated full dispersion in 1 h and no aging via the release of lithium and magnesium ions after 4 days at ambient temperature, indicating the time period during which the non-aggregated dispersion can be safely used for polymerization; TEM images combined to image analysis as well as cryo-TEM indicated that the dispersion contained only few stacks of two to six platelets, with an interlayer thickness of 1 nm.

The coverage of the polymer particles surface by clay platelets was calculated as the ratio of the surface area of platelets' faces discs of 25 nm diameter to the polymer particles' area assuming spherical shape and full clay dispersion (figure 2.1d). For clay concentrations higher than 0.5 g L^{-1} , the area of platelets was enough to cover the total surface of particles and a significant excess of clay platelets was present at the beginning of the polymerization. As the particles grew, this amount became insufficient to cover the full polymer particles' surface, except for 10 g L^{-1} clay. These results suggest successful clay adsorption on the polymer particles' surface to ensure latex stability whatever the clay content. However, clay partitioning between the latex surface and water cannot be evaluated from these data.

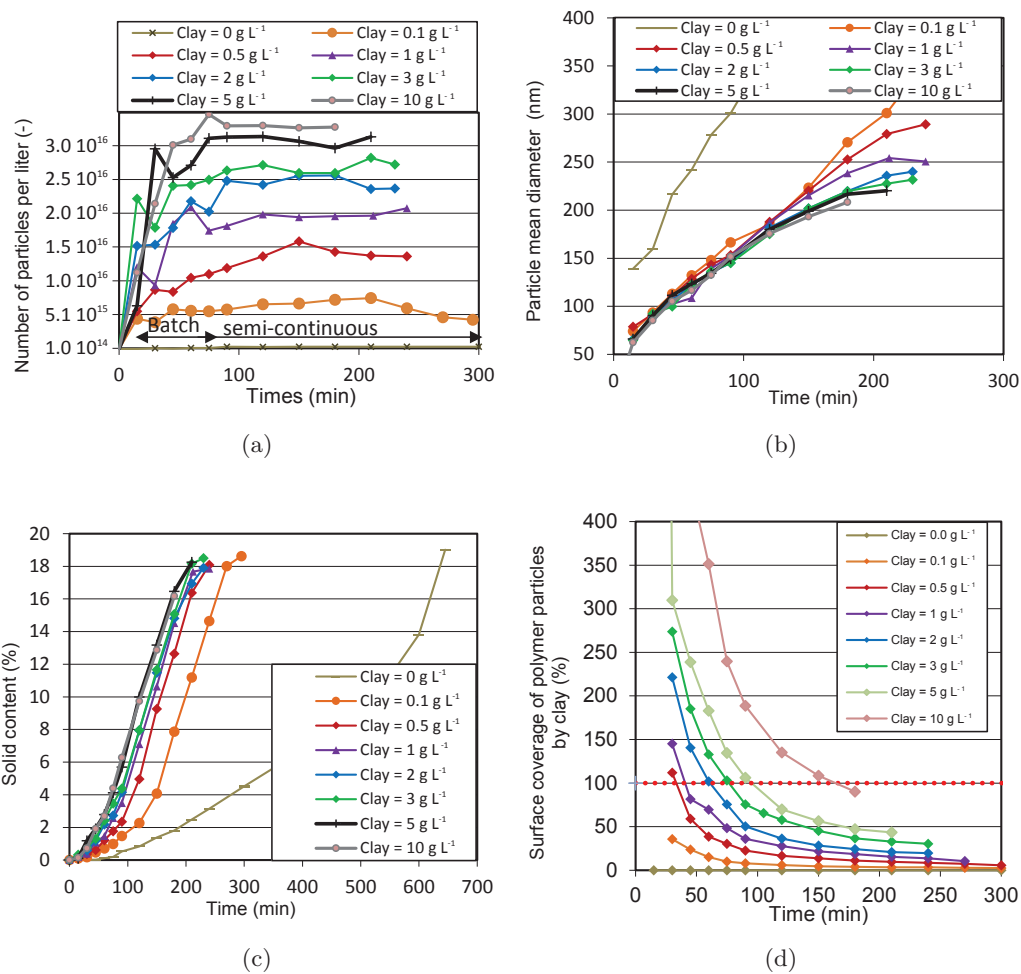


Figure 2.1: Results of the Pickering *ab initio* semi-continuous emulsion polymerization of styrene at 70°C stabilized with different amounts of Laponite RDS®.

2.3.1.2 Effect of clay concentration in seeded emulsion polymerization experiments

These experiments are meant to evaluate the adsorption dynamics of clay on a previously produced clay-armored seed (containing 1 g L^{-1} of clay) and to assess the possible re-nucleation of polymer particles at high clay concentrations.

Two series of experiments were carried out with different clay concentrations, by allowing the clay to equilibrate in the latex for 1 h or 12 h before the reaction. Interestingly, both series gave similar results, which indicated fast adsorption of the clay (less than one hour under the considered experimental conditions: diluted latex at ambient temperature). Moreover, figure 2.2 shows that the number of particles remained constant, after a slight reduction at the beginning of the polymerization, which reveals that the latex particles remained stable and that no further nucleation of polymer particles occurred. The seed particles grew from 280 nm to 470 nm by the end of the reaction. For all clay concentrations higher than 2 g L^{-1} , the area of platelets was higher than that of polymer particles, which would allow total coverage in case of complete adsorption. If only one layer of clay was adsorbed, there should remain a large excess of residual clay platelets in suspension in water. However, no renucleation took place in these experiments. Note that in conventional emulsion polymerization in the presence of surfactants rather than clay, renucleation is possible in seeded experiments upon the addition of high amounts of surfactant that favors the nucleation of new particles at the expense of entry of waterborne oligoradicals into existing seeds; either due to micellar or homogeneous nucleation depending on the concentration of surfactant and solubility of monomer in water. The absence of renucleation suggests that the added clay is predominantly adsorbed on the polymer particles' surface, more precisely forming multilayers, and no significant excess remains in water. This issue is addressed in the second part of the paper dealing with the characterization of the final latexes.

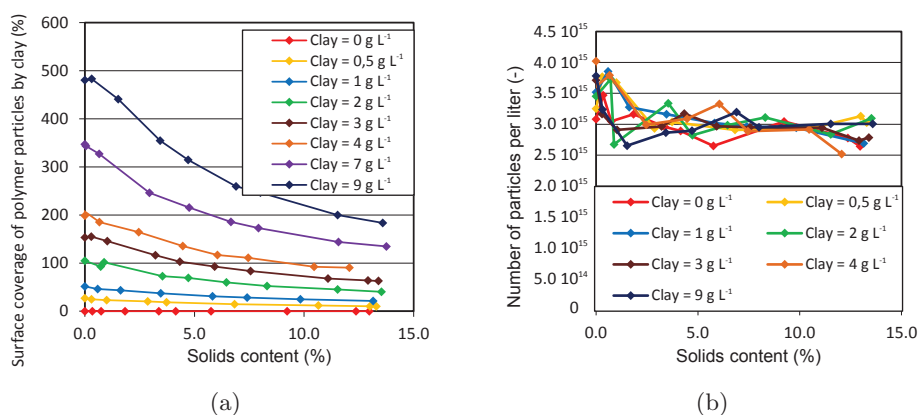


Figure 2.2: (a) Evolution of particle number in seeded semi-continuous emulsion polymerization with different amounts of clay, using an initial seed of 5 wt% solids content containing 1 g L⁻¹ clay. (b) Ratio of the platelets area to the particles' area ($\times 100$).

2.3.1.3 Studying clay adsorption during polymerization using EDS

The latex obtained by the end of a typical batch emulsion polymerization reaction in the presence of 1 wt% Laponite[®] RDS was analyzed by TEM. A thin light contour can be observed around the polystyrene particles indicating that clay platelets are located on the surface of the polymer particles (figure 2.3). An area in this image was selected for EDS analysis (enclosed by an ellipse) shown in figure 2.3b. Two peaks corresponding to the carbon shell and three other peaks corresponding to oxygen, magnesium and silicon elements, respectively, revealed the presence of clay platelets around the polymer particles through the detection of magnesium and silicon in the selected area. The analysis also reveals the presence of copper probably originating from the TEM grid itself.

Mapping of carbon, silicon and magnesium elements as measured by EDS is shown in figure 2.4. The sample was scanned several times to create digital images for each element. The carbon map corresponds to polymer particles while the silicon and magnesium maps are related to the clay. In figure 2.4 Silicon appears tightly bound to the particles surface while a small amount of magnesium is present in the aqueous phase. This might be due to Mg^{2+} ions leaching that was not completely

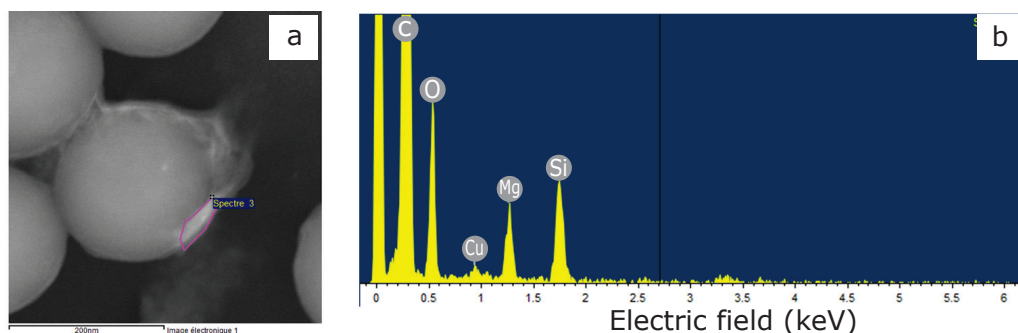


Figure 2.3: (a) Dark-field TEM image of polystyrene latex particles prepared in the presence of 1 wt% Laponite[®] coupled with EDS analysis (scale bar: 200 nm). (b) Intensity of element signal in EDS analysis. Reprinted with permission from Langmuir, 2016, 32, 112-124, copyright 2016 American Chemical Society.

avoided during polymerization at 70°C or during sample preparation. Note that polymerization took place under nitrogen starting at pH 8.8 and reaching pH 8.2 by the end of the reaction due to KPS decomposition. A rough estimate of the thickness of the clay coating is 10-20 nm. In all cases, the maps of silicon are more reliable; they reveal that the clay is mainly present on the surface of the latex particles and that the thickness of the layer of adsorbed clay is larger than the thickness of the elementary clay platelets.

2.3.1.4 Clay adsorption during polymerization using TEM

Evidence for the formation of multilayers of clay platelets on the surface of the polymer particles during surfactant-free emulsion polymerization in the presence of clay was provided by TEM (figure 2.5). Note that full exfoliation of the initial clay dispersions was supported by cryo-TEM analysis (see Supporting Information). Clay platelets are visible as black lines of about 1 nm thickness and 20 nm length. Stacks of platelets are formed on the surface of particles. Clay platelets also form bridges between the particles. Such bridges are not strongly stuck to the particles, as they break up under the electron beam of the microscope at large magnifications, leading to platelets settling down on the particles surface (figure 2.5b).

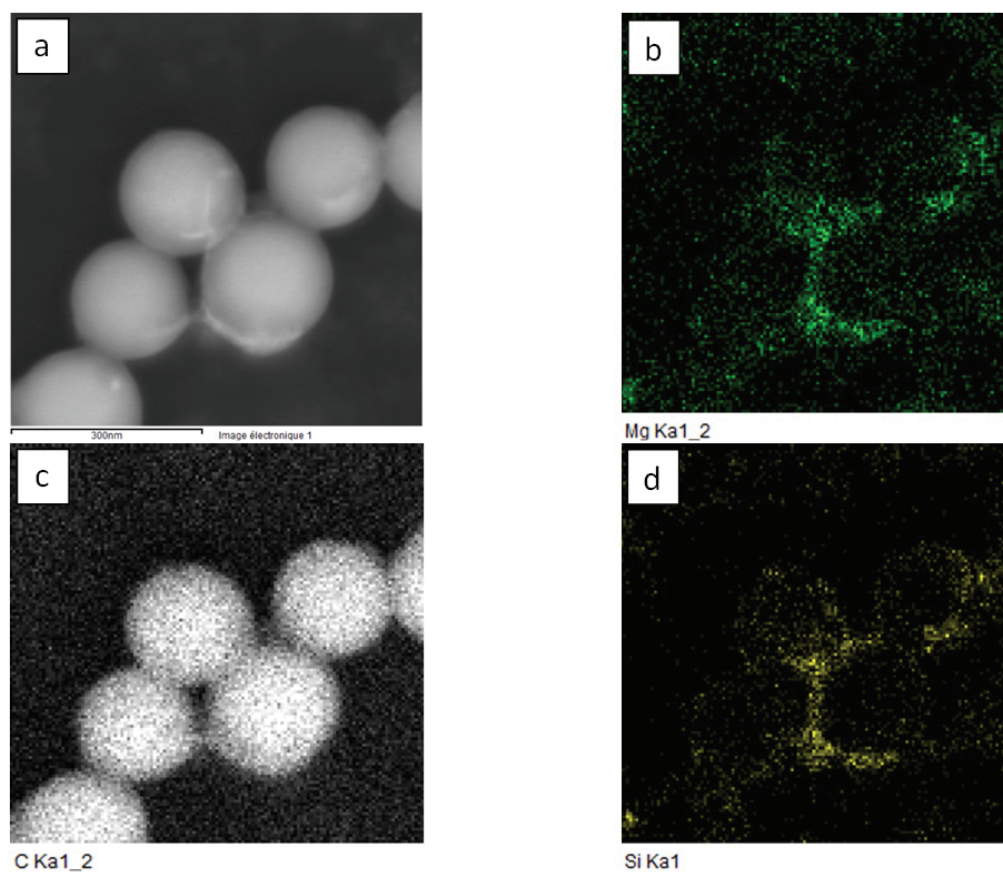


Figure 2.4: a) Dark-field TEM image of polystyrene latex particles prepared in the presence of 1 wt% Laponite[®] (the same latex as in figure 2.3) (scale bar = 300 nm). b-c-d) EDS analysis of the TEM image for magnesium, carbon and silicon respectively. Reprinted with permission from Langmuir, 2016, 32, 112-124, copyright 2016 American Chemical Society.

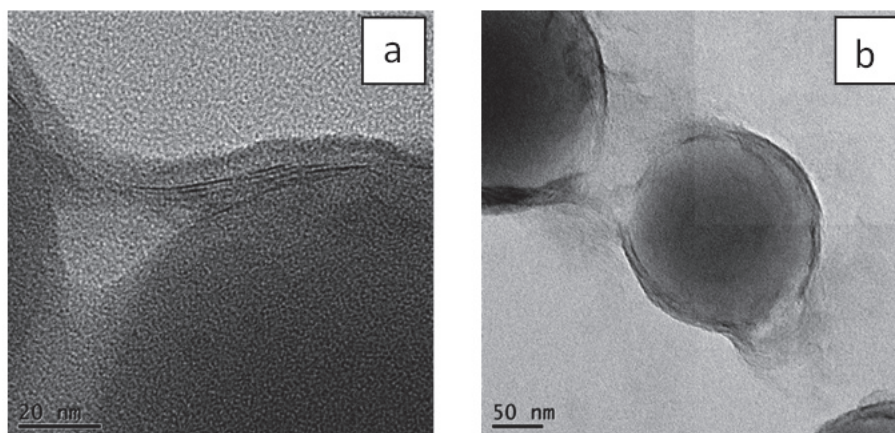


Figure 2.5: TEM images of polystyrene latex particles prepared in the presence of 1 wt% Laponite[®] (the same latex as in figure 2.3) a) Scale bar = 20 nm. b) Scale bar = 50 nm. Reprinted with permission from Langmuir, 2016, 32, 112-124, copyright 2016 American Chemical Society.

2.3.2 Adsorption of Laponite on surfactant-free polystyrene latex particles

Partitioning of clay between water and the surface of polystyrene particles was studied in order to : i) establish whether initially fully exfoliated clay platelets in water subsequently adsorb on the particles surface as multilayers; ii) assess the interaction between clay and polystyrene surfaces and the effect of ionic strength on clay/polymer interaction, and iii) evaluate the residual amount of clay in water. A model of adsorption is sought from these analyses. Three different techniques were used: QCM, conductivity and ICP-AES. Note that a pure polystyrene cell was used for QCM study and a cleaned latex for the conductivity study, in order to assess the affinity between the clay and polystyrene, while both cleaned (adjusted to different ionic strengths) and uncleaned polystyrene latexes were used for the ICP-AES study in order to investigate the adsorption of clay on polystyrene as a function of ionic strength.

2.3.2.1 Quartz crystal microbalance with dissipation (QCM-D)

QCM-D was used to monitor the adsorption of Laponite[®] RDS onto the surface of a commercial polystyrene cell, using two concentrations of Laponite[®] RDS in water: 2 g L^{-1} and 10 g L^{-1} .

Figure 2.6 shows the QCM results, calculated from the third overtone measurements, selected for its better signal-to-noise ratio. The frequency shift (figure 2.6 a) was measured as a function of time: first deionized water was introduced in order to establish a stable baseline after about 2 min (step 0); The periods named 1, 2 and 3 corresponded to the times just after the addition of fresh clay dispersion; Finally, rinsing was applied in order to evaluate the adhesion strength of adsorbed clay on the surface (step 4). The high shift of the resonance frequency since the 1st pass (start of step 1) indicates a fast Laponite[®] RDS adsorption on polystyrene, which reveals a strong affinity with the polystyrene surface. Since the polystyrene surface did not receive a surface modification, the polystyrene cell surface was neutral, which precluded the possibility of charge interactions. Adsorption was thus due to non-electrostatic interactions. The fast adsorption indicates a weak energy barrier against adsorption.

At each new injection of the high clay concentration of 10 g L^{-1} (steps 2 and 3), the frequency stabilized quickly, whereas the frequency continued to decrease slightly as a function of time and did not reach a stationary value after addition of the lower clay concentration of 2 g L^{-1} . This indicated a slow and continuous adsorption from the dilute dispersion of Laponite[®]. When deionized water was used for rinsing after the adsorption study (step 4), all the clay was released into water for the concentration of 10 g L^{-1} , while a small but significant amount remained anchored for the concentration of 2 g L^{-1} . This indicates that the link between the clay and polystyrene is not permanent. Also, there might be different kinds of arrangements of the clay, where non-organized and less dense configurations might be released more easily. In this case, highly concentrated dispersions seem to lead to the formation of such non-organized layers.

In order to calculate the mass of adsorbed material (Δm) from the mea-

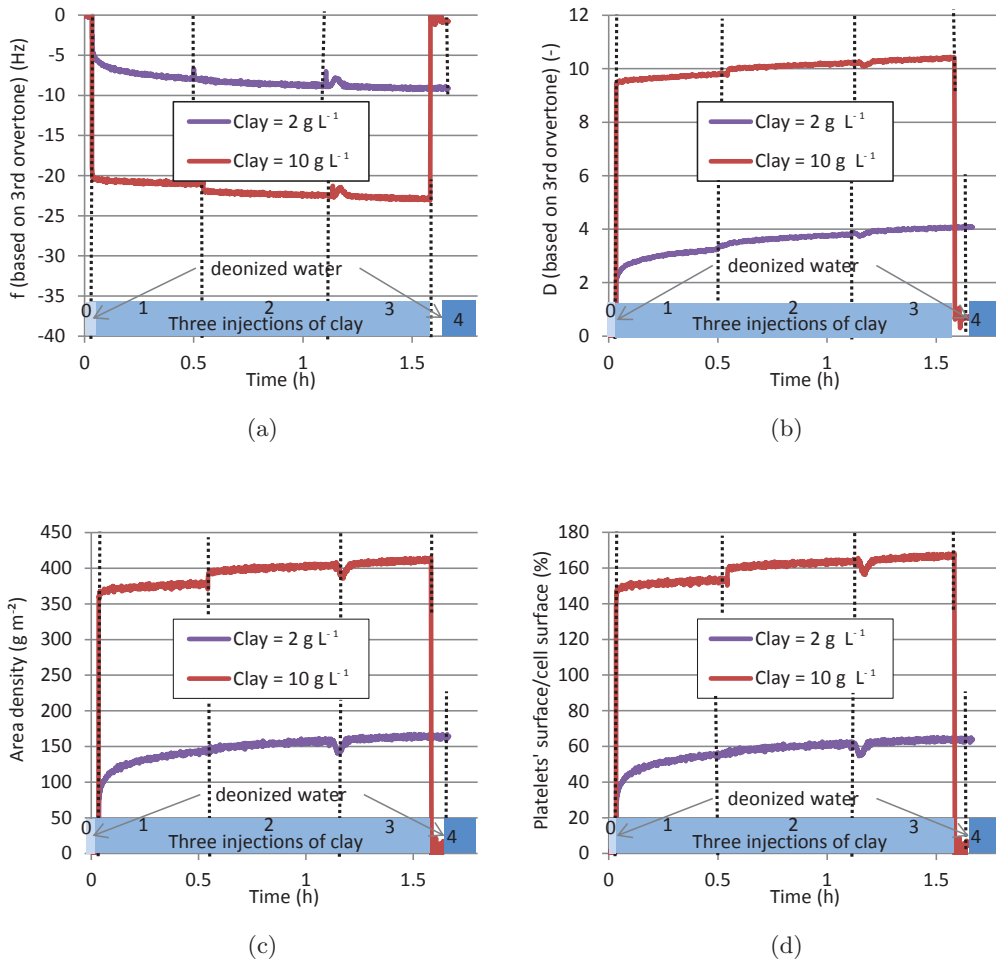


Figure 2.6: QCM resonance frequency and dissipation energy results, and calculated surface density and surface coverage, with a 2 g L^{-1} and 10 g L^{-1} aqueous dispersions of Laponite[®] RDS.

sured frequency shift (Δf), different correlations were proposed in the literature [Xu et al., 2010]. The measured resonance frequencies divided by their overtone number were identical for the three measured harmonics in our case, showing that the adsorbed layer is rigid, which allows using the relationship of Sauerbrey [Sauerbrey, 1959]:

$$\Delta m = -A \underbrace{\left(\frac{\sqrt{\mu\rho_q}}{2f_0^2} \right)}_C n_o \Delta f \quad (2.1)$$

where n_o is the overtone number, $A = 1.54 \text{ cm}^2$ the electrode area and C the mass sensitivity constant. Using the intrinsic crystal frequency $f_0 = 5 \text{ MHz}$, the quartz density $\rho_q = 2.65 \text{ g cm}^{-3}$ and its shear modulus $\mu = 2.95 \times 10^{10} \text{ N m}^{-2}$, one gets $C = 17.7 \text{ ng cm}^{-2} \text{ Hz}^{-1}$. Note that this equation is valid for rigid, non-slip, evenly distributed and sufficiently thin adsorbed layers such that the vibration is completely coupled to the oscillating crystal, ensuring a linear relationship between the adsorbed mass and the frequency. For soft or viscoelastic films causing energy loss during oscillation, both the frequency and the dissipation should be considered in order to calculate the mass, using for instance the Voigt viscoelastic model, or the Kanazawa and Cordon's expression [Keiji Kanazawa and Gordon II, 1985].

The calculated surface density of clay platelets is given in figure 2.6 c. A higher adsorption level was reached instantaneously since the 1st injection for the 10 g L^{-1} clay suspension (375 ng cm^{-2}) compared to the 2 g L^{-1} dispersion (100 ng cm^{-2}). Therefore, the adsorbed amount of clay increases when the concentration of clay in the dispersion is increased. The fast adsorption of clay for both concentrations (of the order of minutes), is favorable to emulsion polymerization in view of the requirement of a fast stabilization of polymer particles.

The area covered by the platelets was estimated from the adsorbed mass of clay and divided by the polystyrene cell surface (1.54 cm^2) (figure 2.6d). As QCM determines the mass of the adsorbed film including trapped solvent, it is necessary to estimate the mass of adsorbed water. The measured water content in the dry powder was 10 wt% and water interlayer measured in the suspension was 0.35 nm

(see Supporting Information), which gives a clay surface density of 35 ng cm^{-2} per layer. As the number of layers is not known, the surface coverage was first calculated without eliminating the water interlayer mass. Figure 2.6d shows the ratio of the calculated clay platelets' area to the cell surface. This value can be considered as the surface coverage, under the assumption that the clay platelets lay flat on the cell surface and that adsorption is not limited by steric hindrance. In all cases, the calculation remains indicative, and it can be seen that the adsorbed amount of clay does not allow saturation of the polystyrene cell surface for the 2 g L^{-1} suspension while the surface was saturated at higher concentration. The observed incomplete coverage at 2 g L^{-1} clay provides a clue as to why the adsorbed amount increased continuously and did not reach equilibrium for the lower clay concentration. With the high clay concentration, overlapping or multilayer formation of clay platelets on the surface seems to take place. Part of the formed layers might be due to the non-exfoliated fraction of the clay, as observed by TEM (see Supporting Information).

The configuration of adsorption and structural (viscoelastic) properties of the adsorbed material can be assessed from the energy dissipation (figure 2.6 b). The dissipation follows a similar behavior as the frequency shift, which indicates that the adsorbed particles are firmly stuck to the surface. Indeed, clay particles extending out into the aqueous solution as non-organized layers would increase the dissipation without affecting the frequency [Xu et al., 2010]. The few works dealing with clay adsorption on solid surfaces, mainly focused on electrostatic interactions because surfaces were coated with cationic polymers such as poly(diallyldimethylammonium chloride), giving a higher adsorption and variations of resonance frequency by QCM [Xu et al., 2010] [Fatisson et al., 2009] [Chen and Elimelech, 2006] [Enarsson and Wagberg, 2008] [Quevedo and Tufenkji, 2009].

It is first concluded that Laponite[®] adsorption on neutral polystyrene takes place even though there is no surface charge. This indicates that non-electrostatic interactions between the clay and the polystyrene surface are operating. Secondly, multilayers of platelets can form on the polymer surface.

2.3.2.2 Conductivity measurements

Partitioning of clay platelets between water and the particles surface was assessed by means of electrical conductivity measurements of suspensions of cleaned surfactant-free seed lattices of three different diameters: 200, 400 and 750 nm to which the clay dispersion was added. The measured conductivity was therefore mainly due to charged species related to the addition of clay, as free ionic species coming from the initiator have been removed during the cleaning process. Moreover, the contribution to the conductivity of Mg^{2+} ions released from the edges of Laponite[®] platelets is relatively small [Jatav and Joshi, 2014]. This was confirmed by the conductivity of aqueous clay dispersions (without latex) staying constant over 4 days, which indicates no Mg^{2+} ions leaching during the measurements (see Supporting Information). Note also that the peptizing agent eliminates rim charges of Laponite[®]. Therefore, the main source of conductivity during the first days is Na^+ counterions released from the Laponite[®] into solution.

Figure 2.7 shows the measured conductivity for latexes containing different amounts of Laponite[®] compared to the conductivity of pure aqueous Laponite[®] dispersions (without latex). The conductivity of clay in the latex was lower than that of the aqueous clay dispersion, which indicates clay adsorption on the polymer particles. Moreover, the higher the particles' surface area, the lower was the conductivity. Finally, the variation of conductivity was linear with respect to the concentration of clay indicating that the mobility of Na^+ ions was maintained identical at the different concentrations and the added clay had the same degree of exfoliation.

2.3.2.3 Inductively Coupled Plasma-Atomic Emission Spectroscopy (ICP-AES)

In order to collect supplementary quantitative data to the previous investigations, clay partitioning between water and the surface of polymer particles was investigated using quantitative ICP-AES analyses of silicon. The concentration of clay in the aqueous phase was measured following two separation techniques: by centrifu-

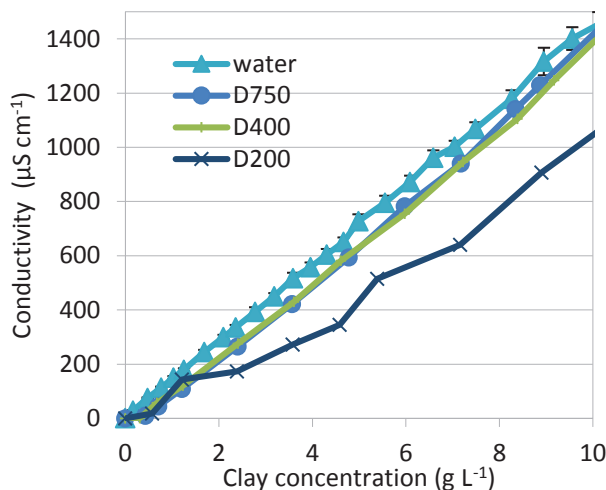


Figure 2.7: Conductivity of Laponite[®] suspensions in pure water and in latex suspensions (5 wt% in water) for three different latex particles diameters, $D = 200$, 400 and 750 nm as a function of clay concentration.

gation or by filtration, where both methods gave identical results (for 3 replicates). The surfactant-free seed latex with a mean diameter of 400 nm was used under three conditions: after cleaning the latex, without cleaning, and using cleaned latex with added KCl salt to adjust the ionic strength. The uncleaned latex allowed studying clay adsorption under the same ionic strength conditions as during the polymerization, i.e. including sulfate anions resulting from initiator decomposition. The cleaned latex allowed evaluating the adsorption rate of clay on pure polystyrene and comparison to QCM and conductivity studies. Finally, the cleaned latex with adjusted ionic strength allowed discriminating the effect of the ionic strength.

Adsorption isotherms of Laponite were obtained from ICP-AES analyses of the Si element as Si is the major component of Laponite[®] (23.3%). Li represents only 0.3% of Laponite[®] giving lower accuracy. Mg^{2+} ions (14.3%) might slightly leach into water and therefore cannot be used to evaluate clay adsorption.

The adsorption isotherm of the uncleaned latex (figure 2.8a) shows two distinct adsorption regimes as a function of the clay concentration: a coexistence of adsorbed

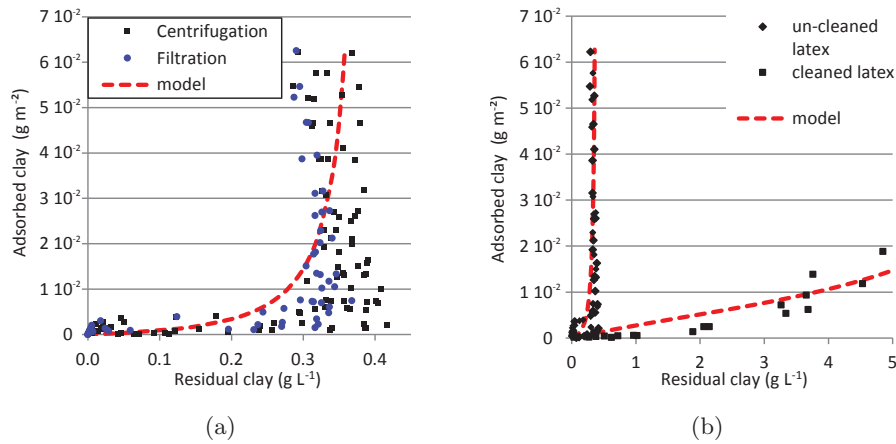


Figure 2.8: Adsorption isotherm of Laponite[®] on polystyrene latex particles (5 wt% solids content and mean diameter 400 nm) measured using Si analysis by ICP-AES a) uncleaned latex (using centrifugation and filtration methods) ; b) both cleaned and uncleaned lattices. The measurements are compared to the isotherm model.

clay particles and residual particles in aqueous suspension was observed for clay concentrations lower than 0.34 g L^{-1} . Above this clay concentration, the adsorption isotherm was almost vertical, showing that clay particles in excess to 0.34 g L^{-1} fully adsorbed onto the latex particles. In the dilute regime where clay platelets partition between the latex surface and bulk water, the adsorbed amount is lower (as calculated below) than the amount allowing full coverage of the polymer surface. Conversely, in the second regime, the adsorbed amount exceeds this later limit for a dense monolayer. Such results strongly suggest that the clay is adsorbing as a monolayer for concentrations lower than 0.34 g L^{-1} and forms adsorbed multilayers for higher concentrations. Therefore, the residual concentration of clay in water cannot be increased because of complete adsorption to the latex. It is important to emphasize that the same mother clay dispersion was used to perform all the ICP-AES experiments, which means that the clay platelets had the same initial degree of dispersion. Moreover, conductometric measurements have shown a linear relationship between the conductivity and the clay concentration, indicating no (or identical) formation of aggregates as a function of the concentration. Therefore, the

formation of multilayers is not due to increased aggregated stacks forming in water upon increasing the clay concentration. Rather, the clay looks well-exfoliated in water in all cases, but forms multilayers on the surface of the particles during their adsorption.

Figure 2.8b shows the adsorption results for the cleaned latex. It can be seen that the adsorption is less effective in this case, which indicates that the presence of initiator residues in the aqueous phase plays an important role in clay adsorption. The sulfate ions in solution lead to an increase in the ionic strength which screens the clay charge and enhances the adsorption to the surface of the negatively charged polystyrene latex. Note that multilayers formation is still taking place with the cleaned latex, but at a lower rate as a function of the clay concentration.

Since it was presumed that the strong adsorption as multilayers to the uncleaned latex was caused by the ionic strength, clay adsorption on the cleaned latex has been investigated at different ionic strengths (15, 25, 35 $mS\ cm^{-1}$) and compared to the results obtained for the uncleaned latex (figure 2.9). The range of ionic strengths was chosen such as to be comparable to the ionic strength of the uncleaned latex by addition of a concentrated KCl solution to the cleaned latex until it attains the conductivity of the uncleaned latex (35 $mS\ cm^{-1}$). Intermediate ionic strengths corresponding to lower conductivities were also tested. Note that the latex did not coagulate upon the addition of KCl in the studied samples, as the particle size measured after the addition of KCl remained unchanged. Moreover, the latex did not reach a visible gel state although the addition of KCl to clay dispersions (without polymer particles) was found to promote gelation (as validated by Nano-ZS size measurements). This supports the assumption that a majority of clay is adsorbed on the particle surface and that only a minor amount remains free in suspension.

Figure 2.9 shows that the addition of salt to the cleaned latex led to an adsorption profile comparable to that of the uncleaned latex, which confirms that the screening effect by the ions in the medium is at the origin of enhanced clay adsorption in the uncleaned latex. A slightly higher adsorption rate was however measured in the presence of KCl compared to the uncleaned latex for a similar ionic

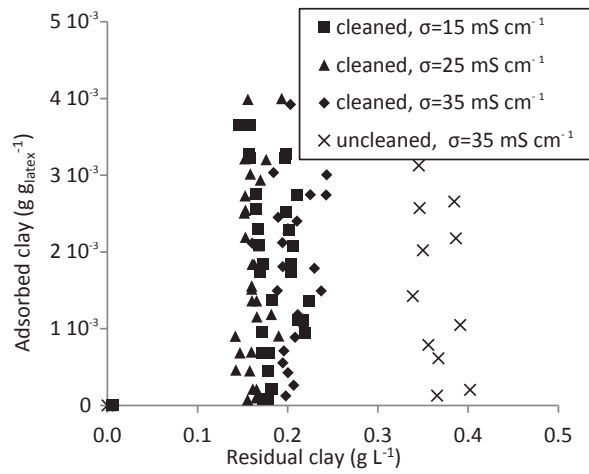


Figure 2.9: Adsorption isotherm of Laponite[®] on polystyrene latex particles (5 wt% solids content and mean diameter 300 nm) measured using ICP-AES analyses of Si, for the uncleaned latex ($\sigma = 35 \text{ mS cm}^{-1}$) as well as cleaned latex adjusted to different ionic strengths by addition of KCl.

strength. It is also noticeable that the majority of the clay introduced is adsorbed on the particle surface whatever the amount of salt introduced with the range of ionic strengths investigated.

It is therefore concluded that during emulsion polymerization, adsorption of clay on polymer particles is due to non-electrostatic attractions with the polymer, possibly dispersion forces, which are predominant when electrostatic repulsions have been weakened by the high ionic strength. The stabilization of polymer particles by adsorbed clay platelets is probably caused by the formation of a rigid crust around the polymer particles that prevent their coalescence. This is the main mechanism put forward for the stabilization of Pickering emulsions [Aveyard et al., 2003] [Chevalier and Bolzinger, 2013]. Moreover, almost full exfoliation of the clay in water is demonstrated, so that multilayer formation on the surface of the polymer latex particles is not due to clay aggregation in water, but to progressive adsorption to the polymer particles surface. The results for the cleaned latex can be compared to the QCM experiments described above (similar ionic strength). For the clay concentration of 2 g L^{-1} , similar results were obtained by QCM and ICP: an adsorbed

amount of clay of $1.5 \times 10^{-3} gm^{-2}$ (corresponding to 60% surface coverage). For the clay concentration of $10 g L^{-1}$, the adsorbed amount of clay measured by QCM was lower, $4 \times 10^{-3} g m^{-2}$ (160% surface coverage) than by ICP, $1.5 \times 10^{-2} g m^{-2}$ (600% surface coverage). But, in both cases multilayer adsorption was detected.

2.3.2.4 Modeling clay adsorption based on ICP-AES

Different models have been proposed in the literature to describe adsorption phenomena. The Langmuir isotherm was first developed to describe gas-solid adsorption, and assumes monolayer adsorption with no lateral interactions or steric hindrance between the adsorbed molecules [Langmuir, 1916]:

$$\frac{q}{q_m} = \frac{K_S C_{eq}}{1 + K_S C_{eq}} \quad (2.2)$$

where C_{eq} ($g L^{-1}$) is the equilibrium solution concentration, q ($mg m^{-2}$) the surface density of adsorbed species, q_m ($mg m^{-2}$) the adsorbed amount at the plateau (maximum surface density for monolayer coverage) and K_S ($L g^{-1}$) the associated equilibrium constant.

For multilayer adsorption, the Brunauer–Emmett–Teller (BET) isotherm is the most widely used [Brunauer et al., 1938]. It allows describing monolayer and multilayer adsorption behaviors. The concept of the theory is an extension of the Langmuir theory under the additional hypothesis that molecules can also physically adsorb by binding to already adsorbed molecules, resulting in the formation of multilayers with no limit regarding the number of layers. This model was originally developed for gas phase adsorption, taking the following form:

$$\frac{q}{q_m} = \frac{cx}{(1-x)(1-x+cx)} \quad (2.3)$$

where x is the ratio of the partial pressure of the adsorbate to its saturation partial pressure at the system temperature and q_m is the surface density of adsorbed species for a hypothetical monolayer at full coverage. c is the BET constant defined as $c = \exp\left(\frac{E_1 - E_N}{k_B T}\right)$ where E_1 is the heat of adsorption for the first layer and E_N is that for the second and higher layers. The BET model was then applied

Table 2.1: Parameters of the BET isotherm model applied for the adsorption of Laponite[®] on polystyrene particles (cleaned and uncleaned latexes).

Parameter	Uncleaned latex	Cleaned latex
$q_m(mg\ m^{-3})$	6.0	8.0
$C_s(mg\ L^{-1})$	3.9×10^2	8.4×10^3
c	0.3	3.5
K_S	9.2×10^{-4}	3.9×10^{-4}
K_L	2.8×10^{-3}	1.1×10^{-4}

to liquid phase adsorption by substituting the partial pressure of the adsorbate by its concentration in the liquid phase [Ebadi et al., 2009] [Prestidge et al., 2004]. Using equation 2.3 with $x = \frac{C_{eq}}{C_S}$ and C_S is taken as an adjustable parameter, the equation has three degrees of freedom (q_m, c, C_S) to be identified by regression to the experimental data. The BET isotherm was used to model the adsorption in this system as it is well-suited to account for multilayer adsorption. The fitted models' parameters are shown in table 2.1 and the modelling results are superimposed to the experimental data in figure 2.8. It can be seen that the model fits very well to the experimental data.

In order to be able to estimate the adsorption energies corresponding to the different layers in adsorption from the liquid phase besides substituting the partial pressure of the adsorbate by the liquid phase concentration, Ebadi et al. [Ebadi et al., 2009] expressed the BET constant c as the ratio of the equilibrium constants of the adsorption equilibria for the first layer and the higher layers: $c = \frac{K_S}{K_L}$, which leads to the following equation [Ebadi et al., 2009] [Prestidge et al., 2004]:

$$\frac{q}{q_m} = \frac{K_S C_{eq}}{(1 - K_L C_{eq})[1 - K_L C_{eq} + K_S C_{eq}]} \quad (2.4)$$

where K_S is the adsorption equilibrium constant of the 1st layer and K_L the adsorption equilibrium constant of upper layers. Upon the assumption $c = \frac{K_S}{K_L}$,

which might be argued, the estimated K_S and K_L parameters in our experiments are shown in table 2.1. It can be seen that the binding constant of Laponite[®] to the uncleaned latex surface, K_S , is 3 times lower than the binding constant of Laponite[®] to the adsorbed Laponite[®] layers, K_L , showing that the formation of multilayers takes place by means of stronger interactions in the upper layers than for the first layer contacting polystyrene. The order of K_S and K_L is reversed in the case of cleaned latex. K_S and K_L are both higher for the uncleaned latex than the cleaned one, indicating stronger adsorption to the uncleaned latex. Indeed electrostatic repulsions acting against adsorption are stronger for the salt-free cleaned latex. For the same reason, the clay concentration at the onset of multilayer formation by surface aggregation is also lower for the uncleaned latex than for the cleaned one. The ratio of the binding constants to the uncleaned and to the cleaned latex provides an estimate of the electrostatic contribution to the adsorption. Such ratio was 2.4 for the first layer and 25 for the higher layers, showing that the electrostatic phenomena give a larger contribution to the clay-clay than to the clay-polystyrene interactions in the adsorbed layer.

2.4 Conclusions

Laponite[®] was found to play an important role in Pickering emulsion polymerization of styrene. It not only ensures stability of polymer particles and determines the number density of produced particles during the nucleation period, but it also controls the reaction rate. In seeded experiments, Laponite[®] ensures effective stabilization whatever the clay content, and no further nucleation of particles occurred even for very high clay concentrations. In order to illustrate the role of clay and its partitioning between water and the surface of the polymer particles, different analysis techniques were used: QCM-D, conductimetry and ICP-AES. Using pure polystyrene, the three methods demonstrated that non-electrostatic attractions between the clay and polystyrene could overcome electrostatic repulsions in order to allow adsorption. Interestingly, multilayer adsorption of platelets on the polymer surface was demonstrated. ICP-AES measurements were also conducted on

uncleaned latex, to mimic the emulsion polymerization conditions. A higher adsorption of clay on the polymer particles was measured in this case, indicating an effect of ionic strength on adsorption due to its screening of the clay surface charges. This was confirmed by adjusting the ionic strength of a series of cleaned latexes by adding different amounts of KCl, to reach an ionic conductivity similar to that of the uncleaned latex containing sulfate ions. TEM and EDS analyses of clay-armored particles synthesized via surfactant-free emulsion polymerization showed that the clay was adsorbed as multilayers on the polystyrene particles, leading to a thick shell. These results show that any added clay adsorbs on the polymer particles and the concentration in the aqueous phase remains constant, preventing further nucleation of new polymer particles by the presence of clay in the suspension during seeded emulsion polymerization experiments. The adsorption behavior was satisfactorily modelled using the BET isotherm, which confirms the hypothesis of multilayer adsorption with cooperative binding. The developed adsorption model will be of use for modelling and understanding the whole polymerization process.

2.5 Supporting Information

2.5.0.5 Dispersion of Laponite RDS in water

Investigation of Laponite[®] RDS dispersion in water was studied by DLS, conductimetry, image analysis of TEM as well as cryo-TEM. Laponite[®] RDS was used as received, without elimination of absorbed water as it was to be dispersed in water throughout the work, but the water content was evaluated experimentally to be 10 wt% (the value announced by the supplier was 8 wt%) and taken into account in the calculations.

2.5.0.6 Conductivity

Due to the high ionic activity of clays, the dispersion was first monitored using conductimetry. Note that exfoliated platelets are expected to give a larger contribution to the conductivity than non-exfoliated ones that share interlayer Na^+ ions of lower mobility. In addition, aging is expected to contribute to the conductivity increase due to leaching of Mg^{2+} and Li^+ ions. The clay powder (2 wt%) was dispersed in water under magnetic stirring at 400 rpm and the resulting dispersion was monitored over 4 days. It was observed that the conductivity reached a high value of around 2.1 mS cm^{-1} in few minutes and stayed at this value over 4 days with no drift. Shahin [Shahin and Joshi, 2012] observed similar stability over 8 days for a 2 wt% Laponite[®] RD dispersion, but the conductivity was lower in their case (0.6 mS cm^{-1}) as no peptizing agent was used, and the dissolution dynamics were not shown. Based on these results, for the characterization studies, the clay was dispersed during 12 h at ambient temperature and used within 24 h to avoid aging. For polymerization reactions, the clay was dispersed during 1 h, and used directly. DLS indicated a stable hydrodynamic diameter of 35 nm after 1 h dispersion at pH = 8.9.

2.5.0.7 Cryo-TEM

Cryo-scanning electron microscopy (cryo-TEM) was performed in a FEI QUANTA 250 FEG scanning electron microscope at the “Centre Technologique des Mi-

crostructures" (CT μ) at the University of Lyon (Villeurbanne, France), at an acceleration voltage of 15 keV. The specimen was first mounted on an appropriate holder, which was itself mounted onto a freezing/vacuum transfer rod. The sample was plunge-frozen in slushy nitrogen and then transferred under vacuum in the cooled stage of the cryo-TEM preparation chamber. The preparation chamber was evacuated by a rotary pump. Finally, the gate valve between the preparation chamber and the SEM was raised, and the specimen was transferred in the cooled stage of the SEM before observation. For this study, dispersions of clay in water were prepared under magnetic stirring at 400 rpm during 12 h in a 1 L closed bottle.

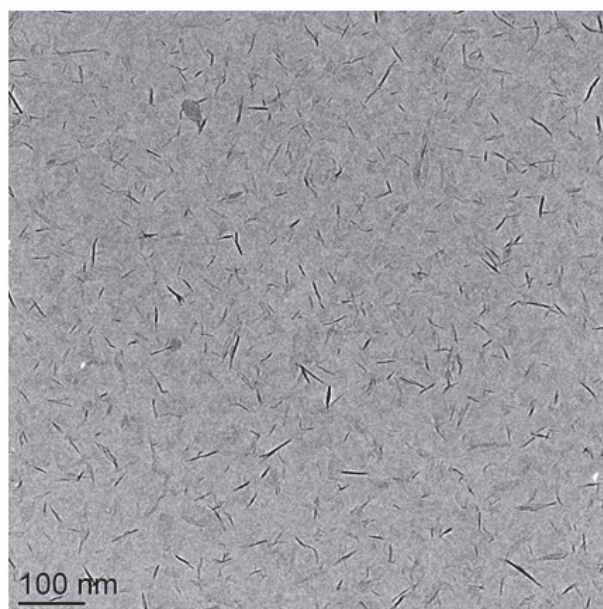


Figure 2.10: Cryo-TEM image of Laponite[®] platelets (obtained by freezing 1 wt% clay dispersion in water), with a selected line for image analysis, scale bar = 100 nm

In figure 2.10, the rim of the platelets can be seen as sticks. Thicker sticks might indicate the presence of stacks of platelets, but single platelets are the most frequent elementary unit. The clay can therefore be assumed mainly exfoliated in water, though the presence of few aggregates was detected.

2.5.0.8 TEM

TEM analysis was also used to investigate clay exfoliation. A number of works assumed that the platelets do not reform stacks after drying in TEM [Thompson and Butterworth, 1992] [Leach et al., 2005] or in other measurement techniques requiring dried samples, such as atomic force microscopy or X-ray scattering [Balnois et al., 2003]. As Laponite[®] RDS contains a peptizing agent, the electrostatic interactions between the anionic basal faces and the cationic charges of the rims were neutralized, and it can be presumed that the state of aggregation of the clay particles does not change during drying the samples on the TEM grid before observation.

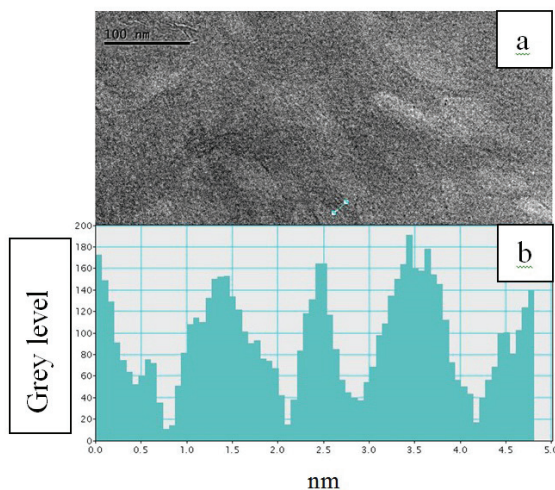


Figure 2.11: a) TEM image of Laponite[®] platelets (obtained by drying 1 wt% clay dispersion in water), with a selected line for image analysis, scale bar = 100 nm. b) Grey level profile as a function of the distance (nm) based on image analysis along the selected line.

TEM images of a dried 1 wt% Laponite[®] dispersion are shown in figure 2.11. Individual platelets can be seen as well as ordered stacks and unordered aggregates of platelets, again with single platelets being the most frequent elementary unit. The number of platelets in ordered stacks was low: 2 to 6 at maximum. Similar trends were found in the literature, but using bare Laponite[®]

without peptizing agent. For instance, light scattering studies of Laponite[®] RD (contains no peptizing agent) revealed doublets, triplets and quadruplets in significant amounts [Rosta and von Gunten, 1990]. In another study, 1H NMR estimated an average number of platelets in a stack of 4.5 (Laponite[®] grade was not indicated) [Fripiat et al., 1982]. Using light scattering, mainly individual disks with some oligomers and a small fraction of very large aggregates were detected [Nicolai and Cocard, 2000].

In order to estimate the individual platelet thickness as well as the interlayer distance in a stack, TEM images were analyzed using the Digital Micrograph software (figure 2.11 b). A zone where several ordered stacks are present was chosen. Image analysis is based on distinguishing the grey level over one dimensional 5 nm distance. Figure 2.11 b indicates the brightness level in the region of interest: High y-axis values are related to voids (no clay or interlayer space) while low values are related to dark pixels, indicating the presence of clay platelets. From this profile, the Laponite[®] platelet thickness was estimated to be 0.90 nm and the interstitial layer thickness around 0.35 nm (corresponding to one-two intercalated water, which is close to the well-known value of 0.30 nm [Nicolai and Cocard, 2000]). These values are consistent with other analysis techniques reported in the literature, such as 1H NMR giving 2.2 water layers meaning an interlayer of 0.75 nm between Laponite[®] sheets (the commercial grade was not indicated) [Fripiat et al., 1982]. For Laponite[®] RD platelets, atomic force microscopy indicated possible ellipsoidal shapes of the platelets of 1 nm height and major and minor radii of 24 ± 6.9 nm and 16.8 ± 4.9 nm respectively, which was in agreement with X-ray scattering measurements and crystallographic data [Balnois et al., 2003].

Chapter 3

Laponite comparison in Pickering emulsion polymerization of styrene

*“ All things are either good or bad
by comparison ”*

Edgar Allan Poe

The research described in this Chapter has been submitted in Langmuir
10.1021/acs.langmuir.6b01080

Abstract : In this work, investigation of four different grades of Laponite[®] is done. First of all, the adsorption isotherm of the different clays is studied using inductively coupled plasma-atomic emission spectroscopy. It was found that the different clays adsorb on the surface of polymer particles forming multilayers under the considered ionic strength (mainly due to the initiator charges). Second, the effect of the clay type and concentration on the number and size of nucleated as well as the reaction rate was studied. While all the clays adsorb similarly on the surface of polymer particles, they do not have the same effect of stabilization. Laponite[®] JS had the lowest stabilization efficiency. Laponite[®] RDS and S482 had almost the same behavior, where increasing the clay concentration allowed the increase in the number of particles without leveling off. Laponite[®] XLS was found to give the same particles size and number as Laponite[®] RDS and S482 at low clay concentrations but it attains a limit in the number of nucleated particles at higher concentrations indicating a kind of saturation.

3.1 Introduction

In surfactant-free heterophase polymerizations known as “Pickering emulsion polymerization”, the adsorbed clay platelets stabilize the dispersion of polymer particles. It is therefore worth investigating to evaluate the partitioning of the platelets on the polymer and the effect of the clay on the reaction rate and polymer properties.

It is worthy to mention that in a number of papers in the literature, the grade of Laponite[®] is not specified and therefore their classification was not evident. Nevertheless, Laponite[®] RD was the frequently used in emulsion or mini-emulsion polymerizations or for the formation of gels. In this work, four grades of clay are investigated: Laponite[®] RDS, S482, XLS and JS, in emulsion polymerization free of any other surfactant. Note that the letter S signifies that a peptizing agent is included in the powder in order to avoid gel formation when dispersing the clay in water.

3.2 Materials and Methods

3.2.1 Materials

The monomer, styrene (Acros Organics, 99% extra pure, stabilized) was stored in a fridge until used. Potassium persulfate (Sigma-Aldrich, minimum 99%) was used as initiator. Deionized water of 18 $M\Omega cm$ resistivity was used throughout the work. Stabilization was ensured using on the four Laponite[®] clays : RDS, XLS, JS and S482, from Rockwood additives. Three grades of Laponite[®] were chosen among the temporary sol forming grades, that are Laponite[®] RDS, XLS and JS. These clays can be well dispersed below 10 wt% in water. While Laponite[®] S482 is used as permanent sol forming grade and can reach 30% of solids content in water.

All used clays are in powder form. They all contain the peptizing agent tetrasodium pyrophosphate ($Na_4P_2O_7$) preventing the thixotropic gel structure. The mean chemical composition of clays is presented in Table 3.1 leading to the following chemical formula [Balnois et al., 2003] [Saunders et al., 1999]:

$$Na_{0.7}^+ \left[(Si_8Mg_{(6-x)}Li_xF_y)O_{20}(OH)_{(4-y)} \right]^{-0.7} \quad (3.1)$$

Table 3.1: Chemical composition for the four Laponite[®] grades

Chemical composition (dry basis)	Laponite [®] RDS	Laponite [®] XLS	Laponite [®] S482	Laponite [®] JS
SiO_2	54.5	54.5	ns	50.2
MgO	26.0	26.0	ns	22.2
Li_2O	0.8	0.8	ns	1.2
F	0	0	ns	4.8
Na_2O	5.6	5.6	ns	7.5
P_2O_5	4.4	4.1	ns	5.4

ns = non specified

Besides, Laponite[®] powder contains up to around 8 wt% water (see Table 3.2) which should be either eliminated before weighing (by heating) or taken into con-

sideration in the calculation of concentrations. In the powder form, the crystals share interlayer Na^+ ions forming stacks.

Table 3.2: Physical properties for the four grades of Laponite[®]

Typical properties	Laponite [®]	Laponite [®]	Laponite [®]	Laponite [®]
	RDS	XLS	S482	JS
Surface Area (m^2g^{-1})	330	330	370	300
Loss in ignition (%)	8	8.2	ns*	8.7
Bulk density (kgm^{-3})	1000	1000	1000	950

3.2.2 Laponite[®] dispersion in water

The clay particles were gently dispersed in water as non-aggregated elementary particles. Indeed, dispersion of clays in water (without latex) was investigated by different methods (see Chapter 2). Conductimetry indicated full dispersion in 1 hour and no aging via the release of lithium and magnesium ions after 4 days at ambient temperature, indicating the time period during which the non-aggregated dispersion can be safely used for polymerization.

3.2.3 *Ab initio* Polymerizations

Reactions were carried out using the reactor set-up and protocol described in chapter 2. The only difference here, is that the reaction is maintained in interval II for a longer period, which means that semi-continuous monomer addition is started before the depletion of monomer droplets.

3.2.4 Surfactant-free polystyrene seed latex

This seed was done for adsorption analyses. It was prepared batch-wise using 4 g potassium persulfate in 800 mL degassed water in a 1 L reactor. The reaction was carried out with 3 wt% of styrene. The final latex had a mean particle size of 300 nm and was concentrated in a Rotavapor[®] up to 20 wt% solids content. Such

high concentration is required since both the adsorption studies involve diluting the latex with a dispersion of clay.

Characterization of the particle size and Inductively Coupled Plasma - Atomic Emission Spectroscopy (ICP-AES) were used following the description in chapter 2.

3.3 Results and discussion

3.3.1 Investigation of clay adsorption on polystyrene

Figure 3.1 shows that the same adsorption isotherm on polymer particle was obtained for all clay grades. Like in chapter 2, the adsorption isotherms show two distinct adsorption regimes as a function of the clay concentration: a coexistence of adsorbed clay particles and residual particles in aqueous suspension was observed for clay concentrations lower than 0.34 g L^{-1} . Above this clay concentration, the adsorption isotherm was almost vertical, showing that clay platelets in excess to 0.34 g L^{-1} fully adsorbed onto the latex particles. In the dilute regime where clay platelets partition between the latex surface and bulk water, the adsorbed amount was lower than the amount allowing full coverage of the polymer surface. Conversely, in the second regime, the adsorbed amount exceeded the limit of one dense monolayer. Such results strongly suggest that the clay was adsorbed as a monolayer for concentrations lower than 0.34 g L^{-1} but formed multilayers for higher concentrations. Therefore, the residual concentration of clay in water cannot be increased because of complete adsorption on the latex particles. Note that the formation of multilayers is not due to increased aggregated stacks forming in water upon increasing the clay concentration as full dispersion of the clay was demonstrated before the adsorption study using cryo-TEM.

For Laponite® S482 and XLS, the residual clay in water could be as high as 1 g L^{-1} when the introduced clay concentration was low ($< 2 \text{ g L}^{-1}$). Exceeding this concentration, the formation of multilayers on the polymer surface starts and the residual clay in water becomes similar as the other clays (0.34 g L^{-1}) and the same isotherm can be used for all the clays afterwards. Note that all the clay dispersions

used for the adsorption study were found to be well-exfoliated in water using cryo-TEM . So, multilayer formation on the surface of the polymer latex particles is not due to clay aggregation in water, but to progressive adsorption to the polymer particles surface.

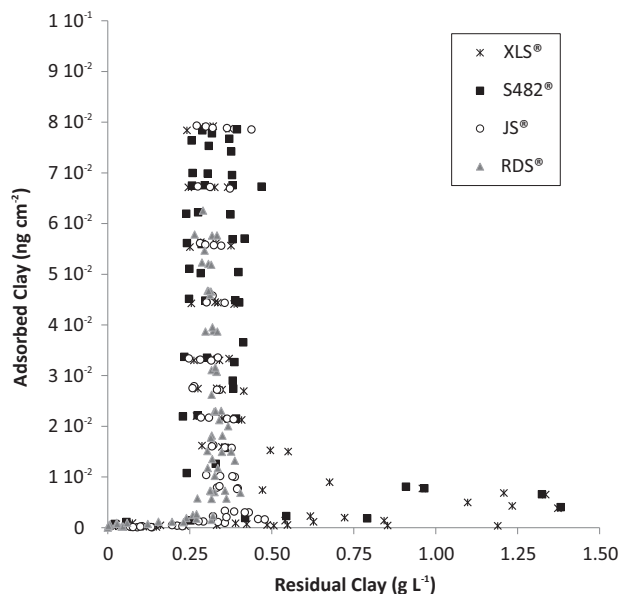


Figure 3.1: Adsorption isotherm of Laponite[®] on polystyrene latex particles (5 wt% solids content and mean diameter 300 nm) measured using Si analysis by ICP-AES.

The Brunauer–Emmett–Teller (BET) isotherm [Brunauer et al., 1938] can be used for multilayer adsorption (chapter 2). It allows describing monolayer and multilayer adsorption behaviors. The concept of the theory is an extension of the Langmuir theory under the additional hypothesis that molecules can also physically adsorb by binding to already adsorbed molecules, resulting in the formation of multilayers with no limit regarding the number of layers.

3.3.2 Investigation of the role of clay in *ab initio* emulsion polymerization

Surfactant-free emulsion polymerization of styrene was carried out in the presence of one of the four grades of Laponite[®] by semi-continuous monomer addition, either in *ab initio* or in seeded modes, in order to infer the role of clay in particles on the

nucleation and stabilization of polymer particles. The objective of these experiments is to investigate the relationships between the clay concentration and the number density of nucleated particles and their stability.

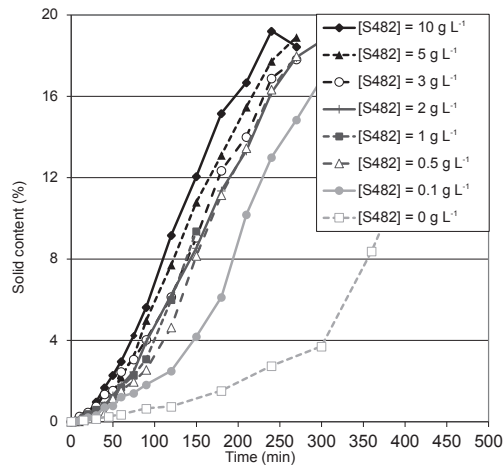
3.3.2.1 Effect of the concentration of Laponite[®] RDS

Investigation of Laponite[®] RDS in *ab initio* semi-continuous emulsion polymerization was presented in chapter 2.

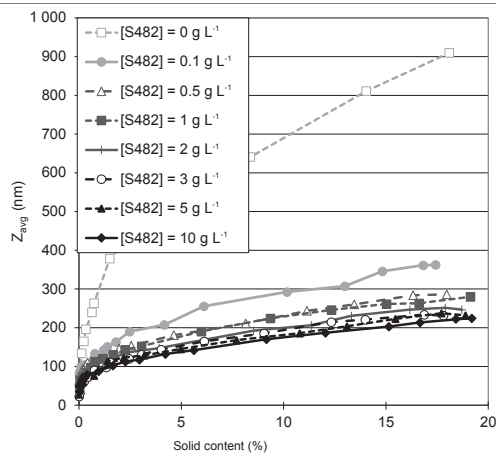
Almost the same results as Laponite[®] RDS were observed for Laponite[®] S482 (figure 3.2). At the beginning, the number of particles increased during the nucleation period (45 to 90 min). Longer nucleation periods were observed for higher clay concentrations. Also, the number of particles increased as a function of the clay concentration. However, at high concentrations, the increase in the particles size slowed down a little. No clear levelling off was though observed. This led to an increase in the reaction rate and the formation of smaller particles at the same solids content.

As a second result, the clay platelets were found to be quite efficient in ensuring particles' stability since the particles number remained constant until the end of the reaction, with SC = 20%, revealing neither coagulation nor renucleation. The stabilization of polymer particles by adsorbed clay platelets is probably caused by the formation of rigid coating around the polymer particles that prevent their coalescence. This is the main mechanism put forward for the stabilization of Pickering emulsions [Aveyard et al., 2003] [Chevalier and Bolzinger, 2013].

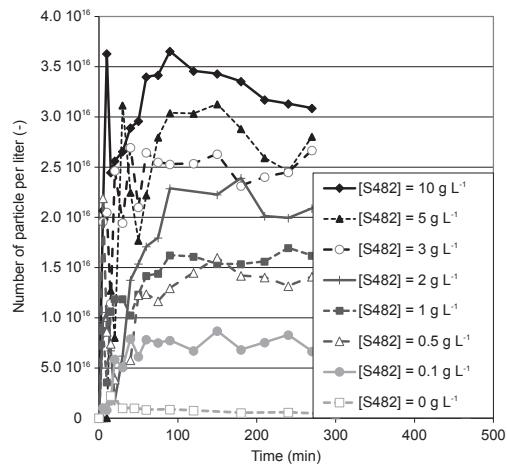
The coverage of the polymer particles surface by clay platelets was calculated as the ratio of the surface area of platelets' faces discs of 25 nm diameter to the polymer particles' area assuming spherical shape and full clay dispersion and were plotted at the beginning and at the end of reaction (figure 3.3). For clay concentrations higher than 0.5 g L^{-1} , the area of platelets was enough to cover the total surface of particles and a significant excess of clay platelets was present at the beginning of the polymerization. As the particles grew, this amount became insufficient to cover the full polymer particles' surface, except for 10 g L^{-1} clay. These results confirm successful clay adsorption on the polymer particles' surface to ensure latex stability



(a)



(b)



(c)

Figure 3.2: Results of the Pickering *ab initio* semi-continuous emulsion polymerization of styrene stabilized with different amounts of Laponite[®] S482

whatever the clay content.

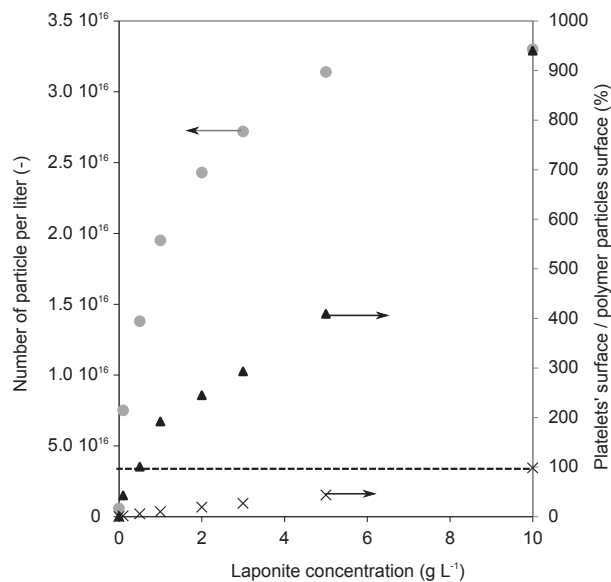


Figure 3.3: Final number of particle (●) and the ratio of platelets surface on polymer surface at the beginning of the reaction ($t=30$ min, ▲) and at the end of reaction (×) for the Pickering emulsion polymerization of styrene with Laponite[®] S482

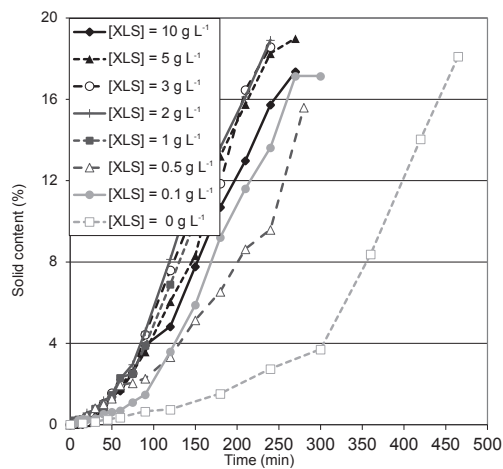
3.3.2.2 Effect of the concentration of Laponite[®] XLS

Figure 3.4 shows the results of *ab initio* emulsion polymerization using different concentrations of Laponite[®] XLS as unique stabilizer.

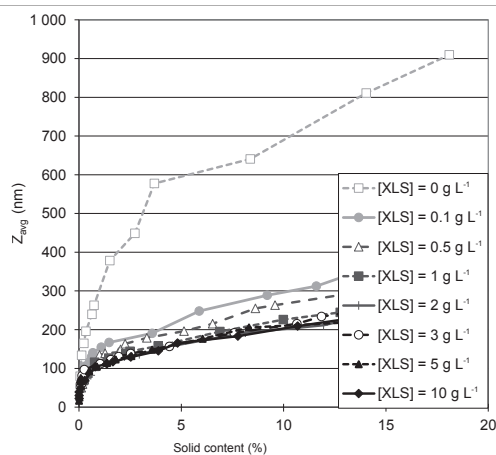
It can be seen that Laponite[®] XLS have the same behavior as Laponite[®] RDS and S482 until a concentration of 2 g L^{-1} (0.05 wt% of clay to monomer). Beyond this concentration the influence of clay concentration fades out to final latexes with 2.10^{16} particles and around 300 nm of diameter. This phasing out was also observed by Bon and coworkers for this clay in Pickering emulsion copolymerization of styrene and n-butyl acrylate at 0.094 of clay : monomer weight ratio [Teixeira et al., 2011].

3.3.2.3 Effect of the concentration of Laponite[®] JS

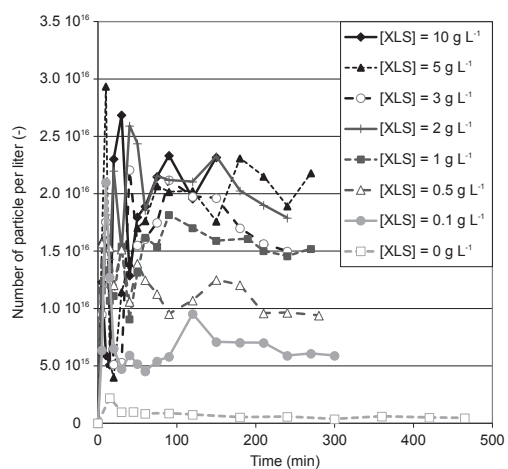
For Laponite[®] JS, a completely different behavior was observed. Like Laponite[®] RDS and S482, the use of an increasing amount of clay led to an increase in the



(a)



(b)



(c)

Figure 3.4: Results of the Pickering *ab initio* semi-continuous emulsion polymerization of styrene stabilized with different amounts of Laponite[®] XLS

number of particles (figure 3.5 and 3.5c) and the formation of smaller particles at the same solid content (figure 3.5b). However, the number of created particles was almost 10 times lower than the other clays, and the obtained latex particles were much bigger (figure 3.5b).

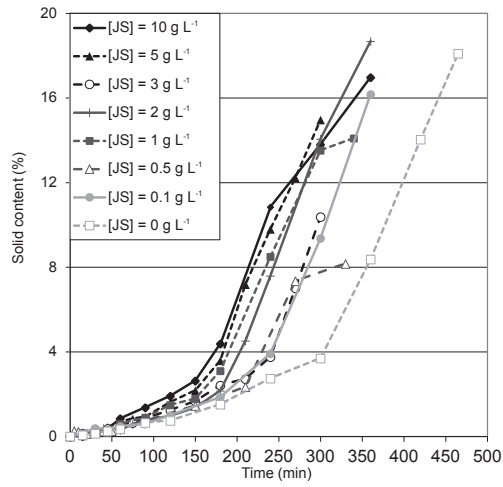
The number of particles was close to the experiment free of clay emulsion polymerization, as the reaction rate. Particle nucleation was slower than the other clays, which extended the nucleation period. Therefore, the batch period (corresponding to interval I and part of interval II, since semi-continuous addition starts during interval II) took longer time, 180 min instead of 60 min for the other clays (figure 3.5a). Therefore, stabilization of Laponite[®] JS seems less efficient. Figure 3.5c shows that a big number of particles are nucleated at the beginning of the reaction (during the first 30 min), that coagulate thereafter and the number of particles stabilizes to a constant number of “mature” particles. This comforts the idea of a nucleative coagulation [Ngai and Bon, 2014].

3.3.2.4 Comparison between Laponites[®]

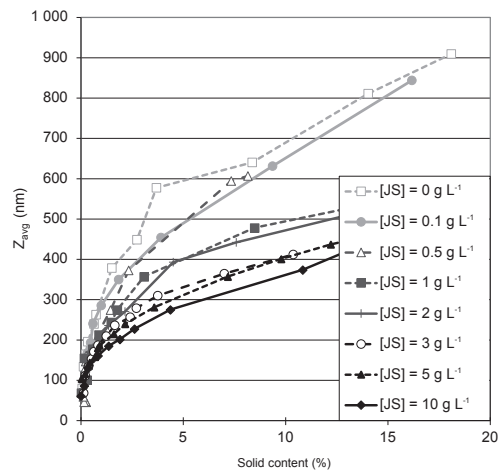
Comparison between the different clay grades can be seen on figure 3.6, for different clay concentrations, 0.5 g L^{-1} (figure 3.6a), 2 g L^{-1} (figure 3.6b), 3 g L^{-1} (figure 3.6c) and 10 g L^{-1} (figure 3.6d).

First of all, according to the adsorption study, section 3.1, almost the same partitioning takes place for all the clays and they all follow the multilayer adsorption mechanism. Therefore, the clay concentration on the surface of particles should be the same for the different clay grades.

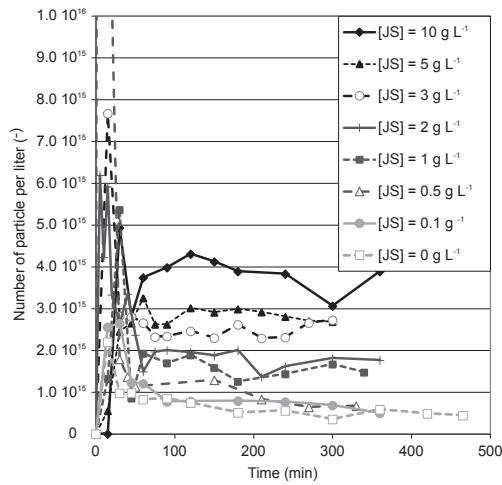
Note also that, the main stabilization by the clay is due to the strong negative face charges (700 elementary charges, due to the release of the Na^+ ions from the surface). Sodium counter-ions Na^+ dispersed in the solution screen the negative charges of the faces forming an electrical double layer composed of a Stern and a diffuse layer. Charges of the rims (produced by protonation of the OH groups with hydrogen atoms of water) are screened due to the presence of a peptizing agent in the different clays (10 wt% tetrasodium pyrophosphate). This decreases the formation of electrostatic bonds between the positively charged rims and the



(a)



(b)



(c)

Figure 3.5: Results of the Pickering *ab initio* semi-continuous emulsion polymerization of styrene stabilized with different amounts of Laponite[®] JS

negatively charged faces, and therefore avoids gelation.

Figure 3.5 shows that Laponite[®] JS leads to the generation of the lowest number of particles at all concentrations. Note that this clay contains fluorine (4.8%) contrarily to the other clays and a higher amount of lithium (1.2% vs 0.8% for the other clays) which should enhance stabilization. Indeed, Saunders [Saunders et al., 1999] reported that clays with higher Li^+ and F^- levels had a higher (more negative) face charge and a lower (less negative) edge charge. However, this clay also contains lower amounts of SiO_2 (50.2% vs 54.5% for the other clays) and MgO (22.2% vs 26% for the other clays). As a result, it seems that as the face charge was lower for this clay. Estimation of the surface charge can be done using DLVO model combined to the population balance equation (as discussed in chapter 6).

Concerning the three other grades, for the two low concentrations (0.5 and 2 g L^{-1}), the number of particles is almost identical for Laponite[®] RDS, S482 and XLS, (much higher than Laponite[®] JS). This indicates similar surface charge for all the grades (the amount of clay on the polymer particles can be considered the same for all the clays as they all follow the same partitioning isotherm). For higher concentrations, the number of particles continues to increase with the clay concentration for Laponite[®] RDS and S482 but stays constant for Laponite[®] XLS. This indicates a kind of saturation of the particles surface by Laponite[®] XLS. As only a small amount of clay could be measured in water during the adsorption study, this indicates that the polymer particles have the same concentration of clay on the surface with the different grades. Two hypotheses can be expressed to explain this effect: (1) packing of the Laponite[®] XLS platelets on the surface is done in a way where only one layer is effectively contributing to the surface charge and the lower layers are screened by the upper layer. That implies the same total surface charge and so the same stabilization with one clay layer or more. (2) Interaction of the platelet-platelet with the Laponite[®] XLS grade is much weaker than platelet-polymer interaction, so multilayer is possible (section 3.1). So Laponite[®] adsorb on the first layer stabilized polymer particle but Laponite[®] on the upper can easily move on continues phase and back to the polymer particle after coagulation. In this case Laponite[®] on the upper layer don't participate to the stabilization (whatever

the repulsion: electrostatic or steric) of the polymer particles that explain the levelling out of the number of particle when Laponite[®] XLS concentration increase.

The electrostatic interaction can explain this observation. Indeed, the stabilization of the polymer particles by the clay can be expressed by two repulsive, steric and electrostatic. The eventuality of a steric stabilization can be dismissed if the clay platelets are strongly adsorbed on the surface because of the same adsorption of each Laponite on polystyrene.

3.4 Conclusion

It was found that the different clays adsorb similarly on the surface of preformed polymer particles under the considered ionic strength. However, the different grades do not have the same stabilizing efficiency. The clay Laponite[®] JS was found the less efficient for stabilizing the latex particles. The global surface charge of this clay should be lower and would be interesting to estimate it using DLVO coupled with the population balance equations. The clays Laponite[®] RDS and S482 are almost similar. Increasing the clay concentration was found to increase the number of particles without leveling off. The clay Laponite[®] XLS has the same behavior as these previous two clays at low clay concentrations. This indicates that, for the three clays, individual platelets have the same surface charge. But, a kind of saturation is observed for Laponite[®] XLS at higher concentrations. Indeed, the nucleated number of particles reaches a limit at a clay concentration of about 3 g L^{-1} . Increasing further the clay concentration does not affect the particles number. As the concentration of all clays on the particles surface is the same, this could be explained by different arrangements of the platelets, where only the upper layer is contributing to the stabilization and the charges of lower layers are screened or hidden by the first upper layer.

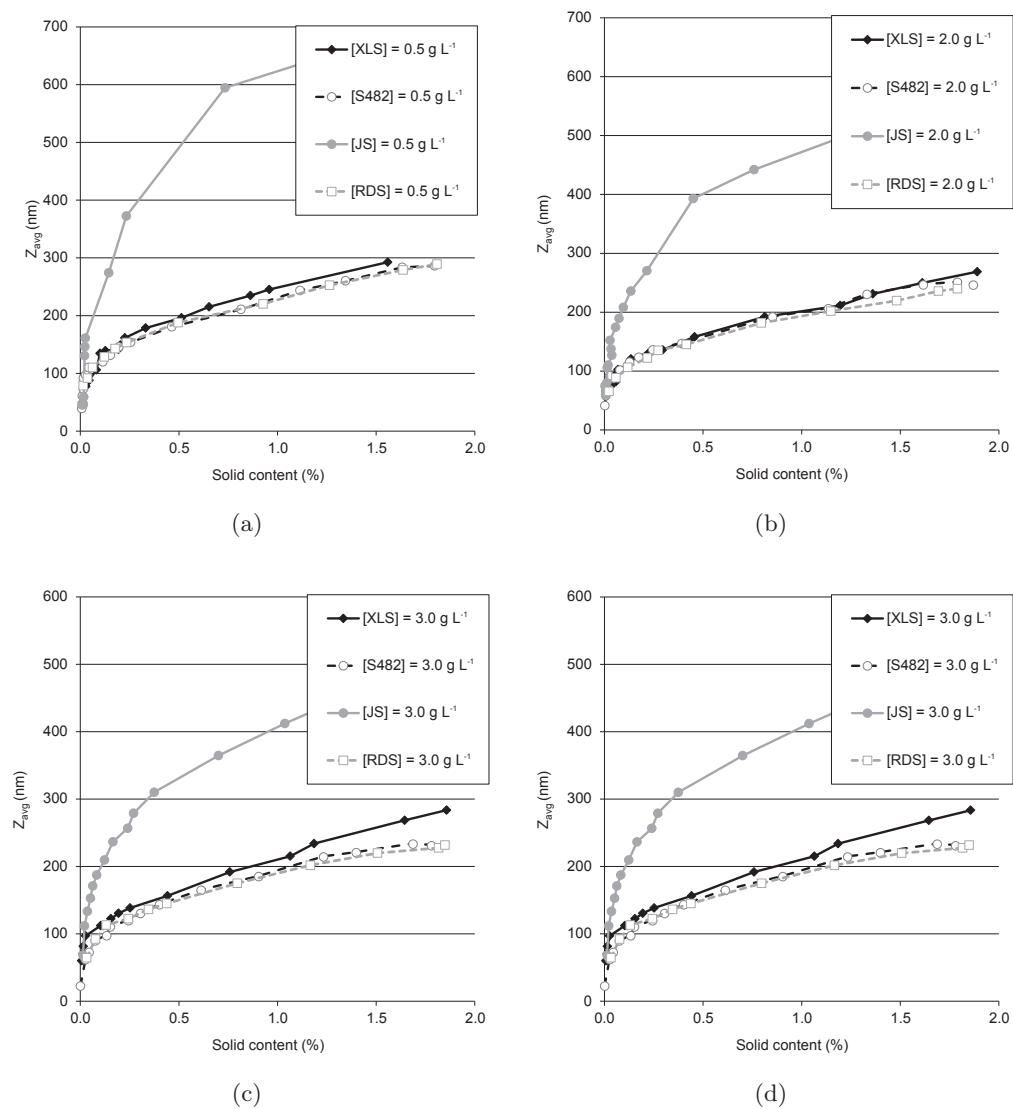


Figure 3.6: Comparison of the Pickering *ab initio* semi-continuous emulsion polymerization of styrene stabilized with different amounts of Laponite®: (a) 0.5 g L^{-1} (b) 2 g L^{-1} (c) 3 g L^{-1} (d) 10.0 g L^{-1}

Chapter 4

Preliminary experimental observations

*“ knowledge is acquired through
experience everything else is just
information ”*

Albert Einstein

Abstract : This part contains all the preliminary results needed to better understand the emulsion polymerization of styrene stabilized with Laponite[®] RDS. All these experiments are needed for the reflection about modeling of Pickering emulsion polymerization but there are not so important to take part to a whole chapter. In other words, the presented experiments in this chapter are necessary to validate some assumption made in the next chapters. Specifically about the mixing effect in order to neglect the orthokinetic coagulation in the coagulation model. The effect of monomer concentration was also investigated to confirm that emulsion polymerization occurred during reaction. This was already noticed with the results of the mixing effect. Reactions were also carried out to check the effect of initiator on the homogeneous nucleation. Different processes of polymerization were noticed with the previous study. Monomer flow rate during semi-continuous Pickering emulsion polymerization was found to play an important role. An increasing of the flow did lead simply to an increasing of the reaction rate. The condition of the reaction play an important role, indeed reaction under starve condition are faster and lead to the same latex (in term of particles size and particles number). A too high monomer flowrate allowed the reaction to come back in phase II and the reaction rate was found smaller. Same conditions were found with conventional emulsion polymerization with sodium dodecyl sulfate. This enhance of reaction is not specific to Pickering emulsion polymerization.

4.1 Introduction

4.2 Materials and Methods

The materials, reactor setup and characterizations of the polymerization were presented in chapter 2. Methods of each reaction were defined before each part. Either Laponite[®] RDS (Rockwood additives) or sodium dodecyl sulfate (SDS) from Sigma Aldrich was used as stabilizers for this study.

4.3 Results and discussion

4.3.1 Effect of mixing

The objective of these experiments is to investigate the effect of stirring rate in emulsion polymerization of styrene stabilized by clay, which is named in this work “Pickering emulsion polymerization”.

Batch reactions were carried out under different stirring speeds. First 800 g of water containing 3 g of clay was stirred for 30 min at ambient temperature and degassed using nitrogen and heating to 70°C in the reactor. This was followed by the addition of 40 g of styrene, heating to 70°C and the polymerization was initiated by adding 1.6 g of potassium persulfate.

Figure 4.1 shows the results of a series of *ab initio* batch experiments with different stirring rates. No particular differences can be noticed in the whole process. The obtained particles size and number are the same under the different stirring speeds (figure 4.1a and 4.1c), which leads to the same reaction rate (figure 4.1c and 4.1d). This indicates that dispersion of monomer droplet in the bulk, (1) does not influence monomer partitioning, that can be considered at equilibrium; (2) and that not nucleation of monomer droplets is taking place, therefore stirring does not influence the nucleation period [Asua, 2002] [Schork et al., 1999]. Therefore, emulsion polymerization process and modelling are considered for the rest of this work.

Nucleating equal number of particles with different stirring speed also means that there is no orthokinetic aggregation. Indeed, an increase of stirring speed enhances the frequency of collisions and the probability of cohesion during collision, and so the orthokinetic aggregation rate, leading to an increase in the particles size and a decrease in their number. This effect was observed only for the highest speed rate (600 rpm) on figure 4.1c and 4.1d. Therefore, for the rest of this work, stirring rate was fixed at 400 rpm, where orthokinetic aggregation can be neglected.

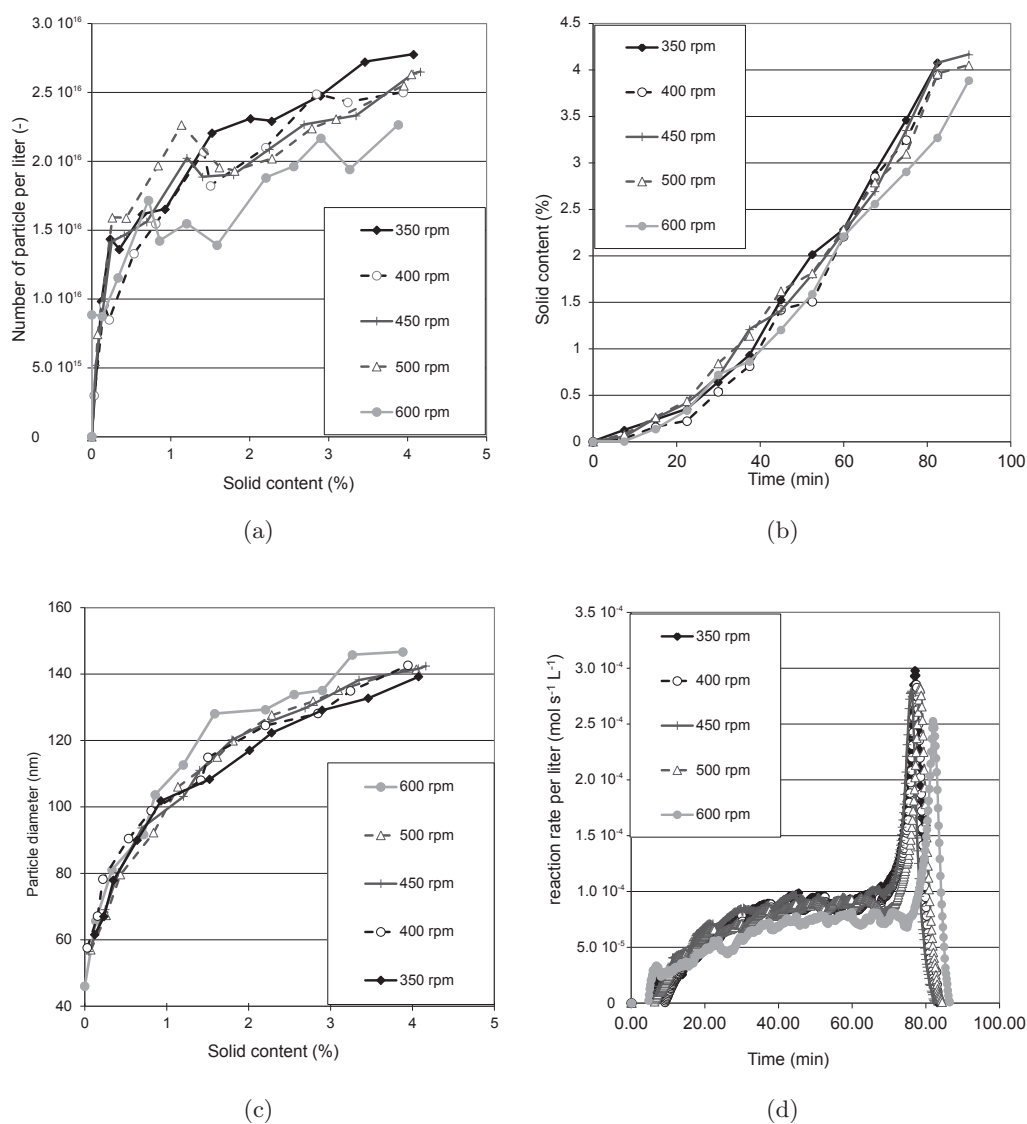


Figure 4.1: Effect of stirring rate on Pickering *ab initio* semi-continuous emulsion polymerization of styrene stabilized with Laponite® RDS (3 g L^{-1}).

4.3.2 Effect of initial concentration of monomer in the bulk medium

The objective of these experiments is to investigate the effect of the initial concentration of monomer on Pickering emulsion polymerization stabilized by clay particles. It is also a way to confirm the emulsion polymerization process.

Batch reactions were considered. The mixture was stirred at 400 rpm. First 800 g of water containing 3 g of clay was stirred for 30 min at ambient temperature and degassed using nitrogen and heating to 70°C in the reactor. This was followed by the addition of different mass of styrene, heating to 70°C and the polymerization was initiated by adding 1.6 g of potassium persulfate.

Figure 4.2 shows the results of a series of *ab initio* batch experiments with different initial concentration of monomer. No particular differences can be noticed on the size and the number of particles (figure 4.2c and 4.2d). The concentration of monomer droplet in the bulk does not influence the nucleation part. While the ratio of monomer/stabilizer is an important parameter of mini-emulsion polymerization [Asua, 2002] [Schork et al., 1999], this ratio was found to have no influence on the number of particle in this system (figure 4.2d). This comforts the use of emulsion polymerization system where nucleation takes place in water and is only affected by concentrations in water (so is independent on the amount and size of droplets).

The reactions end at different solids content (figure 4.2d) depending on the amount of monomer introduced. The Trommsdorff effect (or gel effect) can be observed at around 50% of overall conversion (figure 4.2a). It is due to an increase in the concentration of polymer, and therefore the viscosity inside the particles, leading to a reduction in the mobility of radicals and therefore a decrease in the termination rate coefficient [Ray et al., 1995]. This leads to an increase in the polymerization rate and therefore the heat produced by the reaction. Note that the gel effect has an important impact on the security and polymer properties (leading to an increase in the polymer molecular weight [Tulig and Tirrell, 1981]). Increasing the amount of monomer leads to an increased gel effect as 50% conversion would concern a higher amount of monomer.

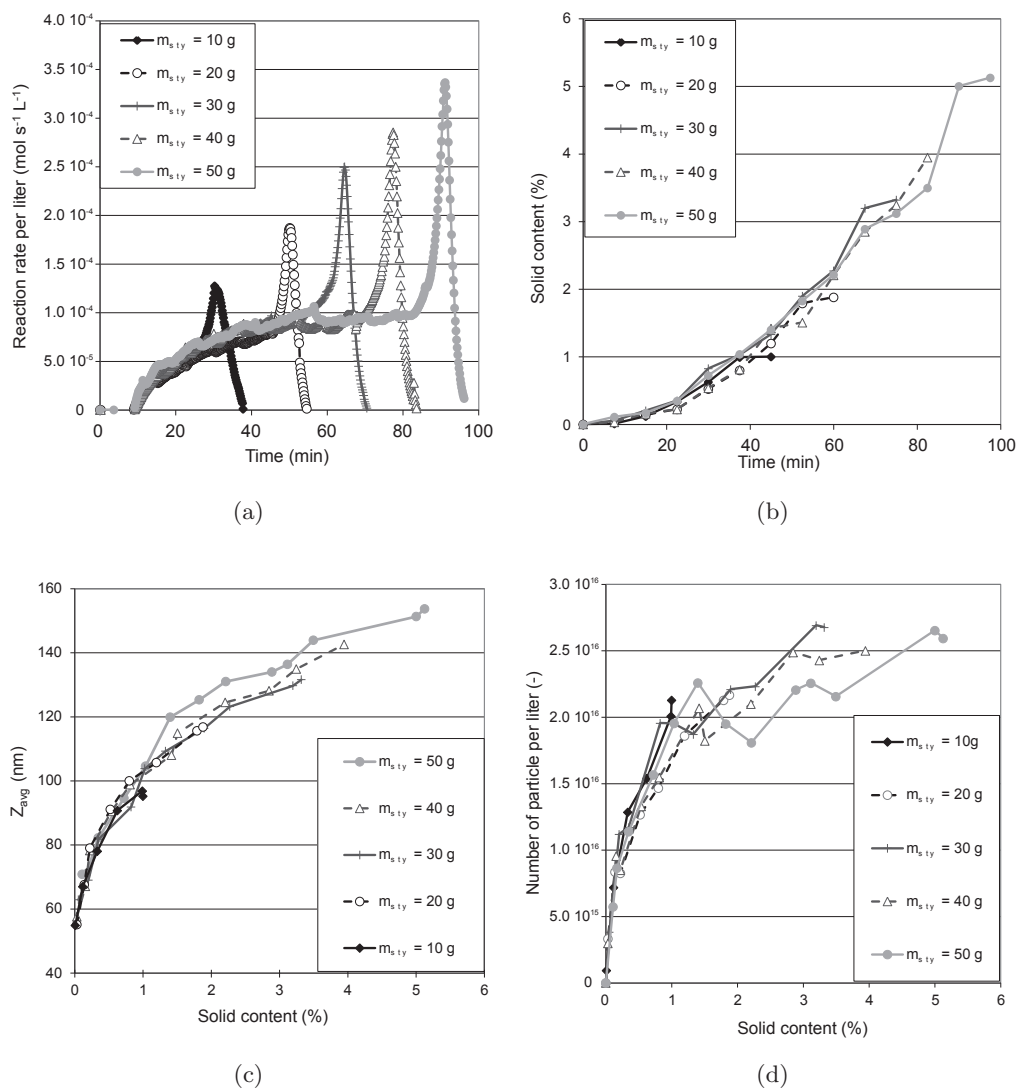


Figure 4.2: Effect of the initial monomer concentration on Pickering *ab initio* semi-continuous emulsion polymerization of styrene stabilized Laponite[®] RDS (3 g L^{-1}).

4.3.3 Effect of initial concentration of initiator

The objective of these experiments was to investigate the effect of the initial concentration of initiator on Pickering emulsion polymerization stabilized by clay particles. A batch period was first considered for particle nucleation followed by a semi-continuous part. First 800 g of water containing 3 g of clay was stirred for 30 min at ambient temperature and degassed using nitrogen and heating to 70°C in the reactor. This was followed by the addition of 40 g of styrene, heating to 70°C and the polymerization was initiated by adding different amount of potassium persulfate. 60 min after the beginning of the reaction, 160 g of monomer was added semi-continuously at a flowrate of 0.02 g s⁻¹.

Figure 4.3 shows the results of a series of *ab initio* semi-continuous experiments with different initial concentration of initiator. First, an increase in the initiator amount leads to a decrease in the particle diameter (figure 4.3c for 2, 3 and 5 g L_{water}⁻¹ of KPS) and an increase in the particles number (figure 4.3d). The greater the amount of initiator, the higher is the production of radicals in the continuous phase (starting by the initiator decomposition followed by propagation with monomer dissolved in the aqueous phase). This leads to the nucleation of a greater number of primary particles by precipitation of oligoradicals, if we assume homogeneous nucleation which is likely to be the case here as no micelle is present and droplet nucleation was precluded. The increase in the number of particles leads to a faster reaction rate (figure 4.3a), and therefore the batch periods ended earlier for a greater amounts of initiator. During the semi-continuous part, the reaction rate was limited by the monomer addition flowrate, which is investigated below.

At the end of the reaction, two reaction regimes can be distinguished: the reaction with gel effect (KPS = 2, 3 and 5 g L_{water}⁻¹) and the reaction without gel effect (KPS = 1 g L_{water}⁻¹). This is due to the lower monomer consumption when a low concentration of KPS was used, which lead to monomer accumulation. The semi-continuous part of this reaction was thus conducted almost totally in interval II while for the other reactions with a higher amount of initiator, the semi-continuous reaction was conducted in interval III.

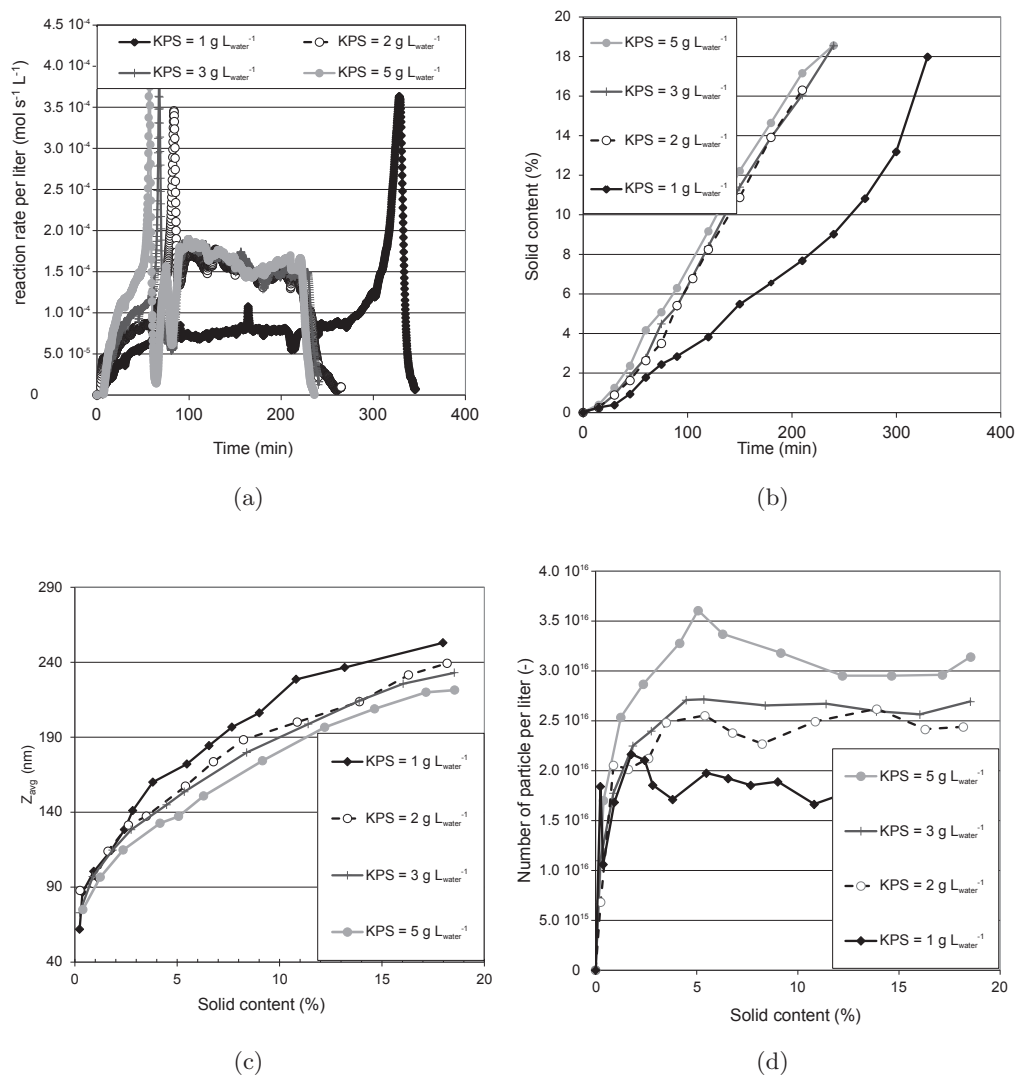


Figure 4.3: Effect of initiator concentration on the Pickering *ab initio* semi-continuous emulsion polymerization of styrene stabilized with Laponite[®] RDS (3 g L^{-1}).

4.3.4 Effect of monomer flowrate

The objective of these experiments was to investigate the effect of the flow rate on Pickering emulsion polymerization stabilized by clay particles. As described above, the reaction rate in the semi-continuous part was found to be limited by the monomer flowrate. This study was carried out to verify this assumption. The same batch period as described above was considered, with 1.6 g of potassium persulfate. 60 min after the beginning of the reaction, 160 g of monomer was added semi-continuously at different flowrates.

Figure 4.4 shows the results of a series of *ab initio* semi-continuous experiments with addition of monomer at different flow rate for the semi-continuous part. At first, monomer flowrate in the semicontinuous part have no influence on the morphology of the final latex, same size (figure 4.4c) and same particles number are obtained. The semi-continuous part plays a role only on the kinetics of the reaction.

If the focus is made on the three low flowrates in the semi-continuous part, it can be seen that a first gel effect takes place at 80 min, and then the reaction rate increases with an increasing monomer flowrate (figure 4.4a). These reaction rates were limited by the monomer addition during the semi-continuous part. Indeed, all the introduced monomer (for example 0.02 g s^{-1}) is immediately consumed, $R_p \approx 2.0 \times 10^{-4} \text{ mol s}^{-1}$ ($\approx 0.02 \text{ g s}^{-1}$ with $MW_{sty} = 104 \text{ g mol}^{-1}$). After the first gel effect, the reaction was carried out under starved condition (phase III) and there was no gel effect at the end of the reaction.

On the other hand, no gel effect occurs at the end of the batch period for the two other reactions, realised with the highest flowrates. The introduction of monomer starts at 60 min and is enough to maintain the reaction in interval II, i.e. with presence of monomer droplets. The conditions are like in a batch mode with 200g of monomer introduced with a high gel effect at the end of reaction.

The monomer flowrate is therefore a good control variable of the reaction time but also the operating security as it allows avoiding the gel effect which might affect the heat of the reaction and the polymer quality.

Interestingly, it can therefore be seen that increasing the monomer flowrate leads

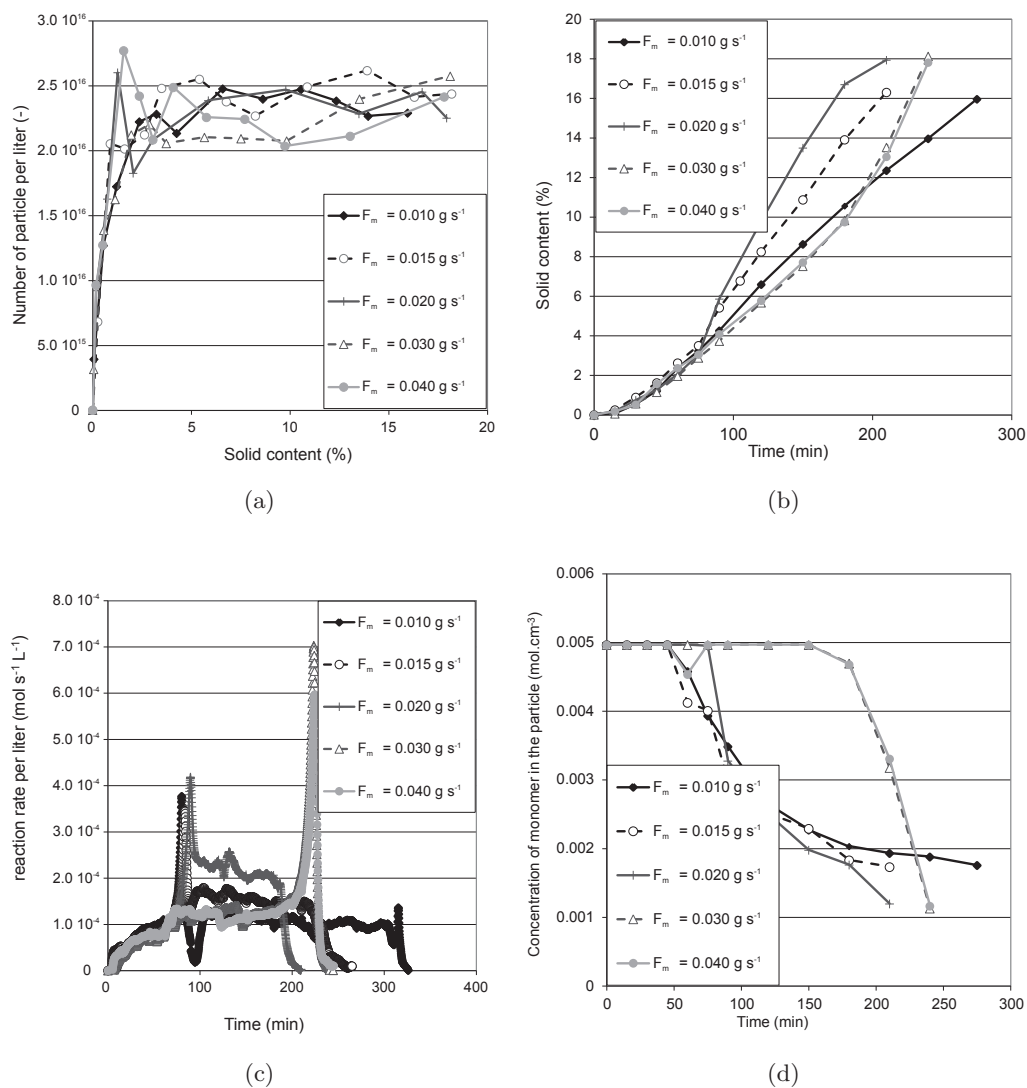


Figure 4.4: Results of the Pickering *ab initio* semi-continuous emulsion polymerization of styrene stabilized with different monomer flowrate.

to an increase in the reaction rate until a limit, where it leads to a drastic decrease in the reaction rate. This limit is related to the saturation of polymer particles. Is this effect specific to Pickering emulsion polymerization systems? This will be studied in the next section with emulsion polymerization using SDS as surfactant.

The different intervals can be better distinguished on the concentration of monomer in the polymer particles (figure 4.5). The total number of particles is superposed on the figure to indicate the end of interval I (the nucleation period). With the monomer flowrate of 0.040 g s^{-1} (figure 4.5a), interval II was ensured at the end of the nucleation. When addition of monomer stopped (150 min), the reaction passed quickly to interval III. A lower monomer flowrate (figure 4.5b) was not enough to keep the reaction in interval II. Therefore, interval III started just after interval II and the concentration of monomer in the polymer particles was always lower than the saturation value.

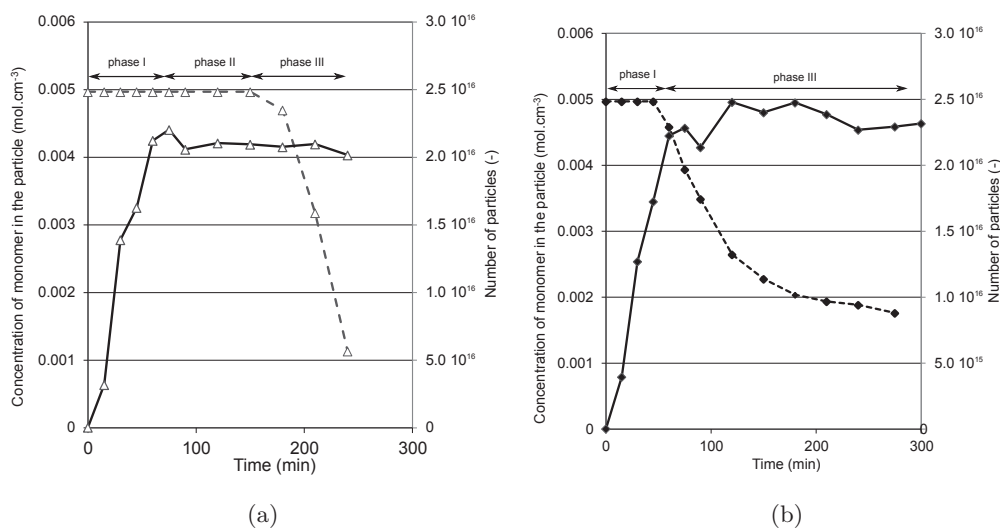


Figure 4.5: Results of the Pickering *ab initio* semi-continuous emulsion polymerization of styrene stabilized with different amounts of Laponite[®] RDS (a) for a flowrate of 0.040 g s^{-1} ; (b) for a flowrate of 0.010 g s^{-1}

4.3.5 Investigation of radical diffusion limitations

The objective of these experiments was to investigate diffusion limitations in conventional emulsion polymerization, namely the possibility of occurrence of a gel effect.

A batch period was first considered for particle nucleation followed by a semi-continuous part. First 800 g of water containing 1 g of SDS was stirred for 30 min at ambient temperature and degassed using nitrogen and heating to 70°C in the reactor. This was followed by the addition of 40 g of styrene, heating to 70°C and the polymerization was initiated by adding 1.6 of potassium persulfate.

Three cases were considered thereafter:

- Case 1: The objective is to maintain the polymer particles under saturation with monomer for a long period (interval II). Therefore, 60 min after the beginning of the reaction (before the depletion of monomer droplets) 160 g of monomer was added semi-continuously at a flowrate of 0.02 g s^{-1} .
- Case 2: The objective is to maintain the reaction in starved conditions for a long period (interval III). Therefore, after the depletion of monomer droplets (as determined by calorimetric estimation of the conversion), which corresponded to about 50% conversion, 160 g of monomer was added semi-continuously at a flowrate of 0.02 g s^{-1} .
- Case 3: The objective is to pass from case 3 to case 2, i.e. first add monomer in starved conditions then in a way to ensure saturation with monomer. Therefore, after the depletion of monomer droplets, 160 g of monomer was added semi-continuously at a flow rate of 0.02 g s^{-1} then after few minutes the flow rate is changed to 0.1 g s^{-1} .

Figure 4.6 shows the results of these the cases of *ab initio* semi-continuous emulsion polymerization stabilized with the surfactant SDS. Cases 1 and 2 confirm the conclusions found when using the clay. In case 1, the addition of monomer starts during interval II and therefore avoids the occurrence of an initial gel effect by the end of the batch period. The concentration of monomer in the polymer particles

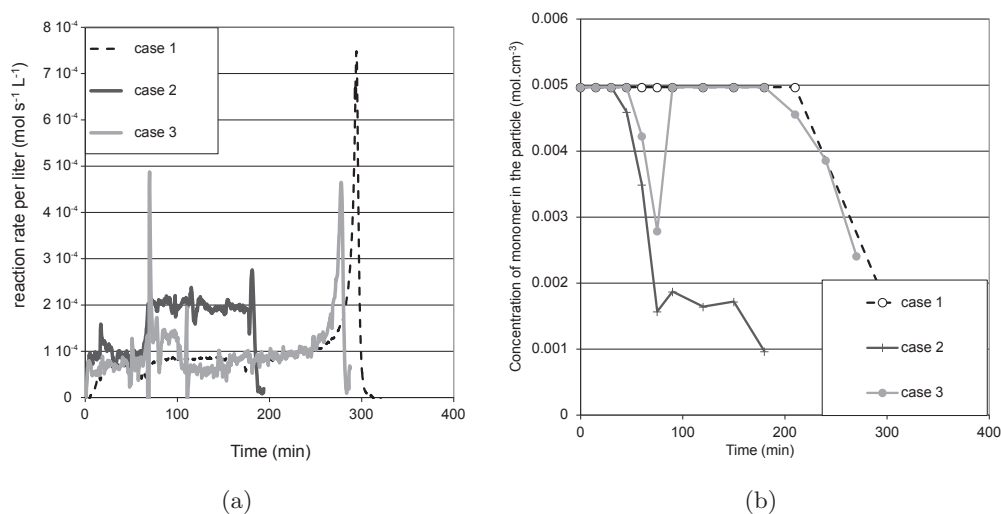


Figure 4.6: *ab initio* semi-continuous emulsion polymerization of styrene stabilized with sodium dodecyl sulfate (1 g) (no clay is used)

stayed at saturation (figure 4.6b) and the reaction was similar to a batch. In case 2, the addition of monomer starts after the start of interval III leading therefore to the occurrence of an initial gel effect at the end of the batch. The flowrate was not enough to stay in phase II, so reaction took place under starved conditions. The reaction rate was limited by the monomer addition flowrate. The reaction was much faster than case 1 (so more interesting) and a small gel effect was observed at the end of the reaction. The increased reaction rate is due to a lower radical diffusion coefficient due to the reduced concentration of monomer in the polymer particles. This leads to a decrease in the termination rate and therefore an increase of total radical number in the particle. However, the higher the addition rate of monomer, the higher is the reaction rate as far as the polymer particles are not saturated with monomer. This is demonstrated in case 3, that passes from case 2 to case 1.

In case 3, monomer addition is started in interval III, ensuring thereby a high reaction rate (equal to the monomer addition flowrate). After few minutes, the monomer flowrate was increased in a way to ensure passing to interval II again. A discontinuity in the reaction rate could be observed as the reaction rate was

proportional to the monomer addition flowrate until the saturation point where it decreased severely (figure 4.6b). It is interesting to notice that the existing models do not describe this phenomenon as diffusion is usually written as a function of the concentration of monomer in the polymer particles. Applying such models, should lead to a decrease in the reaction rate when increasing the monomer flowrate.

In order to avoid diffusion limitations, the modelling study of Pickering emulsion polymerization is realized in interval II. Further investigations in interval III are necessary in order to allow the model to pass from interval II to interval III automatically.

4.4 Conclusion

The experimental work done in this chapter allow to define the operating conditions required for the modelling study, i.e. the stirring speed, initiator concentration, monomer initial concentration and flowrate. Modelling interval II will be considered in this thesis in order to avoid radical diffusion limitations. Also, based on these observations, modelling can be done by decomposing the model of emulsion polymerization (nucleation, growth and coagulation separately).

Part III

Modeling of Pickering Emulsion Polymerization

Chapter 5

Effect of Pickering stabilization on radical exchange in emulsion polymerization

*“ It is more important to know
where you are going than to get
there quickly. Do not mistake
activity for achievement. ”*

Socrates

Abstract: Radical capture and desorption from polymer particles were investigated in semi-continuous Pickering emulsion polymerization systems. The clay concentration is known to affect the particles size and number and therefore the reaction rate. Therefore, it is important to evaluate the impact of the stabilizing layer on radical entry and desorption. The different capture and desorption models were compared during interval II, in conditions that avoid coagulation (nucleation as well). Moreover, this interval reduces diffusion limitations as the polymer particles remain saturated with monomer. This allows using constant values for the coefficients of propagation, termination and diffusion besides constant monomer concentrations in the different phases. Therefore, in this interval, the size of particles changes only due to growth, which is affected by the average number of radicals in the polymer particles (\bar{n}). It was found that for the system underhand, \bar{n} was independent of the surfactant layer and that the observed changes in \bar{n} when increasing the clay concentration were only due to changes in the particle size. Indeed, a model, independent of the clay concentration, could be used to simulate reactions involving different clay concentrations and predict the evolution of the monomer conversion, particle size, and \bar{n} .

5.1 Introduction

Polymer/clay nanocomposites can nowadays be manufactured by in situ free radical emulsion polymerization [Sheibat-Othman et al., 2011]. This implies the production of the composite materials by reacting organic monomers in the presence of pre-formed inorganic colloidal particles [Bourgeat-Lami and Lansalot, 2010] [Bourgeat-Lami et al., 2010]. Laponite[®] was first used in emulsion polymerization in presence of surfactant, after chemical modification of the clay. Such functionalized Laponite[®] was coated with either cationic initiators or monomers through ion exchange, or by the reaction of the edge-hydroxyls with suitable organosilane molecules. Stable colloidal aqueous suspensions of composite particles with diameters in the range 50-150 nm were obtained consisting of a polymer core surrounded by an outer shell of clay platelets [Ruggerone et al., 2009a] [Ruggerone et al., 2009b] [Herrera et al., 2004] [Negrete-Herrera et al., 2006a] [Herrera et al., 2005] [Herrera et al., 2006] [Negrete-Herrera et al., 2007] [Negrete-Herrera et al., 2006b]. It was subsequently shown that bare (non-modified) Laponite[®] particles can be used in emulsion polymerization without addition of surfactant^{12,13}. In such surfactant-free heterophase polymerizations known as "Pickering emulsion polymerization", the adsorption of clay stabilizes the dispersion of polymer particles. However, this adsorption changes the surface property of the polymer particle and its interaction with charged free radicals. The objective of this work is to investigate the impact of the stabilizer layer on radical exchange between the aqueous phase and the polymer particles. Modeling emulsion polymerization systems requires modeling the particle size distribution (PSD), which involves nucleation, coagulation and growth terms. When nucleation and coagulation are not present, the particles size changes only by growth. The growth term depends on the propagation rate coefficient and the concentrations of monomer and radicals in the polymer particles. The propagation rate coefficient is known to be affected by radical diffusion limitations [Soh and Sundberg, 1982] which can be avoided by working under saturation with monomer. Working under saturation with monomer (interval II) also ensures constant monomer concentrations in the water and

polymer phases. Therefore, the growth term becomes only affected by the average number of radicals per particle \bar{n} , which in turn is affected by radical entry and desorption inside the particles. Radical entry. Different mechanisms were proposed to describe radical capture and adsorption. 1) [Smith and Ewart, 1948] first proposed a diffusion-controlled mechanism for radical capture, which assumes that the diffusion of radicals from the bulk phase to the surface of a polymer particle is the rate-controlling step. In this model, the capture rate is proportional to the particle diameter. However, this model was found to yield values that were orders of magnitude larger than the experimental values [Thickett and Gilbert, 2007]. Therefore, a radical capture efficiency term was added to this model by [Ugelstad and Hansen, 1976]. Thereafter, different varieties of the efficiency terms were proposed [Smith and Ewart, 1948] [Ugelstad and Hansen, 1976] [Fontenot and Schork, 1993] [Hernández and Tauer, 2007a] [Nomura et al., 2005] [Coen et al., 1998]. 2) [Gardon, 1968] proposed the collision-controlled mechanism where radical capture was proportional to the particles surface. 3) [A. Penboss et al., 1986] proposed the colloidal model assuming radical entry to be proportional to the particle diameter. 4) [Yeliseyeva and Zuikov, 1977] proposed that the stabilizer layer might hinder radical capture and proposed a mechanism based on stabilizer displacement for radical capture. 5) [Maxwell et al., 1991] then proposed a mechanism where radical capture was conditioned by a critical radical length (z), after propagation in the aqueous phase. The generation of z -mer radicals from $(z-1)$ -mer radicals by a propagation reaction in the aqueous phase is the rate-controlling step and the entry of z -mer radicals is assumed rapid. Radical entry is independent of the particle size in this model. The currently accepted mechanism for radical entry is the propagation-controlled model. The second widely used model is the diffusion-controlled model when combined with radical capture efficiency. The emulsifier layer on the surface of the polymer particles (surface coverage on a particle or its ionic strength) was not found to play a role in radical entry for conventional emulsifiers [Adams et al., 1988] (e.g. electrostatic stabilizer sodium lauryl sulfate, nonionic stabilizer TritonX-405 [Colombié et al., 2000]). However, for some specific cases the stabilization layer was supposed to affect

radical entry which suggested that this layer acted as a barrier for radical entry. This was the case for the steric stabilizer poly(ethylene oxide) nonylphenol (with 30 EO units) [Colombié et al., 2000] [Kusters et al., 1992], the reactive surfactant sodium dodecyl allyl sulfosuccinate [Wang et al., 2001], polymeric surfactants (e.g. electrosteric copolymer of acrylic acid and styrene [Coen et al., 1996], the copolymer of styrene and styrene sulfonate [Cheong and Kim, 1997], poly(acrylic acid) [Vorwerk and Gilbert, 2000] or when the used entering radical was different from the charge of the polyelectrolyte surfactant [Leemans et al., 1998]). Based on these previous results, it appears of interest to determine whether or not the adsorbed layer of clay platelets on the surface of polymer particles acts as a diffusion barrier to the entering radicals and to determine the adapted radical entry model of this system. Note that radical capture concerns radicals issued from initiator decomposition and propagation in water, which are long charged if for instance a persulfate initiator is used. Radical exit. Radical exit, it has been subject to much more debate mainly concerning the competitive reactions inside the particle and the fate of exited radicals. Therefore, the proposed models gained in complexity with time, going from simple diffusion to take into account competitive reactions inside the particle and finally accounting for competitive radicals in the aqueous phase (fate of exited radicals). Note that radical desorption only concerns monomeric radicals, that are small and non-charged, that are issued from the reaction of radical transfer to monomer [Casey et al., 1994] [McAuliffe, 1966]. Therefore, radical desorption is not supposed to be affected by the stabilizer layer and there was no desorption mechanism proposed in the literature that accounts for the stabilizer layer (contrarily to radical capture). This assumption is reasonable and will be assumed in the present work. The desorption models of conventional emulsion polymerization can hence be used in Pickering emulsion polymerization. The objective in studying radical desorption is to determine the adapted desorption model for the present system among those present in the literature, but not to relate it to the concentration of clay on the particles surface. Indeed, these models were usually developed for specific systems (specific monomer solubility, range of particle size and types of surfactants) and no

general model is admitted to be valid independently of the reaction conditions. In this work, Laponite[®] clay is used as stabilizer in surfactant-free Pickering emulsion polymerization. The clay platelets dimension is relatively bigger than conventional surfactants (1 nm in thickness and 25 nm in diameter). Moreover, when dispersed in water, a strongly negative charge (700 elementary charges) appears on their basal faces (due to the release of the Na⁺ ions from the surface) and a weakly positive charge on the rim of the disks (due to protonation of the OH groups with hydrogen atoms of water, for pH < 11) [Tawari et al., 2001] [Ruzicka et al., 2006]. These charges might interact with the charged radicals formed in the aqueous phase and might affect the radical capture rate. The concentration of clay on the polymer particles is estimated based on chapter 2 were the clay was found to adsorb on the polymer particles in multilayers. Semi-continuous Pickering emulsion polymerization of styrene in presence of Laponite[®] was considered in interval II, ensuring no nucleation nor coagulation and flooded polymer particles with monomer. Different clay concentrations were considered.

[Soh and Sundberg, 1982] [McAuliffe, 1966] [Casey et al., 1994]
[Smith and Ewart, 1948] [Ugelstad and Hansen, 1976] [Fontenot and Schork, 1993]
[Coen et al., 1998] [Nomura et al., 2005] [Hernández and Tauer, 2007a]
[Maxwell et al., 1991] [Asua and De La Cal, 1991] [Feeney et al., 1987]
[Yeliseyeva and Zuikov, 1977]

5.2 Materials and Methods

The materials and methods were presented in chapter 2. *Ab initio* semi-continuous reactions were considered, under saturation with monomer.

5.3 Modelling

5.3.1 Polymer particles population balance

The comprehensive particle size distribution model in emulsion polymerization takes into account particle formation by nucleation, growth by polymerization and coag-

ulation mechanisms (Min and Ray [Min and Ray, 1974]):

$$\frac{\partial F(r, t)}{\partial t} + \frac{\partial F(r, t)\mathcal{G}(r, t)}{\partial r} = \mathfrak{R}_n \delta(r - r_{nuc}) - \mathfrak{R}_{coag} \quad (5.1)$$

Where $F(r, t)$ is the number density of particles of radius between r and $r + \delta r$ at time t , $\mathcal{G}(r, t)$ is the growth rate of particle of size r , R_n is the nucleation rate, $\delta(r - r_{nuc})$ is the Dirac delta function which is unity for $r = r_{nuc}$ and zero elsewhere which represents the boundary condition, r_{nuc} is the nucleation radius and R_{coag} is coagulation rate.

As the main objective of this work is to investigate the effect of clay on radical exchange during interval II, without particle nucleation or coagulation, equation 5.1 is resumed to:

$$\frac{\partial F(r, t)}{\partial t} + \frac{\partial F(r, t)\mathcal{G}(r)}{\partial r} = 0 \quad (5.2)$$

The growth rate is given by:

$$\mathcal{G}(r, t) = \frac{dr}{dt} = \frac{k_p \bar{n} [M]_p MW}{4\pi r^2 \rho N_A} = \frac{R_p MW}{4\pi r^2 \rho N N_A} \quad (5.3)$$

Where MW is the monomer molecular weight, ρ is the monomer density, k_p is the propagation rate coefficient, $[M]_p$ is the concentration of monomer in the polymer particles (maintained constant in this study), N_A is Avogadro's number, $N = \int_0^\infty F(r, t) dr$ is the density number of monomer-swollen polymer particles per unit volume of latex and R_p is the polymerization rate per unit volume of latex which mainly proceeds in the polymer particles (i.e. most of the polymer is produced within the polymer particles even though the polymer chains may start in water) [Smith and Ewart, 1948]:

$$R_p = k_p [M]_p \frac{\bar{n}(t)N}{N_A} \quad (5.4)$$

Where $\bar{n}(t) = \frac{1}{N} \int_0^\infty \bar{n}(r, t) F(r, t) dr$. Even though eliminating nucleation and coagulation simplifies equation 5.1 importantly, the growth part is not trivial to model as it depends on $\bar{n}(r, t)$ which requires good estimation of radical entry and desorption as discussed in the following section.

5.3.2 Average number of radicals in the particles

The first quantitative theory for the average number of radicals per particle \bar{n} , was developed by [Smith and Ewart, 1948] based on the model proposed by [Harkins, 1947]. According to this approach, the kinetics of the polymerization in particles is governed by the spread of the monomer in the particles, radical capture into polymer particles, radical desorption from the polymer particles to the aqueous phase and bimolecular radical termination by recombination within the particles. Therefore, the number of particles of size r containing n radicals ($N_n(r)$) can be calculated using the following balance:

$$\frac{\partial N_n(r)}{\partial t} = \rho_e(N_{n-1} - N_n) + k_{des}[(n+1)N_{n+1} - nN_n] + c[(n+2)(n+1)N_{n+2} - n(n-1)N_n] \quad (5.5)$$

where k_{des} is the rate coefficient for radical exit, $c = \frac{k_{tp}}{N_A v_s}$, with k_{tp} the termination rate coefficient and v_s the volume of swollen polymer particles, and rate of radical entry is given by:

$$\rho_e = k_e [R]_w \quad (5.6)$$

with k_e the rate coefficient for radical entry from the aqueous phase and $[R]_w$ the concentration of radicals in the aqueous phase.

The average number of radicals per particle (of size r) is then defined as follows:

$$\bar{n} = \frac{\sum_{n=1}^{n_{max}} n(r) N_n(r)}{N(r)} \quad (5.7)$$

Where $N = \sum_{n=1}^{n_{max}} N_n(r)$ is the total number of particles and n_{max} the maximum number of radicals in a polymer particle.

Smith and Ewart distinguish three polymerization cases depending on the number of radicals per particle, during interval II (i.e. polymer particles are saturated with monomer) [Smith and Ewart, 1948]:

- Case I: The rate of radical desorption is very high compared to the rate of radical capture. The average number of radicals in the particles is much less

than 1.

- Case II: The rate of radical desorption is much lower than the rate of radical capture, at the same time, the termination rate is very high (immediate termination follows the capture of a second radical). In this case, the average number of radicals per particle is 0.5.
- Case III: The rate of radical absorption is high. Several radicals can coexist in a particle. In this case, the average number of radicals in the particles is greater than 1.

Based on this, two limits of the PSD models were defined:

- The zero-one systems: particles may contain only one growing radical as the entry of a second radical into a latex particle results in an instantaneous termination. Therefore, the average number of radicals per particle is significantly smaller than one. In order to model this system, three population balance equations are required: one balance for particles containing no radicals (N_0), one for particles containing a growing polymeric radical (N_1) and one for particles containing a monomeric radical that may exit (N_{1m}). These balances are connected through radical growth, entry or desorption terms. This model is adapted for modeling Cases I and II.

$$\begin{aligned}
 \frac{\partial N_0(r)}{\partial t} &= \rho_e(N_1 + N_m - N_0) + k_{des}N_{1m} \\
 \frac{\partial N_{1m}(r)}{\partial t} &= k_{tr}[M]_p N_1 - (\rho_e + k_{des} + k_p[M]_p)N_{1m} \\
 \frac{\partial N_1(r)}{\partial t} &= \rho_e N_0 + k_p[M]_p N_{1m} - (\rho_e + k_{tr}[M]_p)N_1
 \end{aligned} \tag{5.8}$$

Re-entry of monomeric radicals can be considered by replacing ρ_e by $\rho_e + f_{re}k_{des}\bar{n}$, where f_{re} is a fate parameter expressing the relative importance of re-entry and heterotermination of exited free radicals [Thickett and Gilbert, 2007] [A. Penboss et al., 1986].

- The pseudo-bulk systems: In this type of system, particles contain radicals that can coexist for a significant period (case III). Base on this assumption, equation 5.5 becomes [Ballard et al., 1981]:

$$\frac{\partial \bar{n}(r, t)}{\partial t} = \rho_e - k_{des} \bar{n} - 2c \bar{n}^2 \quad (5.9)$$

Equation 9 is correct when \bar{n} forms a Poisson distribution, which is the case for high values of \bar{n} [Thickett and Gilbert, 2007]. [Stockmayer, 1957] was the first to give an analytical solution for the expression of Smith and Ewart (equation 5.5) assuming steady state of radicals. But, [O'toole, 1965] found that this approach could give physically incorrect results when the rate of desorption of radicals is low. Therefore, he changed the approach of Stockmayer and proposed the determination of \bar{n} from the ratio of the modified Bessel functions:

$$\bar{n} = \frac{h}{4} \frac{I_m(h)}{I_{m-1}(h)} \quad (5.10)$$

with $h = \sqrt{\frac{8\rho_e}{c}} = \sqrt{\frac{8k_e[R]_w N_A v_s}{k_{tp}}}$ and $m = \frac{k_{des}}{c} = \frac{k_{des} N_A v_s}{k_{tp}}$.

[Li and Brooks, 1993] proposed semi-theoretical solutions to this expression:

$$\bar{n}(r, t) = \frac{2H}{m + \left(m^2 + \frac{8H(2H+m)}{2H+m+1}\right)^{1/2}} \quad (5.11)$$

$$\text{with } H = \frac{k_e N_A^2 V_p [R]_w}{k_{tp}} \quad \text{and} \quad m = \frac{k_{des} N_A V_p}{k_{tp}}$$

In the present work, the experimental estimations indicated big particles ($d_p > 200$) and $\bar{n} > 0.5$ (discussed below). Therefore, the pseudo-bulk model will be considered with the Li and Brooks' solution (equations 5.2 and 5.9). In the following section the material balances for radicals in the aqueous phase and the polymer particles are presented.

5.3.3 Aqueous phase reactions

Table 5.1 shows the reaction scheme assumed to take place in Pickering emulsion polymerization involving a water soluble initiator such as persulfates, which is similar to conventional emulsion polymerization.

Table 5.1: Aqueous phase reactions ($i < j_{crit}$)

$I_2 \xrightarrow{k_d} 2I^\bullet$	Decomposition
$I^\bullet + M \xrightarrow{f_I, k_d} IM^\bullet$	Initiation
$IM^\bullet + M \xrightarrow{k_{p1}} IM_2^\bullet$	Propagation
$IM_2^\bullet + M \xrightarrow{k_{p2}} IM_3^\bullet$	
$IM_3^\bullet + M \xrightarrow{k_p} IM_4^\bullet$	
\vdots	
$IM_i^\bullet + M \xrightarrow{k_p} IM_{i+1}^\bullet$	
$IM_i^\bullet + IM_j^\bullet \xrightarrow{k_{tc}} M_{i+j}$	termination by combination
$IM_i^\bullet + IM_j^\bullet \xrightarrow{k_{td}} M_i + M_j$	termination by dismutation
$IM_i^\bullet + M \xrightarrow{k_{fm}} M_i + M^\bullet$	transfer to monomer

Some assumptions are considered in the material balances of radical species in water:

1. Radicals are produced in the aqueous phase through initiator decomposition.
2. The initiation rate coefficient is much higher than the decomposition rate coefficient, and therefore $[IM^\bullet]$ species are limited by initiator decomposition.
3. All radicals may terminate with each other or propagate with monomer dissolved in the aqueous phase.
4. Radical transfer to monomer in the aqueous phase can be neglected due to the low solubility of monomer in water.
5. Only monomeric radicals with one or two monomer units may desorb from particles contributing therefore to the increase in the concentration of radicals in the aqueous phase
6. Radical capture into droplets is negligible due to their lower surface area compared to polymer particles

7. Radical capture into polymer particles concerns only aqueous phase radicals of size $z < i < j_{crit}$, with $z=3$ and $j_{crit}=5$ for styrene [Sajjadi, 2009]
8. A radical can grow in water up to a maximal size of $i=j_{crit}$ after which it precipitates.
9. All chains propagate following the same propagation rate coefficient in the aqueous phase (k_p) except chains with one and two monomer units that are faster (k_{p1} and k_{p2}).
10. No discrimination is done between radical groups originating from initiator decomposition and those produced by transfer to monomer, i.e. $[IM_1^\bullet]_w$ includes desorbed $[M_1^\bullet]_p$ and $[IM_2^\bullet]_w$ includes desorbed $[M_2^\bullet]_p$. This allows reducing the number of equations in the aqueous phase.

Figure 5.1 shows the reaction scheme and the inherent assumptions in the material balances of radicals.

According to the above mentioned assumptions, the following material balance is given for radicals of size 1:

According to the approximation of the Steady state, we can write the following equation for the radicals of size 1 in

$$\frac{d[IM_1^\bullet]_w}{dt} = 0 = 2f_I k_d [I]_w + k_{des} [M_1^\bullet]_p - k_{p1} [M]_w \cdot [IM_1^\bullet]_w - k_{tw} [R]_w [IM_1^\bullet]_w \quad (5.12)$$

Applying the quasi steady state assumption of radicals, gives:

$$[IM_1^\bullet]_w = \frac{2f_I k_d [I]_w + k_{des} [M_1^\bullet]_p}{k_{p1} [M]_w + k_{tw} [R]_w} \quad (5.13)$$

Similarly, the material balances of longer radicals under stationary state hypothesis are:

$$[IM_2^\bullet]_w = \frac{k_{p1} [M]_w [IM_1^\bullet]_w + k_{des} [M_2^\bullet]_p}{k_p [M]_w + k_{tw} [R]_w} \quad (5.14)$$

$$[IM_3^\bullet]_w = \frac{k_{p2} [M]_w [IM_2^\bullet]_w}{k_p [M]_w + k_{tw} [R]_w + \frac{k_e N}{N_A}} \quad (5.15)$$

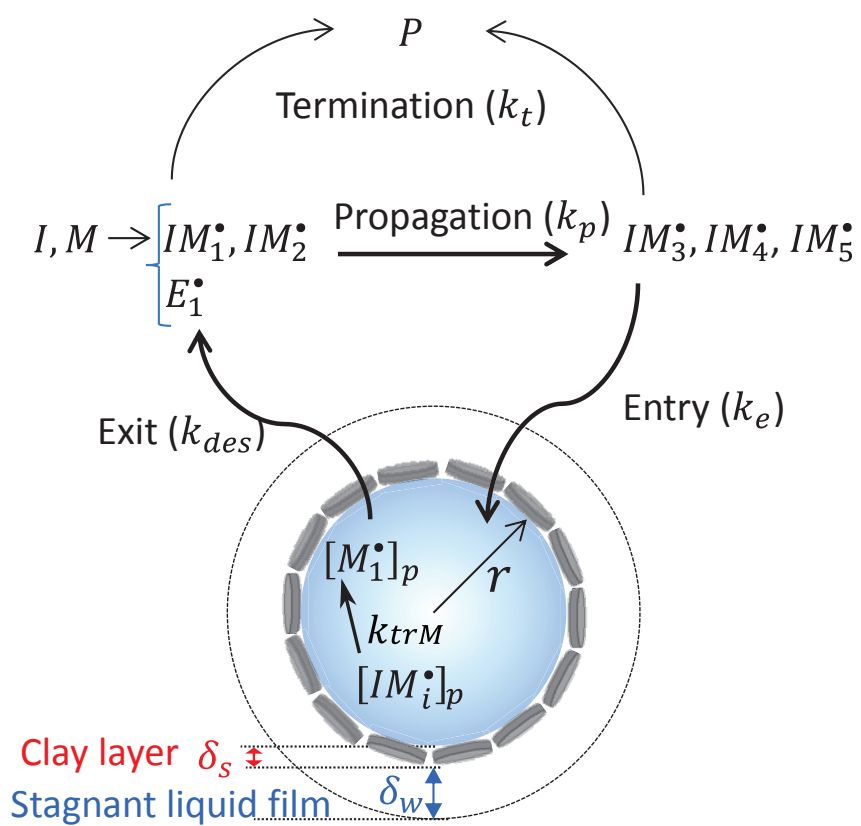


Figure 5.1: Aqueous phase reactions and monomeric radical desorption

$$[IM_4^\bullet]_w = \frac{k_p[M]_w[IM_3^\bullet]_w}{k_p[M]_w + k_{tw}[R]_w + \frac{k_e N}{N_A}} \quad (5.16)$$

$$[IM_5^\bullet]_w = \frac{k_p[M]_w[IM_4^\bullet]_w}{k_{tw}[R]_w + \frac{k_e N}{N_A}} \quad (5.17)$$

The total concentration of radicals in the aqueous phase is given by:

$$[R]_w = \sum_{i=1}^{j_{crit}} [IM_i^\bullet]_w \quad (5.18)$$

5.3.4 Monomeric radicals

As mentioned above, only monomeric radicals, formed by transfer to monomer, of length one $[M_1^\bullet]_p$ or two $[M_2^\bullet]_p$ may desorb from the polymer particles. It is also assumed that transfer to monomer does not concern these monomeric radicals in the polymer particles, which leads to the following balances of primary radicals in the polymer particles:

$$[M_1^\bullet]_p = \frac{k_{fm}[M]_p \frac{1}{N_A} \int_0^\infty \bar{n}(r,t) F(r,t) dr}{k_p[M]_p + k_{des} + k_{tp} \frac{1}{N_A} \int_0^\infty \bar{n}(r,t) F(r,t) dr} \quad (5.19)$$

From this, the concentration of desorbed radicals is given by:

$$[E_1^\bullet]_w = \frac{[M_1^\bullet]_p \frac{1}{N} \int_0^\infty k_{des}(r) F(r,t) dr}{2k_t[R]_w} \quad (5.20)$$

5.3.5 Monomer balance

The variation of the number of moles of residual monomer over time depends on the inlet monomer flowrate F_m , the polymerization rate in the aqueous phase R_{pw} and the polymerization rate in the particles R_{pp} :

$$\frac{dN_m}{dt} = F_m - \underbrace{k_p[M]_w[R]}_{R_{pw}} V_w - \underbrace{k_p[M]_p \frac{\bar{n}N}{N_A}}_{R_{pp}} V_p \quad (5.21)$$

Partitioning of monomer between the phases is admitted fast enough to ensure equilibrium all the time (i.e. consumed monomer within the polymer particles is

instantaneously replaced by monomer from droplets). This partitioning is assumed size independent (which was found to be a good approximation even for small particles [Gilbert and Napper, 1983]). Note that since this work treats interval II, $[M]_w$ and $[M]_p$ are at their saturation values which are known. This interval was usually considered in the literature to study radical entry/exit in order to avoid the nucleation period. Moreover, this interval allows the all the coefficients to be considered constant with time, such as the propagation, termination and radical diffusion coefficient.

5.3.6 Clay partitioning

As the objective of this work is to investigate the effect of the clay layer on radical exchange, it is important to evaluate the amount of clay on the surface of polymer particles. For that, the concentration of clay on the polymer particles was modeled using a BET model as shown in chapter 2.

The clay was found mainly to be adsorbed on the surface of polymer particles forming multilayers, as demonstrated by transmission electron microscopy and Inductively Coupled Plasma-Atomic Emission Spectroscopy, for all clay concentrations studies in this work. The maximal concentration of clay found in the aqueous phase was 0.3 g L^{-1} . For this reason, the use of the concentration of clay on the polymer particles can simply be assumed to be the total clay concentration introduced to the reactor (or calculated by iteration using eq. 5.21 which gives close results).

5.4 Investigation of radical entry and desorption models

Please note that in order to allow easier comparison between the different models proposed in the literature and highlight similarities among them, some models were slightly reformulated (e.g. all models are presented in diameter). This is to not reduce the importance of the original forms that should remain the main references as they reflect the phenomena considered in the development.

5.4.1 Radical entry

Different radical capture mechanisms were reported in the literature (table 5.2):

- **Diffusion-controlled radical capture mechanism:** In the original model proposed by [Smith and Ewart, 1948] the rate of radical entry into a polymer particle is given by the rate of diffusion of free radicals from the aqueous phase with a linear dependency on the particle diameter (equation 5.6, $\rho_e = k_e[R]_w$). With the Smoluchowski equation [Smoluchowski, 1927] for the radical entry coefficient:

$$k_e = 2\pi d_p N_A D_w \quad (5.22)$$

Where the radical diffusion coefficient in water can be approximate by $D_w = \frac{k_B T}{6\pi\eta d_i}$, where d_i is the radical diameter and η is the viscosity of the medium. [Ugelstad and Hansen, 1976] later introduced an efficiency factor $f_e = \frac{U}{W_p}$, with U the reversibility factor and the stability ratio W_p accounts for the electrostatic repulsion, in order to account for the fact that not every radical-particle collision leads to a radical absorption event:

$$k_e = 2\pi d_p N_A D_w f_e \quad (5.23)$$

Where,

$$f_e = \frac{1}{\frac{m \exp(z_\alpha) D_w}{(\tilde{X}_p \coth \tilde{X}_p - 1) D_p} + W_p} \quad (5.24)$$

Where z_α is the zeta potential of the double layer and \tilde{X}_p is proportional to the particle diameter and the reactions inside the particle (table 5.2). In this model, f_e depends on the oligoradical size through the parameters m , D_w , D_p (not indicated for brevity). (Simulated in figure 5.2 for $W_p=5$ and $z_\alpha=1$).

Herrera et al. (2000) used the model of Hansen & Ugelstad to estimate monomeric radical entry efficiency, but proposed a simplified model for polymeric radical entry efficiency as follows [Herrera-Ordóñez and Olayo, 2000]:

$$f_e = \frac{k_p[M]_p + k_{tp} \frac{n(r)(n(r)-1)}{v_p N_A}}{k_0 + k_p[M]_p + k_{tp} \frac{n(r)(n(r)-1)}{v_p N_A}} \quad (5.25)$$

The radical capture efficiency was lower for smaller polymeric radicals and smaller particles and was higher for longer radicals and bigger particles leading to values between $f_e = 10^{-9}$ and $f_e = 1$ for styrene polymerization. For instance, they estimated $f_e \cong 10^{-3}$ for radicals of length $i = 2$ and $d_p = 10 \text{ nm}$ while $f_e \cong 1$ for $i = 4$ and $d_p = 100 \text{ nm}$ (slight depends on $n(r)$). (Simulated in figure 5.2 using $k_0 = \frac{12D_p D_w}{d_p^2(mD_p + 6D_w)}$ and $n(r) = 0.5$).

Using a similar model, Harada et al. (1972) (table 5.2) distinguished efficiency factors for particles and micelles, in order to fit experimental observations (where much lower capture was measured by micelles than by particles) as the difference in size alone could not explain this observation [Harada et al., 1972]. The radical entry rate efficiency was found to be about 100 lower for micelles than for particles. This could be due to the low residence time of radicals into micelles that reduces the probability of propagation before exiting the micelle again. Indeed, radicals are considered captured inside the particles/micelles only if they react therein.

Other forms of f_e where then proposed in the literature (table 5.2).

- **Collision-controlled radical capture mechanism:** In this mechanism, radical capture is proportional to the particle surface and not to the particle surface: [Gardon, 1968] [A. Penboss et al., 1986] [Fitch and Tsai, 1971]:

$$k_e = \sqrt{\frac{8\pi k_B T}{m_i}} N_A d_p^2 \quad (5.26)$$

where m_i is the mass of the entering fee radical (simulated in figure 5.2 for $i=z$).

[Liotta et al., 1997] found this model the most adapted for polystyrene as their experimental data suggested a dependence on $d_p^{1.85}$.

- **Colloidal-controlled radical capture mechanism:** Penboss et al. [A. Penboss et al., 1986] used a mechanism in which the radical entry coefficient is identified as the coagulation rate between a precursor and a latex particle (\approx proportional to the particle diameter):

$$k_e = \frac{k_B T N_A (d_p + d_i)^2}{3\eta W_p d_i d_p} \quad (5.27)$$

Where W_p is the stability ratio calculated using DLVO theory (simulated in figure 5.2 for $i=z$ and $W_p=5$).

- **Radical capture mechanism limited by surfactant layer:** Yeliseyeva [Yeliseyeva and Zuikov, 1977] considered that the surfactant layer around the particle might hinder radical capture, and therefore radical capture requires displacement of surfactant molecules.
- **Propagation-controlled radical capture mechanism:** The admitted entry mechanism nowadays is the propagation-controlled one. Maxwell and Gilbert [Maxwell et al., 1991] proposed to relate the entry rate to an average degree of polymerization in the aqueous phase (z) necessary in order to attain the required surface-activity for entry, thus independently of the particle size or charge, as follows:

$$\rho_e = k_p [M]_w [IM_{z-1}^\bullet]_w \frac{N_A}{N} \quad (5.28)$$

Oligomers that propagate beyond the length z are neglected in this model. k_e can be extracted from this equation using equation 5.22 that is desired to be maintained valid for comparison with other models.

The estimation of the critical length of entry (z) for different monomers was studied based on thermodynamic grounds. For persulfate initiated systems, the following semi-empirical thermodynamic model was proposed:

$$z \cong 1 + \frac{-|\Delta G^{hyd}|}{RT \ln([M]_w^{sat})} \quad (5.29)$$

with $|\Delta G^{hyd}| = 23kJ \text{ mol}^{-1}$ which is the minimum hydrophobic free energy to impart surface activity, (rounded to the closes integer). This gives for styrene, $z = 2 - 3.25$ Similar results are obtained using the two-layer lattice model [Dong and Sundberg, 2002]. Note that for j_{crit} , the same relation was used, with $|\Delta G^{hyd}| = 55kJ \text{ mol}^{-1}$, which gives $j_{crit} = 5$ for styrene. [Coen et al., 1998]

In order to discriminate between the available models in the literature and determine the dependency on the particle size, Asua and de la Cal (1991) proposed the following methodology [Asua and De La Cal, 1991]:

$$k_e = k_e^* d_p^{\alpha_1} \quad (5.30)$$

Where k_e^* and α_1 are adjustable parameters. For instance $\alpha_1 = 0$ in the propagation model, $\alpha_1 = 1$ in the diffusion model and $\alpha_1 = 2$ in the collision model. A similar way was proposed to study the desorption coefficient. This model will be later to investigate the dependency on d_p .

Table 5.2: Absorption efficiency factor

References	k_e	f_e
[Smith and Ewart, 1948]	$k_e = 2\pi d_p N_A D_w$	$f_e = \frac{1}{(X_p \coth X_p - 1) D_p} + W_p; \quad \tilde{X}_p = \frac{d_p}{2} \sqrt{\frac{k_p [M]_p}{D_p} + \frac{k_{tp} n(r)}{N_A v_p D_p}}$ $z_\alpha = \frac{e v \Psi_\alpha}{k_B T}; \quad \Psi_\alpha = \Psi_\delta + \sigma_0 \left(\frac{\delta}{\epsilon}\right)$ $W_p = \frac{d_p}{2} \int_0^\infty \exp\left(\frac{V_T}{k_B T}\right) \frac{dL}{\left(\frac{d_p}{2} + L\right)^2}; \quad V_T = e \Psi_\alpha$
[Hansen and Ugelstad, 1978b]		
[Coen et al., 1998]		$f_e = \begin{cases} \frac{1}{i^2}, & z \leq i < j_{crit} \\ 0, & else \\ 1, & \text{for monomeric radicals} \end{cases}$
herrera 2000		$f_e = \frac{k_p [M]_p + k_{tp} \frac{n(r)(n(r)-1)}{v_p N_A}}{k_0 + k_p [M]_p + k_{tp} \frac{n(r)(n(r)-1)}{N_A v_p}}$
[Nomura et al., 2005]		$f_e = \frac{k_p [M]_p + k_{tp} \frac{n(r)}{v_p N_A}}{k_0 + k_p [M]_p + k_{tp} \frac{n(r)}{N_A v_p}}$
[Hernández and Tauer, 2007b]		$f_e = v \left(\frac{\pi N d_p^3}{6} \right) + 1$
Gardon 1968	$k_e = \sqrt{\frac{8\pi k_B T}{m_i}} N_A d_p^2$	
Penboss 1986	$k_e = \frac{k_B T N_A (d_p + d_i)^2}{3\eta W_p d_i d_p}$, $W_p = \frac{1}{\kappa} \exp\left(\frac{V_T}{k_B T}\right) \left(\frac{d_p + d_i}{2d_p d_i}\right)$, $\kappa = \sqrt{\frac{8\pi e^2 N_A L S}{\epsilon k_B T}}$	
Maxwell 1991	$k_e = k_p [M]_w \frac{N_A}{N} \frac{[M]_{z-1}^{*w}}{[R]_w}$	

Table 5.3: Parameters used for simulation of styrene Emulsion Polymerization at 70 °C

Parameter	Value	Reference
D_p ($dm^2 s^{-1}$)	1.5×10^{-7}	[Sajjadi, 2009]
D_w ($dm^2 s^{-1}$)	1.5×10^{-7}	[Sajjadi, 2009]
j_{crit} (-)	5	[Sajjadi, 2009]
k_p ($dm^3 mol^{-1} s^{-1}$)	480	[Sajjadi, 2009]
k_{pw} ($dm^3 mol^{-1} s^{-1}$)	480	[Sajjadi, 2009]
k_{tw} ($dm^3 mol^{-1} s^{-1}$)	1.16×10^9	[Crowley et al., 2000]
k_{tp} ($dm^3 mol^{-1} s^{-1}$)	6.8×10^7	[Sajjadi, 2009]
k_{fm} ($dm^3 mol^{-1} s^{-1}$)	9.3×10^{-3}	[Sajjadi, 2009]
$m = [M]_w^{sat}/[M]_p^{sat}$ (-)	1.03×10^3	[Asua, 2003]
$[M]_w^{sat}$ ($mol dm^{-3}$)	5.3×10^{-3}	[Vanzo et al., 1965]

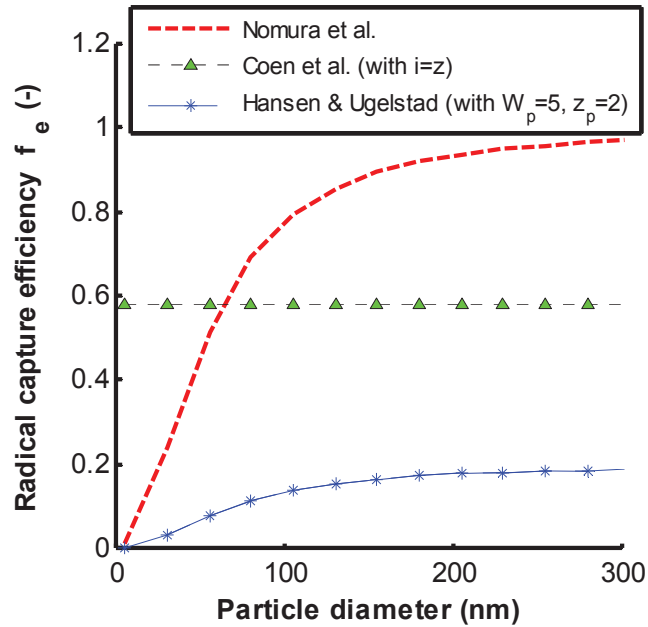


Figure 5.2: Radical entry coefficient obtained with different models reported in table 5.2 with simulation parameter of table 5.3

The above presented radical capture models were simulated using emulsion polymerization parameters (table 5.3). Note that no model has any tuning parameters. But, as these models do not depend on the same set of physical parameters, the presented curves are only indicative. Figure 5.2 shows the simulation results of the radical capture efficiency f_e as a function of the particle diameter. It can be seen that the capture efficiency is increasing with the particle size except for the model of Coen et al. that is only function of the radical degree of polymerization. Hernandez & Tauer suggests that the polymer volume fraction may affect radical collision kinetics. They predicted a Smoluchowski number close to one for polymer volume fraction lower than 10-2 but at higher polymer fractions it increased importantly (up to 10 for 10% volume fraction). The obtained capture efficiency using this model, with the value $v=17.95$ fitted in their experiments, is thus higher than one. In the model of Hansen & Ugelstad (which is more complex), increasing the stability W_p , reduces the radical capture efficiency.

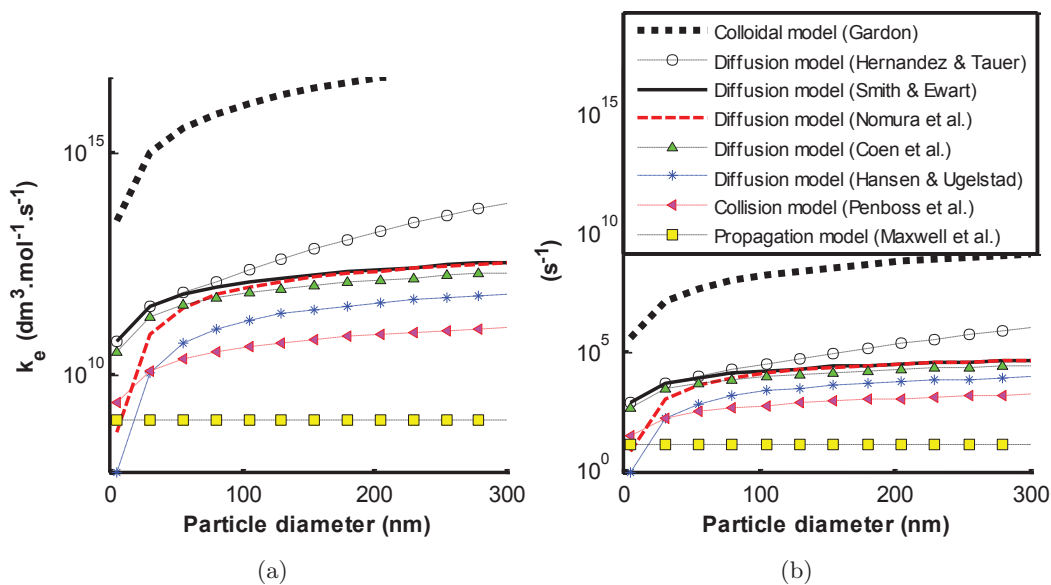


Figure 5.3: The equilibrium desorption rate coefficient (k_0), the desorption probability and the radical desorption coefficient obtained by the different models of table 5.4 using parameters in table 5.3.

Figure 5.3 shows the radical capture coefficient k_e and the radical capture rate ρ_e as a function of the particle size. Note that the diffusion-controlled mechanisms differ only in the way of defining the capture efficiency. For Smith and Ewart (where $f_e=1$), a high radical entry rate was obtained. Whenever the calculated radical capture efficiency was close to one, the models joined that of Smith and Ewart. For instance, the model of Nomura et al. gives $f_e \approx 1$ for bigger particles due to the low desorption rates (which is the case of styrene). In propagation-controlled mechanism, the radical entry rate coefficient is independent of the particle size and is orders of magnitudes lower than that of Smith and Ewart model. The rate of radical entry using the colloidal model is very high. Adams et al. noted that the dimension of colloids in this model attained 50 monomer units which might not be water soluble and is uncoherent with the calculated activation energy of entry [Adams et al., 1988]. Finally, the collisional model is more complex as it requires the calculation of the radical-particle stability ratio as in the Hansen & Ugelstad mechanism. Both of these models were simulated with the same stability ratio ($W_p=5$). It can be seen that the collisional model gives slightly lower values. Note however that much higher values of W_p were considered in the original paper of Penboss et al. which importantly reduces radical entry. Note that these models do not account for the surfactant layer. So, if any of these models is found able to fit Pickering EP experiments with the different clay concentrations, this would indicate that the clay layer does not affect radical entry.

5.4.2 Radical desorption models

For many important emulsion polymerization systems, desorption represents the major cause of the loss of free-radical activity inside a particle as it decreases the concentration of radicals in the particles. As mentioned above, desorption mainly concerns monomeric radicals, derived from the transfer reactions to the monomer. Therefore, it may safely be assumed that the desorption of monomer radicals would not be affected by the surfactant layer due to their small size (1 monomer unit) and to the fact that they are not charged (as the monomer is nonionic and monomeric radicals do not contain an initiator fragment).

The desorption rate is given by $k_{des}\bar{n}$, where the desorption rate coefficient, k_{des} , is supposed reflect all necessary conditions for desorption. For instance, for a free radical to be transferred from the interior of the particle to the continuous phase, it must reach the particle surface and overcome the barrier for desorption exerted by the interface. Moreover, for desorption, radicals must escape concurrent propagation and termination reactions. Finally, desorbed radicals might re-enter the particle, which proportion should not be calculated among desorbed radicals. Therefore, different precision levels accounting for different factors affecting desorption were considered in the desorption models. It is important to keep in mind that the models where usually developed and validated for a particular system, i.e. few monomers (with their specific solubility parameters) and particle size range. The objective here is to find the model adapted to the present system and not to detect the best model to be used in general.

These mechanisms can be resumed as follows (see tables 5.4 to ??):

- **Diffusion-controlled radical desorption mechanism** : The original models by [Smith and Ewart, 1948] followed by [Ugelstad and Hansen, 1976], [Chang et al., 1981], [Asua and De La Cal, 1991], [Morrison et al., 1994], indicate a dependency between the radical desorption coefficient and the particle size:

$$k_{des} = \frac{\beta}{d_p^\alpha} \quad (5.31)$$

Where κ and α are parameters taking different values in the literature ($\alpha=[0:2]$ see table 5.4). This mechanism is known as simple or maximum desorption rate coefficient [Hernandez and Tauer, 2008], because it does not take into account competitive reactions inside the polymer particles (i.e. propagation, termination), nor the fate of the radicals after desorption (possibility of radical re-absorption). Radical desorption is only the result of the diffusive motion of the radicals. Therefore, [Chang et al., 1981] indicated in their model a direct dependency on the diffusion coefficient of the radical inside the polymer particle (D_p).

- **Radical desorption mechanism accounting for polymer phase reactions** (or net desorption): [Harada et al., 1971] where pioneers to propose a mechanism accounting for the competition between radical desorption and other reactions taking place inside the polymer particles. Moreover, a term was introduced in order to account for the different radicals' solubility into the polymer particles and the aqueous phase. Still this mechanism does not take into account the fate of the radicals after desorption. The desorption rate coefficient can generally be written as follows:

$$k_{des} = f_d * P_d \quad (5.32)$$

Where f_d is the frequency at which monomeric radicals (that may exit) are being formed, which mainly concerns transfer to monomer reactions (also to chain transfer agent if present). P is the probability of the radical to escape the particle before undergoing other reactions (propagation and termination inside the particle). For instance, for Harada et al. 1971 [Harada et al., 1971] P is given by:

Where f_d is the frequency at which monomeric radicals (that may exit) are being formed, which mainly concerns transfer to monomer reactions (as well as chain transfer agent if present). P_d is the probability of the radical to escape the particle before undergoing other reactions (propagation and termination inside the particle). For instance, for [Harada et al., 1971] P_d is given by:

$$P_d = \frac{k_0}{k_0 \bar{n} + k_p [M]_p + \frac{k_t \bar{n}}{N_A v_p}} \quad (5.33)$$

Radical partitioning between water and the polymer particles is accounted through the parameter k_0 , also called equilibrium radical desorption [Hernandez and Tauer, 2008], as follows:

$$k_0 = \frac{\kappa \frac{\delta_p}{\delta_w} D_p D_w}{d_p^\alpha (m D_p + \frac{\delta_p}{\delta_w} D_w)} \quad (5.34)$$

Where D_p and D_w are the diffusion rate coefficients in the polymer particles and water respectively and m is the partition coefficient of the radicals between the polymer particles and the aqueous phase $m = R_{pi}^\bullet/R_{wi}^\bullet$ usually approximated by $[M]_w/[M]_p$ or assumed as a tuning parameter. δ_w is the thickness of the stagnant layer in the aqueous phase and δ_p is the thickness of the diffusion layer in the polymer phase.

Brooks and Mekanjuola [Brooks and Mekanjuola, 1981] as well as Hernandez and Tauer [Hernandez and Tauer, 2008] calculated the equilibrium radical desorption by considering the energy barrier for desorption, due to the difference in chemical potential of the radical between the phases as well as the presence of surfactant layers around the particles:

$$k_0 = \frac{\kappa D_p}{d_p^\alpha} e^{-\frac{E_{des}}{k_B T}} \quad (5.35)$$

With E_{des} the activation energy of desorption, k_B is Boltzman constant and T is absolute temperature.

- **Radical desorption mechanism accounting for polymer and aqueous phase reactions**(or effective desorption rate): Asua et al. [Asua et al., 1989] proposed to consider a radical to be effectively desorbed from the particle only after it reacts in the aqueous phase. Desorbed radicals that are reabsorbed by a polymer particle before undergoing any reactions in the aqueous phase are not calculated in the desorption term. Therefore, in the radical desorption mechanism accounting for polymer phase reactions, the probability term is modified as follows to account for aqueous phase reactions:

$$P = \frac{\frac{1}{\bar{n}} \sum_{i=0}^{\infty} \frac{1-P_{p,i+1} N_i}{N_T}}{1 - (1 - Pw) \sum_{i=0}^{\infty} \frac{1-P_{p,i+1} N_i}{N_T}} \quad (5.36)$$

Where the probability of radical reaction inside the particles is given by (k : termination or propagation):

$$P_p = \frac{\sum_k k_{k,p}}{k_0 + \sum_k k_{k,p}} \quad (5.37)$$

And the probability of radical reaction in the continuous phase is:

$$P_w = \frac{\sum_k k_{k,w}}{k_e + \sum_k k_{k,w}} \quad (5.38)$$

Where k_e is the radical capture rate coefficient.

The so named net and effective desorption mechanisms were investigated by simulation using parameters given in table 5.3. The models using almost the same frequency term are not all shown in the figure 5.4. The polystyrene system was considered. Note first that exact comparison between all models is not trivial as they do not all use the same set of parameters (e.g. some models use \bar{n} and others do not). Second, it is important to keep in mind that the models were usually developed and validated for a particular system (with specific solubility parameters and particle size range), and were not validated for different systems during the development. Figure 5.4 shows the calculated equilibrium coefficient k_0 , the probability of radical desorption (P) using the different models as well as the resulting desorption coefficient (k_{des}) from these entities. When \bar{n} was required in the simulation, linearly increasing \bar{n} as a function of d_p was considered, starting from $\bar{n}=0.5$ for $d_p=10$ nm. The following remarks can be outlined:

- A very high probability for small particles ($D_p < 100$ nm) were obtained from models where the probability depends on \bar{n} , as follows $P = \frac{k_0}{k_0 \bar{n} + k_p [M]_p}$ (Harada et al. 1971, Normura et al. 1982.). The model of Asua et al. 1989 is also sensitive to small values of \bar{n} but at a lower extend $P = \frac{\frac{1}{\bar{n}} \sum_{i=0}^{\infty} \frac{1-P_{p,i+1} N_i}{N_T}}{1 - (1-P_w) \sum_{i=0}^{\infty} \frac{1-P_{p,i+1} N_i}{N_T}}$. It is worth to mention that for $\bar{n} > 1$, these models keep limited values of k_{des} for small particle diameters. The model of Ugelstad and Hansen 1976 is independent of \bar{n} , but does not contain k_0 in the denominator as follows $P = \frac{k_0}{k_p [M]_p}$, and so estimates high desorption rates.
- In the models using k_0 of the following form, $k_0 = \frac{12\alpha D_p D_w}{d_p^2 (m D_p + \varepsilon D_w)}$, lower values of ε lead to higher k_0 . Also lower values of m , which means lower ratio of radicals in the polymer to the aqueous phase, lead to higher k_0 . In most

models $\alpha = 1$, except in Nomura 1982 ($\alpha = 4 - 10$), which lead to increased k_0 and Grady 1996 ($\alpha=0.55$), which leads to lower values of k_0 .

- Clearly models containing the term $(1-\bar{n})$ (Harada et al. 1971) are limited to the 0-1 system which is not our case as shown in the experimental observations section

In this work, only models that give limited desorption rate coefficient for small particles and those allowing $\bar{n})>1$ are used in the modelling the whole reaction. These are the models of Lacik et al. 1992, Fontenot and Schork 1993, Grady 1996, and Hernandez and Tauer 2008. The model of Asua 2003 requires the knowledge of D_h and δ_1 that are not easy to estimate in our system.

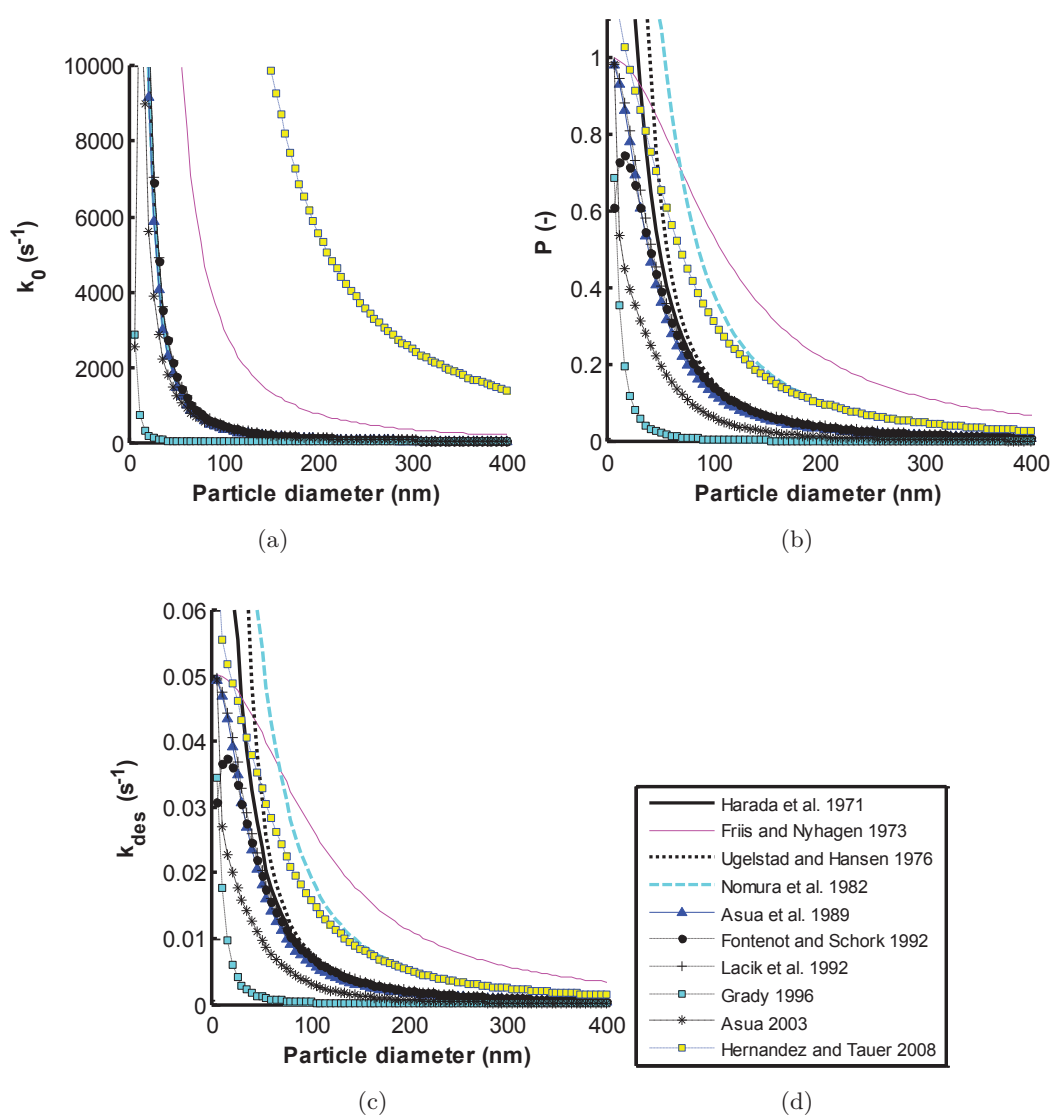


Figure 5.4: The equilibrium desorption rate coefficient (k_0), the desorption probability and the radical desorption coefficient obtained by the different models of tables 5.5 to ?? using parameters in table 5.3.

Table 5.4: Diffusion-controlled radical desorption mechanism

	k_{des}	α	Remarks
[Smith and Ewart, 1948]	$k_{des} = \frac{a_p \kappa'}{v_p} = \frac{6(\frac{\pi}{6})^{\frac{1}{3}} \kappa'}{v_p^{\frac{1}{3}}} = \frac{6\kappa'}{d_p}$		polystyrene case II: ($\bar{n} = 0.5$)
[Ugelstad et al., 1969]	$k_{des} = \frac{\kappa' N_p^{\frac{2}{3}}}{v_p} = \frac{\kappa'(\frac{6}{d_p})^{\frac{2}{3}}}{d_p^{\frac{2}{3}}}$		
[Chang et al., 1981]	$k_{des} = \frac{2D_p}{d_p^2}; \frac{4D_p}{d_p^2}; \frac{5D_p}{d_p^2}$		(centered, edge or anywhere radicals respectively)
[Asua and De La Cal, 1991]	$k_{des} = \frac{\kappa'}{d^\alpha}$	$[0; 3 \times 10^{-4}] \leq [\alpha; \kappa] \leq [2; 1 \times 10^{-13}]$	κ also depends on entry
[Morrison et al., 1994]	$k_{des} = \frac{\kappa}{d^\alpha}$	$\alpha = 1.5 \pm 1.2, \text{ for } \bar{n} < 0.5,$ (case I of Smith Ewart) $\alpha = 2.6 \pm 1.1,$ <i>for</i> $k_{des} \bar{n} < k_p [M]_p$	

Table 5.5: radical desorption mechanism accounting for polymer phase reaction

$k_{des} = P * f$ with $f = k_{fm}[M]_p$				
	Probability	k_0	Remarks	
[Harada et al., 1971]	$P = \frac{k_0}{k_0\bar{n}+k_p[M]_p}$	$k_0 = \frac{12D_pD_w}{d_p^2(mD_p+D_w)}$	$f = k_{fm}[M]_p + k_{fT}[T] + \frac{r_i(1-\bar{n})}{N\bar{n}}$	
[Friis and Nyhagen, 1973]	$P = \frac{k_0}{k_0+k_p[M]_p}$	$k_0 = \frac{8D_p}{d_p^2}$	Polyvinyl acetate 0-1-2 system termination in water neglected	
[Ugelstad and Hansen, 1976]	$P = \frac{k_0}{k_p[M]_p}$	$k_0 = \frac{12D_pD_w}{d_p^2(mD_p+D_w)}$	Distinguishes kp for chain-transfer generated radicals	
[Nomura and Harada, 1981]	$P = \frac{k_0}{k_0+k_p[M]_p} \sum_{i=1}^S \left(\frac{k_p[M]_p}{k_0\bar{n}+k_p[M]_p} \right)^i$	$k_0 = \frac{12D_pD_w}{d_p^2(mD_p+6D_w)}$	Vinyl acetate and vinyl chloride 0-1 system Water-phase termination and propagation are neglected	
[Nomura, 1982]	$P = \frac{k_0}{k_0+k_p[M]_p} \sum_{i=1}^S \left(\frac{k_p[M]_p}{k_0\bar{n}+k_p[M]_p} \right)^i$	$k_0 = \frac{12D_pD_w}{d_p^2(\alpha m D_p + 6D_w)}$	$f = k_{fm}[M]_p + k_{fT}[T]$	$4 \leq \alpha \leq 10$
[Mead and Poehlein, 1989]	$P = \frac{k_0}{k_p[M]_p}$	$k_0 = \frac{12D_pD_w}{d_p^2(mD_p+\varepsilon D_w)}$		
		$\varepsilon = \frac{k^2-3(k \coth(k)-1)}{k^2(k \coth(k)-1)}$		
		$k = \frac{d_p}{2} \sqrt{\frac{k_p[M]_p}{D_p}}$		

[Lacik et al., 1992]	$P = \frac{k_0}{k_0 + k_p} [M]_p$	$k_0 = \frac{12D_p D_w}{m d_p^2}$	Seeded styrene emulsion polymerization 0-1 system
[Fontenot and Schork, 1993]	$P = \frac{k_0}{k_0 + k_p} \frac{k_t \bar{n}}{[M]_p + N_A v_p}$	$k_0 = \frac{12D_p D_w}{d_p^2 (m D_p + \varepsilon D_w)}$ $\varepsilon = \begin{cases} \frac{21 - 21k + 12k^2 - 5k^3}{7(15 - 15k + 9k^2 - 4k^3)} & \text{if } k \leq 0.1 \\ \frac{k^2 - 3(k \coth k - 1)}{k^2 (k \coth k - 1)} & \text{if } k > 0.1 \end{cases}$ $k = \frac{d_p}{2} \sqrt{\frac{k_p [M]_p}{D_p}}$	
[Grady and Jr, 1996]	$P = \frac{k_0 (n_c - 1)}{k_0 (n_c - 1) + k_p [M]_p} \sum_{i=1}^{n_c} \frac{1}{1 + m(i)}$	$k_0 = \frac{20D_p D_w}{3d_p^2 (3D_p + D_w)}$	
[Asua, 2003]	$P = \frac{k_0}{k_p [M]_p + \frac{2k_t(\bar{n}-1)}{N_A v_p}} P_w$ $P_w = \frac{k_0 m v_p N_p + k_i p_w [M]_w + 2k_{tw} [T^*]}{k_0 m v_p N_p + k_i p_w [M]_w + 2k_{tw} [T^*]}$	$k_0 = \frac{2\pi D_p D_w}{d_p^2 (m D_p + m D_w D_p \frac{2\delta_1}{D_h d_p} + \varepsilon D_w)}$ $\varepsilon = \frac{1}{k \coth k - 1}$ $k = \frac{d_p}{2} \sqrt{\frac{k_p [M]_p + \frac{2k_t(\bar{n}-1)}{N_A v_p}}{D_p}}$	

Table 5.6: suite of table 5.5

Table 5.7: radical desorption mechanism for polymer and aqueous phase reactions

$k_{des} = P * f$ with $f = k_{fm}[M]_p$		k_0	Remarks
Probability			
[Asua et al., 1989]	$P = \frac{1}{\bar{n}N_p} \sum_{i=0}^{\infty} P_{p,i} N_i$ $P_{p,i} = \frac{1}{1-(1-Pw)} \frac{1}{N_p} \sum_{i=0}^{\infty} P_{p,i+1} N_i$ $P_{p,i} = \frac{k_0 + k_p[M]_p + \frac{k_t(i-1)}{N_A v p}}{k_0 + k_p[M]_p + k_{tw}[T^*]_w + \frac{k_{cp} N_p \phi_w}{N_A}}$ $P_w = \frac{k_{pw}[M]_w + k_{tw}[T^*]_w + \frac{k_{cp} N_p \phi_w}{N_A}}{k_0 + k_p[M]_p + k_{tw}[T^*]_w + \frac{k_{cp} N_p \phi_w}{N_A}}$	$k_0 = \frac{12D_p D_w}{d_p^2 (mD_p + 2D_w)}$	
[Hernandez and Tauer, 2008]	$P = \frac{P_w P_p}{1-(1-p_w)P_p}$ $P_p = \frac{k_0}{k_0 + k_p[M]_p + \frac{k_t(i-1)}{N_A v p}}$ $P_w = \frac{k_{pw}[M]_w + k_{tw}[T^*]_w + \frac{k_{cp} N_p \phi_w}{N_A}}{k_0 + k_p[M]_p + k_{tw}[T^*]_w + \frac{k_{cp} N_p \phi_w}{N_A}}$	$k_0 = \frac{60D_p}{d_p^2} \exp - \frac{E_{des}}{RT}$	

5.5 Pickering emulsion polymerization (interval II)

The presented models in the previous sections are evaluated in the Pickering emulsion polymerization system in this section. Interval II is considered, where no nucleation or coagulation are taking place and the polymer particles are saturated with monomer. Working under saturation with monomer allows considering constant coefficients during the reaction time (propagation, termination and diffusion). As indicated above, radical desorption may be assumed independent of the clay layer around the particle as it only concerns monomeric radicals that are short and non-charged. The above discussed desorption and capture models are compared in order to evaluate the necessity of making the capture model account for the clay layer around the polymer particles and select an model for radical desorption adapted to the present system.

5.5.1 Experimental observations

Surfactant-free emulsion polymerization of styrene was carried out in the presence of different clay concentrations (figure 5.5). Polymer particles are produced in a batch reaction then monomer addition was started semi-continuously before the depletion of monomer droplets in order to maintain the polymer particles under saturation with monomer reaction (interval II). This avoids reaction diffusion limitations and therefore changes in the reaction coefficients or mechanisms.

First seeded experiments were conducted using the same seed latex to which different clay concentrations were added and reaction was started under saturation conditions. The results of these experiments did not indicate a dependency of \bar{n} on the clay concentration and the estimated differences were within the estimation error. This primary observation would indicate that the clay concentration does not affect radical capture. In order to confirm these results and estimate the dependency of radical capture on the particle size as well, *ab initio* experiments were conducted where the seed particles were produced at the beginning of the reaction using different clay concentrations thus leading to particles of different sizes with different clay coverage.

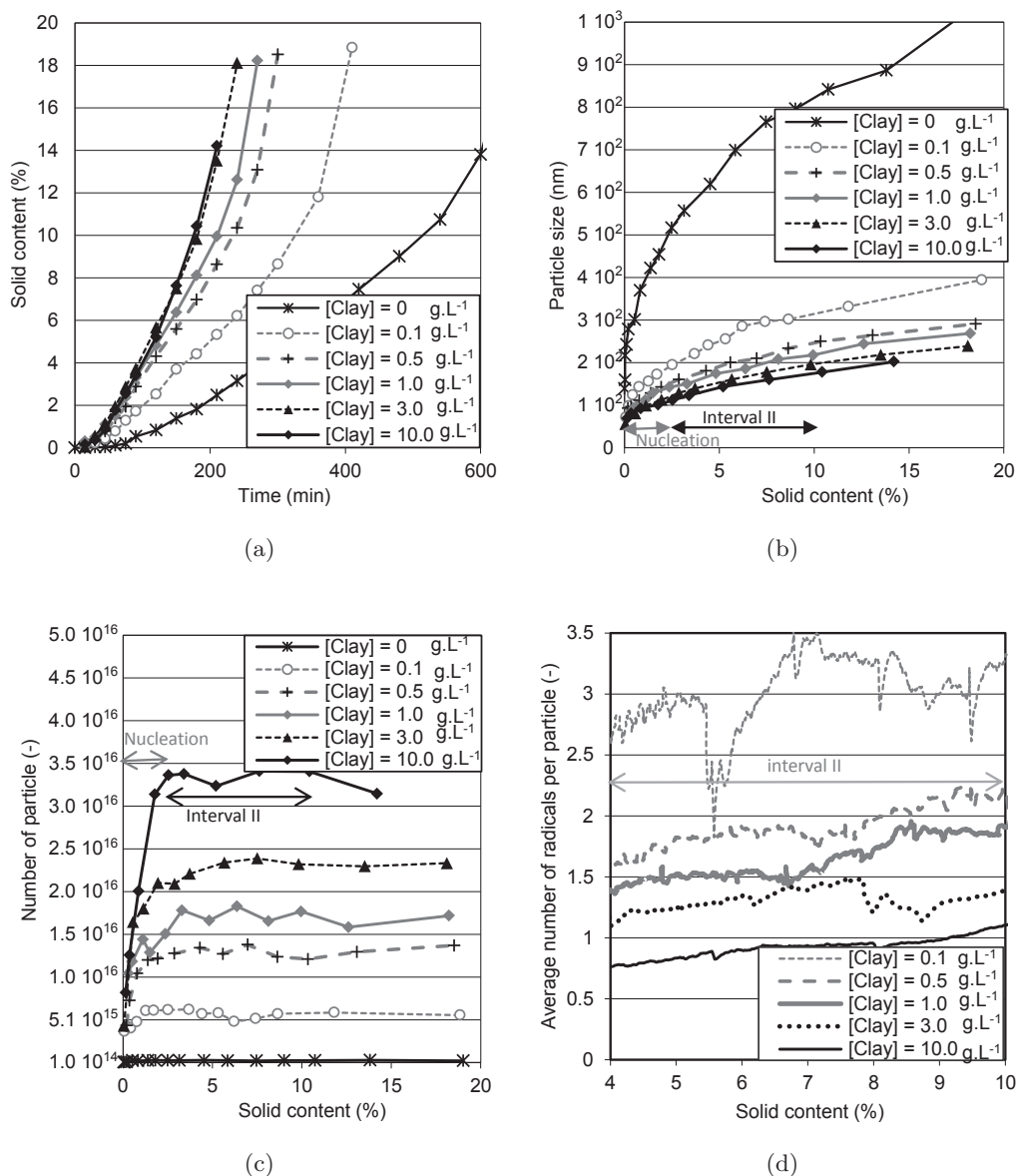


Figure 5.5: Pickering *ab initio* semi-continuous emulsion polymerization of styrene stabilized with different amounts of Laponite RDS[®]. (a) Solid content, (b) Measured particle diameter, (c) Number of particles per liter, (d) Estimated \bar{n} by calorimetry in interval II ($\bar{n}=30$ when [Clay]=0).

The results of *ab initio* experiments are shown in figure 5.5. Even though *ab initio* experiments are presented, only interval II of these experiments will be considered for modeling. It can be seen that increasing the clay concentration led to faster increase in the solid content with time (so to higher reaction rates) as this allowed a better stabilization of nucleated particles reducing thereby the coagulation rate. Therefore, smaller particles were obtained figure 5.5b and a higher number of particles were nucleated figure 5.5c. The number of particles increased at the beginning of the reaction, during a nucleation period, and then stabilized until the end of the reaction. The end of the nucleation period was observed between 45 and 90 min (longer for higher amounts of clay). The end of the nucleation indicates the beginning of interval II as monomer addition was started before the depletion of monomer droplets. The end of interval II and the start of interval III are characterized by the depletion of monomer droplets where the concentration of monomer in the polymer particle becomes lower than the saturation concentration. Note that only interval II will be considered for modeling (so between 4 and 10% solid content). This is possible as the number of particles is constant during this interval (indicating neither nucleation nor coagulation of particles). Therefore, the change in the particles size is only due to growth. The growth term (3)(equation 3) depends on the monomer polymerization rate coefficient and the concentrations of monomer and radicals in the polymer particles. In interval II, the concentration of monomer in the polymer particles is constant. Moreover, radical diffusion in the polymer particles has no particular limitations, and therefore the propagation rate coefficient might be assumed constant and known. Under these assumptions, one may estimate the average number of radicals per particle, \bar{n} (figure 5.5d). It can be seen that increasing the clay concentration led to lower values of \bar{n} . This observation was outlined in similar Pickering emulsion polymerizations [Sheibat-Othman et al., 2011] [Bourgeat-Lami et al., 2010] [Teixeira et al., 2011].

5.5.2 Capture/desorption models for Pickering emulsion polymerization

The different possible combinations of capture and desorption models were simulated and different criterion were investigated (\bar{n} , D_p and the monomer conversion). The simulated radical desorption models are those of Lacik et al. (1992), Fontenot and Schork (1993), Grady (1996) and Hernandez and Tauer (2008). The simulated radical capture models are those of Fontenot and Shork (1993), Maxwell et al. 1991 and Asua and la Cal (1991).

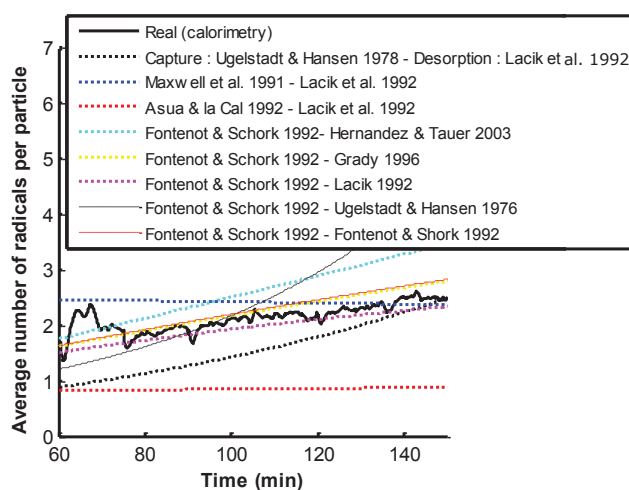


Figure 5.6: The obtained value of \bar{n} from the different combinations of capture-desorption models in a Pickering emulsion polymerisation system

The prediction values of \bar{n} by the different models are depicted on figure 5.6 for a particular experiment. For radical desorption, the closes model to the set of experiments was that of Fontenot and Schork. The desorption model of Ugelstad or Hernandez over estimate \bar{n} . The closes models for capture are those of: Lacik, Grady, or Fontenot and Schork. The propagation-controlled models of Maxwell et al. and Asua gave a decreasing curve of \bar{n} with time. As a result, since the desorption model of Lacik is quite simple and does not involve a big number of parameters, it is selected for modeling the present system. The capture model of Fontenot was the only one adapted to the present system.

Figure 5.7 shows the prediction results of \bar{n} , D_p , monomer conversion and particle size distribution for this experiment using the chosen models of radical capture and desorption. This experiment corresponds to a clay concentration of 0.1 g L^{-1} . A relatively good agreement can be observed for the different variables

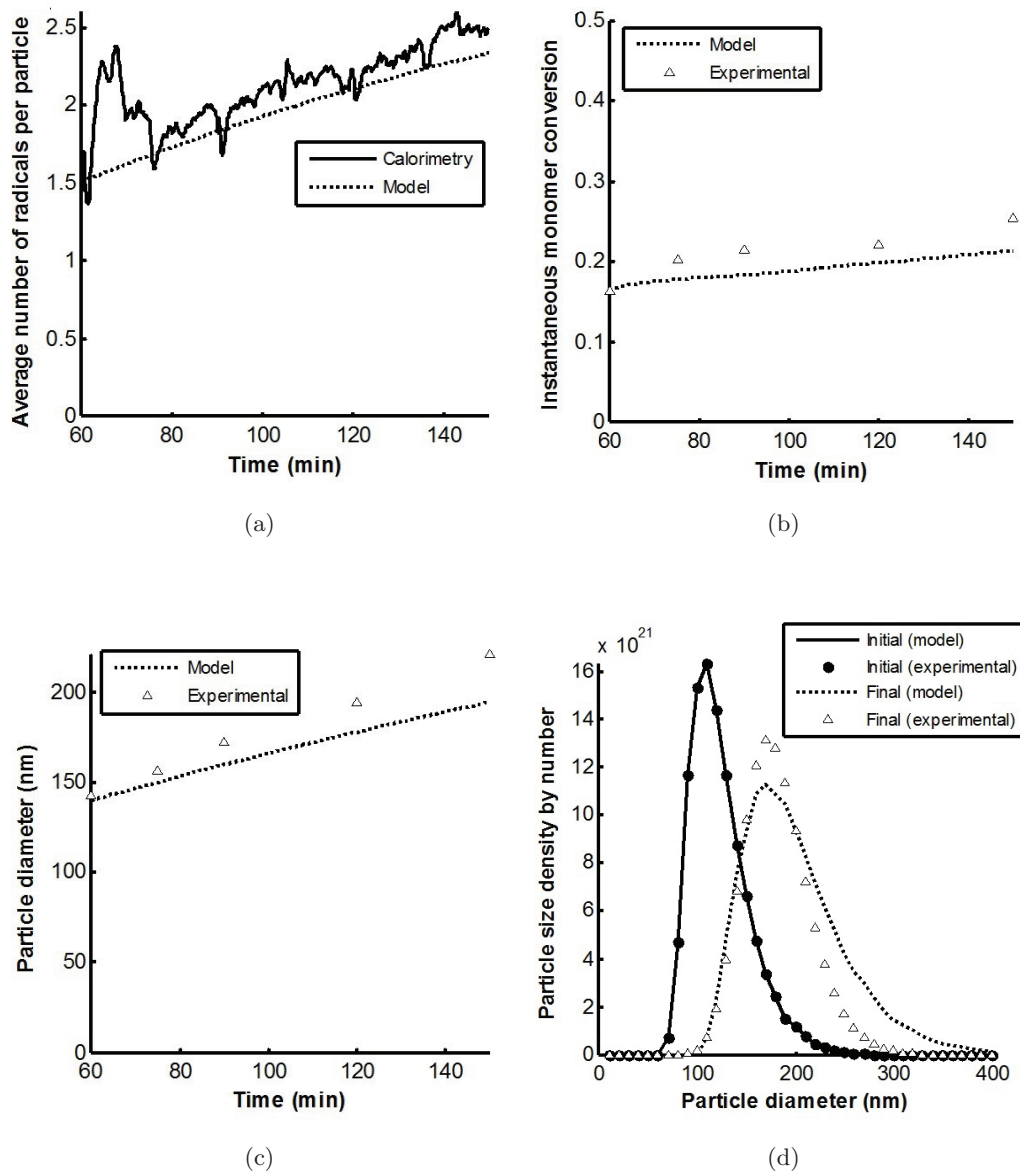


Figure 5.7: Simulation of a Pickering emulsion polymerization involving 0.1 g L^{-1} of clay, using the capture model of Fontentot and Schork (1992) and the desorption model of Lacik et al. (1992)

5.5.3 Effect of clay concentration

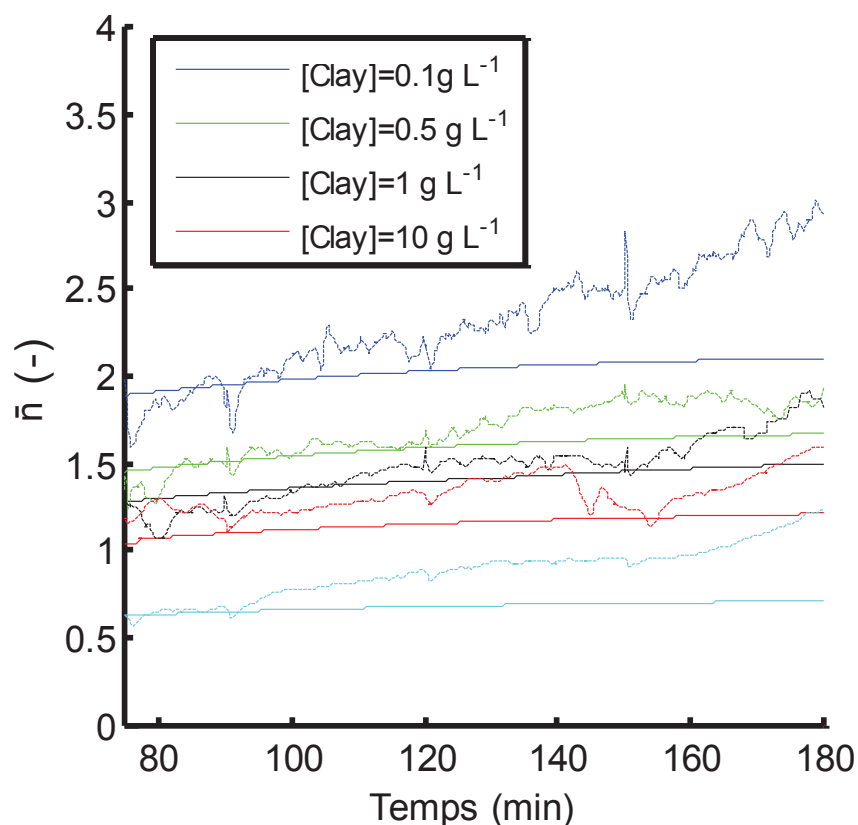


Figure 5.8: Simulation of the Pickering emulsion polymerization system in interval II, for different amount clay concentrations, using the capture model of Fontenot and Schork (1992) and the desorption model of Lacik et al. (1992)

All the experiments with the different clay concentrations were simulated using the selected models (Fontenot and Schork 1992 for radical capture, Lacik et al. 1992 for radical desorption). The simulation results are presented in figure 5.8. It can be seen that the model allows for a pretty good estimation of \bar{n} . Therefore, the clay layer does not seem to affect radical capture. The increase in \bar{n} from one experiment to another is only due to the increase in the particle size. Note that no parameters were fitted in any of the models

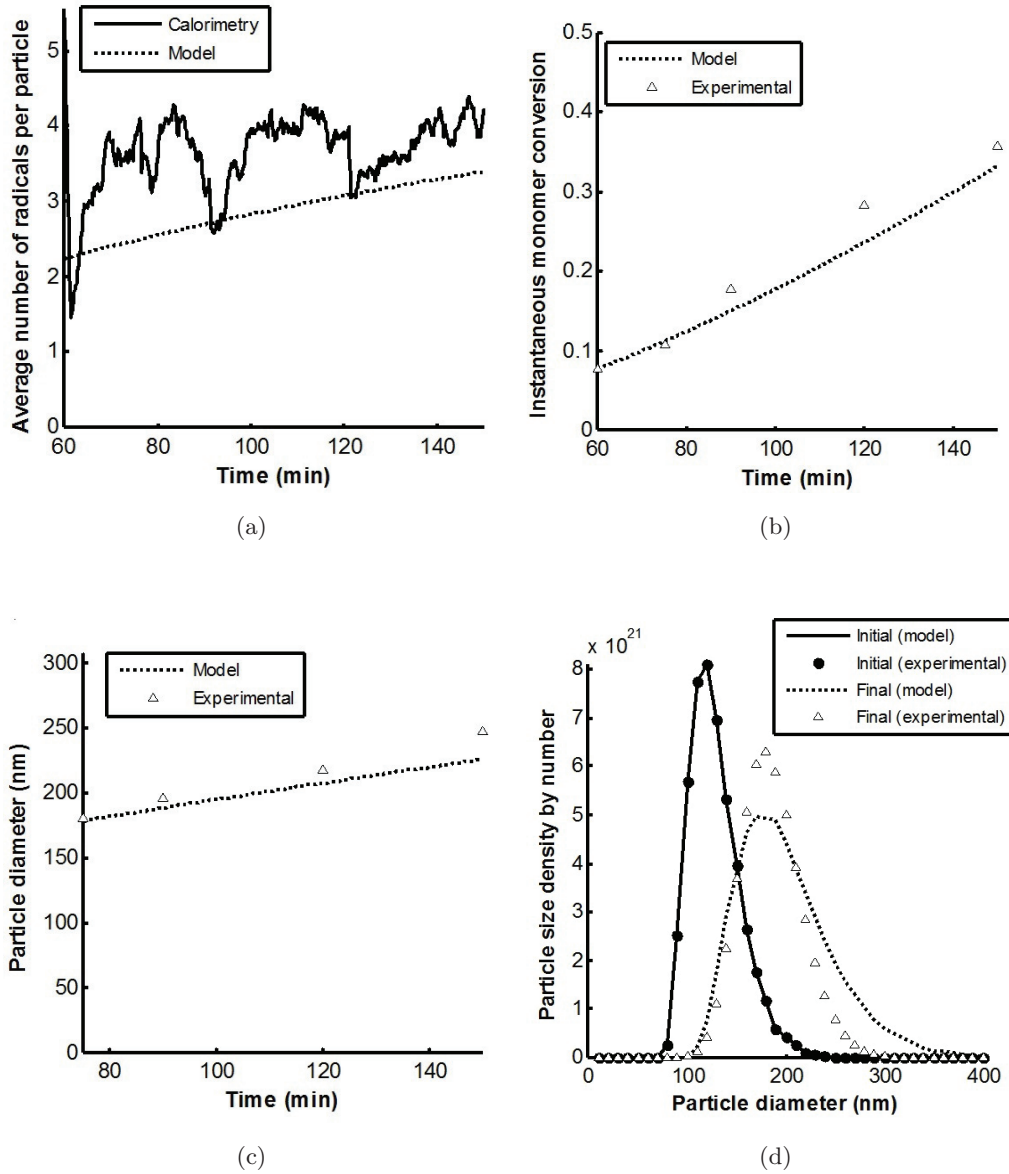


Figure 5.9: Simulation of a conventional emulsion polymerization system stabilised by SDS (0.5 g L^{-1}) using the capture model of Fontenot and Schork (1992) and the desorption model of Lacik et al. (1992)

5.5.4 Comparison to conventional SDS stabilization

The chosen model was used to describe a conventional emulsion polymerization system stabilized by Sodium Dodecyl Sulfate salt, without any clay. Again, interval II was considered in order to avoid diffusion limitations. The initiator and monomer initial concentrations were the same as in the Pickering system, but the obtained particle size and number are quite different from the system stabilized by the clay, which is not surprising due to the different stabilization mechanisms. A higher monomer flowrate was therefore employed in order to ensure saturation conditions, due to the higher number of particles and reaction rate. It can be seen that \bar{n} is well estimated as well as the growth rate which is depicted on the estimated D_p . As the same model was able to predict both a conventional and a Pickering emulsion polymerization system with different clay concentrations, then it can be concluded that the clay in this system does not hinder radical capture.

5.6 Conclusions

Simulations of radical capture and desorption in interval II of Pickering emulsion polymerization of styrene have shown that \bar{n} was independent of the clay concentration. Investigation of the different capture and desorption models show that the validity of the models is limited to particular systems, monomer solubility in water or in polymer, particle size, rate of transfer to monomer and to some extent to particular solid content. The 0-1 or 0-1-2 models are not applicable to the styrene system underhand as the particle size is high which implies high \bar{n} values.

Chapter 6

Modeling of nucleation and coagulation in Pickering emulsion polymerization

*“ Every birth is the rebirth of an
ancestor ”*

African oral tradition

Abstract : Investigation of nucleation in Pickering emulsion polymerization of Styrene is considered. The stabilization efficiency of the polymer particles by the adsorbed Laponite[®] clay was estimated by calculating the effective number of clay platelets contributing to the surface charge of the polymer particles. Coagulative-nucleation mechanism was proposed and the coagulation coefficients were calculated using DLVO theory. The Hamaker constant involved in the attractive potential of this system was measured experimentally. The model was found to fit the experimental data quite well in terms of the nucleated number of particles as well as the nucleation period. The effective number of clay platelets contributing to the surface charge was found higher than the number of platelets allowing full saturation of the surface by the end of the nucleation period. Moreover, the number of particles was found to stabilize against coagulation only for almost full surface coverage.

6.1 Introduction

Modeling of emulsion polymerization systems has attracted a number of scientists and there have been different levels of models proposed to describe these relatively complex systems [Smith and Ewart, 1948] [Coen et al., 1998] [Thickett and Gilbert, 2007] [de Arbina et al., 1996] [Sheibat-Othman et al., 2011] [Immanuel and Doyle Iii, 2003]. Modeling was found important to enhance the understanding of the system and to allow optimization and control of the process [Alamir et al., 2010] [Edouard et al., 2005] [Crowley et al., 2000]. Different stabilization systems were proposed to prevent particle coagulation in emulsion polymerization. Anionic [Colombié et al., 2000] [Castelvetto et al., 2006] or cationic [Ramos and Forcada, 2006] [Zaragoza-Contreras et al., 2002] surfactants were the most widely used stabilizing systems. Steric stabilizers were also employed [Ferguson et al., 2005] [Lazaridis et al., 1999]. More recently, Pickering stabilization was considered by employing different shapes of inorganic particles, such as silica [Colver et al., 2008] [Colard et al., 2010] or clay [Bourgeat-Lami and Lansalot, 2010] [Bourgeat-Lami et al., 2010] [Sheibat-Othman et al., 2011] in view of the production of organic/inorganic nanocomposites. In these surfactant-free heterophase polymerizations known as “Pickering emulsion polymerization”, the adsorption of clay stabilizes the dispersion of polymer particles. The use of Laponite[®] as stabilizers in emulsion polymerization was first carried out in presence of surfactant. A chemically-modified Laponite[®] was used after coating with either cationic initiators or monomers through ion exchange, or by the reaction of the edge-hydroxyls with suitable organosilane molecules. Stable colloidal aqueous suspensions of composite particles with diameters in the range 50-150 nm were obtained consisting of a polymer core surrounded by an outer shell of clay platelets [Ruggerone et al., 2009a] [Ruggerone et al., 2009b] [Herrera et al., 2004] [Negrete-Herrera et al., 2006a] [Herrera et al., 2005] [Herrera et al., 2006] [Negrete-Herrera et al., 2007] [Negrete-Herrera et al., 2006b]. Subsequently bare Laponite[®] platelets were used in emulsion polymerization without addition

of surfactant [Bourgeat-Lami et al., 2007] [Aranda and Ruiz-Hitzky, 1994]. In this work, Laponite[®] clay platelets were used in surfactant-free emulsion polymerization. The objective is to propose a nucleation mechanism of this system that is supposed to be different than surfactant-based polymerizations due to the different particles' surface properties. Nucleation is a determinant step in emulsion polymerization as it determines the number and size of particles and hence the reaction rate. It is commonly admitted that in soap-free emulsion polymerizations the particles formation process occurs through homogeneous nucleation, referred to as the Hansen-Ugelstadt-Fitch-Tsai (HUFT) model of nucleation [Fitch and Tsai, 1971] [Hansen and Ugelstad, 1978b]. In this mechanism, primary latex particles are created in the aqueous phase. This starts by initiator decomposition in the aqueous phase producing primary radicals that propagate with monomer dissolved in water until reaching a critical chain length where they precipitate. Precursor particles swell with monomer and become the loci of polymerization reaction. Stabilization of these precursors is maintained due to sulfate groups of absorbed radicals as well as adsorbed stabilizer from the aqueous phase. With the growth of the particle, its surface area increases and the surface charges might become insufficient to ensure stabilization against coagulation. In order to reduce the surface tension, precursor particles coagulate with each other, until a stable number of growing latex particles is generated. In Pickering emulsion polymerization, the presence of charged inorganic particles on the surface of the polymer particle will supplement the stabilization. The adsorption event of well dispersed charged particles/platelets is important for the nucleation in Pickering emulsion polymerization [Ngai and Bon, 2014]. In this work, surfactant-free emulsion polymerization of styrene is considered in presence of Laponite[®] clay platelets as stabilizers, and potassium persulfate as initiator. Investigation of interval I (related to particle nucleation) and interval II (related to particle growth under saturation with monomer) is done. The models of radical entry and desorption were previously investigated and will be used in this work (chapter 5). Partitioning of clay between the water phase and polymer particles surface was studied in chapter 2 and modeled using the BET model.

To describe the nucleation phenomenon, the coagulative-nucleation mechanism is proposed in this work, using the DLVO theory to calculate the coagulation coefficients. Investigation of the effect of the clay concentration on the nucleation and coagulation rate is considered.

6.2 Materials and Methods

The materials and methods were presented in chapter 2. *Ab initio* semi-continuous reactions were considered, under saturation with monomer. Therefore, semi-continuous monomer injection was started before the depletion of monomer droplets in order to maintain polymer particles under saturation for a longer period. This avoids diffusion limitations and allows the use of constant coefficients in the model (e.g. coefficients of propagation, termination, diffusion in the polymer particles).

6.2.1 Hamaker constant measurement

Latex with 1 g L^{-1} prepared in the ab-initio semi-continuous emulsion polymerization was used for the measurement of the Hamaker constant. This latex was diluted to 5 wt% and the particle size distribution (PSD) of the latex particles was measured by dynamic light scattering (Zetasizer, nano ZS, Malvern) at 25°C at a fixed scattering angle of 90° . Electrolyte solutions were prepared using sodium chloride from Sigma Aldrich. Experimental measurement of the Hamaker constant was done based on the interpretation of the backscattering profile obtained using a Turbiscan Lab[®] with an 850 nm light source [Fortuny et al., 2004]. Samples of 10 mL of latex were placed in the Turbiscan cell. Scan mode was performed before coagulation to acquire transmission and backscattering data. A three blade impeller was used to disperse the salt added during measurement. Once the backscattering signal stable, an aliquot of salt was added under agitation. Agitation was stopped until stabilization of the backscattering signal. Then, salt additions were repeated. Measurements were stopped when backscattering signal stayed constant with the salt addition. Traitement of backscattering measurement allows to estimate the Hamaker constant as described in section 6.4.1.2.

6.3 Modeling

6.3.1 Polymer particles population balances

The comprehensive particle size distribution model in emulsion polymerization takes into account particle formation by nucleation, growth by polymerization and coagulation mechanisms (Min and Ray [Min and Ray, 1974]):

$$\frac{\partial n(r, t)}{\partial t} + \frac{\partial n(r, t)\mathcal{G}(r, t)}{\partial r} = \mathfrak{R}_n\delta(r - r_{nuc}) - \mathfrak{R}_{coag} \quad (6.1)$$

Where $n(r, t)$ is the number of particles of radius between r and $r + \delta r$ at time t , $\mathcal{G}(r, t)$ is the growth rate of particle of size r , R_n is the nucleation rate, $\delta(r - r_{nuc})$ is the Dirac delta function which is unity for $r = r_{nuc}$ and zero elsewhere which represents the boundary condition, r_{nuc} is the nucleation radius and R_{coag} is coagulation rate. The boundary condition of equation 6.1 is therefore given by:

$$n(r_{nuc}, t) = \frac{\mathfrak{R}_n(t)}{\mathcal{G}(r_{nuc}, t)} \quad (6.2)$$

The growth rate is given by:

$$\mathcal{G}(r, t) = \frac{dr}{dt} = \frac{k_p \bar{n} [M]_p MW}{4\pi r^2 \rho N_A} = \frac{R_p MW}{4\pi r^2 \rho N N_A} \quad (6.3)$$

Where MW is the monomer molecular weight, ρ is the monomer density, k_p is the propagation rate coefficient, $[M]_p$ is the concentration of monomer in the polymer particles, N_A is Avogadro's number, N is the number of monomer-swollen polymer particles per unit volume of latex and R_p is the polymerization rate per unit volume of latex which is supposed to proceed mainly in the polymer particles [Smith and Ewart, 1948]:

The value of $\bar{n}(r, t)$ depends on the rates of radical entry, desorption and termination inside the particle, and therefore on the concentration of radicals in the aqueous phase, diffusion inside the particle, and the particle size. An investigation of radical entry and desorption rates was done in chapter 5, and the most adapted model will be used in this chapter because this models can be used in interval I. It

is important to emphasise that it could be concluded that the clay layer around the particle did not affect radical exchange.

In the present Pickering emulsion polymerization system, coagulative-nucleation mechanism is assumed to be the main nucleation mechanism as the system contains no micelles. Particles are mainly formed in water and stabilised by the clay first dispersed in water then adsorbed on the polymer particles surface. Coagulation may take place until the colloidal stabilisation of a tolerable number of particles with reduced surface tension.

The coagulative-nucleation theory calculates the rate of particles formation from the rate of homogenous nucleation and formation of primary precursors based on the Hansen-Ugelstad-Fitch-Tsai theory (HUFT) [Fitch and Tsai, 1971] [Hansen and Ugelstad, 1978b] combined to the kinetics of coagulation among precursor particles, using the Smoluchowski-Muller-Fuch theory [Smoluchowski, 1927] [Fuchs, 1934]. The coagulation rate coefficients may be calculated using DLVO theory. These theories are detailed in the following sections.

6.3.2 Homogeneous nucleation mechanism

In the homogeneous nucleation mechanism, the creation of new particles in the aqueous phase occurs when the oligomers reach the solubility limit j_{crit} and precipitate. These precursors then absorb monomer and radicals and the main monomer consumption occurs within these particles.

The rate of formation of new particles by homogeneous nucleation is given by:

$$\mathfrak{R}_{hom}(t) = k_p[M]_w[IM_{j_{crit}}^\bullet] \quad (6.4)$$

where $[IM_{j_{crit}}^\bullet]$ is the concentration of oligomeric radicals of size j_{crit} in aqueous phase, k_p is the propagation rate constant in the aqueous phase and $[M]_w$ the monomer concentration in the aqueous phase.

6.3.3 Particle coagulation

In emulsion polymerization, particles are stabilized by charges of initiator radicals present on the particles surface as well as those of the adsorbed stabilizer (clay in this

work). Coagulation of latex particles may take place by perikinetic or orthokinetic coagulation [Hermans, 1939] [Melis et al., 1999] [Immanuel and Doyle Iii, 2003]. Perikinetic coagulation is related to the Brownian diffusion of particles and interactions between colloidal particles are typically caused by electrostatic or steric forces. Electrostatic interactions take place when colloidal particles have electrical charges that promote attraction or repulsion from each other. Also charges of continuous and dispersive environments and the mobility of the two phases are factors affecting this interaction. Steric forces may also produce a repulsive steric stabilization force or additional attractive depletion force. Orthokinetic coagulation generated by the shear of the fluid or by the forces of gravity may also enhance the coagulation of particles in emulsion polymerization. The contributions of these two mechanisms are not necessarily additive. This depends on both the medium and the mixing conditions, the size of particles, the shear rate and colloidal stability. Melis et al [Melis et al., 1999] have shown that for stable systems (slow aggregation) the two mechanisms are independent.

In this work, the effect of stirring was examined experimentally and was found not to affect the particles size or number (chapter 4). Therefore, only perikinetic coagulation will be considered.

6.3.3.1 Coagulation rate by volume and by radius

Smoluchowski and coworker [Smoluchowski, 1927] have been working on a mathematical theory and its application to colloidal solutions to describe the particle coagulation kinetics. When discretized by volume, the particle size distribution, $f(v,t)$, can be modeled by:

$$\frac{\partial f(v,t)}{\partial t} + \frac{\partial(f(v,t)\mathcal{G}(v))}{\partial v} = \mathfrak{R}_n(t)\delta(v - v_{nuc}) - \mathfrak{R}_{coag}(v,t) \quad (6.5)$$

and the coagulation rate is expressed as:

$$\mathfrak{R}_{coag}(v,t) = \mathfrak{R}^+(v,t) - \mathfrak{R}^-(v,t) \quad (6.6)$$

with \mathfrak{R}^+ designing the rate of particle creation by coagulation and \mathfrak{R}^- the rate of particles disappearing due to coagulation given by:

$$\begin{cases} \mathfrak{R}^+(v, t) = \int_{v_{nuc}}^{v-v_{nuc}} B(v', v-v') f(v', t) f(v-v', t) dv' \\ \mathfrak{R}^-(v, t) = f(v, t) \int_{v_{nuc}}^{\infty} B(v, v') f(v', t) dv' \end{cases} \quad (6.7)$$

Due to the simplicity due to the additive property of volumes, most works concerning the coagulation express the coagulation rate as a function of volume v ($v = v' + v''$). Immanuel et al. [Immanuel and Doyle Iii, 2002] developed the equivalent coagulation rates discretized as a function of particles radius (r) using the pseudo-bulk model. In order to do so, the volumes of particles of radii r, r', r'' are defined respectively by v, v', v'' and the following change of variables $n(r, t) = f(v, t) \frac{dv}{dr}$ is used. r' and r'' denote the possible particle radii which form a particle with radius r after coagulation. It can be shown that $r^3 = r'^3 + r''^3$. Replacing these terms in equation 6.7, gives:

$$\begin{cases} \mathfrak{R}^+(r, t) = \int_{r_{nuc}}^{(r^3-r_{nuc}^3)^{1/3}} B(r', r'', t) n(r', t) n(r'', t) \frac{dr''}{dr} dr' \\ \mathfrak{R}^-(r, t) = n(r, t) \int_{r_{nuc}}^{\infty} B(r, r', t) n(r', t) dr' \end{cases} \quad (6.8)$$

It can also be demonstrated that:

$$\frac{dr''}{dr} n(r', t) = n(r, t) \quad (6.9)$$

where $dr'' dr$ represents the variation of the particle radius r'' compared to radius r of the formed particle. Hence, the particle formation term becomes:

$$\mathfrak{R}^+(r, t) = \int_{r_0}^{\frac{r}{2^{1/3}}} B(r', r'', t) n(r', t) n(r'', t) \frac{r^2}{(r^3 - (r')^3)^{2/3}} dr' \quad (6.10)$$

with $r'' = (r^3 - r'^3)^{1/3}$

6.3.3.2 DLVO theory

The coagulation rate coefficient B in the Smoluchowski equation 6.10 may be calculated by different methods, the most commonly used in emulsion polymerization

is DLVO theory. This theory have been used for predicting the coagulation of latex particles stabilized by ionic [Coen et al., 1998] [Coen et al., 2004] or nonionic surfactants [Immanuel and Doyle Iii, 2003] and calculate the rate coagulation R_{coag} for the pseudo-bulk model.

The DLVO theory is based on the work of Derjaguin and Landau [Derjaguin and Landau, 1945] and those of Verwey and Overbeek [Verwey and Overbeek, 1948]. It describes the coagulation of colloidal suspension by interpretation of the total energy of interaction between the colloidal particles. The total energy is the combination of repulsive forces and the attractive forces. In emulsion polymerization, interactions between negatively charged particles result mostly from Van der Waals attraction and electrostatic repulsion. These forces are strongly dependent to the interparticle (or center to center) distance R .

6.3.3.3 Coagulation rate coefficients

It is possible to calculate the coagulation rate coefficient B between two particle r and r' at time t , using Muller equation [Müller, 1928]:

$$B(r, r') = B(r', r) = \frac{2k_B T}{3\eta W(r, r')} \left(2 + \frac{r}{r'} + \frac{r'}{r} \right) \quad (6.11)$$

where η is the viscosity of the medium, k_B is Boltzman constant, T is absolute temperature and $W(r, r')$ is the stability ratio of particles of radius r and r' . Fuchs [Fuchs, 1934] studied the collision of particles in Brownian motion in the presence of repulsion and attraction forces of Van der Waals and defined the stability ratio as an equivalent to the inverse of the efficiency of aggregation as follows:

$$W(r, r') = \frac{r + r'}{4\kappa r r'} \int_2^\infty \frac{\exp\left(\frac{\Phi_T}{k_B T}\right)}{R^2} dR \quad (6.12)$$

where κ is the Debye length, R is the center-to-center distance separating two particles of swollen radii r and r' and Φ_T is the total potential.

According to DLVO, two particles can coagulate if they get over the potential barrier, which precisely corresponds to the integral of the curve of total potential

positive. Usually, the curve of the total energy (attraction – repulsion, Φ_T) passes through a maximum $\Phi_{T,max}$. Exceeding this maximum is necessary for particles aggregation. So, Overbeek (Verwey and Overbeek 1948) proposed the following simplification:

$$\int_{r+r'}^{\infty} \exp\left(\frac{\Phi_T}{k_B T}\right) \frac{dR}{R^2} \approx \frac{1}{2R} \exp\left(\frac{\Phi_{T,max}}{k_B T}\right) \quad (6.13)$$

The total potential between two particles is given by:

$$\Phi_T = \Phi_A + \Phi_R \quad (6.14)$$

6.3.3.4 Attractive potential

The attractive potential is given by:

$$\Phi_A = \frac{-A}{6} \left[\frac{2rr'}{R^2 - (r+r')^2} + \frac{2rr'}{R^2 - (r-r')^2} + \ln \left(\frac{R^2 - (r+r')^2}{R^2 - (r-r')^2} \right) \right] \quad (6.15)$$

where A is the Hamaker constant.

6.3.3.5 Repulsive potential

The repulsive potential is given by Hogg Healy and Fürstenau formula [Hogg et al., 1966]:

$$\Phi_R = \frac{\varepsilon r r' (\zeta^2 + \zeta'^2)}{4(r+r')} \left[\frac{2\zeta\zeta'}{\zeta^2 + \zeta'^2} \ln \left(\frac{1 + e^{-\kappa L}}{1 - e^{-\kappa L}} \right) + \ln(1 - \exp(-2\kappa L)) \right] \quad (6.16)$$

where $L = R + (r + r')$, is the edge-to-edge distance between particles.

The zeta potential of the particles is given by:

$$\zeta = \left(\frac{2k_B T}{z_+ e} \right) \ln \left(\frac{\exp(\lambda_4) + 1}{\exp(\lambda_4) - 1} \right) \quad (6.17)$$

with:

$$\lambda_4 = \delta\kappa + \ln \left(\frac{\exp(\lambda_5) + 1}{\exp(\lambda_5) - 1} \right) \quad (6.18)$$

$$\lambda_5 = \frac{z_+ e \Psi}{2k_B T} \quad (6.19)$$

where e is the electron charge, z the counter ion valence, δ_s is the thickness of the stern layer and Ψ is the surface potential is given by:

$$\Psi = \frac{2k_B T}{e} \sinh^{-1} \frac{2\pi e \sigma_T}{\varepsilon \kappa k_B T} \quad (6.20)$$

where σ_T is the surface charge of the polymer particles and $\varepsilon = 4\pi\varepsilon_0\varepsilon_r$ is the relative permittivity of the medium, with ε_0 the vacuum permittivity and ε_r the water relative permittivity. If κr is greater than 1, the particle surface is approximately a flat surface, but if κr is less than 1, the curvature of the particle is not negligible, and hence the surface potential is replaced by (both terms have the same value for $\kappa r_s = 1$) :

$$\Psi = \frac{4\pi r \sigma_T}{\varepsilon(1 + \kappa r)} \quad (6.21)$$

The Debye length κ characterizes the thickness of the double electric layer and describes the diffuse layer of the free ions in opposite aqueous phase to the particle surface:

$$\kappa = \sqrt{\frac{8\pi N_A F i^2}{\varepsilon k_B T}} \quad (6.22)$$

where N_A is the Avogadro number and $F_i = \sum C_{e,i} z_i^2$ is the ionic strength ($C_{e,i}$ is the electrolyte concentration of ionic species i and z_i is its respective ionic valence).

The total surface charge of the polymer particles come from the decomposition of the initiator, σ_I , and the presence of charged inorganic particles, σ_{stab} , on their surface:

$$\sigma_T = \sigma_{stab} + \sigma_I \quad (6.23)$$

The contribution of the ions formed by the decomposition of the initiator at the time t is given by:

$$\sigma_I = \frac{2([I_0] - [I(t)])V_w z_+ e N_a}{A_{tot}} \quad (6.24)$$

where $[I_0]$ and $[I(t)]$ are respectively the concentrations of initiator at initial time and at the time t , and A_{tot} the total surface of polymer particles defined as follow:

$$A_{tot} = \int_0^\infty 4\pi n(r)r^2 dr \quad (6.25)$$

While the contribution of the clay surface charge charge is given by:

$$\sigma_{stab} = \frac{q_c}{A_{tot}} \quad (6.26)$$

q_c is the total charge brought by the clay platelets. It is going to be investigated during the experiments.

6.3.4 Radical, monomer and surfactant balances in the different phases

6.3.4.1 Average number of radicals in the particles

Please refer to chapter 5 for the model of \bar{n}

6.3.4.2 Radical entry and desorption

Radical entry and desorption was studied in the absence of nucleation or coagulation in chapter 5. A propagation-controlled model was found the most appropriate to describe radical entry [Asua and De La Cal, 1991] while radical desorption the model of Lacik [Lacik et al., 1992] was found adapted.

6.3.4.3 Aqueous phase reactions

Aqueous phase reactions are presented in chapter 5.

6.3.4.4 Monomer Balance and partitioning

Monomer balance was presented in chapter 5. As modeling is considered exclusively in interval II, all phases (i.e. polymer and aqueous phases) may be assumed to be saturated with monomer, if we assume instantaneous equilibration of the monomer concentration in the different phases during the reaction. The saturation concentrations are supposed not to be affected by the clay layer.

6.3.4.5 Stabilizer partitioning

In chapter 2, the clay was found to be mainly adsorbed on the surface of polymer particles forming multilayers, as demonstrated by transmission electron microscopy and Inductively Coupled Plasma-Atomic Emission Spectroscopy, for all clay concentrations studies in this work. The BET model can be used to calculate the concentration of clay on the surface of polymer particles and in water. It was also found by QCM measurements that the adsorption phenomenon is relatively fast (5 min), and therefore equilibrium partitioning can be assumed during the reaction.

The adsorption isotherm was found to be affected by the ionic strength of the system. At higher ionic strength (mainly due to initiator decomposition), adsorption of clay platelets was enhanced. This was explained by the fact that the sulfate ions in solution screen the clay charge and enhances the adsorption to the surface of the negatively charged polystyrene latex. Therefore, it might be guessed that the stabilization efficiency of the clay will be affected by the ionic strength and not only by the amount of adsorbed clay. The ionic strength was not varied in this work, but was high enough to ensure full clay adsorption. Therefore, the stabilization efficiency of the clay is estimated only in these ionic strength conditions.

6.4 Results and discussion

The presented models were evaluated in Pickering emulsion polymerization system of styrene stabilized by Laponite®. The models related to radical exchange and growth were validated in chapter 5, in the absence of nucleation and coagulation, and during interval II and reused in this chapter (interval I). During interval I,

diffusion limitations are not an issue, and therefore the different coefficients could be assumed constant with time (i.e. propagation, termination and diffusion). Clay partitioning was calculated using BET model (chapter 2).

Before modeling, some experimental observations are presented and the Hamaker constant involved in the attractive potential, is identified experimentally. This is followed by modeling the population balance equation, where nucleation is described by the homogeneous coagulative nucleation model.

6.4.1 Experimental observations

6.4.1.1 Effect of the clay concentration

In order to examine the role of clay on nucleation and stabilization of polymer particles, surfactant-free emulsion polymerization of styrene was carried out in the presence of clay, in *ab initio* batch or semi-continuous modes. The objective of these experiments was to investigate relationships between the clay concentration and the nucleated number of particles.

Surfactant-free emulsion polymerization of styrene was carried out in the presence of different clay concentrations (figure 6.1). It can be seen that increasing the clay concentration lead to an increase in the nucleated number of particles (figure 6.1a). Indeed, increasing the amount of clay allowed a better stabilization of nucleated particles reducing thereby the coagulation rate. Increasing the number of particles is usually accompanied by an increase in the reaction rate with time (figure 6.1b). Therefore, at the same solid content, smaller particles were obtained when increasing the clay concentration (figure 6.1c). These results suggest successful clay adsorption on the polymer particles' surface as demonstrated in chapter 2. Figure 6.1d also shows that the number of particles increased at the beginning of the reaction during the nucleation period, and then stabilized until the end of the reaction. The nucleation period was longer for higher amounts of clay. The end of the nucleation period was observed between 45 and 90 min. It indicates the beginning of interval II.

The particles' coverage rate by the clay in these experiments was estimated as

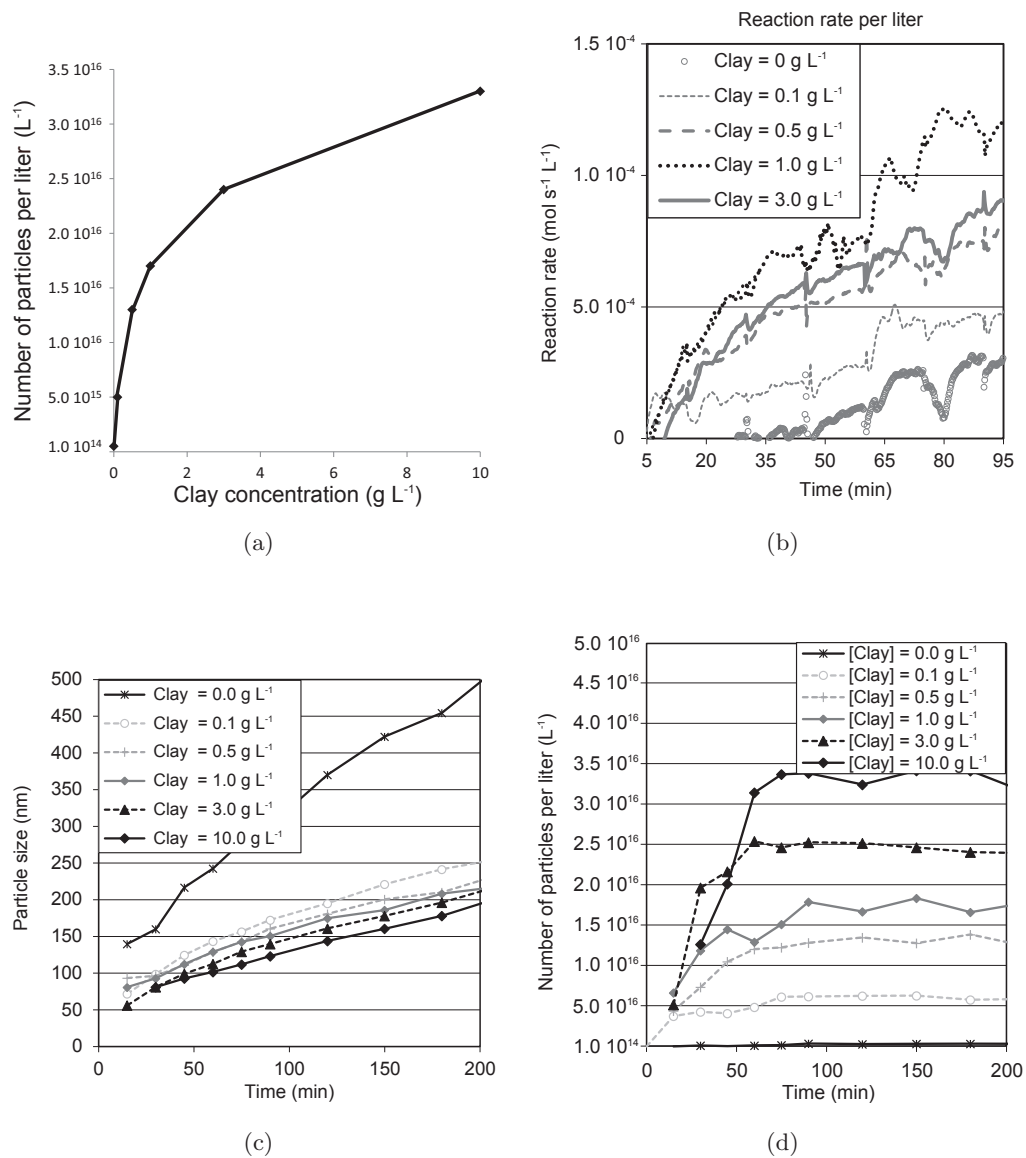


Figure 6.1: Pickering *ab initio* semi-continuous emulsion polymerization of styrene stabilized by different amounts of Laponite RDS[®]. (a) Final number of particles per liter versus Laponite[®] concentration, (b) Reaction rate (c) Average particle size (d) Evolution of the number of particles during E.P.

the ratio of the surface area of platelets' discs of 25 nm diameter to the polymer particles' area assuming spherical shape and full clay dispersion (i.e. no aggregates of clay in water). Figure 6.2 shows that for clay concentrations higher than 0.5 g L^{-1} , the area of platelets was enough to cover the total surface area of particles and a significant excess of clay platelets was present at the beginning of the polymerization. As the particles grew, this amount became insufficient to cover the full polymer particles' surface, except for 10 g L^{-1} clay.

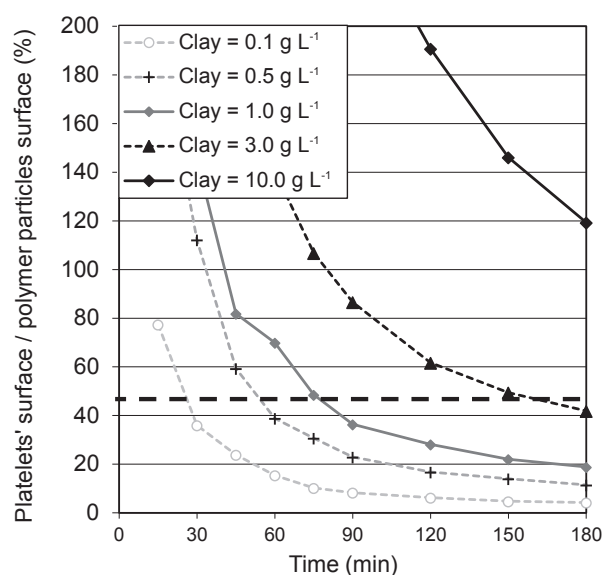


Figure 6.2: Ratio of the surface area of platelets' faces discs to the polymer particles' area

In chapter 2 it was demonstrated that almost full adsorption of clay platelets on the polymer particles takes place under the present reactions conditions (e.g. ionic strength) and only a slight amount may be observed in water. The BET model presented in chapter 2 can be used to calculate surfactant partitioning between the phases. However, the stabilization efficiency of the clay was not evaluated. The objective of the next sections is therefore to determine the influence of charge interactions created by the clay on particle stabilization and to propose a nucleation mechanism for the present Pickering emulsion polymerization system.

6.4.1.2 Measurement of the Hamaker constant

Provoked coagulation experiments were realized to evaluate the Hamaker constant by adding a monovalent electrolyte (Sodium chloride, NaCl) on polystyrene latex coated with clay. The principle of this experimental approach is based on that used by Fortuny et al. [Fortuny et al., 2004].

The collected data are plotted on figure 6.3, and treated with the following empirical equation [Fortuny Heredia, 2002] [Fortuny et al., 2004] [Abismail et al., 2000]:

$$W = \frac{\left(\frac{d\tau}{dt}\right)_{0, C_e > CCC}}{\left(\frac{d\tau}{dt}\right)_{0, C_e}} \quad (6.27)$$

where W is the experimental stability ratio, $\frac{d\tau}{dt}$ the variation of the turbidity as a function of time, C_e is the electrolyte concentration and CCC is the critical coagulation concentration.

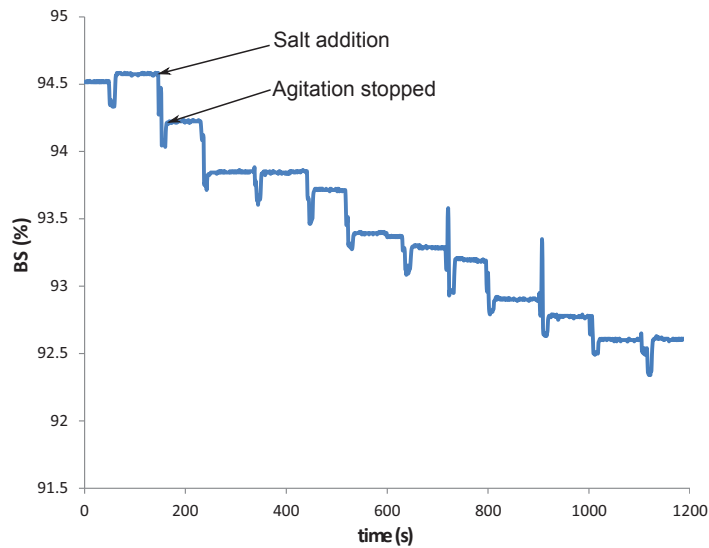


Figure 6.3: Variation of the backscattering of polystyrene (5 wt%) covered with Laponite RDS (1 wt% of latex)

First of all, the backscattering signal was normalized by division by the initial

value (before adding salt) and the effect of dilution was eliminated (by subtracting signal due to the addition of water without salt) [Fortuny et al., 2004]. An average value for each plateau was then calculated to determine the differential back scattering values that were used to replace the turbidities in equation 6.27. The stability ratio was obtained by dividing the differential turbidity by the value of differential turbidity obtained at the plateau (figure 6.4).

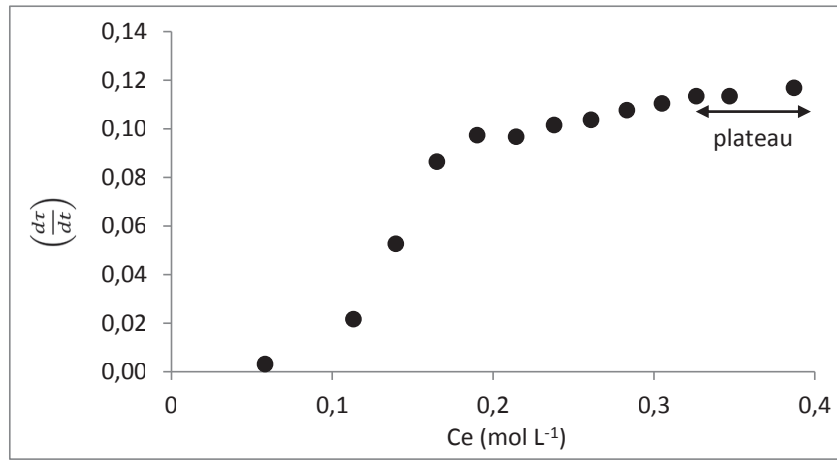


Figure 6.4: Differential turbidity of polystyrene (5 wt%) armored with Laponite RDS (1 wt% of latex)

Once the experimental stability ratio obtained (figure 6.5), Hamaker constant was found by fitting the experimental data using DLVO theory (equations 6.11 to 6.26) using the least squares method.

The estimated value of A was 1.89×10^{-21} J. Hamaker constant can also be estimated from Lifshitz theory [Lifshitz, 1955] using Tabor-Winterton assumption [Israelachvili, 1992]. According to this theory, for two identical entities (i.e. two Laponite[®] platelets in our case) across a medium (water), the Hamaker constant is given by:

$$A = \frac{3}{4}k_B T \left(\frac{\varepsilon_{r1} - \varepsilon_{r2}}{\varepsilon_{r1} + \varepsilon_{r2}} \right)^2 + \frac{3h\nu_e}{16\sqrt{2}} \frac{(n_1^2 - n_2^2)^2}{(n_1^2 + n_2^2)^{3/2}} \quad (6.28)$$

Where h is Planck constant, n is the refractive index, ε is a dielectric constant and ν_e is the frequency of electron cloud oscillations, commonly estimated

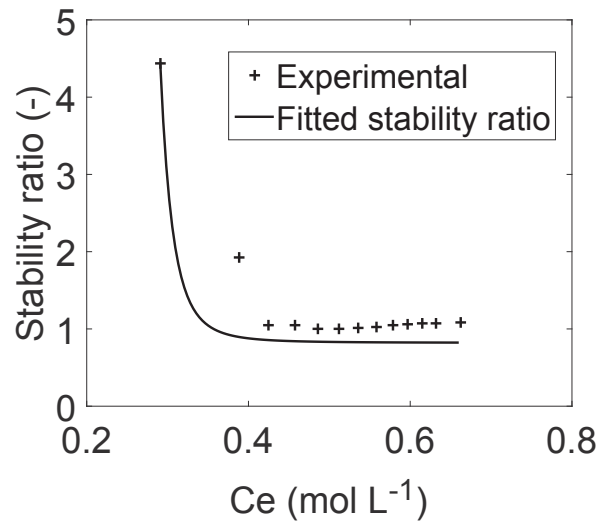


Figure 6.5: Experimental stability ratio and fitted stability ratio by DVLO theory for polystyrene (5 wt%) armored with Laponite RDS (1 wt% of latex)

to be $v_e = 3 \times 10^{15} \text{ s}^{-1}$. For the clay, the refractive index was given by $n_1 \approx 1.336$ [Kumar et al., 2008] and a dielectric (or relative permittivity) by $\epsilon_{r1} \approx 3.5$ [Laxton and Berg, 2006]. For water, the following constants were considered: $n_2 \approx 1.334$ and $\epsilon_{r2} \approx 63.9$ [Malmberg and Maryott, 1956] at 70°C. This results in a Hamaker constant of $A = 2.96 \times 10^{-21} \text{ J}$. This value is close and comfort the order of magnitude of the value found by the experimental fitting. The experimental value is used in the DLVO model as it takes into account possible aggregates of clay in water.

6.4.2 Modeling

6.4.2.1 Evidence for coagulation during nucleation

Figure 6.6 shows the estimation of the coagulation rate B for a clay concentration of 1 g L^{-1} . The figure shows that coagulation is high for very small particles and decreases rapidly for bigger particles. Also, it can be seen that small particles coagulate preferentially with the biggest particle.

Homogeneous nucleation presented in equation 6.4 was then used either alone or

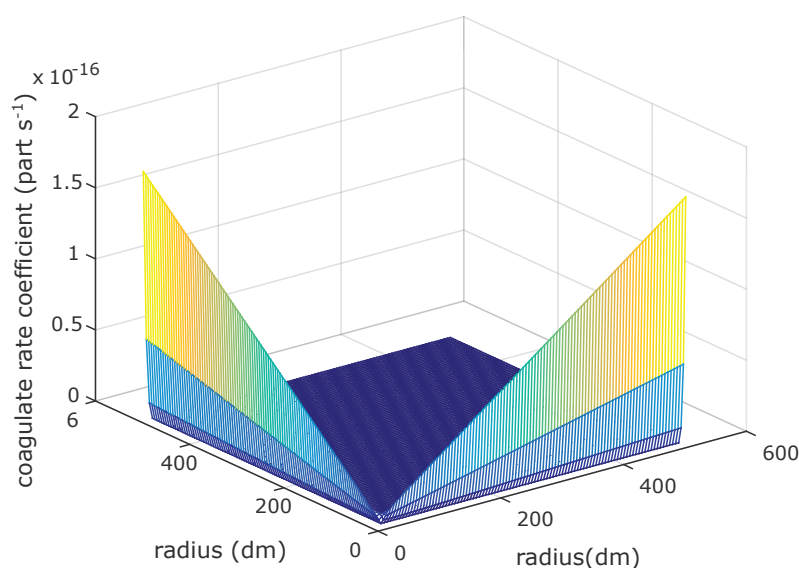


Figure 6.6: The coagulation rate coefficient B , eq. 6.11, of a Pickering emulsion polymerization system stabilized by Laponite[®] RDS (1 g L^{-1})

combined to coagulation (coagulative-nucleation) to predict the nucleated number of particles. Figure 6.7 shows that the number of particles created by homogeneous nucleation without coagulation was much higher than the real measured one. By assuming homogeneous nucleation combined to coagulation in the model, a more realistic number of particles was estimated (figure 6.7). This estimation is plausible, as a big numbers of precursors may be produced due to the high concentration of radicals, monomer and stabilizer in the aqueous phase. However, growth of these precursors leads to a fast increase in their surface area, which requires a huge amount of stabilizer to be protected against coagulation. The present amount of clay quickly adsorbs on the surface of particles, but may not cover all the surface of precursor particles, especially with the increasing surface due to particle growth. In order to enhance their stability, precursor particles hence coagulate to reduce their surface tension. It was noticed that the number of particles stabilizes when the coverage surface area by the clay attains about 100%. This simulation gives evidence for coagulation during nucleation that should therefore be taken into account in the model.

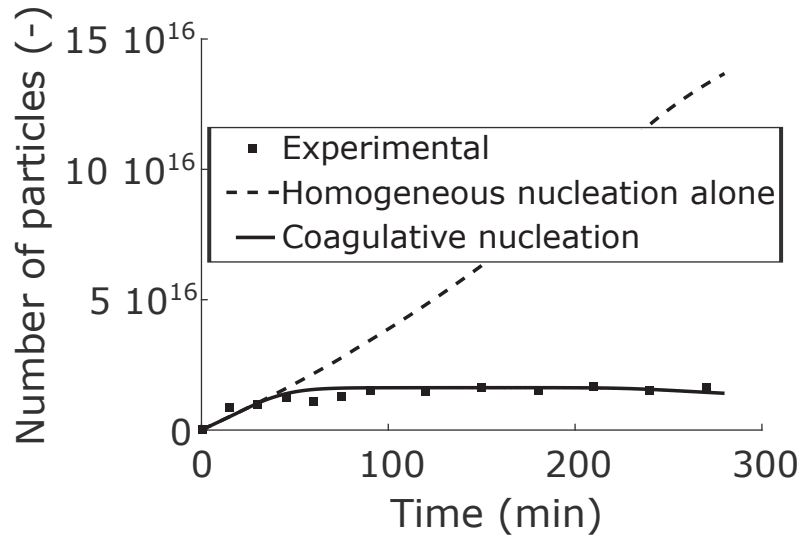


Figure 6.7: Nucleation in Pickering emulsion polymerization stabilized by Laponite[®] RDS (1 g L^{-1})

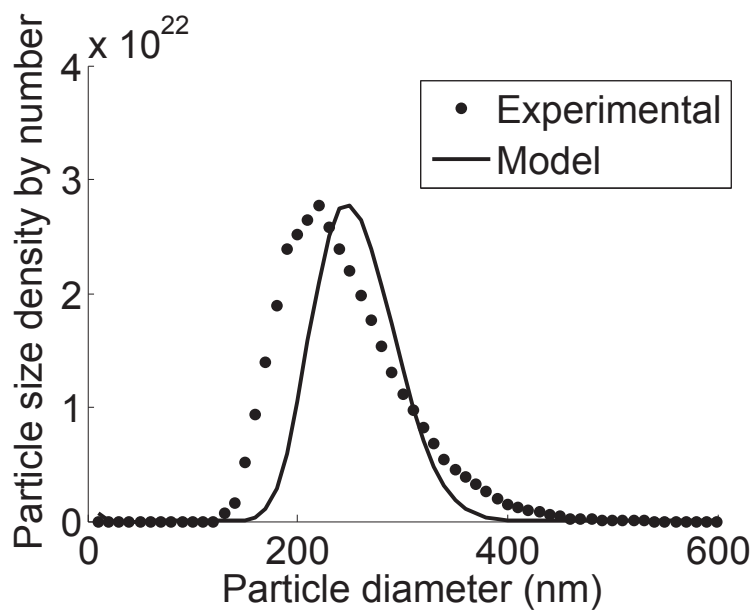


Figure 6.8: Particle sizer distribution obtained by the end of the reaction (Pickering emulsion polymerization stabilized by 1 g L^{-1} Laponite[®] RDS)

Figure 6.8 shows that the estimated final particle size distribution by model is in good agreement with the experimental data. The quasi Gaussian distribution confirms that the coagulation concerns mainly small particles.

6.4.2.2 Estimation of the surface charge due to the clay

In this section, homogeneous nucleation combined to coagulation is considered to describe nucleation in this Pickering system. DLVO is used to calculate the coagulation coefficient. The charge due to the clay, q_c , will be used as the only fitting parameter allow evaluating the stabilizing efficiency of the clay.

First of all, the charge due to the clay was identified individually for each experiment. The simulation results of the different clay concentrations are presented in figure 6.9 compared to the experimental data. The resulting charge from fitting is shown in figure 6.10 as a function of the clay concentration. A relatively good agreement can be observed for the total number of particles. Interestingly, the number of particles seems to stabilize usually when the surface coverage by the clay attains about 100%, except for 10 g L^{-1} (figure 6.2).

The individually fitted parameters are presented in figure 6.10 as a function of the clay concentration. As expected, the total charge of clay increased with the clay concentration. Indeed, almost all clay platelets are adsorbed on the polymer particles, and the higher the clay concentration the higher the charge is expected to be. However, the charge is not increasing linearly with the concentration. This can be explained by the multilayer adsorption mechanism. Upper layers may screen the charge of lower layers. In the following section, the effective number of platelets on the surface contributing to the charge is estimated in order to be able to estimate the effective charge based on the clay concentration without any parameter fitting.

6.4.3 Effective number of platelets contributing to surface charge

The charge due to the adsorbed clay on the polymer surface can be described by the following relation:

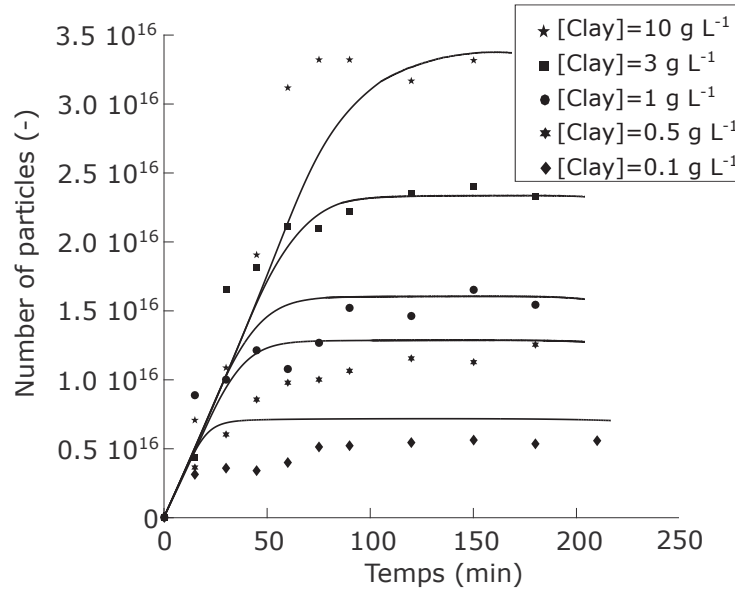


Figure 6.9: Estimation of the particle number in Pickering emulsion polymerization for different clay concentrations using charge of clay as a fitting parameter. The continuous lines represent the model and the points are experimental.

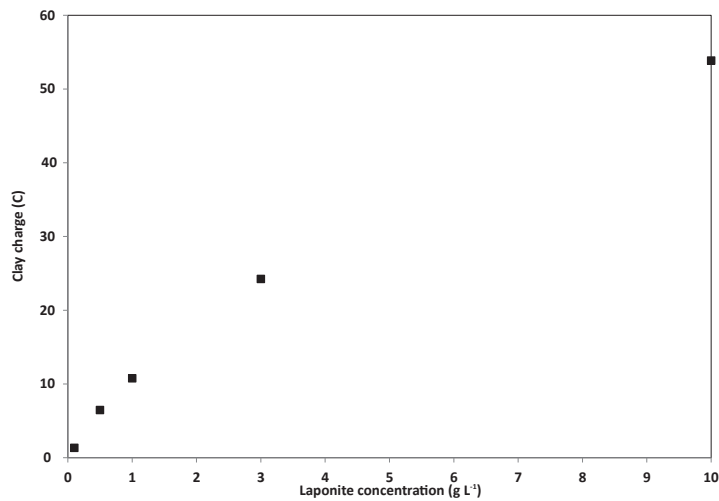


Figure 6.10: Total charge of Laponite[®] as fitted for the simulation of particle nucleation in Pickering emulsion polymerization for different amount clay concentrations

$$q_c = \sigma_0 S_c N_c \quad (6.29)$$

Where S_c is the surface of the face of a clay platelet, σ_0 the surface charge of clay (Laponite[®]) per unit of volume and N_c is the number of clay platelets introduced in the reaction medium calculated as follows:

$$N_c = \frac{m_c}{4\pi r_c^2 h_c \rho_c} \quad (6.30)$$

Where m_c is the introduced mass of clay, $r_c = 25$ nm and $h_c = 1$ nm are respectively the radius and the thickness of a Laponite[®] platelet and $\rho_c = 2570$ kg m⁻³ the density of Laponite[®] (Ruzicka, Zulian, and Ruocco 2006).

The assumption of no multilayer adsorption can be made for a clay concentration of 0.1 g L⁻¹ (the introduced amount is not sufficient to cover more than once the polymer particles, assuming perfect dispersion of the clay in water before the reaction). So this experiment can be used to evaluate the surface charge of one clay platelet (σ_0). Indeed, the surface coverage in this experiment is the lowest (<80%, figure 6.2) and therefore interactions between the platelets adsorbed on the surface of the polymer particles might be neglected. The estimated total charge during this experiment can therefore be divided by the surface of the clay platelets. This gives a value of $\sigma_0 = 0.216e$ nm⁻². Note that this is close to the one given in the literature for free Laponite[®] RD clay platelets ($\sigma_0 = 0.3e$ nm⁻²) [Li et al., 2005].

The estimated surface charge per platelet can then be used to estimate the effective number of platelets contributing to the total charge and eliminating the platelets for which the charge was screened either due to the ionic strength or to higher layers of platelets on the particles' surface. This is done as follows:

$$N_c^{eff} = \frac{q_c}{\sigma_0 S_c} \quad (6.31)$$

The resulting estimations of N_c^{eff} are given in figure 6.11. It can be seen that for low clay concentration (< 1 g L⁻¹), all the clay platelets were contributing to the charge as the effective number of clay platelets was equal to the experimental one. Moreover, for such concentrations, the polymer particles were completely saturated

with the clay at the end of the nucleation period. For clay concentrations higher than 3 g L^{-1} , only part of the clay was effectively contributing to the charge. This might be due to screening of lower layers charges or for having these charges hidden by upper layers. However, the effective number of clay was slightly higher than the number of clays required to ensure saturation of the polymer surface. This was probably a result of arrangement of multilayers of clay on the surface. Note that all the clay was however adsorbed on the surface of particles as demonstrated in chapter 2.

An interpolation curve was developed to allow getting a relation between the effective number of platelets as a function of the clay concentration, under the considered ionic strength. This allows modeling the nucleation phenomena without any fitting parameters.

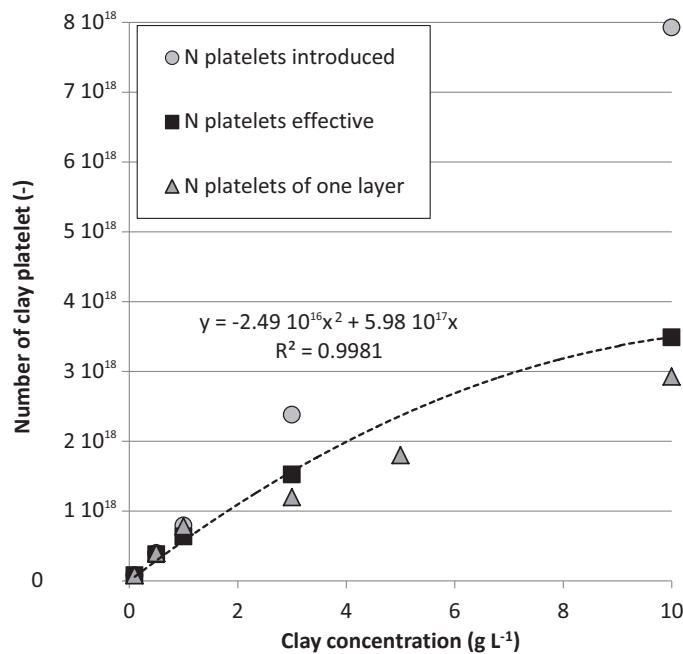


Figure 6.11: The introduced number of platelets is compared to the effective number of platelets contributing to the charge of the polymer particle and to the number of platelets required to saturate the polymer particle with the clay. (–) interpolation curve.

6.5 Conclusion

Clay was found to have an important role in stabilizing polymer particles in surfactant free emulsion polymerization. Smaller particles could be obtained at the same solid content when increasing the clay concentration, which lead to a bigger number of stabilized particles by the end of the reaction. In order to describe this phenomenon, coagulative-nucleation mechanism was assumed. Homogeneous nucleation takes place in parallel to coagulation. DLVO was used to describe the coagulation parameters. As the clay platelets might not be perfectly dispersed in water, the Hamaker constant, included in the attractive potential, was estimated experimentally, but the obtained value was close to the theoretical one. Contrarily to surfactant stabilized systems, multilayers of clay could be observed on the surface of particles. This explains the nonlinear relationship between the total number of particles versus the clay concentration. Therefore, the stabilization efficiency of the clay is not straightforward to estimate as higher layers may partly screen the charge of lower layers. Therefore, the effective number of clay platelets contributing to the stabilization of the system was estimated experimentally and a relationship was proposed as a function of the clay concentration. The obtained model should allow the prediction of the rates of particle nucleation and coagulation as a function of the clay concentration.

Part IV

Conclusion

The objective of this work was to develop a methodology for modeling of fundamental surfactant-free emulsion polymerization stabilized by inorganic particles, called “Pickering emulsion polymerization”. The developed model is able to describe the reaction kinetics in the various phases, mass transfer between phases (eg radicals.) and the evolution of the particle size distribution (PSD), which is an important property of final latex.

The fundamental differences between conventional emulsion polymerization (with surfactant) and Pickering emulsion polymerization were highlighted through experimental results and modeling.

In a first part, it was necessary to study the partitioning of the clay during the polymerization process. The adsorption isotherm was realized on previously formed polystyrene latex particles produced in the same conditions (i.e. same ionic strength). A multilayer adsorption was found, while the clay was found to be well dispersed in water before adsorption. BET isotherm was able to model this adsorption. Several analytical methods were used to support this hypothesis: QCM-D, conductivity study and ICP-AES. The same study on pure polystyrene has shown that non-electrostatic interactions between the clay and polystyrene can overcome electrostatic repulsion required for adsorption. The presence of electrolyte improves the adsorption of the organic clay. The presence of multilayers was verified by TEM microscopy coupled to a method of energy dispersive spectroscopy (EDS).

Secondly, Pickering emulsion polymerizations were carried out in order to understand the different experimental factors involved in the styrene polymerization process stabilized by inorganic clay. The polymerization of styrene initiated by a water-soluble initiator (potassium persulfate) was chosen as reaction reference in the literature. The stirring rate and the initial monomer concentration have no effect on the population of polymer particles obtained; this excludes the possibility of droplet nucleation, confirms the use of conventional monomer partitioning model and avoids the necessity to model orthokinetic coagulation. Semi-continuous polymerization allowed to better understand how to control the polymerization reaction. A first batch part allows the formation of the polymer particles, this number then remains constant during the rest of the reaction. Moreover, by varying the speed

rate and time of start of injection, it is possible to maintain the reaction in the saturated regime or starved regime.

Thirdly, several Laponite[®] grades were used in *ab initio* semi-continuous emulsion polymerization. Laponite[®] RDS, XLS, S482 and JS were compared and the differences of each on the polymer particles stabilization have been described experimentally. All the clays adsorb similarly on the latex particles. The less efficient clay for stabilizing the latex particles was Laponite[®] JS. The clays RDS and S482 were almost equivalent, where the number of particles increased with the clay concentration without leveling off. The behavior of the clay XLG was a little different as it was found similar to the clays RDS and S482 at low concentration but reaches a kind of saturation in the nucleated number of particles at higher concentrations.

In a second part, models were proposed to describe the growth of the polymer particles. This was made possible by the adjustment of the absorption coefficient and the desorption coefficient. Several models from the literature were described and confronted to the results of *ab initio* of Pickering emulsion polymerization. As conclusion, the presence of inorganic particles seems to have no influence on the entry and exit of the radicals inside the polystyrene particles.

Once the growth mechanism being determined, a coagulative nucleation model was used to describe the mechanisms involved in the formation of polymer particles. Homogeneous nucleation generates a large number of primary particles. After growth, these particles are unstable in water and coagulate to improve their stability. The inorganic particles stabilize these primary particles. The greater the number of clay platelets, the better is the polymer particles stabilization and therefore the greater is the number of particles. The number of particles effectively participating in the stabilization was determined using the DLVO theory.

The modeling methodology is established, and is able to be applied to other clay particles to better understand their stabilization effect on Pickering emulsion polymerization.

Appendix A

Transition from interval II to interval III in emulsion polymerizationn

*“ Be the change you want to see in
the world ”*

Mahatma Gandhi

The research described in this Appendix has been published in the Canadian Journal of Chemical Engineering

Abstract : Modelling of emulsion polymerization in intervals II and III is investigated in order to properly represent the evolution of the broadening of the particle size distribution and take into account diffusion limitations inside the particles. In these intervals, if particle nucleation and coagulation are avoided, the particles grow as a consequence of radical capture, desorption and termination inside the particles. As diffusion limitations are negligible in interval II (under saturation with monomer), radical entry and capture models are investigated in this interval with the criteria of fitting the total particle size distribution (not only the mean particle size) and the reaction rate. Indeed, the broadening of the particle size distribution was found to reveal a dependency of radical capture on the particle size. If only the mean particle size is considered, this effect would be misestimated. Interval III is then investigated in order to account for the variation of radical diffusion limitations. The advantages of operating in interval III are highlighted, namely the increased reaction rate and better control of the reaction rate. The global model describes both intervals II and III.

A.1 Introduction

Emulsion polymerization modelling has been subject of numerous studies in the literature both for process and property modelling. The polymer quality in emulsion polymerization is determined by the particle size distribution (PSD) and the molecular weight distribution (MWD). The MWD determines the mechanical properties of the final polymer while the PSD determines the reaction rate and the latex viscosity which impacts its transfer and processing post-treatments. The PSD may also affect the optical properties of the produced films. In emulsion polymerization, the course of the reaction can be divided in three intervals almost independently of the used monomer or process [Smith and Ewart, 1948] [Harkins, 1947]: In interval I, particle nucleation takes place by different mechanisms (micellar, homogeneous); in interval II primary nucleation stops and particles grow under saturation with monomer (monomer droplets exist); in interval III no monomer droplets are present and particles grow under unsaturated (up to starved) conditions. During interval III, a gel effect may occur where the termination rate is reduced due to the extremely high viscosity in the polymer particles. The propagation and monomer diffusion rate coefficients may also be reduced due to the glass effect at very low monomer concentration. Modelling the PSD is done through population balance modelling (PBM) that includes the particle nucleation, growth and coagulation terms. Modelling each of these terms involves a particular difficulty and it is therefore preferred to model each of term separately, when possible. For instance, modelling particle growth can be considered alone if particle nucleation and coagulation are avoided, which represents the concern of this work. Particle growth depends on the concentrations of monomer and radicals in the polymer particles. The concentration of radicals in the polymer particles in turn depends on radical capture by the polymer particles, radical desorption from the polymer particles to the aqueous phase and bimolecular radical termination by recombination within the particles. Investigation of radical capture and exit from the polymer particles was usually studied in interval II [Smith and Ewart, 1948] [Ugelstad and Hansen, 1976] [Maxwell et al., 1991] [A. Penboss et al., 1986] [Gardon, 1968] [Harada et al., 1971]. This allows elimi-

nating difficulties in modelling the nucleation and coagulation terms. Moreover, by forcing saturation of particles by monomer, no change in the diffusion limitations needs to be considered which leads to unvarying reaction coefficients at a certain temperature (diffusion of radicals, propagation, termination, etc.). Diffusion limitations should however be correctly represented in interval III, that represents an important part of the reaction. Indeed, operating in interval III has a number of advantages such as the enhanced control of the reaction rate, temperature and polymer properties. An improved productivity can also be obtained in interval III compared to interval II as diffusion limitations might lead to a lowered chain termination rate. Thus, most semi-continuous industrial operations are operated in interval III. In this work, modelling the growth rate was considered in both intervals II and III. Radical entry and desorption models were discriminated in interval II by comparison to the whole particle size distribution. Modeling radical diffusion limitations was studied in interval III. Ab initio styrene emulsion polymerizations were conducted where a seed was first produced at the beginning of the reaction; then, interval II, or alternatively interval III, were extended by manipulating the monomer addition flow rate semi-continuously. Modelling of only intervals II and III was considered where the number of particles was maintained constant (no nucleation or coagulation).

A.2 Materials and methods

A.2.1 Materials

The monomer, styrene (Acros Organics, 99% extra pure, stabilized) was stored in a fridge until used. Potassium persulfate (Sigma-Aldrich, minimum 99%) was used as initiator. Sodium dodecyl sulfate (SDS) was used as surfactant. Deionized water of 18 M Ω *cm* resistivity was used throughout the work.

A.2.2 Ab initio semi-continuous polymerization experiments

The polymerization reaction started by a batch period for polymer particle nucleation followed by a semi-continuous part to allow their growth. A 1 L reactor was

used with mechanical stirring at 400 rpm using a three blades Bohlender propeller. First, the surfactant was dispersed in 800 g of water for 30 min under stirring in the reactor at ambient temperature and degassed using nitrogen. The mixture was next heated to 70 °C using a thermostated bath. Then, 40 g of styrene was added and the polymerization was initiated by adding 1.6 g of potassium persulfate. During the reaction, the stream of nitrogen was moved upwards off the reaction medium to the top of the reactor to maintain saturation of the gaseous atmosphere with nitrogen. Semi-continuous monomer addition started by adding 160 g of monomer at different flow rates covering different ranges in interval III (starved conditions) up to interval II (saturation conditions). Samples were withdrawn at specific time intervals to measure the solids content (SC, i.e. mass fraction of solid) using a thermogravimetric balance and the particle size (using a Malvern Nano ZS®). The solids content was used to calculate the amount of polymer and the monomer conversion, after subtracting the mass of surfactant and initiator. Both measurements allowed calculating the particle number density.

A.3 Modeling

A.3.1 Polymer particles population balances

Please refer to chapter 6 for the model of the population balance

A.3.1.1 Average number of radicals in the particles

Please refer to chapter 5 for the model of \bar{n}

A.3.1.2 Aqueous phase reactions

Aqueous phase reactions are presented in chapter 5.

A.3.1.3 Monomer Balance and partitioning

Radical exchange was presented in chapter 5.

A.3.2 Radical exchange

Monomer balance was presented in chapter 5.

A.3.3 Diffusion limitation

Diffusion limitations in the polymer particles are due to the decrease in the concentration of monomer in interval III. As a first effect, diffusion of long molecules (polymeric radicals) is observed. This effect is described by a decrease in the radical termination rate coefficient in the polymer particles [Hawket et al., 1981]. In this work, the following relation is used:

$$k_t = k_{t_0} \exp[-\alpha_t(w_p - w_p^{sat})] \quad (\text{A.1})$$

Where w_p^{sat} is the weight fraction of polymer in the particles in interval II, α_t is a fitting parameter (estimated in this work for the present reaction conditions), and w_p is the weight fraction of polymer in the particles, given by:

$$w_p = \frac{V_{pp}\rho_p}{V_{pp}\rho_p + V_{mp}\rho_m} \quad (\text{A.2})$$

A glass effect might also take place at very low monomer fractions for polymers with high glass transition temperature which consists in a decrease in the diffusion of monomer or monomeric radicals in the polymer particles. This effect is usually described by a reduction in the propagation rate coefficient and radical diffusion rate coefficient in the polymer particles. The glass effect is described by a reduction in the diffusion of small molecules (monomer, monomeric radicals, oligoradicals) in the polymer particles as follows ($V_f < V_{f_{cr}}$) [Sundberg et al., 1981]:

$$D_p = D_{p_0} \exp \left[-0.5 \left(\frac{1}{V_f} - \frac{1}{V_{f_{cr}}} \right) \right] \quad (\text{A.3})$$

Where D_{p_0} is the monomer diffusion coefficient in the polymer particles under saturation, $V_{f_{cr}}$ is the critical free volume in the particles at the onset of the glass effect and V_f is the free volume in the particles given by:

$$V_f = V_{f_m} \frac{V_{m_p}}{V_p} + V_{f_p} \frac{V_{p_p}}{V_p} \quad (\text{A.4})$$

V_{f_m} and V_{f_p} are the monomer and polymer contributions to particle free volume respectively given by the following semi-empirical relations [Sajjadi, 2009] :

$$\begin{aligned} V_{f_m} &= 0.025 + \alpha_m(T - T_{g_m}) \\ V_{f_p} &= 0.025 + \alpha_p(T - T_{g_p}) \end{aligned} \quad (\text{A.5})$$

Where α_m and α_p are the thermal expansion coefficients of monomer and polymer and T_{g_m} and T_{g_p} are the glass transition temperatures of monomer and polymer, respectively. The propagation rate and transfer to monomer rate coefficients, k_p and k_f can then be obtained as follows (Sundberg et al. 1981)[Sundberg et al., 1981]:

$$\begin{aligned} k_p &= k_{p_0} \frac{D_p}{D_{p_0}} \\ k_f &= k_{f_0} \frac{D_p}{D_{p_0}} \end{aligned} \quad (\text{A.6})$$

A.4 Results and discussion

A.4.1 Experimental observations

A.4.1.1 PSD broadening

Figure A.1 shows the measured particle size distribution at the beginning and at the end of interval II in a semi-continuous experiment (thus conducted under saturation). In both samples the number of particles was identical indicating stable latex (no coagulation or secondary nucleation). The number of particles was calculated based on the distributions combined to the mass of polymer. A further test of stability was realized by mixing the final latex under the same conditions (temperature, concentration, stirring rate) but without reaction which led to no change in the PSD. Thus, the observed broadening of the distribution in Figure A.1 is not due to coagulation. This indicates that the growth rate, and so \bar{n} , are diameter dependent. This means that the radical termination, entry and/or desorption rates depend on the particles diameter. The dependency of the termination rate on the particle size is described by $c = \frac{k_{tp}}{N_A v_s}$ (where $v_s = \frac{\pi}{6} d_p^3$, in equation 5.7). Concerning the radical

desorption rate, in most of the proposed mechanisms it is assumed to depend on the particle surface (d_p^2). Regarding the radical entry rate, three mechanisms can be distinguished: no dependency on d_p (propagation controlled) [Maxwell et al., 1991], depending on d_p (diffusion controlled) [Smith and Ewart, 1948], and depending on d_p^2 (collision-controlled) [Gardon, 1968]. The first objective of this work is therefore to evaluate if the dependency of termination and desorption on the particle size is sufficient to describe the broadening of the distribution in interval II or it is required to use a radical entry model that depends on d_p .

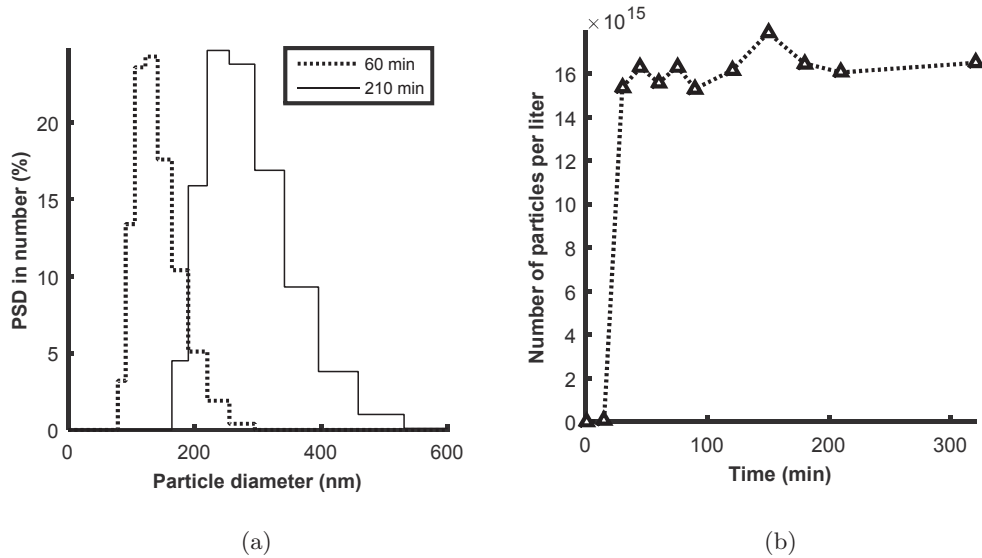


Figure A.1: Evolution of the particle size distribution in number (measured by Nano-ZS) in interval II of a semi-continuous emulsion polymerization

A.4.1.2 Interests of interval III

Figure A.2 shows the evolution of the reaction rate as a function of the concentration of monomer in the polymer particles in an emulsion polymerization experiment undergoing a gel effect at the end of the reaction. It can be seen that lower reaction rates were obtained in interval II (with $[M]_p$ under saturation) than in interval III. In interval III, the reaction rate increased when $[M]_p$ decreases. At very low $[M]_p$, the gel effect took place where the reaction rate increased importantly. At very

low monomer concentrations, the reaction rate decreased and stopped due to the glass effect. The increase in the reaction rate in interval III compared to interval II is attributed to the decrease in radical diffusion in the polymer particles when $[M]_p$ decreases. This leads to a decrease in the termination rate coefficient, leading to an increase in \bar{n} . The second objective of this work is thus to determine the dependency of k_{tp} on $[M]_p$ in interval III. A clear effect of $[M]_p$ on R_p is observed when passing from interval II to interval III.

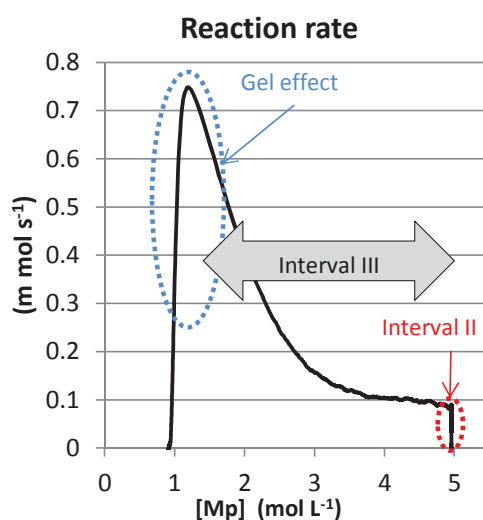


Figure A.2: The reaction rate as a function of the monomer concentration in emulsion polymerization of styrene (semi-continuous reaction with extension of interval II)

The observed effect of $[M]_p$ on R_p was further investigated in semi-continuous experiments by varying the monomer addition flow rate. Figure A.3 shows the obtained average polymerization rate in the semi-continuous part of the reaction as a function of the monomer flow rate for 5 different reactions. The experiments can be divided in two groups: experiments where the monomer flow rate is high and are therefore conducted in interval II and experiments with low monomer flow rate thus operated in interval III. In the first group, the employed flow rate is high enough to allow saturating the polymer particles with monomer and in this case the

reaction rate was relatively low. In the second group (operated in interval III), the reaction rate was equal to the monomer flow rate. In the studied flow rate range, $[M]_p$ varied between $0.3 \times [M]_p^{sat}$ to $[M]_p^{sat}$. This indicates that the limiting factor in this interval is the concentration of monomer while the concentration of radicals in the polymer particles seems to be high enough and not a limiting factor. Similar diffusion limitations can thus be perceived in this group of experiments although $[M]_p$ is varying. It appears from these experiments that in order to increase the reaction rate and reduce the process time in semi-continuous experiments, it is more interesting to work in interval III. Moreover, the monomer flow rate should be maximized with a constraint of working in interval III and avoid saturating the polymer particles, which may improve some control strategies [Alamir et al., 2007] [Sáenz de Buruaga et al., 1997].

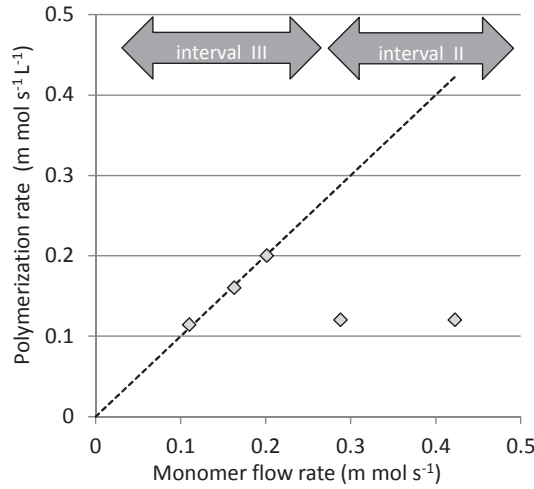


Figure A.3: Effect of the monomer flow rate on the polymerization rate in seeded semi-continuous emulsion polymerization of styrene (in all experiments the initial solid content is 4 wt%, $N = 2 \times 10^{16}$ and initial particle diameter $d_p=130$ nm).

Another interesting feature of operating in interval III in the semi-continuous reactions is related to the controllability of the reaction. Figure A.4 compares two reactions starting from the same batch conditions, followed by different semi-continuous flow rates where in one experiment an extension of interval II was done

(figure A.4a) while in the other experiment, interval III was extended (Figure A.4b). In both experiments, the same number of particles was obtained at the end of the batch and was maintained stable during the semi-continuous part. The monomer mass was 40 g in the batch followed by 160 g added semi-continuously. The solid content and therefore the particle size were identical at the end of both reactions. Again, it can be seen that the reaction rate was higher in the experiment conducted in interval III, and the reaction time was reduced from 300 to 200 minutes. More interestingly, it can be seen that the final gel effect could almost be eliminated in the reaction mainly conducted in interval III. A better control of the reaction rate, temperature and properties (molecular weight) is thus ensured in this case.

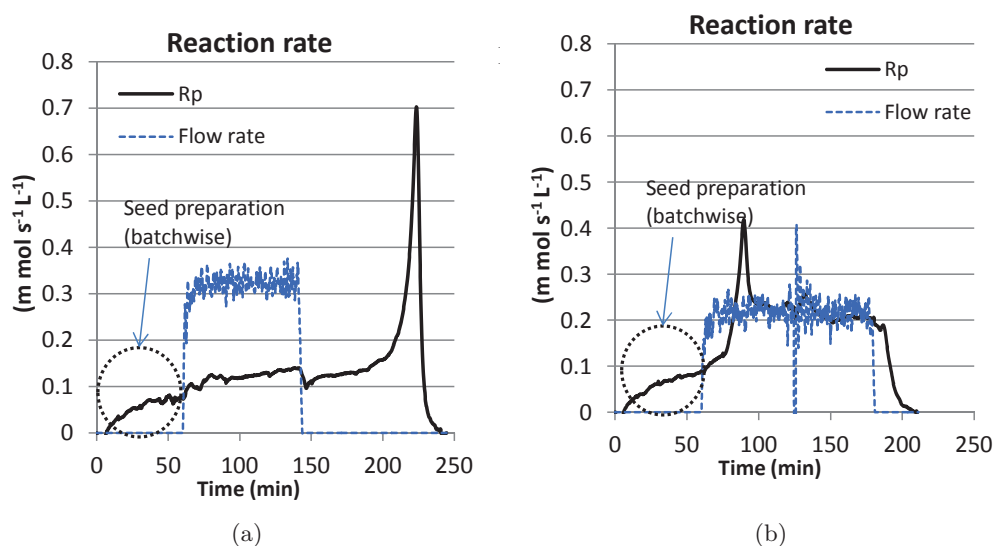


Figure A.4: Effect of the monomer flow rate on the polymerization rate: A: the semi-continuous part is operated in interval II, B: the semi-continuous part is operated in interval III (in both experiments $N = 2.1 \times 10^{16}$, particle diameter at the end of the batch is $d_p=120$ nm and the final solids content = 20 wt%).

A.4.2 Modelling intervals II and III

In order to model both intervals II and III, first data of interval II is used in order to identify the radical entry and desorption models then data of interval III is used to

identify the diffusion limitations (i.e. identify α_t in equation A.1).

A.4.2.1 Identifying radical entry and exit models based on interval II

A comparison between the capture and desorption models proposed in the literature was done first in interval II. As discussed above, in this interval the number of particles is constant (no nucleation or coagulation were observed) and $[M]_p$ is maintained under saturation, which lead to constant radical diffusion coefficients (both for small and long radicals), thus leading to constant coefficients of termination, transfer as well as desorption. The desorption rate is admitted to depend on d_p^2 in most desorption models. In order to account for competitive reactions of the event of desorption, i.e. propagation and termination within the particle and radical re-entry after desorption, the model proposed by [Hernandez and Tauer, 2008] was used (see chapter 5). However, the model proposed by [Harada et al., 1971] was used to calculate the equilibrium radical desorption coefficient (k_0) as the activation energy of desorption is not known for the present system. In order to evaluate the dependency of radical capture on the particle diameter, the strategy proposed by [Asua and De La Cal, 1991] was adopted as a first attempt to allow selecting an adapted phenomenological model in a next step. This methodology consists in identifying the parameters of the following empirical relationship:

$$k_e = k_e^* d_p^{\alpha_e} \tag{A.7}$$

Where k_e^* and α_e are adjustable parameters. For instance, $\alpha_e=0$ in the propagation model, $\alpha_e=1$ in the diffusion model and $\alpha_e=2$ in the collision model. The minimization criterion is the monomer conversion and the PSD.

Figure A.5 compares the fitting results for $\alpha_e=0,1$ and 2. The parameters used in the simulations are given in Table 1. It can be seen that a better representation of the broadening of the PSD is obtained with the capture model proportional to d_p^2 rather than with d_p^1 or d_p^0 . All models fit correctly the mean particle size and the monomer conversion, which indicates that model selection should not be based only on these measurements. The methodology allows therefore detecting a clear depen-

dependency of the radical entry coefficient on the particle size. Simulations with $\alpha_e=2$ gives $k_e^* = 1.4 \times 10^{21} \text{ dm mol}^{-1} \text{ s}^{-1}$). This value is relatively high, which is due to the high reaction temperature (70°C). Liotta et al. (1997) estimated a dependency on $d_p^{1.85}$ for polystyrene with sizes varying from 100 to 300 nm in diameter, thus privileging the collision mechanism [Liotta et al., 1997]. If we consider the different terms in equation 5.7, at 200 nm, the termination rate at this reaction temperature is estimated at $2c\bar{n}^2 = 150 \text{ s}^{-1}$, the desorption rate at $k_{des}\bar{n} = 6 \times 10^{-3} \text{ s}^{-1}$, and thus the fitting algorithm aligned the radical entry rate to the termination rate to maintain the desired reaction rate (constant in this interval), leading to $\rho_e = 150 \text{ s}^{-1}$. From this numerical analysis, it appears that radical desorption has no contribution under the considered reaction conditions (i.e. temperature, particle size). Thus, discriminating between the radical desorption models is not appropriate under these conditions.

The existing fundamental capture models were then investigated. Note that these models do not have any adjustable parameters. As expected from Figure A.5, the size independent capture model could not fit the PSD broadness [Maxwell et al., 1991]. Moreover, it was found to importantly underestimate the reaction rate. This is probably due to the big particle sizes considered in this work. Indeed, in experiments involving smaller particles, particle growth did not lead to PSD broadening as much as bigger particles. Moreover, the reaction temperature is 70°C in these experiments involving thus a high radical entry rate, while a lot of data in the literature is available for 50°C , where radical termination, propagation and entry are lower. As the PSD involves a number of parameters that are temperature dependent, it becomes more difficult to define generic models for radical entry. The other radical capture models proposed in the literature were found to overestimate the reaction rate ([Smith and Ewart, 1948], [Coen et al., 1998], [Hernández and Tauer, 2007a], [Nomura et al., 2005], [Gardon, 1968]). The models proposed by [Ugelstad and Hansen, 1976] and [A. Penboss et al., 1986] depend on the calculation of the radical stability by DLVO theory which makes them more complicated. [Mead and Poehlein, 1989] and [Fontenot and Schork, 1993] rather proposed to use an empirical relationships to estimate the stability ratio. In this

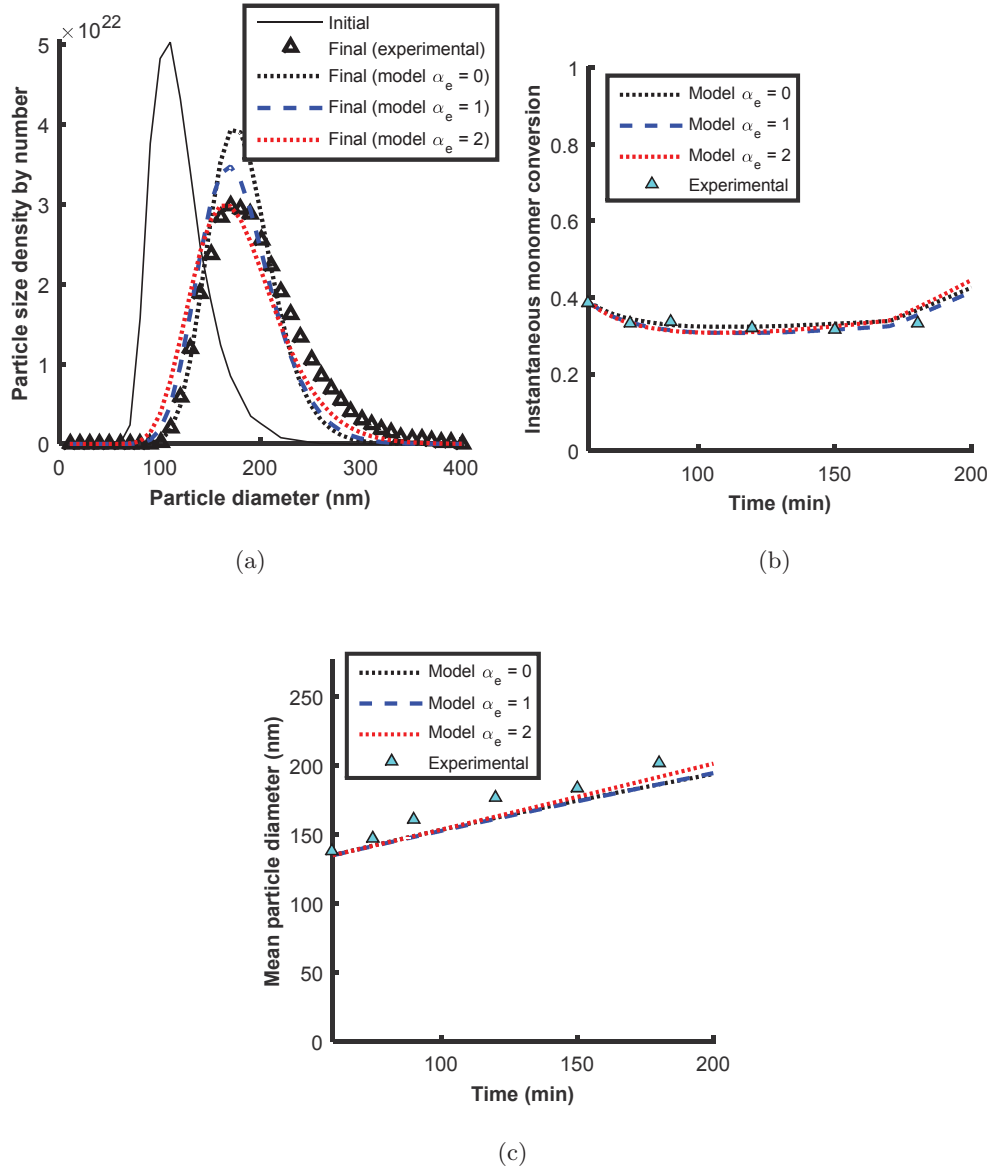


Figure A.5: Dependence of the capture rate on the particle size demonstrated through its effect on representing the broadening of the PSD (interval II)

sense, these models may be tuned to fit the experimental results. None of these models is applicable without correction. For the simulation of interval III I the next section, the desorption model proposed by [Hernandez and Tauer, 2008] with k_0 proposed by [Harada et al., 1971] was used (can be neglected). It was combined to the model proposed by [A. Penboss et al., 1986] ($\propto d_p^1$) where the stability ratio was fitted to experimental data during interval II.

voir table

In order to model interval III, the model parameters should take into account the diffusion limitations characterizing this interval that mainly affect k_{tp} (gel effect), but also the glass effect (affecting diffusion of small molecules, and thus k_p , k_{tr} D_p and so k_{des}) [Sajjadi, 2009] [Crowley et al., 2000]. Identification of α_t , characterizing the effect of the polymer weight fraction on the termination rate coefficient through equation A.1 and onset of the gel effect are estimated based on three experiments realized in quit varying conditions. These experiments start by the same batch conditions. At the end of the nucleation period (once the number of particles is stabilized), the reaction is continued semi-continuously to attain different transitions between intervals II and III:

- Figure A.6 shows the results of an experiment where monomer addition started during interval II, which avoided the occurrence of a gel effect at the end of the batch period. Interval II was thus extended. Interval II of this reaction was used in the previous section to discriminate between radical entry and desorption mechanisms. When monomer addition stopped, the reaction consumed the available monomer slowly and attained interval III.
- Figure A.7 corresponds to a reaction operated in interval III since the end of the batch period. Diffusion limitations are therefore present during the whole simulation time.
- Figure A.8 shows the results of an experiment starting by interval III, followed by interval II then finishing by interval III.

In Figure A.6, both the gel and glass effects can be observed at the end of the

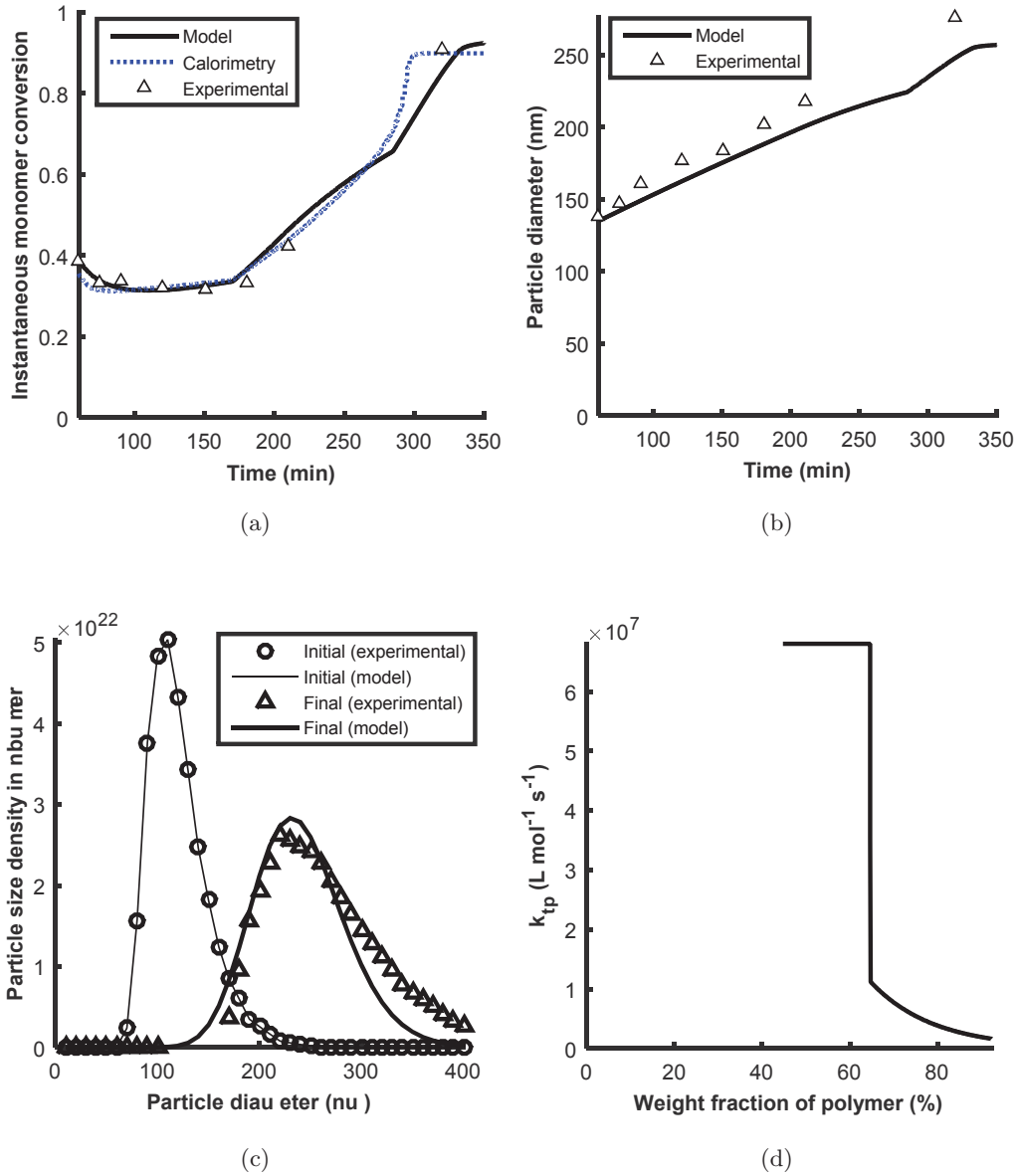


Figure A.6: Semi-continuous emulsion polymerization of styrene stabilized with 1g SDS, operated in interval II

reaction. The start of the gel effect is revealed by a change in the slope of the conversion estimated by calorimetry, which is approximately $[M]_p = 3.2 \text{ mol L}^{-1}$ ($w_p = 65.8 \text{ wt\%}$, $V_f = 0.079$). The reduction in k_{t_p} as a function of w_p is represented by the parameter α_t in equation A.1. It was fitted based on the three experiments described above, leading to $\alpha_t = 7$. From figure A.6, it appears that the gel effect is a little under estimated, but this compromise was required in order to fit the other two experiments. Note that the number of particles was stable in this part of the reaction (figure A.1). The glass effect can be detected from calorimetric estimations at about $[M]_p = 1 \text{ mol L}^{-1}$ ($w_p = 90 \text{ wt\%}$), which corresponds to $V_{f_{cr}}=0.034$. This is in accordance with the value used by [Sajjadi, 2009], $V_{f_{cr}}=0.033$.

A.5 Conclusion

In this work modelling of intervals II and III in emulsion polymerization of styrene at 70°C in presence of 1 g of SDS as stabilizer is considered. The benefits of interval II in modelling radical capture and desorption are known: avoiding particle nucleation, coagulation and assuming constant diffusion of radicals and monomer in the polymer particles. Therefore, this interval is considered the best for the discrimination between radical capture and desorption models. A number of radical capture and desorption models were proposed in the literature on the basis of different phenomenological basis. It is suggested in this work to use the whole PSD combined to the monomer reaction rate in order to allow discrimination between these models. As a conclusion, under the present reaction conditions (particle size, temperature and monomer solubility), it is found that radical desorption is negligible and radical entry and termination are much higher than the known values for reactions at 50°C . Thus, the available radical desorption models could not be discriminated under these conditions where desorption is negligible. A dependency of radical entry on the particle surface was observed. The available radical capture models were found to overestimate radical entry, except for the propagation mechanism that underestimated radical entry, which might be due to the high reaction temperature in this work. As none of these models has a tuning parameter, the

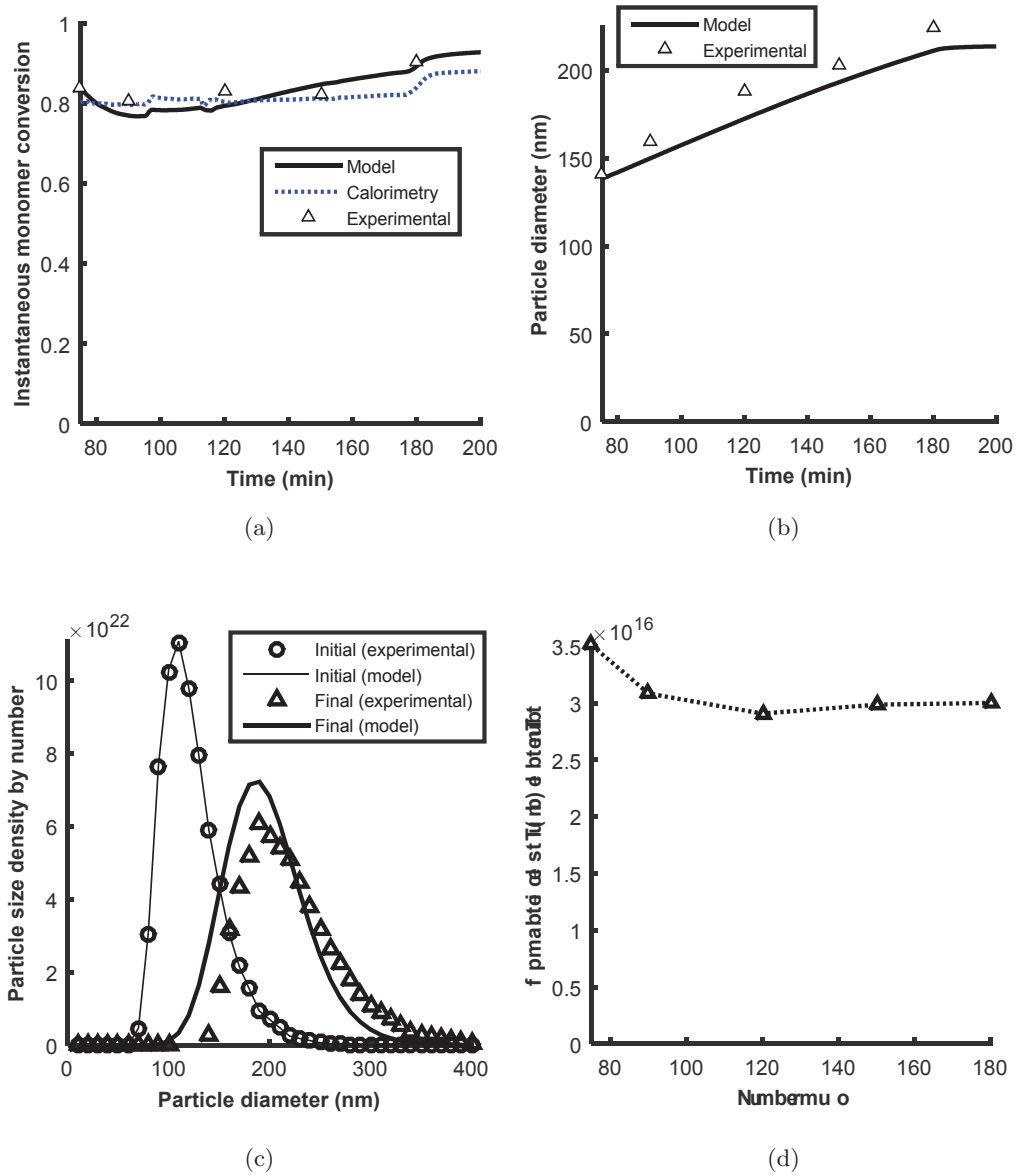


Figure A.7: Semi-continuous emulsion polymerization of styrene stabilized with 1g SDS, operated in interval III

stability ratio is used as a fitting parameter in order to account for the change in the reaction temperature. While interval II is useful for modelling, interval III remains more beneficial for industrial operations as it allows a better control of the reaction rate and polymer properties and an improved productivity. Therefore, modelling this interval is essential. In interval III, the same radical capture and desorption

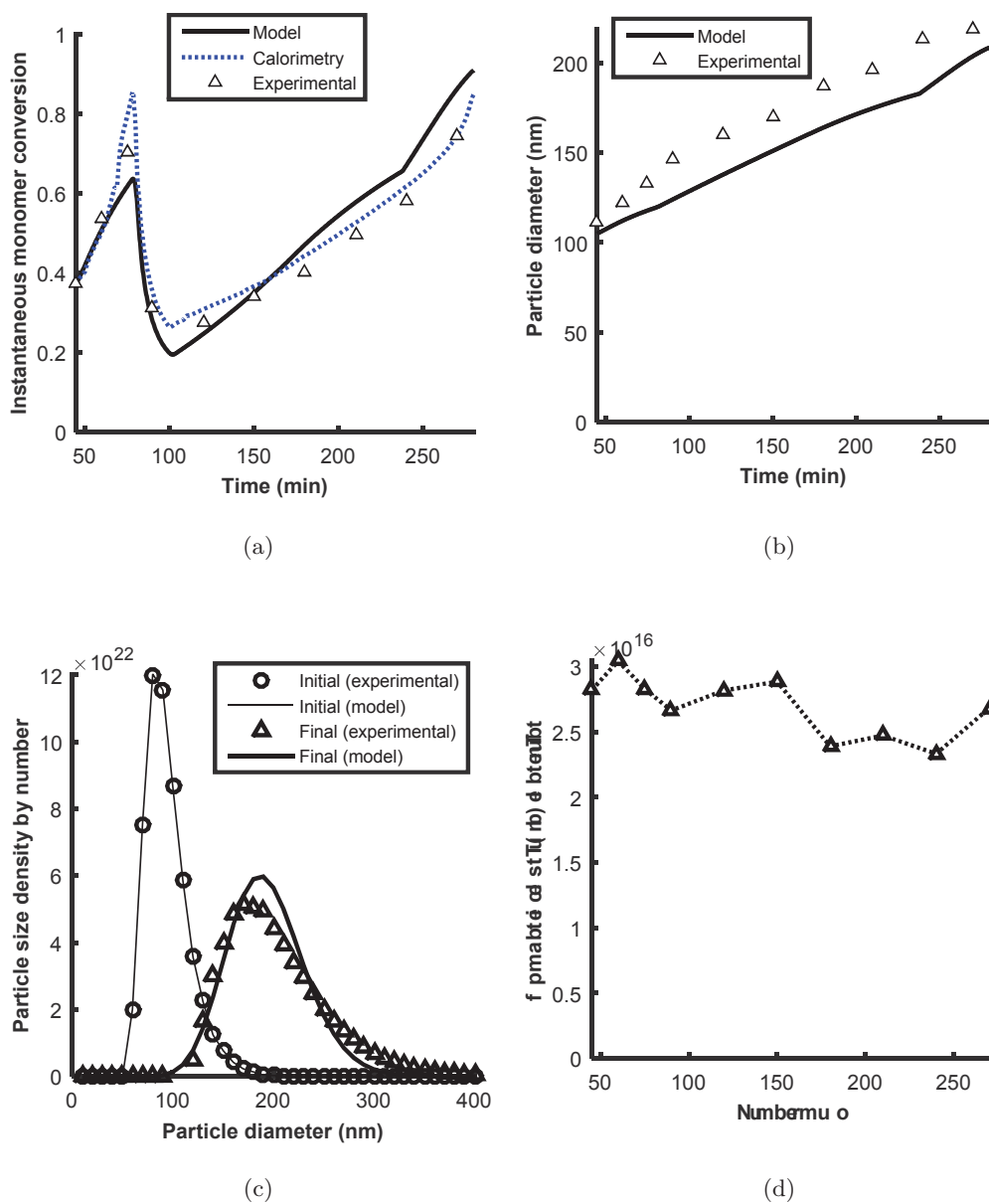


Figure A.8: Semi-continuous emulsion polymerization of styrene stabilized with 1g SDS, with variable flow rates (starting in interval III, to interval II, then again to interval III)

model can be used, but diffusion limitations of long radical polymer chains, small monomer and monomeric radicals inside the polymer particles should be considered. This is usually described by a variation of the termination rate coefficient as

a function of the weight fraction of polymer (gel effect) and monomer diffusion coefficient inside the polymer particles as a function of the free volume (glass effect). Accordingly, one needs to detect the onset of these two effects, and the decrease rate. In this work, it is suggested to base the identification of these parameters on different reaction configurations in order to ensure their genericity. Calorimetric estimations were found of great use in order to detect the onset of these effects. A good estimation is obtained for the reaction rate and the PSD using the same set of parameters for all experiments: radical desorption can be neglected; radical capture could be described using the model of [A. Penboss et al., 1986] ($\propto d_p^1$) with $W_p=34$; the onset of gel effect takes place at $[M]_p= 3.2 \text{ mol L}^{-1}$ ($w_p=65.8 \text{ wt}\%$, $V_f=0.079$), the decrease in k_{t_p} can be described by equation A.2 with $\alpha_t = 7$; the onset of the glass effect takes place at $V_{f_{cr}}=0.033$ and the parameters proposed in equations A.4 and A.6 remain valid.

Appendix B

Modelling of Emulsion Polymerization

The model of emulsion polymerization presented throughout this work (5 and chapter 6) can be completed with the balance of initiator and monomer as follow.

B.1 Initiator balance

The initiator decomposes according to the following mass balance:

$$\frac{d[I]}{dt} = -f_I k_I [I] \quad (\text{B.1})$$

where $[I]$ is the initiator concentration and k_I the decomposition coefficient of the initiator.

B.2 Monomer balance

B.2.1 Total monomer balance

The total monomer mass balance is given by the following equation :

$$\frac{dN_m}{dt} = F_m - R_{p_p} - R_{p_w} \quad (\text{B.2})$$

where N_m is the number of moles of free monomer in the reactor, F_m the molar flow rate of monomer, R_{pw} the rate of reaction in the aqueous phase and R_{pp} the reaction rate in the particle defined as follow :

$$R_{pp} = \frac{k_p[M]_p\bar{n}N}{N_A} \quad (\text{B.3})$$

where k_p is the propagation coefficient of the monomer in the particles, $[M]_p$ the monomer concentration in the particles, \bar{n} the average number of radicals in the particles of all sizes and N total number of particles obtained by integration of the particle size distribution $n(r, t)$:

$$N(t) = \int_{r_{nuc}}^{\infty} n(r, t) dr \quad (\text{B.4})$$

The reaction rate in water is defined as follow :

$$R_{pw} = k_p[M]_w V_w [R]_w \quad (\text{B.5})$$

The average number of radicals in the particles of all sizes is given by:

$$\bar{n}(t) = \frac{\int_{r_{nuc}}^{\infty} \bar{n}(r, t) n(r, t) dr}{\int_{r_{nuc}}^{\infty} n(r, t) dr} \quad (\text{B.6})$$

B.2.2 Monomer partitioning

In emulsion polymerization, conversion of monomer occurs principally in the monomer-swollen particles. Monomer concentration in the particles is restock by the monomer droplets by diffusion through the water phase. The polymer particles can absorb a certain amount of monomer that is limited by thermodynamic equilibrium. This leads to a monomer partitioning between particles, water phase and droplets. On one hand, the monomer concentration can limit the reaction rate in the particle. On the other hand, the solubility of monomer in the water phase influences the reaction rate in the aqueous phase and controls the homogeneous nucleation rate. Therefore, determining the monomer partitioning is important for the rest of the reaction model.

The distribution of the monomer in the droplets, particles and the aqueous phase depends on both the volumetric fraction between the different phases defined as follow

$$\begin{aligned}\Phi_p^p &= \frac{V_p^p}{V_p} \\ \Phi_m^p &= \frac{V_m^p}{V_p} \\ \Phi_m^w &= \frac{V_m^w}{V_w}\end{aligned}\tag{B.7}$$

Φ_m^j is the volumetric fraction of the monomer in the phase j (p for particle, w for aqueous phase and d for monomer droplet), V_m^j is the volume of monomer in phase j , V_j is the total volume of the phase j .

Assuming that the water cannot dissolve in the polystyrene particles or pure monomer, the material balance between the phases can be written as follows :

$$\begin{aligned}V_w &= V_w^w + V_m^w \\ V_p &= V_m^p + V_p^p \\ V_d &= V_m^d \\ V_m &= V_m^d + V_m^w + V_m^p\end{aligned}\tag{B.8}$$

The polymer particles are saturated with monomer if the following condition is met:

$$V_m > V_p \Phi_m^p + V_w \Phi_m^w\tag{B.9}$$

The end of the interval II is characterized by the disappearance of the droplets in the reactor (i.e. $V_d = V_m^d = 0$). The remaining monomer is shared between the aqueous phase and particles.

There are several models in the literature to predict the distribution of monomer in the different phases [Sheibat-Othman, 2000]. These models are based on theoretical laws (thermodynamic), empirical or semi-empirical relationships.

- **A model based on the theoretical thermodynamic consideration** based on the classical Flory-Huggins lattice theory for monomer-polymer mixtures. At equilibrium, the swelling forces are counterbalanced by the interfacial free energy between latex particles and the aqueous phase. The monomer concentration is determined by the balance at this equilibrium. This model

predicts with good accuracy the partitioning of monomer. However, several parameter are needed, many of them are difficult to measure or completely unknown.

- **semi-empirical equations of maxwell** [Maxwell et al., 1992b] [Maxwell et al., 1992a] [Maxwell et al., 1993]. The authors found that partitioning was insensitive to temperature, latex particles radius, polymer composition and polymer molecular weight. The swelling ability of monomer in the polymer particles controls the monomer partitioning. This model is simple to use but some effects can't be predicted by this equations like the effect of adding inorganic salt [Said and Fataftah, 1996].
- **Partition coefficient model** is based on the equilibrium distribution among the droplets, particles and water though empirical partition coefficient. The partition coefficient model takes into account the balance between the distribution of the monomer in the different phases by sharing sets of empirical coefficients constant during the reaction

There are several definitions for these coefficients [Guillot, 1985]. The definition given by Gugliotta [Gugliotta et al., 1995] has been chosen to simulate interval II in this work.

$$k_m^j = \frac{\Phi_m^j}{\Phi_m^w} \quad \text{with } j = p \text{ or } d \quad (\text{B.10})$$

where k_m^j is the partition coefficient of monomer between phase j and the aqueous phase. Therefore for the particles:

$$\begin{aligned} k_m^p &= \frac{\Phi_m^p}{\Phi_m^w} = \frac{V_m^p}{V_p} \frac{V_w}{V_m^w} \\ k_m^p &= \frac{V_m^p \frac{\rho_m}{MW_m}}{V_p} \frac{V_w}{V_m^w \frac{\rho_m}{MW_m}} \\ k_m^p &= \frac{[M_p]^{sat}}{[M_w]^{sat}} \end{aligned} \quad (\text{B.11})$$

Similarly, for the monomer droplets:

$$k_m^d = \frac{\rho_m}{MW_m [M_w]^{sat}} \quad (\text{B.12})$$

Knowing the value of the volumetric fraction of the monomer in the particles to saturation, one can calculate the saturation concentration in the particles:

$$\begin{aligned}\Phi_m^p &= 0.6 = \frac{V_m^p}{V_p} = [M_p]^{sat} \frac{MW_m}{\rho_m} \\ [M_p]^{sat} &= 0.6 \frac{\rho_m}{MW_m} \\ [M_p]^{sat} &= 4.96\end{aligned}\tag{B.13}$$

These parameters will be inserted in the empirical partition coefficient model. This model was chosen with an optimized algorithm proposed by Omi [Omi et al., 1985] to converge to the solution of the 6 equations with 6 unknowns. This algorithm is described below. Note that it is necessary to differentiate the case where the medium contains droplets of monomer (Phase I and II) where there are no more droplets (stage III and IV):

The iteration algorithm used to calculate monomer concentration in phase I and II is :

1. Choice of initial values for V_p , V_d and V_w .
2. Calculating V_m^p with the following equation:

$$V_m^p = \frac{V_m}{1 + \frac{k_m^d}{k_m^p} \frac{V_d}{V_p} + \frac{V_w}{V_p k_m^p}}\tag{B.14}$$

3. Calculating V_m^d and V_m^w with the following equation:

$$\begin{aligned}V_m^d &= \frac{k_m^d}{k_m^p} \frac{V_m^p}{V_p} V_d \\ V_m^w &= \frac{V_m^p}{k_m^p} \frac{V_w}{V_p}\end{aligned}\tag{B.15}$$

4. Calcul de V_p , V_d and V_w :

$$\begin{aligned}V_d &= V_m^d \\ V_p &= V_m^p + V_p^p \\ V_w &= V_w^w + V_m^w\end{aligned}\tag{B.16}$$

5. Iteration until convergence of V_p , V_d and V_w .

The iteration algorithm used to calculate monomer concentration in phase III:

1. Choice of initial values for V_p and V_w .
2. Calculating V_m^p with the following equation:

$$V_m^p = \frac{V_m}{1 + \frac{V_w}{V_p k_m^p}}\tag{B.17}$$

3. Calculating V_m^w with the following equation:

$$V_m^w = \frac{V_m^p}{k_m^p} \frac{V_w}{V_p} \quad (\text{B.18})$$

4. Calculating V_p and V_w :

$$\begin{aligned} V_p &= V_m^p + V_p^p \\ V_w &= V_w^w + V_m^w \end{aligned} \quad (\text{B.19})$$

5. Iteration until convergence of V_p and V_w .

Then the monomer concentration in different phases can be calculated as follows:

$$\begin{aligned} [M_p] &= \frac{N_m^p}{V_p} = \frac{V_m^p}{\rho_m} MW_m V_p \\ [M_w] &= \frac{N_m^w}{V_w} = \frac{V_m^w}{\rho_m} MW_m V_w \end{aligned} \quad (\text{B.20})$$

Bibliography

- [A. Penboss et al., 1986] A. Penboss, I., G. Gilbert, R., and H. Napper, D. (1986). Entry rate coefficients in emulsion polymerization systems. *Journal of the Chemical Society, Faraday Transactions 1: Physical Chemistry in Condensed Phases*, 82(7):2247–2268. (Quoted pages 96, 101, 109, 167, 177 and 183.)
- [Abismail et al., 2000] Abismail, B., Canselier, J., Wilhelm, A., Delmas, H., Gourdon, C., et al. (2000). Emulsification processes: on-line study by multiple light scattering measurements. *Ultrasonics Sonochemistry*, 7(4):187–192. (Quoted page 149.)
- [Adams et al., 1988] Adams, M. E., Trau, M., Gilbert, R. G., Napper, D. H., and Sangster, D. F. (1988). The entry of free radicals into polystyrene latex particles. *Australian Journal of Chemistry*, 41(12):1799–1813. (Quoted pages 21, 96 and 114.)
- [Alamir et al., 2007] Alamir, M., Sheibat-Othman, N., and Othman, S. (2007). Constrained nonlinear predictive control for maximizing production in polymerization processes. *Control Systems Technology, IEEE Transactions on*, 15(2):315–323. (Quoted page 174.)
- [Alamir et al., 2010] Alamir, M., Sheibat-Othman, N., and Othman, S. (2010). Measurement Based Modeling and Control of Bimodal Particle Size Distribution in Batch Emulsion Polymerization. *Aiche Journal*, 56(8):2122–2136. (Quoted page 135.)

- [Alexandre and Dubois, 2000] Alexandre, M. and Dubois, P. (2000). Polymer-layered silicate nanocomposites: preparation, properties and uses of a new class of materials. *Materials Science and Engineering Reports*, 28:1–63. (Quoted page 12.)
- [Aranda and Ruiz-Hitzky, 1994] Aranda, P. and Ruiz-Hitzky, E. (1994). New polyelectrolyte materials based on smectite polyoxyethylene intercalation compounds. *Acta Polymerica*, 45:59–67. (Quoted pages 14 and 135.)
- [Ariga et al., 1999] Ariga, K., Lvov, Y., Ichinose, I., and Kunitake, T. (1999). Ultrathin films of inorganic materials (SiO_2 nanoparticle, montmorillonite microplate, and molybdenum oxide) prepared by alternate layer-by-layer assembly with organic polyions. *Applied Clay Science*, 15:137–152. (Quoted page 28.)
- [Asua, 2002] Asua, J. M. (2002). Miniemulsion polymerization. *Progress in polymer science*, 27(7):1283–1346. (Quoted pages 79 and 81.)
- [Asua, 2003] Asua, J. M. (2003). A New Model for Radical Desorption in Emulsion Polymerization. *Macromolecules*, 36(16):6245–6251. (Quoted pages 112 and 123.)
- [Asua and De La Cal, 1991] Asua, J. M. and De La Cal, J. C. (1991). Entry and exit rate coefficients in emulsion polymerization of styrene. *Journal of Applied Polymer Science*, 42(7):1869–1877. (Quoted pages 98, 110, 115, 121, 145 and 176.)
- [Asua et al., 1989] Asua, J. M., Sudol, E. D., and El-Aasser, M. S. (1989). Radical desorption in emulsion polymerization. *Journal of Polymer Science Part A: Polymer Chemistry*, 27(12):3903–3913. (Quoted pages 117 and 124.)
- [Aveyard et al., 2003] Aveyard, R., Binks, B. P., and Clint, J. H. (2003). Emulsions stabilised solely by colloidal particles. *Advances in Colloid and Interface Science*, 100–102:503–546. (Quoted pages 20, 51 and 67.)
- [Ballard et al., 1981] Ballard, M. J., Gilbert, R. G., and Napper, D. H. (1981). Improved methods for solving the smith—ewart equations in the steady state. *Journal of Polymer Science: Polymer Letters Edition*, 19(11):533–537. (Quoted page 101.)

- [Balnois et al., 2003] Balnois, E., Durand-Vidal, S., and Levitz, P. (2003). Probing the Morphology of Laponite Clay Colloids by Atomic Force Microscopy. *Langmuir*, pages 6633–6637. (Quoted pages 16, 58, 59 and 63.)
- [Binks and Lumsdon, 1999] Binks, B. P. and Lumsdon, S. O. (1999). Stability of oil-in-water emulsions stabilised by silica particles. *Physical Chemistry Chemical Physics*, 1(12):3007–3016. (Quoted page 20.)
- [Bon and Colver, 2007] Bon, S. A. and Colver, P. J. (2007). Pickering Miniemulsion Polymerization Using Laponite Clay as a Stabilizer. *Langmuir*, pages 8316–8322. (Quoted pages 12 and 14.)
- [Bourgeat-Lami et al., 2007] Bourgeat-Lami, E., Herrera, N. N., Putaux, J.-L., Perro, A., Reculosa, S., Ravaine, S., and Duguet, E. (2007). Designing Organic/Inorganic Colloids by Heterophase Polymerization. *Macromolecular Symposia*, 248:213–226. (Quoted pages 14 and 135.)
- [Bourgeat-Lami and Lansalot, 2010] Bourgeat-Lami, E. and Lansalot, M. (2010). Organic/Inorganic Composite Latexes: The Marriage of Emulsion Polymerization and Inorganic Chemistry. In van Herk, A. M. and Landfester, K., editors, *Hybrid Latex Particles*, number 233 in Adv. Polym. Sci., pages 53–123. Springer Berlin Heidelberg. (Quoted pages 95 and 135.)
- [Bourgeat-Lami et al., 2010] Bourgeat-Lami, E., Sheibat-Othman, N., and Dos Santos, A. M. (2010). Polymer-Clay Nanocomposite Particles and Soap-free Latexes Stabilized by Clay Platelets: State of the Art and Recent Advances. In Mittal, V., editor, *In Polymer Nanocomposites by Emulsion and Suspension*, pages 269–311. RSC Publishing. (Quoted pages 13, 14, 31, 95, 127 and 135.)
- [Brooks and Mankanjuola, 1981] Brooks, B. and Mankanjuola, B. (1981). Measurements of the rate of radical desorption from polymer latices during emulsion polymerisation. *Journal of the Chemical Society, Faraday Transactions 1: Physical Chemistry in Condensed Phases*, 77(11):2659–2667. (Quoted page 117.)

- [Brunauer et al., 1938] Brunauer, S., Emmett, P. H., and Teller, E. (1938). Adsorption of Gases in Multimolecular Layers. *Journal of the American Chemical Society*, 60(2):309–319. 16446. (Quoted pages 52 and 66.)
- [Caruso et al., 2001] Caruso, R. A., Susha, A., and Caruso, F. (2001). Multilayered Titania, Silica, and Laponite Nanoparticle Coatings on Polystyrene Colloidal Templates and Resulting Inorganic Hollow Spheres. *Chemistry of Materials*, pages 400–409. (Quoted page 12.)
- [Casey et al., 1994] Casey, B. S., Morrison, B. R., Maxwell, I. A., Gilbert, R. G., and Napper, D. H. (1994). Free radical exit in emulsion polymerization. I. Theoretical model. *Journal of Polymer Science Part A: Polymer Chemistry*, 32(4):605–630. (Quoted pages 97 and 98.)
- [Castelvetto et al., 2006] Castelvetto, V., De Vita, C., Giannini, G., and Giaiacopi, S. (2006). Role of anionic and nonionic surfactants on the control of particle size and latex colloidal stability in the seeded emulsion polymerization of butyl methacrylate. *Journal of applied polymer science*, 102(4):3083–3094. (Quoted pages 20 and 135.)
- [Chang et al., 1981] Chang, K. H. S., Litt, M. H., and Nomura, M. (1981). The Reinvestigation of Vinyl Acetate Emulsion Polymerization (I) -The Rate of Polymerization. In El-Aasser, M. S. and Vanderhoff, J. W., editors, *Emulsion Polymerization of Vinyl Acetate*, pages 89–136. Springer Netherlands. (Quoted pages 115 and 121.)
- [Chen et al., 2008] Chen, J. H., Cheng, C.-Y., Chiu, W.-Y., Lee, C.-F., and Liang, N.-Y. (2008). Synthesis of zno/polystyrene composites particles by pickering emulsion polymerization. *European Polymer Journal*, 44(10):3271–3279. (Quoted page 13.)
- [Chen and Elimelech, 2006] Chen, K. L. and Elimelech, M. (2006). Aggregation and Deposition Kinetics of Fullerene (C60) Nanoparticles. *Langmuir*, 22:10994–11001. (Quoted page 46.)

- [Cheong and Kim, 1997] Cheong, I.-W. and Kim, J.-H. (1997). Effects of surface charge density on emulsion kinetics and secondary particle formation in emulsifier-free seeded emulsion polymerization of methyl methacrylate. *Colloid and Polymer Science*, 275(8):736–743. (Quoted page 96.)
- [Chern, 2006] Chern, C. S. (2006). Emulsion polymerization mechanisms and kinetics. *Progress in Polymer Science*, 31(5):443–486. (Quoted page 19.)
- [Chevalier and Bolzinger, 2013] Chevalier, Y. and Bolzinger, M.-A. (2013). Emulsions stabilized with solid nanoparticles: Pickering emulsions. *Colloids and Surfaces A: Physicochemical and Engineering Aspects*, 439:23–34. (Quoted pages 20, 51 and 67.)
- [Choi et al., 2001] Choi, Y. S., Choi, M. H., Wang, K. H., Kim, S. O., Kim, Y. K., and Chung, I. J. (2001). Synthesis of exfoliated pmma/na-mmt nanocomposites via soap-free emulsion polymerization. *Macromolecules*, 34(26):8978–8985. (Quoted page 13.)
- [Coelho et al., 2007] Coelho, A. C. V., Santos, P., and Santos, H. (2007). Argilas especiais: argilas quimicamente modificadas-uma revisão. *Química Nova*, 30:1282. (Quoted page 29.)
- [Coen et al., 1998] Coen, E. M., Gilbert, R. G., Morrison, B. R., Leube, H., and Peach, S. (1998). Modelling particle size distributions and secondary particle formation in emulsion polymerization. *Polymer*, 39(26):7099–7112. (Quoted pages 96, 98, 110, 111, 135, 141 and 177.)
- [Coen et al., 1996] Coen, E. M., Lyons, R. A., and Gilbert, R. G. (1996). Effects of Poly(acrylic acid) Electrosteric Stabilizer on Entry and Exit in Emulsion Polymerization. *Macromolecules*, 29(15):5128–5135. (Quoted page 96.)
- [Coen et al., 2004] Coen, E. M., Peach, S., Morrison, B. R., and Gilbert, R. G. (2004). First-principles calculation of particle formation in emulsion polymerization: pseudo-bulk systems. *Polymer*, 45(11):3595–3608. (Quoted page 141.)

- [Colard et al., 2010] Colard, C. A., Teixeira, R. F., and Bon, S. A. (2010). Unraveling mechanistic events in solids-stabilized emulsion polymerization by monitoring the concentration of nanoparticles in the water phase. *Langmuir*, 26(11):7915–7921. (Quoted page 135.)
- [Colombié et al., 2000] Colombié, D., Landfester, K., Sudol, E. D., and El-Aasser, M. S. (2000). Competitive adsorption of the anionic surfactant sls and the nonionic surfactant triton x-405 on polystyrene latex particles. *Langmuir*, 16(21):7905–7913. (Quoted pages 20, 96 and 135.)
- [Colver et al., 2008] Colver, P. J., Colard, C. A., and Bon, S. A. (2008). Multilayered nanocomposite polymer colloids using emulsion polymerization stabilized by solid particles. *Journal of the American Chemical Society*, 130:16850–16851. (Quoted pages 13 and 135.)
- [Crowley et al., 2000] Crowley, T. J., Meadows, E. S., Kostoulas, E., and Doyle III, F. J. (2000). Control of particle size distribution described by a population balance model of semibatch emulsion polymerization. *Journal of Process Control*, 10(5):419–432. (Quoted pages 112, 135 and 179.)
- [de Arbina et al., 1996] de Arbina, L. L., Barandiaran, M. J., Gugliotta, L. M., and Asua, J. (1996). Emulsion polymerization: particle growth kinetics. *Polymer*, 37(26):5907–5916. (Quoted page 135.)
- [Derjaguin and Landau, 1945] Derjaguin, B. and Landau, L. (1945). Theory of stability of highly charged liophobic sols and adhesion of highly charged particles in solutions of electrolytes. *Zhurnal Eksperimentalnoi I Teoreticheskoi Fiziki*, 15(11):663–682. (Quoted page 141.)
- [Dong and Sundberg, 2002] Dong, Y. and Sundberg, D. C. (2002). Radical entry in emulsion polymerization: estimation of the critical length of entry radicals via a simple lattice model. *Macromolecules*, 35(21):8185–8190. (Quoted page 110.)
- [Dupin et al., 2007] Dupin, D., Schmid, A., Balmer, J. A., and Armes, S. P. (2007). Efficient synthesis of poly (2-vinylpyridine)-silica colloidal nanocomposite par-

- ticles using a cationic azo initiator. *Langmuir*, 23(23):11812–11818. (Quoted page 13.)
- [Ebadi et al., 2009] Ebadi, A., Mohammadzadeh, J. S. S., and Khudiev, A. (2009). What is the correct form of BET isotherm for modeling liquid phase adsorption? *Adsorption*, 15:65–73. (Quoted pages 52 and 53.)
- [Edouard et al., 2005] Edouard, D., Sheibat-Othman, N., and Hammouri, H. (2005). Observer design for particle size distribution in emulsion polymerization. *AIChE Journal*, 51(12):3167–3185. (Quoted page 135.)
- [Enarsson and Wagberg, 2008] Enarsson, L.-E. and Wagberg, L. (2008). Conformation of preadsorbed polyelectrolyte layers on silica studied by secondary adsorption of colloidal silica. *Journal of colloid and interface science*, 325:84–92. (Quoted page 46.)
- [Fatisson et al., 2009] Fatisson, J., Domingos, R. F., Wilkinson, K. J., and Tufenkji, N. (2009). Deposition of TiO₂ Nanoparticles onto Silica Measured Using a Quartz Crystal Microbalance with Dissipation Monitoring. *Langmuir*, 25:6062–6069. (Quoted page 46.)
- [Feeney et al., 1984] Feeney, P. J., Napper, D. H., and Gilbert, R. G. (1984). Coagulative nucleation and particle size distributions in emulsion polymerization. *Macromolecules*, 17(12):2520–2529. (Quoted page 11.)
- [Feeney et al., 1987] Feeney, P. J., Napper, D. H., and Gilbert, R. G. (1987). Surfactant-free emulsion polymerizations: predictions of the coagulative nucleation theory. *Macromolecules*, 20(11):2922–2930. (Quoted page 98.)
- [Ferguson et al., 2005] Ferguson, C. J., Hughes, R. J., Nguyen, D., Pham, B. T., Gilbert, R. G., Serelis, A. K., Such, C. H., and Hawket, B. S. (2005). Ab initio emulsion polymerization by raft-controlled self-assembly §. *Macromolecules*, 38(6):2191–2204. (Quoted pages 20 and 135.)
- [Fitch and Tsai, 1971] Fitch, R. M. and Tsai, C. H. (1971). Particle Formation in Polymer Colloids, III: Prediction of the Number of Particles by a Homogeneous

- Nucleation Theory. In Fitch, R. M., editor, *Polymer Colloids*, pages 73–102. Springer US. (Quoted pages 10, 109, 135 and 138.)
- [Fontenot and Schork, 1993] Fontenot, K. and Schork, F. J. (1993). Simulation of Mini/Macro Emulsion Polymerizations I. Development of the Model. *Polymer Reaction Engineering*, 1(1):75–109. (Quoted pages 96, 98, 123 and 177.)
- [Fortuny et al., 2004] Fortuny, M., Graillat, C., and McKenna, T. F. (2004). Coagulation of anionically stabilized polymer particles. *Industrial & engineering chemistry research*, 43(23):7210–7219. (Quoted pages 137, 147 and 149.)
- [Fortuny Heredia, 2002] Fortuny Heredia, M. (2002). *Modelisation de procedes pour la synthese de latex multipopules*. Thèse de doctorat, Universite Claude Bernard, Lyon, France. (Quoted pages 7 and 149.)
- [Friis and Nyhagen, 1973] Friis, N. and Nyhagen, L. (1973). A Kinetic Study of the Emulsion Polymerization of Vinyl Acetate. *Journal of Applied Polymer Science*, 17(8):2311–2327. (Quoted page 122.)
- [Fripiat et al., 1982] Fripiat, J., Cases, J., Francois, M., and Letellier, M. (1982). Thermodynamic and microdynamic behavior of water in clay suspensions and gels. *Journal of Colloid and Interface Science*, 89(2):378–400. 00169. (Quoted pages 29 and 59.)
- [Fuchs, 1934] Fuchs, N. (1934). Über die Stabilität und Aufladung der Aerosole. *Zeitschrift für Physik*, 89(11-12):736–743. (Quoted pages 139 and 142.)
- [Gardon, 1968] Gardon, J. L. (1968). Emulsion polymerization. I. Recalculation and extension of the Smith-Ewart theory. *Journal of Polymer Science Part A-1: Polymer Chemistry*, 6(3):623–641. (Quoted pages 96, 109, 167, 171 and 177.)
- [Gilbert and Napper, 1983] Gilbert, R. G. and Napper, D. H. (1983). The direct determination of kinetic parameters in emulsion polymerization systems. *Journal of Macromolecular Science-Reviews in Macromolecular Chemistry and Physics*, 23(1):127–186. (Quoted page 106.)

- [Grady and Jr, 1996] Grady, M. C. and Jr, R. R. M. (1996). Small-molecule exchange in emulsion polymerization. *Journal of Computer-Aided Materials Design*, 3(1-3):296–302. (Quoted page 123.)
- [Gugliotta et al., 1995] Gugliotta, L. M., Arzamendi, G., and Asua, J. M. (1995). Choice of monomer partition model in mathematical modeling of emulsion copolymerization systems. *Journal of Applied Polymer Science*, 55(7):1017–1039. (Quoted page 188.)
- [Guillot, 1985] Guillot, J. (1985). Some thermodynamic aspects in emulsion copolymerization. *Die Makromolekulare Chemie*, 10(Suppl. 10-11):235–264. (Quoted page 188.)
- [Hansen and Ugelstad, 1978a] Hansen, F. K. and Ugelstad, J. (1978a). Particle nucleation in emulsion polymerization. I. A theory for homogeneous nucleation. *Journal of Polymer Science: Polymer Chemistry Edition*, 16(8):1953–1979. (Quoted page 10.)
- [Hansen and Ugelstad, 1978b] Hansen, F. K. and Ugelstad, J. (1978b). Particle nucleation in emulsion polymerization. I. A theory for homogeneous nucleation. *Journal of Polymer Science: Polymer Chemistry Edition*, 16(8):1953–1979. (Quoted pages 111, 135 and 138.)
- [Harada et al., 1971] Harada, M., Nomura, M., Eguchi, W., and Nagata, S. (1971). Studies of the Effect of Polymer Particles on Emulsion Polymerization. *Journal of Chemical Engineering of Japan*, 4(1):54–60. (Quoted pages 115, 116, 122, 167, 176 and 177.)
- [Harada et al., 1972] Harada, M., Nomura, M., Kojima, H., Eguchi, W., and Nagata, S. (1972). Rate of emulsion polymerization of styrene. *Journal of Applied Polymer Science*, 16(4):811–833. (Quoted page 108.)
- [Harkins, 1945] Harkins, W. D. (1945). A General Theory of the Reaction Loci in Emulsion Polymerization. *The Journal of Chemical Physics*, 13(9):381–382. (Quoted page 9.)

- [Harkins, 1947] Harkins, W. D. (1947). A general theory of the mechanism of emulsion polymerization. *Journal of the American Chemical Society*, 69(6):1428–44. (Quoted pages 7, 17, 99 and 167.)
- [Hawket et al., 1981] Hawket, B. S., Napper, D. H., and Gilbert, R. G. (1981). Analysis of interval iii kinetic data for emulsion polymerizations. *Journal of the Chemical Society, Faraday Transactions 1: Physical Chemistry in Condensed Phases*, 77(10):2395–2404. (Quoted page 170.)
- [Hermans, 1939] Hermans, J. (1939). Orthokinetic coagulation due to oscillations. *Recueil des Travaux Chimiques des Pays-Bas*, 58(2):164–173. (Quoted page 139.)
- [Hernandez and Tauer, 2008] Hernandez, H. F. and Tauer, K. (2008). Radical Desorption Kinetics in Emulsion Polymerization. 1. Theory and Simulation. *Industrial & Engineering Chemistry Research*, 47(24):9795–9811. (Quoted pages 115, 116, 117, 124, 176 and 177.)
- [Hernández and Tauer, 2007a] Hernández, H. F. and Tauer, K. (2007a). Brownian Dynamics Simulation of the Capture of Primary Radicals in Dispersions of Colloidal Polymer Particles. *Industrial & Engineering Chemistry Research*, 46(13):4480–4485. (Quoted pages 96, 98 and 177.)
- [Hernández and Tauer, 2007b] Hernández, H. F. and Tauer, K. (2007b). Brownian Dynamics Simulation Studies on Radical Capture in Emulsion Polymerization. *Macromolecular Symposia*, 259(1):274–283. (Quoted page 111.)
- [Herrera et al., 2004] Herrera, N. N., Letoffe, J.-M., Putaux, J.-L., David, L., and Bourgeat-Lami, E. (2004). Aqueous Dispersions of Silane- unctinalized Laponite Clay Platelets. A First Step toward the Elaboration of Water-Based Polymer/Clay Nanocomposites. *Langmuir*, pages 1564–1571. (Quoted pages 14, 95 and 135.)
- [Herrera et al., 2005] Herrera, N. N., Letoffe, J.-M., Reymond, J.-P., and Bourgeat-Lami, E. (2005). Silylation of laponite clay particles with monofunctional and

- trifunctional vinyl alkoxysilanes. *Journal of Materials Chemistry*, 15:863–871. (Quoted pages 14, 95 and 135.)
- [Herrera et al., 2006] Herrera, N. N., Persoz, S., Putaux, J.-L., David, L., and Bourgeat-Lami, E. (2006). Synthesis of polymer latex particles decorated with organically-modified laponite clay platelets via emulsion polymerization. *Journal of Nanosciences and Nanotechnologies*, 6:421–431. (Quoted pages 14, 95 and 135.)
- [Herrera-Ordóñez and Olayo, 2000] Herrera-Ordóñez, J. and Olayo, R. (2000). On the kinetics of styrene emulsion polymerization above CMC. II. Comparison with experimental results. *Journal of Polymer Science Part A: Polymer Chemistry*, 38(12):2219–2231. (Quoted page 108.)
- [Hogg et al., 1966] Hogg, R., Healy, T., and Fuerstenau, D. (1966). Mutual coagulation of colloidal dispersions. *Transactions of the Faraday Society*, 62:1638–1651. (Quoted page 143.)
- [Immanuel and Doyle Iii, 2002] Immanuel, C. D. and Doyle Iii, F. J. (2002). Open-loop control of particle size distribution in semi-batch emulsion copolymerization using a genetic algorithm. *Chemical Engineering Science*, 57(20):4415–4427. (Quoted page 140.)
- [Immanuel and Doyle Iii, 2003] Immanuel, C. D. and Doyle Iii, F. J. (2003). Computationally efficient solution of population balance models incorporating nucleation, growth and coagulation: application to emulsion polymerization. *Chemical Engineering Science*, 58(16):3681–3698. (Quoted pages 135, 139 and 141.)
- [Israelachvili, 1992] Israelachvili, J. N. (1992). Intermolecular and surface forces: With applications to colloidal and biological systems (colloid science). (Quoted page 151.)
- [Jatav and Joshi, 2014] Jatav, S. and Joshi, Y. M. (2014). Chemical stability of Laponite in aqueous media. *Applied Clay Science*, 97–98:72–77. (Quoted page 46.)

- [Keiji Kanazawa and Gordon II, 1985] Keiji Kanazawa, K. and Gordon II, J. G. (1985). The oscillation frequency of a quartz resonator in contact with liquid. *Analytica Chimica Acta*, 175:99–105. (Quoted page 45.)
- [Kim et al., 2013] Kim, Y. J., Liu, Y. D., Seo, Y., and Choi, H. J. (2013). Pickering-emulsion-polymerized polystyrene/fe₂o₃ composite particles and their magneto-responsive characteristics. *Langmuir*, 29(16):4959–4965. (Quoted page 13.)
- [Kiparissides, 1996] Kiparissides, C. (1996). Polymerization reactor modeling: a review of recent developments and future directions. *Chemical Engineering Science*, 51(10):1637–1659. (Quoted page 3.)
- [Kumar et al., 2008] Kumar, N. R., Muralidhar, K., and Joshi, Y. M. (2008). On the refractive index of ageing dispersions of laponite. *Applied Clay Science*, 42(1):326–330. (Quoted page 151.)
- [Kusters et al., 1992] Kusters, J. M., Napper, D. H., Gilbert, R. G., and German, A. L. (1992). Kinetics of particle growth in emulsion polymerization systems with surface-active initiators. *Macromolecules*, 25(25):7043–7050. (Quoted page 96.)
- [Lacik et al., 1992] Lacik, I., Casey, B. S., Sangster, D. F., Gilbert, R. G., and Napper, D. H. (1992). Desorbed free radicals in emulsion polymerizations: effect of aqueous-phase spin trap. *Macromolecules*, 25(16):4065–4072. (Quoted pages 123 and 145.)
- [Langmuir, 1916] Langmuir, I. (1916). The constitution and fundamental properties of solids and liquids. part i. solids. *Journal of the American Chemical Society*, 38:2221–2295. (Quoted page 51.)
- [Laxton and Berg, 2006] Laxton, P. B. and Berg, J. C. (2006). Relating clay yield stress to colloidal parameters. *Journal of colloid and interface science*, 296(2):749–755. (Quoted page 151.)
- [Lazaridis et al., 1999] Lazaridis, N., Alexopoulos, A. H., Chatzi, E. G., and Kiparissides, C. (1999). Steric stabilization in emulsion polymerization using

- oligomeric nonionic surfactants. *Chemical engineering science*, 54(15):3251–3261. (Quoted pages 20 and 135.)
- [Leach et al., 2005] Leach, E. S. H., Hopkinson, A., Franklin, K., and van Duijnveltdt, J. S. (2005). Nonaqueous Suspensions of Laponite and Montmorillonite. *Langmuir*, 21:3821–3830. (Quoted page 58.)
- [Leemans et al., 1998] Leemans, L., Jerome, R., and Teyssie, P. (1998). Diffusive Radical Entry as the Rate-Determining Step in Amphiphilic Block Polyelectrolyte Mediated Emulsion Polymerization. *Macromolecules*, 31(17):5565–5571. (Quoted page 96.)
- [Li and Brooks, 1993] Li, B.-G. and Brooks, B. W. (1993). Prediction of the average number of radicals per particle for emulsion polymerization. *Journal of Polymer Science Part A: Polymer Chemistry*, 31(9):2397–2402. (Quoted page 101.)
- [Li et al., 2005] Li, L., Harnau, L., Rosenfeldt, S., and Ballauff, M. (2005). Effective interaction of charged platelets in aqueous solution: Investigations of colloid laponite suspensions by static light scattering and small-angle x-ray scattering. *Physical Review E*, 72(5):051504. (Quoted page 156.)
- [Lifshitz, 1955] Lifshitz, E. (1955). Zh. eksp. teor. fiz. *Soviet Physics JETP*, 29:94. (Quoted page 151.)
- [Lin et al., 2006] Lin, K.-F., Lin, S.-C., Chien, A.-T., Hsieh, C.-C., Yen, M.-H., Lee, C.-H., Lin, C.-S., Chiu, W.-Y., and Lee, Y.-H. (2006). Exfoliation of montmorillonite by the insertion of disklike micelles via the soap-free emulsion polymerization of methyl methacrylate. *Journal of Polymer Science Part A: Polymer Chemistry*, 44(19):5572–5579. (Quoted page 13.)
- [Lin et al., 2008] Lin, Z., Renneckar, S., and Hindman, D. P. (2008). Nanocomposite-based lignocellulosic fibers 1. Thermal stability of modified fibers with clay-polyelectrolyte multilayers. *Cellulose*, 15:333–346. (Quoted page 28.)
- [Liotta et al., 1997] Liotta, V., Georgakis, C., Sudol, E. D., and El-Aasser, M. S. (1997). Manipulation of Competitive Growth for Particle Size Control in Emul-

- sion Polymerization. *Industrial & Engineering Chemistry Research*, 36(8):3252–3263. (Quoted pages 109 and 176.)
- [Lu and Larock, 2007] Lu, Y. and Larock, R. C. (2007). New hybrid latexes from a soybean oil-based waterborne polyurethane and acrylics via emulsion polymerization. *Biomacromolecules*, 8(10):3108–3114. (Quoted page 13.)
- [Malmberg and Maryott, 1956] Malmberg, C. and Maryott, A. (1956). Dielectric constant of water from 0 0 to 1000 0 c. *Journal of Research of the National Bureau of Standards*, 56:1–8. (Quoted page 151.)
- [Maxwell et al., 1992a] Maxwell, I. A., Kurja, J., Van Doremale, G. H., and German, A. L. (1992a). Thermodynamics of swelling of latex particles with two monomers. *Die Makromolekulare Chemie*, 193(8):2065–2080. (Quoted page 188.)
- [Maxwell et al., 1992b] Maxwell, I. A., Kurja, J., Van Doremale, G. H., German, A. L., and Morrison, B. R. (1992b). Partial swelling of latex particles with monomers. *Die Makromolekulare Chemie*, 193(8):2049–2063. (Quoted page 188.)
- [Maxwell et al., 1991] Maxwell, I. A., Morrison, B. R., Napper, D. H., and Gilbert, R. G. (1991). Entry of free radicals into latex particles in emulsion polymerization. *Macromolecules*, 24(7):1629–1640. (Quoted pages 96, 98, 110, 167, 171 and 177.)
- [Maxwell et al., 1993] Maxwell, I. A., Noel, L. F., Schoonbrood, H. A., and German, A. L. (1993). Thermodynamics of swelling of latex particles with two monomers: a sensitivity analysis. *Macromolecular Theory and Simulations*, 2(2):269–274. (Quoted page 188.)
- [McAuliffe, 1966] McAuliffe, C. (1966). Solubility in water of paraffin, cycloparaffin, olefin, acetylene, cycloolefin, and aromatic hydrocarbons¹. *The Journal of Physical Chemistry*, 70(4):1267–1275. (Quoted pages 97 and 98.)
- [Mead and Poehlein, 1989] Mead, R. N. and Poehlein, G. W. (1989). Free-radical transport from latex particles. *Journal of Applied Polymer Science*, 38(1):105–122. (Quoted pages 122 and 177.)

- [Melis et al., 1999] Melis, S., Verduyn, M., Storti, G., Morbidelli, M., and Baldyga, J. (1999). Effect of fluid motion on the aggregation of small particles subject to interaction forces. *AIChE journal*, 45(7):1383–1393. (Quoted pages 139 and 140.)
- [Min and Ray, 1974] Min, K. W. and Ray, W. H. (1974). On the Mathematical Modeling of Emulsion Polymerization Reactors. *Journal of Macromolecular Science, Part C: Polymer Reviews*, 11(2):177–255. (Quoted pages 98 and 137.)
- [Mongondry et al., 2004] Mongondry, P., Nicolai, T., and Tassin, J.-F. (2004). Influence of pyrophosphate or polyethylene oxide on the aggregation and gelation of aqueous laponite dispersions. *Journal of Colloid and Interface Sciences*, 275(1):191–196. (Quoted pages 15 and 30.)
- [Morrison et al., 1994] Morrison, B. R., Casey, B. S., Lacik, I., Leslie, G. L., Sangster, D. F., Gilbert, R. G., and Napper, D. H. (1994). Free radical exit in emulsion polymerization. II. Model discrimination via experiment. *Journal of Polymer Science Part A: Polymer Chemistry*, 32(4):631–649. (Quoted pages 115 and 121.)
- [Müller, 1928] Müller, H. (1928). Zur allgemeinen theorie ser raschen koagulation. *Fortschrittsberichte über Kolloide und Polymere*, 27(6):223–250. (Quoted page 141.)
- [Negrete-Herrera et al., 2006a] Negrete-Herrera, N., Putaux, J.-L., and Bourgeat-Lami, E. (2006a). Synthesis of polymer/Laponite nanocomposite latex particles via emulsion polymerization using silylated and cation-exchanged Laponite clay platelets. *Progress in solid state chemistry*, 34(2):121–137. (Quoted pages 14, 95 and 135.)
- [Negrete-Herrera et al., 2006b] Negrete-Herrera, N., Putaux, J.-L., David, L., and Bourgeat-Lami, E. (2006b). Polymer/Laponite Composite Colloids through Emulsion Polymerization: Influence of the Clay Modification Level on Particle Morphology. *Macromolecules*, 39:9177–9184. (Quoted pages 14, 95 and 135.)

- [Negrete-Herrera et al., 2007] Negrete-Herrera, N., Putaux, J.-L., David, L., Haas, F. D., and Bourgeat-Lami, E. (2007). Polymer/Laponite composite latexes: Particle morphology, film microstructure, and properties. *Macromol. Rapid Commun.*, 28:1567–1573. (Quoted pages 14, 95 and 135.)
- [Ngai and Bon, 2014] Ngai, T. and Bon, S. A. (2014). *Particle-stabilized emulsions and colloids*, volume 3. Royal Society of Chemistry. (Quoted pages 71 and 136.)
- [Nicolai and Cocard, 2000] Nicolai, T. and Cocard, S. (2000). Light Scattering Study of the dispersion of Laponite. *Langmuir*, pages 8189–8193. (Quoted page 59.)
- [Nomura, 1982] Nomura, M. (1982). Desorption and Reabsorption. *Emulsion polymerization*, page 191. (Quoted page 122.)
- [Nomura and Harada, 1981] Nomura, M. and Harada, M. (1981). Rate coefficient for radical desorption in emulsion polymerization. *Journal of Applied Polymer Science*, 26(1):17–26. (Quoted page 122.)
- [Nomura et al., 2005] Nomura, M., Tobita, H., and Suzuki, K. (2005). Emulsion Polymerization: Kinetic and Mechanistic Aspects. In Okubo, M., editor, *Polymer Particles*, number 175 in Advances in Polymer Science, pages 1–128. Springer Berlin Heidelberg. (Quoted pages 96, 98, 111 and 177.)
- [Omi et al., 1985] Omi, S., Kushibiki, K., Negishi, M., and Iso, M. (1985). Generalized computer modeling of semi-batch, n-component emulsion copolymerization systems and its applications. *Zairyo Gijutsu*, 3(426). (Quoted page 189.)
- [O’toole, 1965] O’toole, J. T. (1965). Kinetics of emulsion polymerization. *Journal of Applied Polymer Science*, 9(4):1291–1297. (Quoted page 101.)
- [Podsiadlo et al., 2009] Podsiadlo, P., Shim, B. S., and Kotov, N. A. (2009). Polymer/clay and polymer/carbon nanotube hybrid organic–inorganic multilayered composites made by sequential layering of nanometer scale films. *Coord. Chem. Rev.*, 253:2835–2851. (Quoted page 28.)

- [Prestidge et al., 2004] Prestidge, C. A., Barnes, T., and Simovic, S. (2004). Polymer and particle adsorption at the PDMS droplet-water interface. *Advances in colloid and interface science*, 108:105–118. (Quoted pages 52 and 53.)
- [Quevedo and Tufenkji, 2009] Quevedo, I. R. and Tufenkji, N. (2009). Influence of Solution Chemistry on the Deposition and Detachment Kinetics of a CdTe Quantum Dot Examined Using a Quartz Crystal Microbalance. *Environmental Science & Technology*, 43:3176–3182. (Quoted page 46.)
- [Ramos and Forcada, 2006] Ramos, J. and Forcada, J. (2006). Modeling the emulsion polymerization of amino-functionalized latex particles. *Polymer*, 47(4):1405–1413. (Quoted pages 20 and 135.)
- [Ray et al., 1995] Ray, A. B., Saraf, D., and Gupta, S. K. (1995). Free radical polymerizations associated with the trommsdorff effect under semibatch reactor conditions. i: Modeling. *Polymer Engineering & Science*, 35(16):1290–1299. (Quoted page 81.)
- [Rosta and von Gunten, 1990] Rosta, L. and von Gunten, H. R. (1990). Light scattering characterization of laponite sols. *Journal of Colloid and Interface Science*, 134:397–406. (Quoted page 59.)
- [Ruggerone et al., 2009a] Ruggerone, R., Plummer, C. J., Herrera, N. N., Bourgeat-Lami, E., and Manson, J.-A. E. (2009a). Highly filled polystyrene-laponite nanocomposites prepared by emulsion polymerization. *European Polymer Journal*, 45(3):621–629. (Quoted pages 14, 95 and 135.)
- [Ruggerone et al., 2009b] Ruggerone, R., Plummer, C. J., Herrera, N. N., Bourgeat-Lami, E., and Manson, J. A. E. (2009b). Mechanical properties of highly filled latex-based polystyrene/laponite nanocomposites. In *Solid State Phenomena*, volume 151, pages 30–34. Trans Tech Publ. (Quoted pages 14, 95 and 135.)
- [Ruzicka et al., 2006] Ruzicka, B., Zulian, L., and Ruocco, G. (2006). More on the Phase Diagram of Laponite. *Langmuir*, 22:1106–1111. (Quoted pages 29, 30 and 97.)

- [Sáenz de Buruaga et al., 1997] Sáenz de Buruaga, I., Armitage, P. D., Leiza, J. R., and Asua, J. M. (1997). Nonlinear control for maximum production rate of latexes of well-defined polymer composition. *Industrial & engineering chemistry research*, 36(10):4243–4254. (Quoted page 174.)
- [Said and Fataftah, 1996] Said, Z. F. and Fataftah, Z. A. (1996). Saturation swelling and the seeded emulsion polymerisation of styrene at high ionic strength. *Polymer international*, 40(4):307–313. (Quoted page 188.)
- [Sajjadi, 2009] Sajjadi, S. (2009). Population balance modeling of particle size distribution in monomer-starved semibatch emulsion polymerization. *AIChE Journal*, 55(12):3191–3205. (Quoted pages 103, 112, 170 and 179.)
- [Sauerbrey, 1959] Sauerbrey, G. Z. (1959). Use of quartz vibration for weighing thin films on a microbalance. *Physik Journal*, 155:206–212. (Quoted page 43.)
- [Saunders et al., 1999] Saunders, J. M., Goodwin, J. W., Richardson, R. M., and Vincent, B. (1999). A Small-Angle X-ray Scattering Study of the Structure of Aqueous Laponite Dispersions. *The Journal of Physical Chemistry B*, 103:9211–9218. (Quoted pages 63 and 73.)
- [Schmid et al., 2009] Schmid, A., Armes, S. P., Leite, C. A., and Galembeck, F. (2009). Efficient preparation of polystyrene/silica colloidal nanocomposite particles by emulsion polymerization using a glycerol-functionalized silica sol. *Langmuir*, 25(4):2486–2494. (Quoted page 13.)
- [Schork et al., 1999] Schork, F. J., Poehlein, G., Wang, S., Reimers, J., Rodrigues, J., and Samer, C. (1999). Miniemulsion polymerization. *Colloids and Surfaces A: Physicochemical and Engineering Aspects*, 153(1):39–45. (Quoted pages 79 and 81.)
- [Schrade et al., 2011] Schrade, A., Mikhalevich, V., Landfester, K., and Ziener, U. (2011). Synthesis and characterization of positively charged, alumina-coated silica/polystyrene hybrid nanoparticles via pickering miniemulsion polymeriza-

- tion. *Journal of Polymer Science Part A: Polymer Chemistry*, 49(22):4735–4746. (Quoted page 13.)
- [Shahin and Joshi, 2012] Shahin, A. and Joshi, Y. M. (2012). Physicochemical Effects in Aging Aqueous Laponite Suspensions. *Langmuir*, 28:15674–15686. (Quoted page 56.)
- [Sheibat-Othman, 2000] Sheibat-Othman, N. (2000). *Advanced strategies for composition control in Semi-continuous emulsion polymerization*. PhD thesis, Université Claude Bernard - Lyon I. (Quoted page 187.)
- [Sheibat-Othman and Bourgeat-Lami, 2009] Sheibat-Othman, N. and Bourgeat-Lami, E. (2009). Use of silica particles for the formation of organic- inorganic particles by surfactant-free emulsion polymerization. *Langmuir*, 25(17):10121–10133. (Quoted page 13.)
- [Sheibat-Othman et al., 2011] Sheibat-Othman, N., Cenacchi-Pereira, A.-M., Santos, A. M. D., and Bourgeat-Lami, E. (2011). A kinetic investigation of surfactant-free emulsion polymerization of styrene using laponite clay platelets as stabilizers. *Journal of Polymer Science Part A: Polymer Chemistry*, 49:4771–4784. (Quoted pages 12, 13, 14, 95, 127 and 135.)
- [Sherman and Ford, 2005] Sherman, R. L. and Ford, W. T. (2005). Small Core/Thick Shell Polystyrene/Poly(methyl methacrylate) Latexes. *Industrial & Engineering Chemistry Research*, 44:8538–8541. (Quoted page 12.)
- [Sill et al., 2009] Sill, K., Yoo, S., and Emrick, T. (2009). Polymer–Nanoparticle Composites. In *Dekker Encyclopedia of Nanoscience and Nanotechnology, Second Edition*, pages 3487–3500. Taylor & Francis. (Quoted page 12.)
- [Smith and Ewart, 1948] Smith, W. V. and Ewart, R. H. (1948). Kinetics of Emulsion Polymerization. *The Journal of Chemical Physics*, 16(6):592–599. (Quoted pages 21, 95, 96, 98, 99, 100, 107, 111, 115, 121, 135, 138, 167, 171 and 177.)

- [Smoluchowski, 1927] Smoluchowski, M. (1927). Versuch einer mathematischen theorie der koagulationskinetik kolloider losungen. *Pisma Mariana Smoluchowskiego*, 2(1):595–639. (Quoted pages 107, 139 and 140.)
- [Soh and Sundberg, 1982] Soh, S. K. and Sundberg, D. C. (1982). Diffusion-controlled vinyl polymerization. III. Free volume parameters and diffusion-controlled propagation. *Journal of Polymer Science: Polymer Chemistry Edition*, 20(5):1331–1344. (Quoted pages 95 and 98.)
- [Song et al., 2009] Song, X., Zhao, Y., Wang, H., and Du, Q. (2009). Fabrication of polymer microspheres using titania as a photocatalyst and Pickering stabilizer. *Langmuir*, 25(8):4443–4449. (Quoted page 13.)
- [Stockmayer, 1957] Stockmayer, W. H. (1957). Note on the kinetics of emulsion polymerization. *Journal of Polymer Science*, 24(106):314–317. (Quoted page 101.)
- [Sun et al., 2004] Sun, Q., Deng, Y., and Wang, Z. L. (2004). Synthesis and Characterization of Polystyrene-Encapsulated Laponite Composites via Miniemulsion Polymerization. *Macromolecular Materials and Engineering*, 289:288–295. 00087. (Quoted page 12.)
- [Sundberg et al., 1981] Sundberg, D., Hsieh, J., Soh, S., and Baldus, R. (1981). Diffusion-controlled kinetics in the emulsion polymerization of styrene and methyl methacrylate. In *Emulsion Polymers and Emulsion Polymerization*, volume 165, pages 327–343. American Chemical Society. (Quoted pages 170 and 171.)
- [Tang et al., 2014] Tang, M., Wang, X., Wu, F., Liu, Y., Zhang, S., Pang, X., Li, X., and Qiu, H. (2014). Au nanoparticle/graphene oxide hybrids as stabilizers for pickering emulsions and au nanoparticle/graphene oxide@ polystyrene microspheres. *Carbon*, 71:238–248. (Quoted page 13.)
- [Tawari et al., 2001] Tawari, S. L., Koch, D. L., and Cohen, C. (2001). Electrical Double-Layer Effects on the Brownian Diffusivity and Aggregation Rate of

- Laponite Clay Particles. *Journal of Colloid and Interface Sciences*, 240:54–66. (Quoted pages 15, 30 and 97.)
- [technical bulletin, 2003] technical bulletin, L. (2003). Laponite - synthetic layered silicate - its chemistry, structure and relationship to natural clays. (Quoted page 14.)
- [Teixeira et al., 2011] Teixeira, R. F., McKenzie, H. S., Boyd, A. A., and Bon, S. A. (2011). Pickering emulsion polymerization using laponite clay as stabilizer to prepare armored “soft” polymer latexes. *Macromolecules*, 44(18):7415–7422. (Quoted pages 31, 69 and 127.)
- [Thickett and Gilbert, 2007] Thickett, S. C. and Gilbert, R. G. (2007). Emulsion polymerization: state of the art in kinetics and mechanisms. *Polymer*, 48(24):6965–6991. (Quoted pages 96, 101 and 135.)
- [Thickett and Zetterlund, 2013] Thickett, S. C. and Zetterlund, P. B. (2013). Preparation of composite materials by using graphene oxide as a surfactant in ab initio emulsion polymerization systems. *ACS Macro Letters*, 2(7):630–634. (Quoted page 13.)
- [Thompson and Butterworth, 1992] Thompson, D. W. and Butterworth, J. T. (1992). The nature of laponite and its aqueous dispersions. *Journal of Colloid and Interface Science*, 151:236–243. (Quoted page 58.)
- [Tulig and Tirrell, 1981] Tulig, T. J. and Tirrell, M. (1981). Molecular theory of the trommsdorff effect. *Macromolecules*, 14(5):1501–1511. (Quoted page 81.)
- [Ugelstad and Hansen, 1976] Ugelstad, J. and Hansen, F. K. (1976). Kinetics and Mechanism of Emulsion Polymerization. *Rubber Chemistry and Technology*, 49(3):536–609. (Quoted pages 96, 98, 107, 115, 122, 167 and 177.)
- [Ugelstad et al., 1969] Ugelstad, J., Mork, P. C., Dahl, P., and Rangnes, P. (1969). A kinetic investigation of the emulsion polymerization of vinyl chloride. *Journal of Polymer Science Part C: Polymer Symposia*, 27(1):49–68. (Quoted page 121.)

- [Vanderhoff, 1993] Vanderhoff, J. W. (1993). Recent advances in the preparation of latexes. *Chemical Engineering Science*, 48(2):203–217. (Quoted page 10.)
- [Vanzo et al., 1965] Vanzo, E., Marchessault, R., and Stannett, V. (1965). The solubility and swelling of latex particles. *Journal of Colloid Science*, 20(1):62–71. (Quoted page 112.)
- [Verwey and Overbeek, 1948] Verwey, E. J. W. and Overbeek, J. T. G. (1948). *Theory of the Stability of Lyophobic Colloids*. Elsevier. (Quoted page 141.)
- [Verwey et al., 1999] Verwey, E. J. W., Overbeek, J. T. G., and Overbeek, J. T. G. (1999). *Theory of the stability of lyophobic colloids*. Courier Corporation. (Quoted page 20.)
- [Vorwerg and Gilbert, 2000] Vorwerg, L. and Gilbert, R. G. (2000). Electrosteric stabilization with poly (acrylic) acid in emulsion polymerization: Effect on kinetics and secondary particle formation. *Macromolecules*, 33(18):6693–6703. (Quoted page 96.)
- [Wang et al., 2001] Wang, X., Boya, B., Sudol, E. D., and El-Aasser, M. S. (2001). Effect of a reactive surfactant and its polymeric counterpart on the kinetics of seeded emulsion polymerization of styrene. *Macromolecules*, 34(26):8907–8912. (Quoted page 96.)
- [Xu et al., 2010] Xu, D., Hodges, C., Ding, Y., Biggs, S., Brooker, A., and York, D. (2010). A QCM Study on the Adsorption of Colloidal Laponite at the Solid/Liquid Interface. *Langmuir*, 26:8366–8372. (Quoted pages 28, 43 and 46.)
- [Xu et al., 2005] Xu, Y., Higgins, B., and Brittain, W. J. (2005). Bottom-up synthesis of PS–CNF nanocomposites. *Polymer*, 46:799–810. (Quoted page 12.)
- [Yamak, 2013] Yamak, H. B. (2013). Emulsion polymerization: Effects of polymerization variables on the properties of vinyl acetate based emulsion polymers. *InTech*, 44(19):35–70. (Quoted page 20.)

- [Yan and Masliyah, 1994] Yan, N. and Masliyah, J. H. (1994). Adsorption and desorption of Clay Particles at the Oil-Water Interface. *Journal of Colloid and Interface Sciences*, pages 386–392. (Quoted page 28.)
- [Yeliseyeva and Zuikov, 1977] Yeliseyeva, V. I. and Zuikov, A. V. (1977). Emulsion polymerization of polar monomers. *Polymer Science U.S.S.R.*, 19(11):3021–3031. (Quoted pages 96, 98 and 109.)
- [Yin et al., 2012] Yin, D., Du, X., Liu, H., Zhang, Q., and Ma, L. (2012). Facile one-step fabrication of polymer microspheres with high magnetism and armored inorganic particles by pickering emulsion polymerization. *Colloids and Surfaces A: Physicochemical and Engineering Aspects*, 414:289–295. (Quoted page 13.)
- [Yin et al., 2013] Yin, G., Zheng, Z., Wang, H., Du, Q., and Zhang, H. (2013). Preparation of graphene oxide coated polystyrene microspheres by pickering emulsion polymerization. *Journal of colloid and interface science*, 394:192–198. (Quoted page 13.)
- [Zaragoza-Contreras et al., 2002] Zaragoza-Contreras, E. A., Navarro-Rodríguez, D., and Maldonado-Textle, H. (2002). Evolution of molecular weight and molecular weight distribution in ab initio styrene emulsion polymerizations using series of rigid rodlike cationic amphiphiles as surfactants. *Journal of applied polymer science*, 84(8):1513–1523. (Quoted pages 20 and 135.)
- [Zhao et al., 2010] Zhao, Y., Wang, H., Song, X., and Du, Q. (2010). Fabrication of two kinds of polymer microspheres stabilized by modified titania during pickering emulsion polymerization. *Macromolecular Chemistry and Physics*, 211(23):2517–2529. (Quoted page 13.)

